Studies on π-interactions in liquid phase separations

Eisuke Kanao

2020

Contents

Chapter 3. Separation of Halogenated Benzenes Enabled by Investigation of Halogen-π Interactions with Carbon Materials

Chapter 4. Isotope Effects on Hydrogen Bonding and CH/CD-π Interaction

Chapter 1

General Introduction

1-1 Nanotechnology

Nanotechnology is a technology conducted at the nanoscale between 1 to 100 nanometers. The nanotechnology is studied and applied for extremely small things, and the technology can be used across all the scientific fields, including chemistry, biology, physics, materials science, and engineering.[1-6] There are two general approaches for synthesizing nanomaterials and/or fabricating nanostructures. The first approach is the "top-down approach". This approach uses larger (macroscopic) initial structures, which can be externally-controlled in processing nanostructures. At the moment, the most common top-down approach is well known as lithography.[7-10] It has been used for a while to manufacture the computer chips and produced the structures smaller than 100 nm. Gordon Moore, who is the Intel® co-founder, empirically predicted "The number of transistors incorporated in a chip will approximately double every 24 months." This predict is widely known as the Moore's law.[11] In accordance with the Moore's law, we have reached the level, at which 50 nm transistors can be mass-produced with the development of lithography techniques. Although the concept of photolithography is pretty simple, the actual implementation is very complex and expensive. Furthermore, this technique is slow and not suitable for a large-scale production by nature.

Another approach is the "bottom-up approach". This approach includes the miniaturization of materials components (up to atomic level) with further self-assembly

process leading to the formation of nanostructures.[12-14] During self-assembly, the physical forces operating at nanoscale are used to combine basic units into larger stable structures. A typical example is the quantum dot formation during epitaxial growth and formation of nanoparticles from colloidal dispersion.[15-19] Inspiration for bottom-up approaches comes from biological systems, where nature has harnessed chemical forces to create essentially all the structures needed by life.[20-22] For example, living matters synthesize proteins and lipid molecules from DNA, and autonomously build cells and organs. This process is ultimate in the bottom-up approaches. In the bottom-up approaches, we can produce the desired nano-structures by only mixing the required materials without large scale factories, complicated machines, and operations. As the component size decreases in nanofabrication, the bottom-up approaches provide an increasingly important complement to the top-down techniques. Researchers hope to replicate nature's ability to produce small clusters of specific atoms, which can be self-assembled into more-elaborate structures.

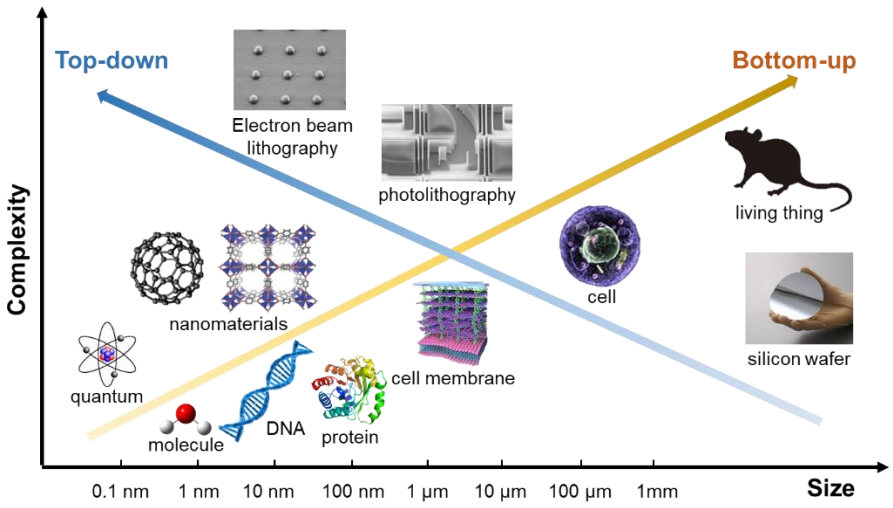

Figure 1. Limitation of the top-down nanotechnologies and potentials of the bottom-up nanotechnologies.

1-2 Supramolecular Chemistry

Supramolecular chemistry is one of the key research fields to develop the bottom-up nanotechnology. In molecular chemistry, strong association forces such as covalent and ionic bonds are used to assemble atoms into discrete molecules and hold them together. In contrast, supramolecular chemistry has been defined as a "chemistry beyond the molecule". It aims at designing and implementing functional chemical systems based on molecular components held together by weaker noncovalent intermolecular forces, such as hydrogen bonding, coordinate bonding, hydrophilic–hydrophobic interactions, and π interactions.[23-25] Supramolecular chemistry has grown into a major field over the last half century and fueled numerous developments at the interfaces in biology and physics between basic knowledge and applications.

The concept of supramolecular chemistry was proposed by Jean-Marie Lehn, who introduced the cage-shaped molecule "cryptands".[26] He was awarded the Nobel Prize in Chemistry in 1987 together with Charles J. Pedersen and Donald J. Cram. After their works, many chemists have made attentions on cavities formed by certain types of molecules. Cations, anions, or neutral molecules can enter the cavities of specifically designed compounds and are held there by the intermolecular forces. In this instance, they are called the host and guest, respectively.[27-32] Such a host–guest inclusion has relatively high stability, providing reliable and robust connection. During past a few decades, a series of host molecules and their derivatives have been developed for energy storage,[33, 34] self-healing materials,[35, 36] drug delivery,[37] and bioimaging[38, 39] (or with simple interest).

As mentioned above, the origin of supramolecular chemistry is the host-guest chemistry. At present, the research scope of supramolecular chemistry has expanded to complex structures composed of a certain number of molecules and crystal structures formed by

spontaneous assembly of large number of molecules.[40-44] Furthermore, higher order structures of biopolymers and ligand recognition of proteins *in vivo* are also studied in this field.[45, 47] As an important point, these substances and phenomena are related to molecular recognition. Broadly speaking, supramolecular chemistry is the study of intermolecular interactions. Therefore, elucidating intermolecular interactions in these various tissues, crystals, and biomolecules are significant starting points for developing the bottom-up nanotechnologies.

1-3 Intermolecular Interaction in Molecular Recognition

Typically, molecular recognition is derived from strong intermolecular interaction forces, such as hydrophobic interaction and hydrogen bonding. For example, cyclodextrins (CDs) are typical supramolecular hosts, which utilize the hydrophobic interaction. CDs are cyclic oligosaccharides, in which several molecules of D-glucose are linked by α-1,4-glycosidic bonds to form a cyclic structure. CDs are used for designing functional materials, such as *in vivo* drug, gene delivery, self-healing gels and stimuli-responsive sol-gel switching materials, because they have the ability to enhance the solubility of hydrophobic molecules in water by encapsulating hydrophobic molecules inside.[48-50] A hydrogen bonding is the most common intermolecular noncovalent interactions for molecular recognition, because the hydrogen bonding has an energy of 25 to 40 kJ/mol, and other intermolecular interactions have energies lower than 10 kJ/mol.[51, 52] The hydrogen bonding particularly plays an important role in molecular recognition in life activities, such as assembly of biological macromolecules (RNA and DNA helices), antigen-antibody reaction and chelation.[53-55]

On the other hand, weak and attractive π interactions recently have received considerable attention as a principal factor governing molecular recognition and self-assembly, as accumulated in the database on proximate arrangements in structures of supramolecular.[56-59] π interactions involve π-orbitals of any compound and are common in aromatic rings. Depending on the target of the interaction, there are various types in π interaction, such as π-π interaction, CH-π interaction, and halogen-π (X-π) interaction. These interactions are caused by induced dipole interaction, which is a very weak attraction resulting from disturbing the arrangement of electrons in the nonpolar species.[60-62] These weak intermolecular interactions are important for precise structure

control because they are highly directional dependent. For example, Qing et al. successfully synthesized uniform hexamers made of phenylacetylene molecules on an Au (111) surface and suggested that the CH-π interaction was critical for supramolecular self-assembly, dictating the number of molecules within the assembly and their relative orientation.[63] Butterfield et al reported that the π-π interaction played an important role in stabilizing monomeric α-helical structure by circular dichroism analysis of the Ala-Lys host peptides.[64] As can be observed by these and many other reports, a deep understanding and the ability to control the π interactions will greatly facilitate supramolecular chemistry.

1-4 Evaluation Method of π Interactions

Generally, it is challenging to study the π interactions especially in the presence of other molecular interactions because the π interactions are much weaker than most molecular interactions, such as the hydrophobic interaction, hydrogen bonding, and electrostatic bonding. Computer simulation methods, such as Monte Carlo and molecular dynamics, have proven to be powerful tools for studying intermolecular interactions.[61, 65-67] These calculations, however, only generate theoretical hypotheses that still need experimental verification. Also, various molecular spectroscopies, such as UV-Vis spectroscopy, fluorescence spectroscopy, and nuclear magnetic resonance spectroscopy, have been successfully applied to study strong molecular interactions, such as the hydrophobic interaction and hydrogen bonding.[68-70] However, these molecular spectroscopies often lack sufficient sensitivity to detect the weak π interactions. Therefore, a straightforward experimental method that can directly determine the π interactions are strongly required.

Liquid chromatography (LC) is a powerful separation technique that is able to distinguish the partition coefficients of solutes between the mobile and stationary phases and can sensitively reflect the strength of molecular interactions. By using LC, Kimata et al. determined the differences of the strength in the π interactions between allotropes by studying the retention behavior of fullerene allotropes in pyrenylethyl-modified columns.[71] In another study, Chen et al. evaluated the influence of metal species on the strength of the π-π interactions using a metallo protoporphyrins covalently-linked-silica surface.[72] As these studies evaluating the retention behavior in the columns, which immobilized various aromatic compounds on the stationary phases, the strength of the π interactions between these compounds and solutes can be directly elucidated.

Nano-carbon materials, *e.g.*, graphene, fullerene, corannulene (Crn) and carbon

nanotubes, have specific properties, such as a high specific surface area, physical strength, and conductivity.[73-76] Therefore, a variety of applications had been carried out for electronic materials,[77, 78] reinforced materials,[79] medicals,[80] and others.[81, 82] Furthermore, carbon-based nanomaterials have many π-electrons and show strong π interactions.[83, 84] In analytical chemistry, they are expected to fabricate a separation medium that exhibits an unprecedented strong π interaction by immobilizing the nanocarbon material onto the surface of separation substrates.[85-87] For example, Kubo et al. have succeeded in immobilizing C60-fullerene (C60) onto a surface of the silica-monolith in a capillary, which was effectively interacted with aromatic hydrocarbons.[88, 89] They evaluated the C60-coated column by LC, and then several polycyclic aromatic hydrocarbons (PAHs) were successfully separated by the effective interaction based on the π-electrons arise from C60 in the capillary. Therefore, the weak π interaction can be accurately evaluated by using a new separating media with the immobilized nanocarbon material.

1-5 Application of π Interaction in Separation Science

The π interactions can contribute to the separations of various samples, which are difficult to be achieved by the existing retention mechanisms. For example, the π-π interaction, which is the most famous and a common π interaction, is effective for the separation of aromatic compounds. Kayillo et al. reported that a phenyl group-bonded silica provided more effective separation of PAHs compared to a typical hydrophobic adsorbent, octadecylsilyl bonded silica.[90] Croes et al. compared the retention selectively in a phenyl group-bonded silica versus alkyl silica columns, and proved the importance of the π–π interaction in the phenyl stationary phase.[91] In addition, there were some reports of using the CH-π interaction and X-π interaction for the LC mechanism. For example, Turowski et al. succeeded in the separation of protiated/deuterated (H/D) isotopologue pairs with aryl groups-bonded silica-based adsorbents in reversed phase LC (RPLC).[92] In order to explain this phenomenon, they proposed a plausible model that includes specific contributions from the CH/D-π interactions. Their report provided important hints on the technology for the purification of the deuterated drugs. Furthermore, the X-π interaction is seemed to be effective in separating halogenated aromatic compounds. Gómara et al. succeeded in separating halogenated benzenes, such as poly chlorinated biphenyls and polybrominated diphenyl ethers by using pyrenylethyl-modified columns.[93] Because these solutes have been used mainly as capacitors and flame retardants, the strict usage regulations are imposed as their high toxicity and bioconcentration risk, and the separation techniques of these solutes are very important.[94, 95] Moreover, these LC columns are currently commercially available as π-based columns, because there are demands for separation media utilizing the π interaction in advanced chemistry field, in which we handling complex structural organic compounds.

1-6 Purpose and Contents of the Thesis

The π interactions play an important role in the molecular recognition processes in supramolecular chemistry and the key intermolecular interaction for the bottom-up nanotechnology. Therefore, there are pressing needs to elucidate the properties of the π interactions, such as their strength and structural dependence. Furthermore, the π interactions are suitable for separating H/D isotopologue pairs and halogenated compounds, which are difficult to be separated with the existing separation mechanisms. The aim of this thesis is twofold. The first aim is clarifying the natures of the π interactions by evaluating various nano-carbon materials-coated columns in LC and applying the π interactions to the specific separation analysis. Another aim is applying various π interactions to the specific separation analysis.

In Chapter 2, the author developed novel silica-monolithic capillary columns, which were modified with C_{70}-fullerene (C70) via a particular thermal reactive molecule, and evaluated the retention selectivity for PAHs of the columns in LC. Since C70 is an allotrope of C60 and has more π-electrons, the author expected that the C70-coated column retains PAHs more effectively. Also, C70 has not spherical as C60 but asymmetric elliptic sphere, so that the C70-coated column may show a different molecular recognition ability compared to the C60-coated column. To understand the specific intermolecular interactions of fullerenes and PAHs, the computational simulations were carried out. Also, alterations in the absorption spectra during the interaction between C70 and Crn were examined.

In Chapter 3, the author experimentally evaluated the strength of the X–π interaction

between carbon materials and a variety of halogenated benzenes using normal phase LC (NPLC). The hydrophobic interaction was completely suppressed in this technique, and thus the π interactions could be simply examined. Furthermore, the author accurately evaluated the π interactions between halogenated benzenes and C70 using ultraviolet-visible and ^{1}H NMR spectroscopy. Finally, the one-pot separation of the entirety of the brominated benzenes (11 analogues) was demonstrated by optimizing the mobile phase conditions to control the X–π interactions.

In Chapter 4, the author investigated the effect of solvents in the mobile phase and isotopologues as the solutes in LC evaluations with a variety of columns. He discussed the contribution of the intramolecular interactions to the separation of isotopologues by RPLC and evaluated the isotopologic separation based on the hydrogen bonding. Furthermore, the author examined the effect of the CH-π interaction with the C70 column to confirm the strength of the CH-π interaction and the effect of the CH-π interaction on the separation of isotopologues by NPLC.

In Chapter 5, the author evaluated the mechanism of the isotope effect by LC based on the interactions of isotopologues of aromatic molecules with polar functional groups and with π-conjugated moieties. Various analytes with a number of stationary phases and mobile phases were employed in NPLC. The author utilized a few hydrophilic stationary phases modified with polar functional groups and a C70 column. Based on the isothermal evaluations from NPLC, the dependence of enthalpy and entropy on the H/D isotope effects was estimated by the van't Hoff equations. Furthermore, the influence of the dielectric constant of the mobile phases on the H/D isotope effects was examined.

Following these experiments, the H/D separations by harnessing the complementary behaviors of the CH-π interactions with a stationary phase and OH-π interactions with a mobile phase were demonstrated.

In Chapter 6, the author developed the new Crn-coated silica monoliths for the precise understanding of the π interactions on the curved π-conjugated surface using LC. Crn is known to have the convex and concave surfaces, which is expected to lead to different molecular recognition at each surface. Toward this end, the author developed two kinds of Crn-functionalized silica monoliths, namely the Crn-ester column and Crn-PFPA (perfluorophenyl azide) columns. In the Crn-ester column, both surfaces of the Crn structure can interact with solutes. On the other hand, only concave surface of the Crn structure can interact with solutes in the Crn-PFPA column. Using these two new columns, the strength of the π interactions between Crn and several PAHs was evaluated by NPLC. To further understand the π-π interactions between the Crn structure on the stationary phase and Crn as a solute, computational simulations were carried out. In addition, ^{1}H NMR spectroscopy was employed to examine the interaction between Crn and coronene in detail and found multiple CH-π interactions between bucky bowls and planar π-conjugated surface.

1-7 References

1. Heath, J. R., Nanotechnologies for biomedical science and translational medicine. *Proc. Natl. Acad. Sci. USA* **2015,** *112*, 14436.
2. Song, W.; Anselmo, A. C.; Huang, L., Nanotechnology intervention of the microbiome for cancer therapy. *Nat. Nanotechnol.* **2019,** *14*, 1093-1103.
3. Balzani, V., Nanoscience and Nanotechnology: A Personal View of a Chemist. *Small* **2005,** *1*, 278-283.
4. Senellart, P.; Solomon, G.; White, A., High-performance semiconductor quantum-dot single-photon sources. *Nat. Nanotechnol.* **2017,** *12*, 1026-1039.
5. Hamley, I. W., Nanotechnology with Soft Materials. *Angew. Chem. Int. Ed.* **2003,** *42*, 1692-1712.
6. Sarikaya, M.; Tamerler, C.; Jen, A. K. Y.; Schulten, K.; Baneyx, F., Molecular biomimetics: nanotechnology through biology. *Nat. Mater.* **2003,** *2*, 577-585.
7. Achal, R.; Rashidi, M.; Croshaw, J.; Churchill, D.; Taucer, M.; Huff, T.; Cloutier, M.; Pitters, J.; Wolkow, R. A., Lithography for robust and editable atomic-scale silicon devices and memories. *Nat. Commun.* **2018,** *9*, 2778.
8. Ito, T.; Okazaki, S., Pushing the limits of lithography. *Nature* **2000,** *406*, 1027-1031.
9. Shim, W.; Braunschweig, A. B.; Liao, X.; Chai, J.; Lim, J. K.; Zheng, G.; Mirkin, C. A., Hard-tip, soft-spring lithography. *Nature* **2011,** *469*, 516-520.
10. Sreenivasan, S. V., Nanoimprint lithography steppers for volume fabrication of leading-edge semiconductor integrated circuits. *Microsyst. Nanoeng.* **2017,** *3*, 17075.
11. Moore, G. E., Cramming more components onto integrated circuits. *Electronics* **1965,** *38*, 114.
12. Guido, N. J.; Wang, X.; Adalsteinsson, D.; McMillen, D.; Hasty, J.; Cantor, C. R.;

Elston, T. C.; Collins, J. J., A bottom-up approach to gene regulation. *Nature* **2006,** *439*, 856-860.

13. Murugavel, R.; Walawalkar, M. G.; Dan, M.; Roesky, H. W.; Rao, C. N. R., Transformations of Molecules and Secondary Building Units to Materials: A Bottom-Up Approach. *Acc. Chem. Res.* **2004,** *37*, 763-774.
14. Villagómez, C. J.; Sasaki, T.; Tour, J. M.; Grill, L., Bottom-up Assembly of Molecular Wagons on a Surface. *J. Am. Chem. Soc.* **2010,** *132*, 16848-16854.
15. Mano, T.; Kuroda, T.; Sanguinetti, S.; Ochiai, T.; Tateno, T.; Kim, J.; Noda, T.; Kawabe, M.; Sakoda, K.; Kido, G.; Koguchi, N., Self-Assembly of Concentric Quantum Double Rings. *Nano Lett.* **2005,** *5*, 425-428.
16. Wang, D.; Rogach, A. L.; Caruso, F., Semiconductor Quantum Dot-Labeled Microsphere Bioconjugates Prepared by Stepwise Self-Assembly. *Nano Lett.* **2002,** *2*, 857-861.
17. Urban, J. J.; Talapin, D. V.; Shevchenko, E. V.; Murray, C. B., Self-Assembly of PbTe Quantum Dots into Nanocrystal Superlattices and Glassy Films. *J. Am. Chem. Soc.* **2006,** *128*, 3248-3255.
18. Zhang, J.; Li, Y.; Zhang, X.; Yang, B., Colloidal Self-Assembly Meets Nanofabrication: From Two-Dimensional Colloidal Crystals to Nanostructure Arrays. *Adv. Mater.* **2010,** *22*, 4249-4269.
19. Juárez, J. J.; Bevan, M. A., Feedback Controlled Colloidal Self-Assembly. *Adv. Funct. Mater.* **2012,** *22*, 3833-3839.
20. Dujardin, E.; Mann, S., Bio-inspired Materials Chemistry. *Adv. Mater.* **2002,** *14*, 775-788.
21. Ren, Y.; Kan, W. H.; Thangadurai, V.; Baumgartner, T., Bio-Inspired Phosphole-

Lipids: From Highly Fluorescent Organogels to Mechanically Responsive FRET. *Angew. Chem. Int. Ed.* **2012,** *51*, 3964-3968.

22. Xia, F.; Jiang, L., Bio-Inspired, Smart, Multiscale Interfacial Materials. *Adv. Mater.* **2008,** *20*, 2842-2858.
23. Amabilino, D. B.; Smith, D. K.; Steed, J. W., Supramolecular materials. *Chem. Soc. Rev.* **2017,** *46*, 2404-2420.
24. Huang, F.; Anslyn, E. V., Introduction: Supramolecular Chemistry. *Chem. Rev.* **2015,** *115*, 6999-7000.
25. Mako, T. L.; Racicot, J. M.; Levine, M., Supramolecular Luminescent Sensors. *Chem. Rev.* **2019,** *119*, 322-477.
26. Lehn, J.-M., Supramolecular Chemistry-Scope and Perspectives Molecules, Supermolecules, and Molecular Devices. *Angew. Chem. Int. Ed.* **1988,** *27*, 89-112.
27. Srivastava, S. K.; Gupta, V. K.; Jain, S., PVC-Based 2,2,2-Cryptand Sensor for Zinc Ions. *Anal. Chem.* **1996,** *68*, 1272-1275.
28. Xue, M.; Yang, Y.; Chi, X.; Zhang, Z.; Huang, F., Pillararenes, A New Class of Macrocycles for Supramolecular Chemistry. *Acc. Chem. Res.* **2012,** *45*, 1294-1308.
29. Liu, S.; Ruspic, C.; Mukhopadhyay, P.; Chakrabarti, S.; Zavalij, P. Y.; Isaacs, L., The Cucurbit[n]uril Family: Prime Components for Self-Sorting Systems. *J. Am. Chem. Soc.* **2005,** *127*, 15959-15967.
30. Alberto, R.; Ortner, K.; Wheatley, N.; Schibli, R.; Schubiger, A. P., Synthesis and Properties of Boranocarbonate: A Convenient in Situ CO Source for the Aqueous Preparation of [99mTc(OH2)3(CO)3]+. *J. Am. Chem. Soc.* **2001,** *123*, 3135-3136.
31. Pedersen, C. J., Cyclic polyethers and their complexes with metal salts. *J. Am. Chem. Soc.* **1967,** *89*, 7017-7036.

32. Szejtli, J., Introduction and General Overview of Cyclodextrin Chemistry. *Chem. Rev.* **1998,** *98*, 1743-1754.

33. Cui, X.; Chen, K.; Xing, H.; Yang, Q.; Krishna, R.; Bao, Z.; Wu, H.; Zhou, W.; Dong, X.; Han, Y.; Li, B.; Ren, Q.; Zaworotko, M. J.; Chen, B., Pore chemistry and size control in hybrid porous materials for acetylene capture from ethylene. *Science* **2016,** *353*, 141.

34. Peng, H.-J.; Hou, T.-Z.; Zhang, Q.; Huang, J.-Q.; Cheng, X.-B.; Guo, M.-Q.; Yuan, Z.; He, L.-Y.; Wei, F., Strongly Coupled Interfaces between a Heterogeneous Carbon Host and a Sulfur-Containing Guest for Highly Stable Lithium-Sulfur Batteries: Mechanistic Insight into Capacity Degradation. *Adv. Mater. Interfaces* **2014,** *1*, 1400227.

35. Kakuta, T.; Takashima, Y.; Nakahata, M.; Otsubo, M.; Yamaguchi, H.; Harada, A., Preorganized Hydrogel: Self-Healing Properties of Supramolecular Hydrogels Formed by Polymerization of Host–Guest-Monomers that Contain Cyclodextrins and Hydrophobic Guest Groups. *Adv. Mater.* **2013,** *25*, 2849-2853.

36. Appel, E. A.; del Barrio, J.; Loh, X. J.; Scherman, O. A., Supramolecular polymeric hydrogels. *Chem. Soc. Rev.* **2012,** *41*, 6195-6214.

37. Douglas, T.; Young, M., Host–guest encapsulation of materials by assembled virus protein cages. *Nature* **1998,** *393*, 152-155.

38. Zhang, J.; Ma, P. X., Host–guest interactions mediated nano-assemblies using cyclodextrin-containing hydrophilic polymers and their biomedical applications. *Nano Today* **2010,** *5*, 337-350.

39. Mohandoss, S.; Sivakamavalli, J.; Vaseeharan, B.; Stalin, T., Host-guest molecular recognition based fluorescence On-Off-On chemosensor for nanomolar level

detection of Cu2+ and Cr2O72− ions: Application in XNOR logic gate and human lung cancer living cell imaging. *Sens. Actuator B-Chem.* **2016,** *234*, 300-315.

40. Zheng, Y.-R.; Zhao, Z.; Wang, M.; Ghosh, K.; Pollock, J. B.; Cook, T. R.; Stang, P. J., A Facile Approach toward Multicomponent Supramolecular Structures: Selective Self-Assembly via Charge Separation. *J. Am. Chem. Soc.* **2010,** *132*, 16873-16882.
41. Kühne, D.; Klappenberger, F.; Krenner, W.; Klyatskaya, S.; Ruben, M.; Barth, J. V., Rotational and constitutional dynamics of caged supramolecules. *Proc. Natl. Acad. Sci. USA* **2010,** *107*, 21332.
42. Tanaka, H.; Ikeda, T.; Takeuchi, M.; Sada, K.; Shinkai, S.; Kawai, T., Molecular Rotation in Self-Assembled Multidecker Porphyrin Complexes. *ACS Nano* **2011,** *5*, 9575-9582.
43. Eddaoudi, M.; Kim, J.; Rosi, N.; Vodak, D.; Wachter, J.; Keeffe, M.; Yaghi, O. M., Systematic Design of Pore Size and Functionality in Isoreticular MOFs and Their Application in Methane Storage. *Science* **2002,** *295*, 469.
44. Lee, J.; Farha, O. K.; Roberts, J.; Scheidt, K. A.; Nguyen, S. T.; Hupp, J. T., Metal–organic framework materials as catalysts. *Chem. Soc. Rev.* **2009,** *38*, 1450-1459.
45. Buck, L.; Axel, R., A novel multigene family may encode odorant receptors: A molecular basis for odor recognition. *Cell* **1991,** *65*, 175-187.
46. Heil, F.; Hemmi, H.; Hochrein, H.; Ampenberger, F.; Kirschning, C.; Akira, S.; Lipford, G.; Wagner, H.; Bauer, S., Species-Specific Recognition of Single-Stranded RNA via Toll-like Receptor 7 and 8. *Science* **2004,** *303*, 1526.
47. Nelson, J. C.; Saven, J. G.; Moore, J. S.; Wolynes, P. G., Solvophobically Driven Folding of Nonbiological Oligomers. *Science* **1997,** *277*, 1793.
48. Hu, Q.-D.; Tang, G.-P.; Chu, P. K., Cyclodextrin-Based Host–Guest Supramolecular

Nanoparticles for Delivery: From Design to Applications. *Acc. Chem. Res.* **2014,** *47*, 2017-2025.

49. Simões, S. M. N.; Rey-Rico, A.; Concheiro, A.; Alvarez-Lorenzo, C., Supramolecular cyclodextrin-based drug nanocarriers. *Chem. Commun.* **2015,** *51*, 6275-6289.
50. Harada, A.; Takashima, Y.; Nakahata, M., Supramolecular Polymeric Materials via Cyclodextrin–Guest Interactions. *Acc. Chem. Res.* **2014,** *47*, 2128-2140.
51. Wendler, K.; Thar, J.; Zahn, S.; Kirchner, B., Estimating the Hydrogen Bond Energy. *J. Phys. Chem. A* **2010,** *114*, 9529-9536.
52. Zhao, Y.; Truhlar, D. G., Density Functionals for Noncovalent Interaction Energies of Biological Importance. *J. Chem. Theory Comput.* **2007,** *3*, 289-300.
53. Johnson, E. R.; Keinan, S.; Mori-Sánchez, P.; Contreras-García, J.; Cohen, A. J.; Yang, W., Revealing Noncovalent Interactions. *J. Am. Chem. Soc.* **2010,** *132*, 6498-6506.
54. Reinmuth, M.; Pramanik, S.; Douglas, J. T.; Day, V. W.; Bowman-James, K., Structural Impact of Chelation on Phytate, a Highly Phosphorylated Biomolecule. *Eur. J. Inorg. Chem.* **2019,** *2019*, 1870-1874.
55. Jia, C.; Wang, Q.-Q.; Begum, R. A.; Day, V. W.; Bowman-James, K., Chelate effects in sulfate binding by amide/urea-based ligands. *Org. Biomol. Chem.* **2015,** *13*, 6953-6957.
56. Zang, L.; Che, Y.; Moore, J. S., One-Dimensional Self-Assembly of Planar π-Conjugated Molecules: Adaptable Building Blocks for Organic Nanodevices. *Acc. Chem. Res.* **2008,** *41*, 1596-1608.
57. Schenning, A. P. H. J.; Meijer, E. W., Supramolecular electronics; nanowires from

self-assembled π-conjugated systems. *Chem. Commun.* **2005,** *26*, 3245-3258.

58. Metrangolo, P.; Resnati, G., Halogen Bonding: A Paradigm in Supramolecular Chemistry. *Chem.: Eur. J.* **2001,** *7*, 2511-2519.
59. Gibson, H. W.; Yamaguchi, N.; Hamilton, L.; Jones, J. W., Cooperative Self-Assembly of Dendrimers via Pseudorotaxane Formation from a Homotritopic Guest Molecule and Complementary Monotopic Host Dendrons. *J. Am. Chem. Soc.* **2002,** *124*, 4653-4665.
60. Wheeler, S. E., Understanding Substituent Effects in Noncovalent Interactions Involving Aromatic Rings. *Acc. Chem. Res.* **2013,** *46*, 1029-1038.
61. Tsuzuki, S.; Honda, K.; Uchimaru, T.; Mikami, M.; Tanabe, K., The Magnitude of the CH/π Interaction between Benzene and Some Model Hydrocarbons. *J. Am. Chem. Soc.* **2000,** *122*, 3746-3753.
62. Riley, K. E.; Hobza, P., On the Importance and Origin of Aromatic Interactions in Chemistry and Biodisciplines. *Acc. Chem. Res.* **2013,** *46*, 927-936.
63. Li, Q.; Han, C.; Horton, S. R.; Fuentes-Cabrera, M.; Sumpter, B. G.; Lu, W.; Bernholc, J.; Maksymovych, P.; Pan, M., Supramolecular Self-Assembly of π-Conjugated Hydrocarbons via 2D Cooperative CH/π Interaction. *ACS Nano* **2012,** *6*, 566-572.
64. Butterfield, S. M.; Patel, P. R.; Waters, M. L., Contribution of Aromatic Interactions to α-Helix Stability. *J. Am. Chem. Soc.* **2002,** *124*, 9751-9755.
65. Wells, R. A.; Kellie, J. L.; Wetmore, S. D., Significant Strength of Charged DNA–Protein π–π Interactions: A Preliminary Study of Cytosine. *J. Phys. Chem. B* **2013,** *117*, 10462-10474.
66. Huber, R. G.; Margreiter, M. A.; Fuchs, J. E.; von Grafenstein, S.; Tautermann, C. S.; Liedl, K. R.; Fox, T., Heteroaromatic π-Stacking Energy Landscapes. *J. Chem. Inf.*

Model. **2014,** *54*, 1371-1379.

67. Senthilkumar, K.; Grozema, F. C.; Bickelhaupt, F. M.; Siebbeles, L. D. A., Charge transport in columnar stacked triphenylenes: Effects of conformational fluctuations on charge transfer integrals and site energies. *J. Chem. Phys.* **2003,** *119*, 9809-9817.
68. He, A.; Kang, X.; Xu, Y.; Noda, I.; Ozaki, Y.; Wu, J., Investigation on intermolecular interaction between berberine and β-cyclodextrin by 2D UV–Vis asynchronous spectra. *Spectrochim. Acta A* **2017,** *185*, 343-348.
69. Kohn, S. C.; Dupree, R.; Smith, M. E., Proton environments and hydrogen-bonding in hydrous silicate glasses from proton NMR. *Nature* **1989,** *337*, 539-541.
70. Del Bene, J. E.; Perera, S. A.; Bartlett, R. J., Hydrogen Bond Types, Binding Energies, and 1H NMR Chemical Shifts. *J. Phys. Chem. A* **1999,** *103*, 8121-8124.
71. Kimata, K.; Hosoya, K.; Araki, T.; Tanaka, N., [2-(1-Pyrenyl)ethyl]silyl silica packing material for liquid chromatographic separation of fullerenes. *J. Org. Chem.* **1993,** *58* (1), 282-283.
72. Chen, S.; Meyerhoff, M., Shape-Selective Retention of Polycyclic Aromatic Hydrocarbons on Metalloprotoporphyrin−Silica Phases: Effect of Metal Ion Center and Porphyrin Coverage. *Anal. Chem.* **1998,** *70*, 2523-2529.
73. Krätschmer, W.; Lamb, L. D.; Fostiropoulos, K.; Huffman, D. R., Solid C60: a new form of carbon. *Nature* **1990,** *347*, 354-358.
74. Iijima, S., Helical microtubules of graphitic carbon. *Nature* **1991,** *354*, 56-58.
75. Geim, A. K.; Novoselov, K. S., The rise of graphene. *Nat. Mater.* **2007,** *6*, 183-191.
76. Nestoros, E.; Stuparu, M. C., Corannulene: a molecular bowl of carbon with multifaceted properties and diverse applications. *Chem. Commun.* **2018,** *54*, 6503-6519.

77. Tans, S. J.; Verschueren, A. R. M.; Dekker, C., Room-temperature transistor based on a single carbon nanotube. *Nature* **1998,** *393*, 49-52.

78. de Heer, W. A.; Châtelain, A.; Ugarte, D., A Carbon Nanotube Field-Emission Electron Source. *Science* **1995,** *270*, 1179.

79. Popov, M.; Kyotani, M.; Nemanich, R. J.; Koga, Y., Superhard phase composed of single-wall carbon nanotubes. *Phys. Rev. B* **2002,** *65*, 033408.

80. Kam, N. W. S.; Connell, M.; Wisdom, J. A.; Dai, H., Carbon nanotubes as multifunctional biological transporters and near-infrared agents for selective cancer cell destruction. *Proc. Natl. Acad. Sci. USA* **2005,** *102*, 11600.

81. Wang, X.; Tao, S.; Xing, B., Sorption and Competition of Aromatic Compounds and Humic Acid on Multiwalled Carbon Nanotubes. *Environ. Sci. Technol.* **2009,** *43*, 6214-6219.

82. Velzeboer, I.; Kwadijk, C. J. A. F.; Koelmans, A. A., Strong Sorption of PCBs to Nanoplastics, Microplastics, Carbon Nanotubes, and Fullerenes. *Environ. Sci. Technol.* **2014,** *48*, 4869-4876.

83. Kar, T.; Bettinger, H. F.; Scheiner, S.; Roy, A. K., Noncovalent π−π Stacking and CH-π Interactions of Aromatics on the Surface of Single-Wall Carbon Nanotubes: An MP2 Study. *J. Phys. Chem. C* **2008,** *112*, 20070-20075.

84. Zhang, Z.; Huang, H.; Yang, X.; Zang, L., Tailoring Electronic Properties of Graphene by π–π Stacking with Aromatic Molecules. *J. Phys. Chem. Lett.* **2011,** *2*, 2897-2905.

85. Scida, K.; Stege, P. W.; Haby, G.; Messina, G. A.; García, C. D., Recent applications of carbon-based nanomaterials in analytical chemistry: Critical review. *Anal. Chim. Acta* **2011,** *691*, 6-17.

86. Valcárcel, M.; Cárdenas, S.; Simonet, B. M., Role of Carbon Nanotubes in Analytical Science. *Anal. Chem.* **2007,** *79*, 4788-4797.

87. Sitko, R.; Zawisza, B.; Malicka, E., Graphene as a new sorbent in analytical chemistry. *Trends Anal. Chem..* **2013,** *51*, 33-43.

88. Kubo, T.; Murakami, Y.; Tominaga, Y.; Naito, T.; Sueyoshi, K.; Yan, M.; Otsuka, K., Development of a C_{60}-fullerene bonded open-tubular capillary using a photo/thermal active agent for liquid chromatographic separations by π–π interactions. *J. Chromatogr. A* **2014,** *1323*, 174-178.

89. Kubo, T.; Murakami, Y.; Tsuzuki, M.; Kobayashi, H.; Naito, T.; Sano, T.; Yan, M.; Otsuka, K., Unique Separation Behavior of a C60 Fullerene-Bonded Silica Monolith Prepared by an Effective Thermal Coupling Agent. *Chem.: Eur. J.* **2015,** *21*, 18095-18098.

90. Kayillo, S.; Dennis, G. R.; Shalliker, R. A., An assessment of the retention behaviour of polycyclic aromatic hydrocarbons on reversed phase stationary phases: Selectivity and retention on C18 and phenyl-type surfaces. *J. Chromatogr. A* **2006,** *1126*, 283-297.

91. Croes, K.; Steffens, A.; Marchand, D. H.; Snyder, L. R., Relevance of π–π and dipole–dipole interactions for retention on cyano and phenyl columns in reversed-phase liquid chromatography. *J. Chromatogr. A* **2005,** *1098*, 123-130.

92. Turowski, M.; Yamakawa, N.; Meller, J.; Kimata, K.; Ikegami, T.; Hosoya, K.; Tanaka, N.; Thornton, E. R., Deuterium Isotope Effects on Hydrophobic Interactions: The Importance of Dispersion Interactions in the Hydrophobic Phase. *J. Am. Chem. Soc.* **2003,** *125*, 13836-13849.

93. Gómara, B.; García-Ruiz, C.; González, M. J.; Marina, M. L., Fractionation of

chlorinated and brominated persistent organic pollutants in several food samples by pyrenyl-silica liquid chromatography prior to GC–MS determination. *Anal. Chim. Acta* **2006,** *565*, 208-213.

94. Mullins, M. D.; Pochini, C. M.; McCrindle, S.; Romkes, M.; Safe, S. H.; Safe, L. M., High-resolution PCB analysis: synthesis and chromatographic properties of all 209 PCB congeners. *Environ. Sci. Technol.* **1984,** *18*, 468-476.
95. Hites, R. A., Polybrominated Diphenyl Ethers in the Environment and in People: A Meta-Analysis of Concentrations. *Environ. Sci. Technol.* **2004,** *38*, 945-956.

Chapter 2

Specific Intermolecular Interactions by the Localized π-Electrons in C_{70}-fullerene

2-1 Introduction

Based on the unique properties, such as high specific surface area, physical strength, and conductivity,[1-3] nano-carbon materials have been widely applied for a variety of fields, including electronic materials, reinforced materials, medicines, and so on.[4-8] Additionally, most of the nano carbon materials show a specific π-stacking property based on their huge π-conjugated surface. Therefore, the possibility of separating aromatic compounds by nano carbon materials is expected.[9-13] Generally, the π-π interaction, by which a pair of aromatic rings is stabilized as an overlapping shape, is caused mainly by the London dispersion.[14] The polarizability of certain molecules provides the London dispersion since the induced dipole interaction works among the dipole moments of the molecules generated by the momentary electronic fluctuation.[15-17] Aromatic compounds with larger π-conjugation surface provide higher polarity, in fact a simulation was reported that the strength of the π-π interaction between benzene and polycyclic aromatic hydrocarbon (PAH) in vacuum depended on the number of carbon atoms in PAHs.[14]

As previous studies, PAHs can be easily separated by the column modified with aromatic moiety in liquid chromatography (LC),[18] especially Kimata et al. reported the effective separation of PAHs and fullerenes by the column modified with pyrene.[19] These reports suggested the utility of the π-π interaction for separations of complicated aromatic

mixtures.[20-22] Here, the nano-carbon materials are expected as new separation media for PAHs. However, we have to overcome the issues of both low solubility and poor reactivity of nano-carbon materials to realize new separation media. Although some researchers reported the usefulness of nano-carbon materials as the separation media, complicated reaction processes and unexpected interactions based on introduced functional groups should be eliminated. Recently, we have reported a C60-fullerene (C60) bonded silica-monolithic column via a thermal reactive compound, perfluorophenyl azide (PFPA), which is effectively reacted with nano-carbon materials generating a covalent bonding.[23-27] The C60 bonded column allowed the effective separation of PAHs even in a normal phase mode with *n*-hexane as a mobile phase by the strong π-π interaction.[28-30] Also, an unique retention behavior was revealed[30], in which a hemispherical molecule, corannulene (Crn),[31-36] was selectively retained on the column by the spherical recognition due to C60.

In this study, we report the development of another column with C70-fullerene (C70) for further understanding of the intermolecular interaction by fullerenes. As well known, C70 has a spherical surface and more electrons compared to C60,[37-41] therefore we expected that the different molecular retention ability could be obtained. We prepared a C70 bonded silica-monolithic column in a capillary and evaluated in LC. To understand the specific intermolecular interaction of fullerenes and PAHs, the computational simulations were carried out. Also, alterations in the absorption spectra during the interaction between C70 and Crn were examined. This is the first report regarding the evaluation of such a specific interaction ability of C70.

2-2 Experimental Section

2-2-1 Materials

Chlorobenzene, ethyl acetate, *n*-hexane, methanol, toluene, dichloromethane, acetone, diethylether, magnesium sulfate, sodium hydroxide, and chloroform were purchased from Nacalai Tesque (Kyoto, Japan), methyl pentafluorobenzoate, polycyclic aromatic hydrocarbons (PAHs), alkylbenzenes, diethyl amine, urea, acetic acid, and tetramethyl orthosilicate (TMOS) from Tokyo Chemical Industry (Tokyo, Japan), sodium azide, *N*-hydroxysuccinimide (NHS), and 1-ethyl-3-(3-dimethylaminopropyl)carbodiimide (EDAC) from Wako Pure Chemical Industries (Osaka, Japan), 3-aminopropyltrimethoxysilane (APTMS), polyethylene glycol (PEG) (Mn=10,000), C_{60}-fullerene, and C_{70}-fullerene from Sigma-Aldrich Japan (Tokyo, Japan), respectively. Deionized water was obtained from a Milli-Q Direct-Q 3UV system (Merck Millipore, Tokyo, Japan). A COSMOSIL PYE® was purchased from Nacalai Tesque, and a fused-silica capillary from Polymicro Technologies Inc. (Phoenix, AZ).

2-2-2 Instruments

A capillary liquid chromatographic system consisted of a DiNa S (KYA Technologies Co., Tokyo, Japan) as a pump, CE-2070 (JASCO, Tokyo, Japan) as a UV detector, CHEMINERT (Valco Instruments Co., Huston, TX) as a sample injector, and Chemco capillary column conditioner Model 380-b (Chemco Co. Osaka, Japan) as a column oven. An HPLC system consisted of a Prominence series (Shimadzu Co., Kyoto, Japan). FT-IR, NMR, elemental analysis, and fast atom bombardment mass spectrometry (FABMS) were carried out by a Nicolet iS5 ATR (Thermo Fisher Scientific K. K., Yokohama, Japan), JNM-ECA500 spectrometer (JEOL, Tokyo, Japan), Flash EA1112 (Thermo

Fisher Scientific K. K.), and JMS-700 (JEOL), respectively.

2-2-3 Synthesis of PFPA conjugated C_{70}-fullerene

4-azido-2,3,5,6-tetrafluorophenyl succinate (PFPA-NHS)

Methyl pentafluorobenzoate (MPFB, 18.3 mmol) and sodium azide (20 mmol) was dissolved in water/acetone = 5/12 (v/v), and the mixture was stirred at 120 °C for 20 h under N_2 atmosphere. After extraction with diethyl ether and dried over sodium sulfate, the solvent was evaporated to give PFPA-CO_2CH_3. Then, the residue was dissolved in methanol/10% NaOH aq. = 4/1 (v/v), and the mixture was stirred at room temperature for 30 min. After neutralization with 6 M HCl to pH ~1, the solution was extracted with chloroform, the organic layer was dried over sodium sulfate, and the solvent was removed. The product (PFPA-CO_2H, 17.4 mmol) was dissolved in dichloromethane with EDAC (17.2 mmol) and NHS (17.2 mmol), and the mixture was stirred at room temperature for 16 h under N_2 atmosphere. The mixture was washed with water to remove unreacted EDAC and NHS. The chloroform layer was dried over sodium sulfate and the solvent was removed. Finally, 4-azido-2,3,5,6-tetrafluorophenyl succinate (PFPA-NHS) was obtained after purification by silica-gel column chromatography with dichloromethane as the eluent.

PFPA-NHS conjugated C_{70}-fullerene

C_{70}-fullerene (C70) of 0.12 mmol and PFPA-NHS of 0.24 mmol were dispersed into chlorobenzene. The mixture was reacted at 108 ºC in an oil bath for 120 h under N_2 atmosphere. After removal of the solvent, the residue was purified by silica-gel column chromatography using toluene/ethyl acetate =10/1 (v/v) as a solvent to remove excess of

unreacted compounds. Then, the products were dissolved in small amount of toluene and add excess of *n*-hexane for precipitation of a product. The precipitation was washed with *n*-hexane and methanol. Finally, the objective product (C70-NHS-PFPA) was isolated and characterizations were carried out by FT-IR, FABMS and elemental analysis.

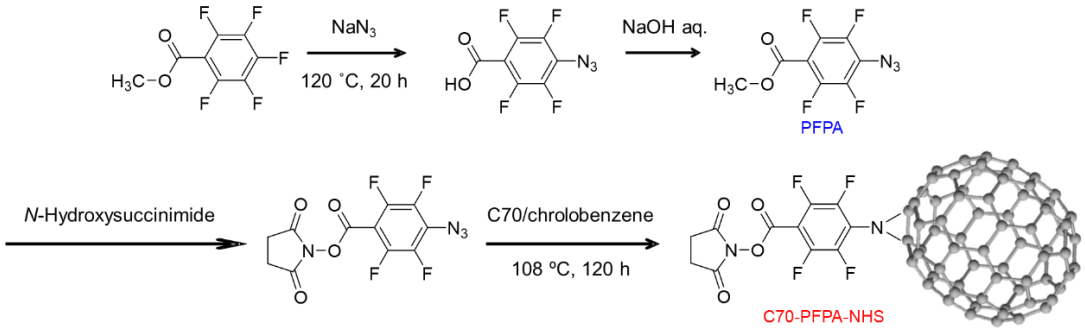

Scheme 1. Synthesis of C70-PFPA-NHS.

2-2-4 Preparation of C70 column

Preparation of silica-monolithic capillary

A fused-silica capillary (2-3 m in length) was treated with a 1.0 M aqueous sodium hydroxide solution at 40 °C for 3 h. Then, the capillary was washed with water and acetone, and dried. TMOS (56 mL) was added to a solution of PEG (11.9 g) and urea (9.0 g) in 0.01 M acetic acid (100 mL), and the mixture stirred at 0 °C for 30 min. The resulting homogeneous solution was charged into the fused-silica capillary and remained at 30 °C overnight. The resulting monolithic silica column was treated for 3 h at 120 °C to form mesopores with ammonia generated by the hydrolysis of urea, followed by water and methanol washes. After drying, a heat treatment was carried out at 330 °C for 25 h, resulting in the decomposition of the organic moieties in the capillary.

Surface modification of the silica monolith with C70-PFPA-NHS

The silica-monolithic capillary was treated with 1.0 M aqueous sodium hydroxide at 40 ºC for 3 h. After washing with water and methanol, APTMS in methanol (10%, v/v) was passed through the silica-monolithic capillary for 24 h and washed with methanol (NH2-monolith). C70-PFPA-NHS in toluene (3.0 mg mL^{-1}) was charged into the NH2-monolith for 24 h at room temperature, and washed with toluene and methanol. To evaluate by elemental analysis, the bulk type silica monolith was also prepared with the same compositions as the capillary. The bulk monolith was crashed and similar surface modification was also carried out with C70-PFPA-NHS.

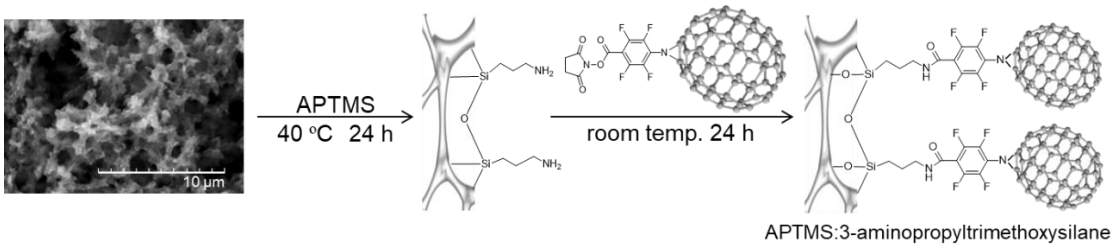

Scheme 2. Preparation of C70 bonded silica monolithic capillary.

2-2-5 Computational methods

To obtain the initial 3D molecular coordinates of NHS-PFPA-fullerenes, Chem3D version 7.0 was used. *Ab initio* calculations using Gaussian 03 were performed on a Linux Cluster. All geometrical optimizations were carried out by using the RB3LYP/3- 21G basis set. Calculations of charges based on Merz-Singh-Kollman were carried out by using the B3LYP/3-21G basis set, which can be applied to large molecules. This method required no significant calculation time. During *ab initio* calculations, all internal coordinates were optimized by means of the Berny algorithm, and convergence was tested against criteria for the maximum force component, root-mean-square force, maximum displacement component, and root-mean-square displacement.

2-3 Results and Discussion

2-3-1 Characterizations of PFPA derivatives and the modified silica monoliths

Since effective protons are not existing in each PFPA derivative and PFPA-NHS conjugated C70, ^{1}H-NMR was not suitable for the qualitative analysis. Therefore, the FT-IR spectra of each derivative described in Scheme 1 are summarized in Figure 1. Specific absorbance based on an azide group was obviously confirmed around 2200 cm^{-1} in each derivative containing the PFPA moiety. Additionally, the peak shifts caused by the difference of carbonyl groups among PFPA-CO_2H, PFPA-NHS and C70-PFPA-NHS were also confirmed around 1600 to 1700 cm^{-1}. Results of FABMAS and elemental analysis of the final product (C70-PFPA-NHS) were summarized in Figure 2, and Table 1, respectively. According to these spectroscopic data and elemental analysis, C70-PFPA-NHS was well identified.

Additionally, to improve the reaction efficiency, the microwave reaction was also employed. C70 of 20 mg (0.03 mmol) and PFPA-NHS of 15.6 mg (0.047 mmol) were dissolved in chlorobenzene (8 mL), and then the mixture was treated at 130 ºC for 2 h by microwave (2.45 GHz). As comparison between a typical thermal reaction in an oil bath and a microwave reaction, the yield against C70 were 18.2% and 24.5%, respectively. Although the reaction time by the microwave was significantly shorter than that of the oil bath, the yield was much higher.

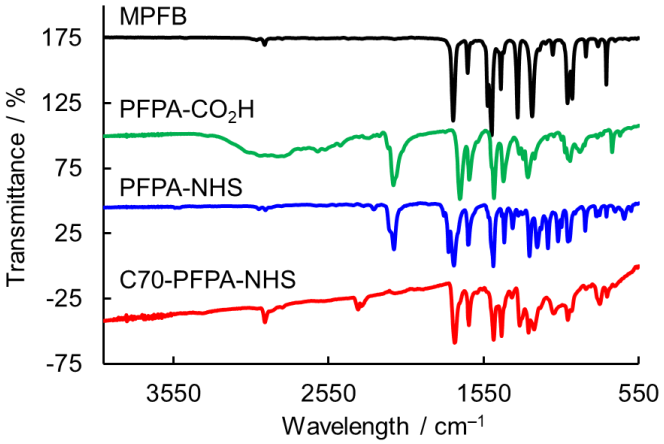

Figure 1. FT-IR spectra of each compounds.

Table 1. Elemental analysis of C70-PFPA-NHS.

	C/%	H/%	N/%
Theoretical	84.9	0.35	2.45
Results	84.1	0.91	2.44

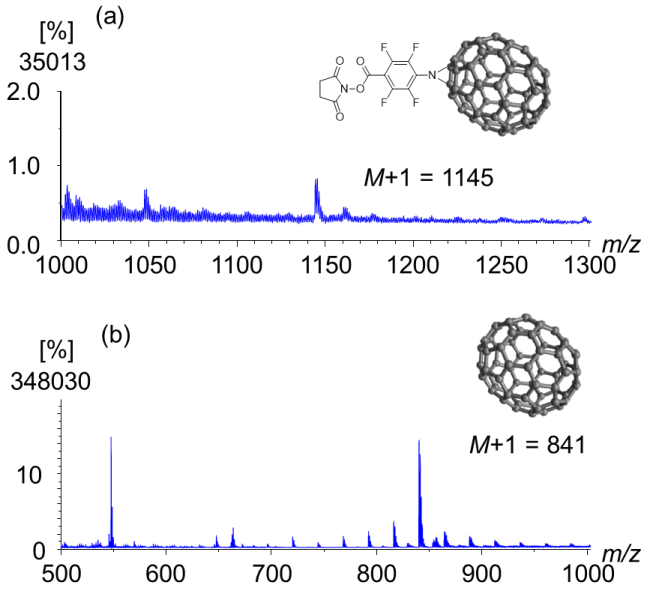

Figure 2. FABMS spectra of C70-PFPA-NHS. The spectrum was obtained by using 4-nitrobenzylalcohol as a matrix. (a) 1000 to 1300, (b) 500 to 1000 m/z.

2-3-2 Modification of silica-monoliths with C70

To estimate the immobilized C70, bulk type monoliths were also treated with the same conditions and evaluated by an elemental analysis. As shown in Table 2, the densities of C60 and C70 onto the silica monolith were estimated as 0.83 and 0.44 mmol mg^{-1}, respectively. The lower density of C70 (almost the half of C60) might be caused by the steric hindrance of a larger molecular size of C70.

Furthermore, to confirm the immobilization of C70, the prepared capillaries were evaluated with a typical reversed phase mode in LC. Figure 3 showed the relation between the logarithms of the retention factor, k (k=(t_R–t_0)/t_0; t_R, retention time of a solute; t_0, elution time of non-retained solute (acetone)) toward the water/octanol partition coefficient (Log $P_{O/W}$) of alkylbenzenes in the capillary columns. The results also supported the immobilization of C70 because the logarithms of the retention factor of alkylbenzenes increased along with Log $P_{O/W}$. On the other hand, although the immobilization density of the C70 bonded monolith was lower than that of the C60, the absolute retentions obtained in both columns were similar. Additionally, the slope, which is depended on the hydrophobicity, of the C60 bonded monolith was higher than the C70. These results suggest that alkylbenzenes were retained in the monoliths by both the π-π interaction and hydrophobicity. In brief, we predicted that the relative strength of the π-π interaction was higher in C70, whereas the hydrophobic interaction was more dominate in C60 in a reversed phase mode.

Table 2. Elemental analysis of the prepared monolith.

	C/%	H/%	N/%	Density (μmol mg^{-1})
Silica-monolith	2.07	0.57	0.04	2.45
NH_2-modified	6.42	1.41	1.27	2.44
C60 monolith	23.9	1.08	1.14	0.83
C70 monolith	18.1	1.17	1.15	0.44

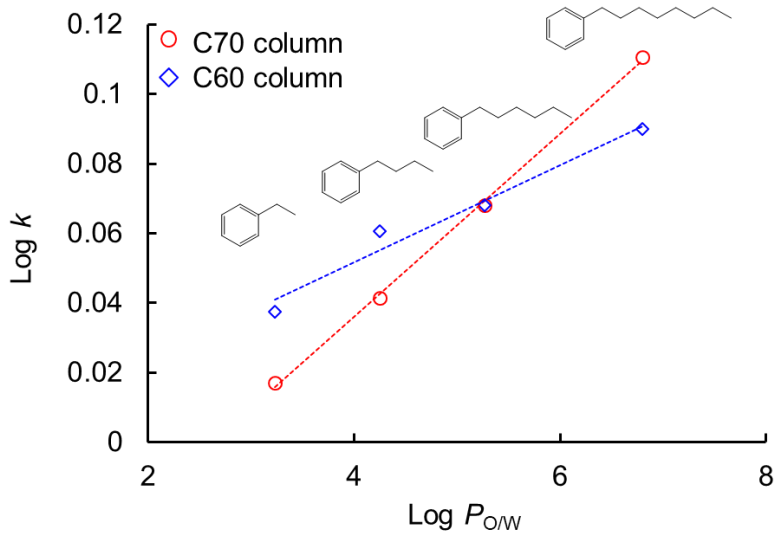

Figure 3. Log *k* vs. log $P_{o/w}$ in each column with alkylbenzenes. LC conditions: columns, C60 column (19.6 cm × 100 μm i.d.), C70 column (15.4 cm × 100 μm i.d.); mobile phase, water/methanol = 1/9; samples, 72 mM ethylbenzene, 60 mM butylbenzene, 50 mM hexylbenzene, 42 mM octylbenzene; UV absorption (254 nm).

2-3-3 Retention behaviors of PAHs with different π electron numbers

To clarify the hypothesis, which the higher π-stacking worked in C70 than C60, the monoliths were evaluated with a normal phase mode in LC. Under the condition with *n*-hexane as a mobile phase, the hydrophobic interaction can be completely neglected and the dipole interactions, such as the electrostatic interaction and hydrogen bonding, are dominant. When nonpolar molecules like alkylbenzenes and PAHs are employed as solutes in the condition, simplified interactions based on aromatic moieties may be examined. In fact, all the alkylbenzenes were not retained completely in both the C60 and C70 bonded monoliths with the *n*-hexane mobile phase. Then, a variety of PAHs were evaluated by using the C60 and C70 bonded monoliths. For a comparison, a commercially available LC column for the effective π-π interaction, PYE® (Nacalai Tesque, Kyoto, Japan), in which the spherical silica particles modified with pyrene groups are packed, was employed under the same LC conditions. The typical chromatograms obtained by a normal phase mode of PAHs, including phenanthrene, pyrene, chrysene, triphenylene, benzo[a]pyrene, and Crn, are shown in Figure 4.

As unexpected, all the PAHs were barely retained in the PYE column. On the other hand, the retentions of PAHs in both the fullerene columns were much higher than in the PYE. As shown in these chromatograms, hemispherical Crn was significantly retained compared to other PAHs. In our previous study, Kubo, T. et al. concluded that the specific retention of Crn on C60 was just caused by the special recognition of a buckyball structure of C60.[30] Interestingly, the retention of Crn was much higher in C70 even though the immobilized density of C70 was half of that of C60 as mentioned above. In these evaluations, the length of each capillary was the same to avoid the effects in length, so

that an extra interaction other than the spherical recognition should be worked in these retention behaviors.

To confirm the retention selectivity in the C70 bonded monolith, the retention factor for each PAH is plotted against the number of π electrons of each PAH. As shown in Figure 5 (a), in the PYE column a linear relation was observed in spite of low retention for all the PAHs. Similarly, as shown in Figure 2 (b), the retention of most PAHs increased as higher π electrons in the fullerene bonded monoliths except for Crn. In both the C60 and C70 bonded monoliths, Crn was significantly retained independently of the number of π electrons. Here, as mentioned above, the estimated density of the immobilized fullerene was different in each other. Therefore, the corrected retention factors were calculated with considering each density. As a result, the retention of Crn in C70 was estimated as almost thrice as that of C60 (see Figure 6). According to these results obtained from the LC evaluations, we assumed that the significant retention of Crn in C70 was caused by not only the spherical structural recognition but also the states of the partial electron density in each molecule.

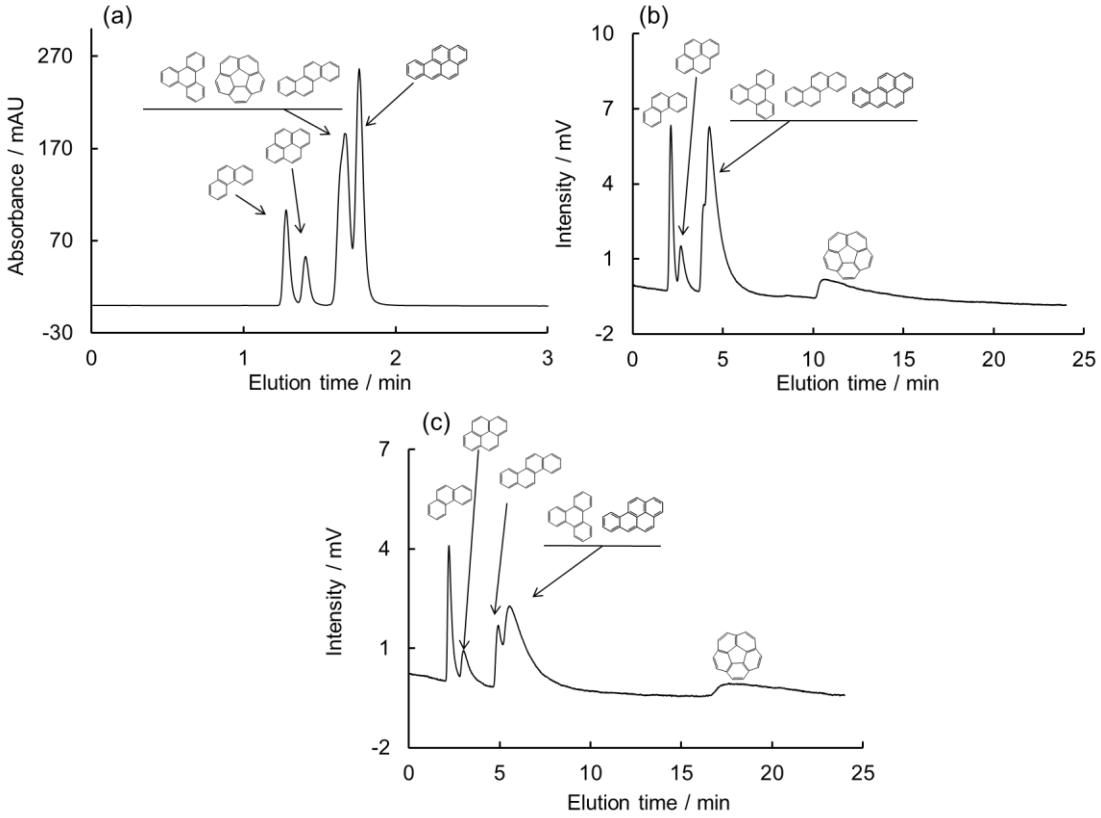

Figure 4. Chromatograms of PAHs with *n*-hexane as a mobile phase.
Conditions: column, (a) PYE® (Nacalai Tesque, 150 mm × 4.6 mm i.d.), (b) C60 column (12.1 cm × 100 mm i.d.), (c) C70 column (12.1 cm × 100 mm i.d.); flow rate, (a) 2.0 mL min^{-1}, (b)(c) 2.0 mL min^{-1}; detection, UV 254 nm.

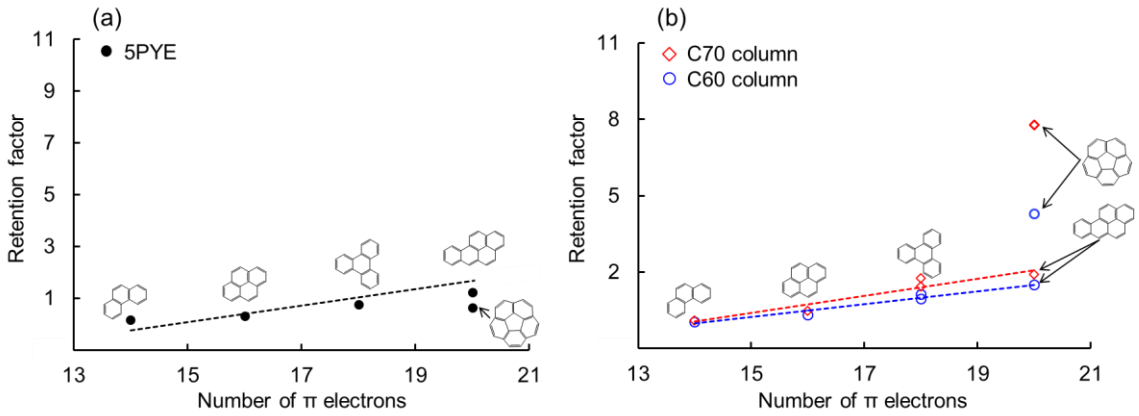

Figure 5. Relations between the retention factors and the number of π electrons in PAHs. (a) PYE column, (b) C60 and C70 monoliths. LC conditions were the same as Figure 4.

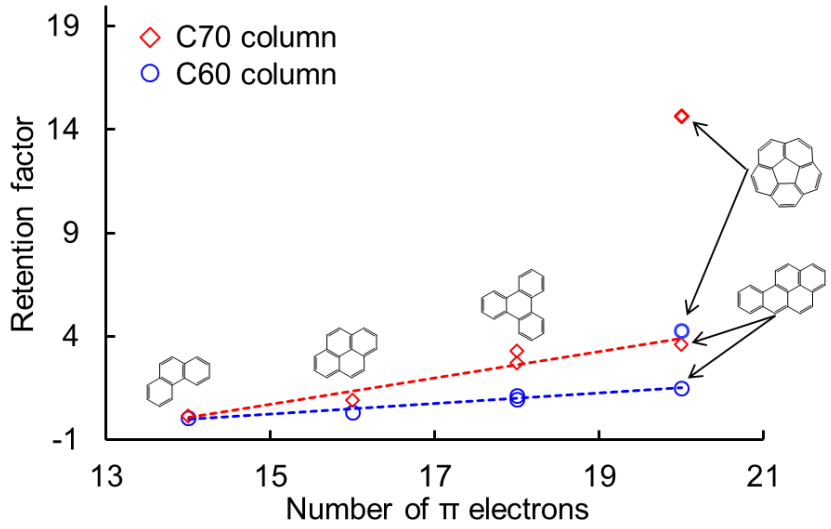

Figure 6. Corrected retention factors of PAHs. LC conditions were the same as Figure 5. The corrected retention factor was estimated by the retention factor divided with the density of each fullerene shown in Table 2.

2-3-4 Computer simulations of atomic charges in PAHs and C60/C70-PFPA-NHS

Then, in order to understand the atomic charge and polarity of each PAH, a computational simulation was carried out. Figure 7 shows the atomic charges of C60/C70-PFPA-NHS. Here, the coordinated number of carbon atoms was defined as follows; the farthest carbon from an N atom, which is bonded to fullerene, was at number 1. The figure shows the results for the half of carbon atoms from free edge of fullerenes. Any charge deflection was not observed in C60- and C70-conjugated molecule. The result supposed that the selective interaction between Crn and fullerenes might be occurred by induced-dipole interactions. Therefore, the polarity of PAHs and fullerene-PFPA-NHS was also estimated. As shown in Figure 7 (b), only Crn and fullerene conjugations shows higher dipole moment, whereas no dipole moment was observed in any other PAHs. Especially, the aspect of the dipole moment in Crn was identified at vertical direction as against the face of Crn, which supported the efficient interaction of Crn and fullerenes by both the structural recognition and induced-dipole interaction. Consequently, these results by LC evaluations and the computational calculation suggested that the specific interaction between Crn and fullerenes were caused by both the structural recognition on fullerenes and the induced-dipole interaction, especially we anticipated that the induced interaction was much stronger in C70.

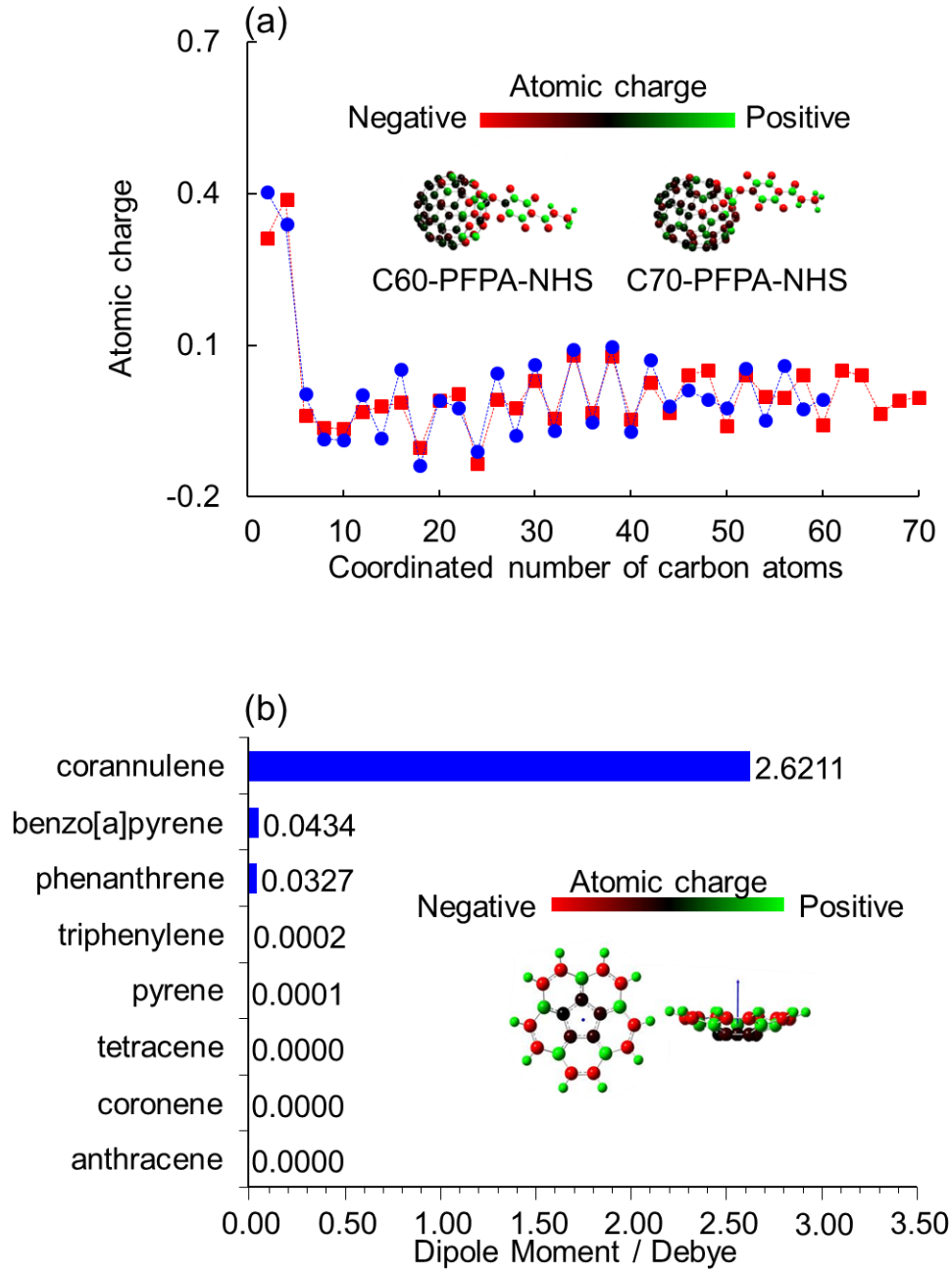

Figure 7. Computer simulations of fullerenes. (a) Atomic charges of carbon atoms in fullerenes. The farthest carbon from N attached to fullerene was coordinated at number 1. (b) The dipoles of each PAH and fullerene conjugated PFPA.

2-3-5 Absorption spectra changing caused by the intermolecular interaction between Crn and free fullerenes

An observation of absorption spectra changing caused by the intermolecular interaction between Crn and free fullerenes was carried out to find the difference of the interaction strength on C60 or C70. The absorption spectrum of C60 or C70 with/without Crn was evaluated. The spectrum changing of the C70 solution by alteration of the concentration of added Crn is summarized in Figure 8 (a)(b). A significant decrease of the absorption at 468 nm was observed by adding Crn into the C70 solution, while the C60 solutions did not show any spectrum changing. Furthermore, as shown in Figure 8 (c), the visible color of the mixture of C70 and Crn was dramatically changed. These results strongly supported that the significant changing of the polarity based on the electron density on C70 was occurred by the interaction with Crn. Further investigations including an X-ray structure analysis and an estimation of the binding energy will allow us to understand the mechanism of the specific interaction on C70. We believe that the result described in this study is the first finding for the specific interaction on C70 depending on the localized π-electrons by the consideration of chromatography, simulation and spectroscopic analysis.

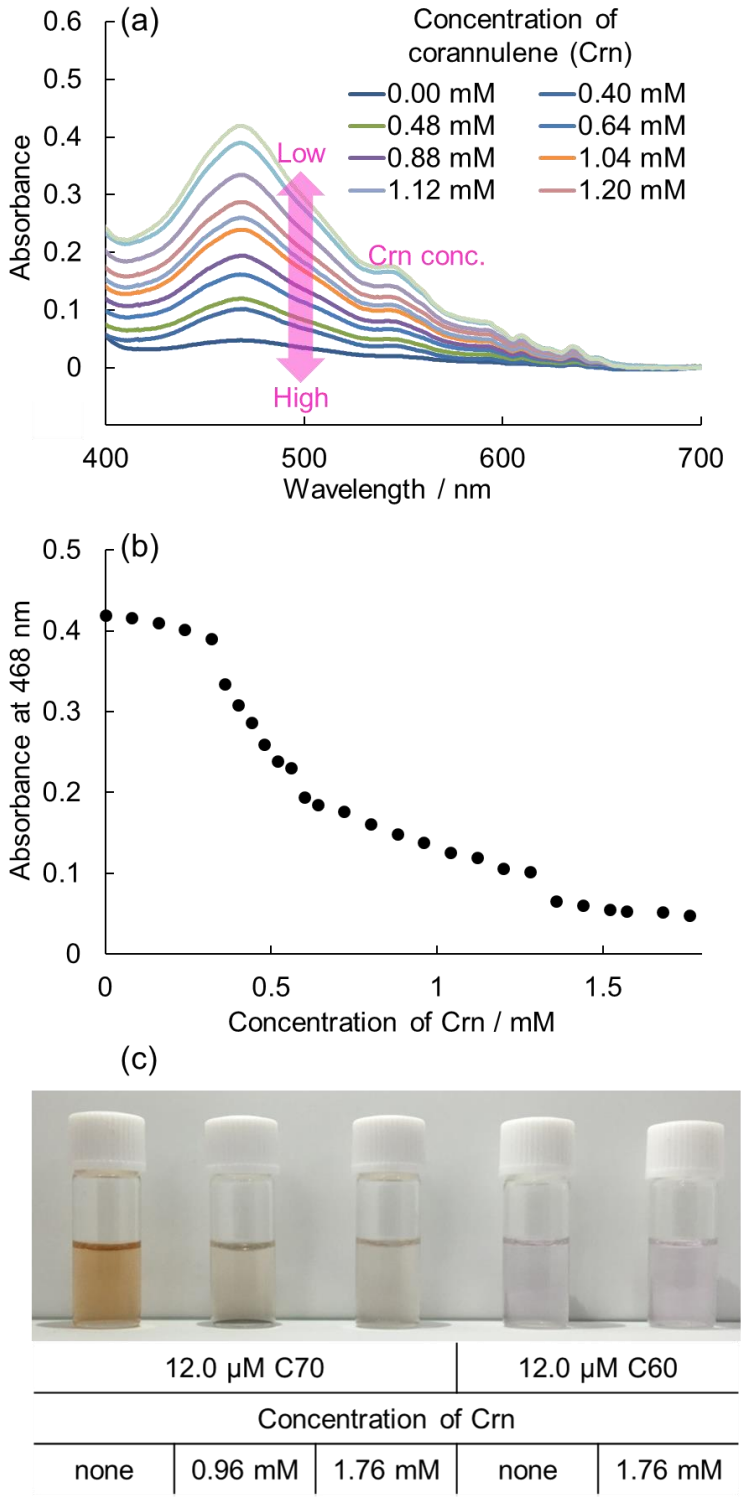

Figure 8. The alteration of absorption spectra in free C70 with Crn. (a) Absorption spectra of free C70 solution in n-hexane with various concentrations of Crn. (b) The changing of absorbance at 468 nm by adding Crn. (c) Physical appearances of free C60 and C70 solutions with/without Crn.

2-3-6 Separation of the aromatic compounds with C70 column and porous graphite carbon

As well known, the carbon-based materials are useful for the separation of aromatic compounds. Porous graphite carbon (PGC) is the best adsorbent for the separation, in brief, Hypercarb^{TM} has been widely applied for the separation of aromatic compounds, racemic mixture, and polymers.[42-46] Then, we finally demonstrated the separation of aromatic compounds with the C70 column comparted to the separation by the PGC column. The results of chromatographic separation of PAHs and brominated benzenes are summarized in Figure 9 and Figure 10. As we expected, the PGC column provided the significantly strong retention ability toward PAH described in Figure 9 (a). Although the separation of PAHs was also achieved in the C70 column, the absolute retention was much lower than that of the PGC column (Figure 10 (a)). The PGC column was packed with the spherical porous graphite carbon, so that the total amount of graphite is much higher than any other silica-gel based columns. Accordingly, the higher retention was obtained in the PGC column. On the other hand, similar separations were obtained for brominated benzenes in both columns (Figure 9 (b), Figure 10 (b)). Comparted to the separation of PAHs, the relative retention to brominated benzenes in C70 was much higher. In other words, C70 provided the selective retention ability for the polarized aromatic ring or bromine atoms. In either case, the weaker induced-dipole interactions seemed to be contributed the selective retentions. Consequently, we expect that the C70 bonded column is useful not only for PAHs but also polarized aromatic compounds in non-polar solvents by LC. Further investigations will contribute the effective separations based on the weak interaction, such as induced dipole interactions.

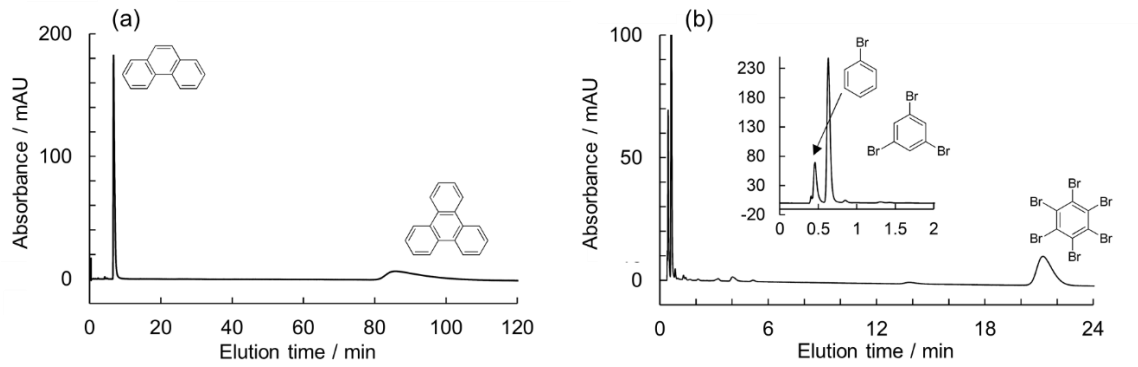

Figure 9. Separations of PAHs and brominated benzenes in the PGC column. (a) separations of PAHs, (b) separations of brominated benzenes, LC conditions: PGC column, Hepercarb™ (30 mm × 2.1 mm i.d.); flow rate, 2.0 mL min^{-1}; mobile phase, *n*-hexane/chloroform = 7/3.

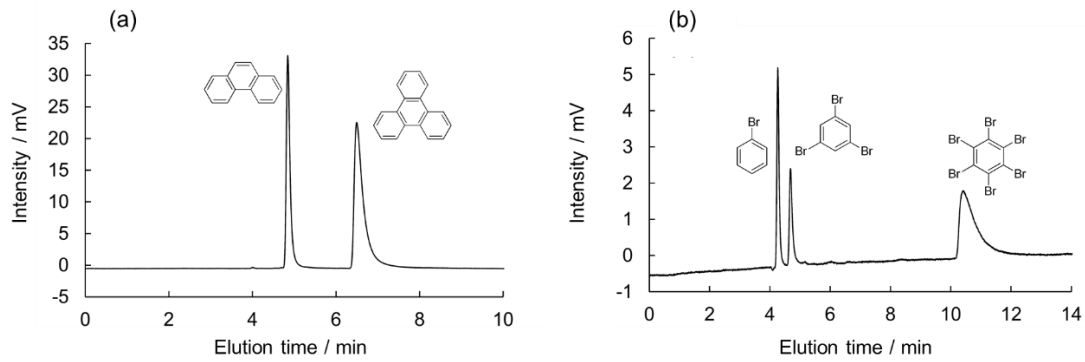

Figure 10. Separations of PAHs and brominated benzenes in the C70 column. (a) separations of PAHs, (b) separations of brominated benzenes, LC conditions: column, C70 column (66.5 cm × 100 μm i.d.); flow rate, 2.0 μL min^{-1}; mobile phase, *n*-hexane/chloroform = 7/3.

2-4 Conclusions

In conclusion, we successfully prepared the C70 bonded silica-monolith via PFPA conjugated compounds. The C70 monolith allowed the strong π-π interaction toward a variety of PAHs even in a normal phase LC mode with *n*-hexane as a mobile phase as well as our previous study using C60. Additionally, the C70 monolith showed the higher retention ability for Crn than that of C60. The computer simulation and the evaluation of absorption spectra for the interaction between fullerenes and Crn suggested that C70 was effectively interacted with Crn by the induced-dipole interaction. Furthermore, comparison of the LC separations between the C70 and PGC column supposed that the C70 column showed the unique separation ability for brominated aromatic compounds by induced-dipole interactions. We expect that this effective induced-dipole interaction should be utilized as a new separation mechanism for liquid phase separation techniques including LC as one of dispersion interactions.

2-5 References

1. Krätschmer, W.; Lamb, L. D.; Fostiropoulos, K.; Huffman, D. R., Solid C60: a new form of carbon. *Nature* **1990,** *347*, 354-358.
2. Iijima, S., Helical microtubules of graphitic carbon. *Nature* **1991,** *354*, 56-58.
3. Schedin, F.; Geim, A. K.; Morozov, S. V.; Hill, E. W.; Blake, P.; Katsnelson, M. I.; Novoselov, K. S., Detection of individual gas molecules adsorbed on graphene. *Nat. Mater.* **2007,** *6*, 652-655.
4. De Heer, W. A.; Châtelain, A.; Ugarte, D., A Carbon Nanotube Field-Emission Electron Source. *Science* **1995,** *270*, 1179.
5. Tans, S. J.; Verschueren, A. R. M.; Dekker, C., Room-temperature transistor based on a single carbon nanotube. *Nature* **1998,** *393*, 49-52.
6. Popov, M.; Kyotani, M.; Nemanich, R. J.; Koga, Y., Superhard phase composed of single-wall carbon nanotubes. *Phys. Rev. B* **2002,** *65*, 033408.
7. Kam, N. W. S.; Connell, M.; Wisdom, J. A.; Dai, H., Carbon nanotubes as multifunctional biological transporters and near-infrared agents for selective cancer cell destruction. *Proc. Natl. Acad. Sci. USA* **2005,** *102*, 11600.
8. Velzeboer, I.; Kwadijk, C. J. A. F.; Koelmans, A. A., Strong Sorption of PCBs to Nanoplastics, Microplastics, Carbon Nanotubes, and Fullerenes. *Environ. Sci. Technol.* **2014,** *48*, 4869-4876.
9. Jinno, K.; Tanabe, K.; Saito, Y.; Nagashima, H., Separation of Polycyclic Aromatic Hydrocarbons With Various C60 Fullerene Bonded Silica Phases in Microcolumn Liquid Chromatography. *Analyst* **1997,** *122*, 787-791.
10. Tournus, F.; Latil, S.; Heggie, M. I.; Charlier, J. C., π-π stacking interaction between carbon nanotubes and organic molecules. *Phys. Rev. B* **2005,** *72*, 075431.

11. Stankovich, S.; Dikin, D. A.; Piner, R. D.; Kohlhaas, K. A.; Kleinhammes, A.; Jia, Y.; Wu, Y.; Nguyen, S. T.; Ruoff, R. S., Synthesis of graphene-based nanosheets via chemical reduction of exfoliated graphite oxide. *Carbon* **2007,** *45*, 1558-1565.
12. Dreyer, D. R.; Park, S.; Bielawski, C. W.; Ruoff, R. S., The chemistry of graphene oxide. *Chem. Soc. Rev.* **2010,** *39*, 228-240.
13. Cao, M.; Fu, A.; Wang, Z.; Liu, J.; Kong, N.; Zong, X.; Liu, H.; Gooding, J. J., Electrochemical and Theoretical Study of π–π Stacking Interactions between Graphitic Surfaces and Pyrene Derivatives. *J. Phys. Chem. C* **2014,** *118*, 2650-2659.
14. Zeinalipour-Yazdi, C. D.; Pullman, D. P., Correlation of Polarizabilities with Van Der Waals Interactions in π-systems. *J. Phys. Chem. B* **2006,** *110*, 24260-24265.
15. Bradshaw, D. S.; Andrews, D. L., Interparticle Interactions: Energy Potentials, Energy Transfer, and Nanoscale Mechanical Motion in Response to Optical Radiation. *c A* **2013,** *117*, 75-82.
16. Tkatchenko, A.; DiStasio, R. A.; Car, R.; Scheffler, M., Accurate and Efficient Method for Many-Body van der Waals Interactions. *Phys. Rev. Lett.* **2012,** *108*, 236402.
17. Amovilli, C.; Floris, F. M., Study of Dispersion Forces with Quantum Monte Carlo: Toward a Continuum Model for Solvation. *J. Phys. Chem. A* **2015,** *119*, 5327-5334.
18. Kayillo, S.; Dennis, G. R.; Shalliker, R. A., An assessment of the retention behaviour of polycyclic aromatic hydrocarbons on reversed phase stationary phases: Selectivity and retention on C18 and phenyl-type surfaces. *J. Chromatogr. A* **2006,** *1126*, 283-297.
19. Kimata, K.; Hosoya, K.; Araki, T.; Tanaka, N., [2-(1-Pyrenyl)ethyl]silyl silica packing material for liquid chromatographic separation of fullerenes. *J. Org. Chem.*

1993, *58*, 282-283.

20. Willcox, M. K.; Woodward, L. A.; Ylitalo, G. M.; Buzitis, J.; Atkinson, S.; Li, Q. X., Organochlorines in the free-ranging Hawaiian monk seal (Monachus schauinslandi) from French Frigate Shoals, North Pacific Ocean. *Sci. Total Environ.* **2004,** *322*, 81-93.
21. Troshin, P. A.; Avent, A. G.; Darwish, A. D.; Martsinovich, N.; Abdul-Sada, A.; a, K.; Street, J. M.; Taylor, R., Isolation of two seven-membered ring C_{58} fullerene derivatives: $C_{58}F_{17}CF_3$ and $C_{58}F_{18}$. *Science* **2005,** *309*, 278.
22. Gómara, B.; García-Ruiz, C.; González, M. J.; Marina, M. L., Fractionation of chlorinated and brominated persistent organic pollutants in several food samples by pyrenyl-silica liquid chromatography prior to GC–MS determination. *Anal. chim. Acta* **2006,** *565*, 208-213.
23. Liu, L.-H.; Yan, M., Simple Method for the Covalent Immobilization of Graphene. *Nano Lett.* **2009,** *9*, 3375-3378.
24. Liu, L.-H.; Yan, M., Perfluorophenyl Azides: New Applications in Surface Functionalization and Nanomaterial Synthesis. *Acc. Chem. Res.* **2010,** *43*, 1434-1443.
25. Liu, L.-H.; Zorn, G.; Castner, D. G.; Solanki, R.; Lerner, M. M.; Yan, M., A simple and scalable route to wafer-size patterned graphene. *J. Mater. Chem.* **2010,** *20*, 5041-5046.
26. Kubo, T.; Wang, X.; Tong, Q.; Yan, M., Polymer-Based Photocoupling Agent for the Efficient Immobilization of Nanomaterials and Small Molecules. *Langmuir* **2011,** *27*, 9372-9378.
27. Liu, L.-H.; Yan, M., Functionalization of pristine graphene with perfluorophenyl azides. *J. Mater. Chem.* **2011,** *21*, 3273-3276.

28. Kubo, T.; Murakami, Y.; Tominaga, Y.; Naito, T.; Sueyoshi, K.; Yan, M.; Otsuka, K., Development of a C60-fullerene bonded open-tubular capillary using a photo/thermal active agent for liquid chromatographic separations by π–π interactions. *J. Chromatogr. A* **2014,** *1323*, 174-178.
29. Kubo, T.; Murakami, Y.; Naito, T.; Otsuka, K., C60-Fullerene Bonded Silica Monolithic Capillary for Specific Separations of Aromatic Compounds. *CHROMATOGRAPHY* **2015,** *36*, 105-113.
30. Kubo, T.; Murakami, Y.; Tsuzuki, M.; Kobayashi, H.; Naito, T.; Sano, T.; Yan, M.; Otsuka, K., Unique Separation Behavior of a C60 Fullerene-Bonded Silica Monolith Prepared by an Effective Thermal Coupling Agent. *Chem.: Eur. J.* **2015,** *21*, 18095-18098.
31. Steiner, E.; Fowler, P. W.; Jenneskens, L. W., Counter-Rotating Ring Currents in Coronene and Corannulene. *Angew. Chem. Int. Ed.* **2001,** *40*, 362-366.
32. Kennedy, M. R.; Burns, L. A.; Sherrill, C. D., Buckyplates and Buckybowls: Examining the Effects of Curvature on π–π Interactions. *J. Phys. Chem. A* **2012,** *116*, 11920-11926.
33. Vijay, D.; Sakurai, H.; Subramanian, V.; Sastry, G. N., Where to bind in buckybowls? The dilemma of a metal ion. *Phys. Chem. Chem. Phys.* **2012,** *14*, 3057-3065.
34. Li, J.; Liu, Y.; Qian, Y.; Li, L.; Xie, L.; Shang, J.; Yu, T.; Yi, M.; Huang, W., Describing curved–planar π–π interactions: modeled by corannulene, pyrene and coronene. *Phys. Chem. Chem. Phys.* **2013,** *15*, 12694-12701.
35. Li, X.; Kang, F.; Inagaki, M., Buckybowls: Corannulene and Its Derivatives. *Small* **2016,** *12*, 3206-3223.
36. Schmidt, B. M.; Osuga, T.; Sawada, T.; Hoshino, M.; Fujita, M., Compressed

Corannulene in a Molecular Cage. *Angew. Chem. Int. Ed.* **2016,** *55*, 1561-1564.

37. Cox, D. M.; Behal, S.; Disko, M.; Gorun, S. M.; Greaney, M.; Hsu, C. S.; Kollin, E. B.; Millar, J.; Robbins, J., Characterization of C60 and C70 clusters. *J. Am. Chem. Soc.* **1991,** *113*, 2940-2944.
38. Howard, J. B.; McKinnon, J. T.; Makarovsky, Y.; Lafleur, A. L.; Johnson, M. E., Fullerenes C60 and C70 in flames. *Nature* **1991,** *352*, 139-141.
39. Johansson, J. O.; Campbell, E. E. B., Probing excited electronic states and ionisation mechanisms of fullerenes. *Chem. Soc. Rev.* **2013,** *42*, 5661-5671.
40. Kishi, N.; Akita, M.; Yoshizawa, M., Selective Host–Guest Interactions of a Transformable Coordination Capsule/Tube with Fullerenes. *Angew. Chem. Int. Ed.* **2014,** *53*, 3604-3607.
41. Li, Y.; Xu, D.; Gan, L., Selective Multiamination of C70 Leading to Curved π Systems with 60, 58, 56, and 50 π Electrons. *Angew. Chem. Int. Ed.* **2016,** *55*, 2483-2487.
42. Chaimbault, P.; Elfakir, C.; Lafosse, M., Comparison of the retention behavior of polyethoxylated alcohols on porous graphitic carbon and polar as well as apolar bonded-silica phases. *J. Chromatogr. A* **1998,** *797*, 83-91.
43. Chaimbault, P.; Petritis, K.; Elfakir, C.; Dreux, M., Ion-pair chromatography on a porous graphitic carbon stationary phase for the analysis of twenty underivatized protein amino acids. *J. Chromatogr. A* **2000,** *870*, 245-254.
44. Karlsson, A.; Karlsson, O., Chiral ion-pair chromatography on porous graphitized carbon using N-blocked dipeptides as counter ions. *J. Chromatogr. A* **2001,** *905*, 329-335.
45. Chitta, R.; Macko, T.; Brüll, R.; Kalies, G., Elution behavior of polyethylene and

polypropylene standards on carbon sorbents. *J. Chromatogr. A* **2010,** *1217*, 7717-7722.

46. Lu, T.; Olesik, S. V., Homogeneous Edge-Plane Carbon as Stationary Phase for Reversed-Phase Liquid Chromatography. *Anal. Chem.* **2015,** *87*, 3616-3622.

Chapter 3

Separation of Halogenated Benzenes Enabled by Investigation of Halogen-π Interactions with Carbon Materials

3-1 Introduction

Advances in computational chemistry have enabled investigations of large charge deflections in halogen atoms. The low electron density region along the σ bonding axis of bonded halogen atoms, known as the "σ hole," interacts propitiously with electron donor species.[1] This halogen bonding interaction has attracted interest in many fields, such as molecular biology[2] and crystal engineering,[3] due to its high molecular selectivity and linear directionality.[4] In particular, halogen bonding has been positively applied to develop new functional materials[5] since Nguyen et al. first synthesized liquid crystals designed with halogen bonds in 2004.[6] An example is the Roxane structure with iodo groups synthesized by Barendt et al. that selectively recognized nitrogen anions via halogen bonding, producing drastic color changes.[7] Another example is the iodoperfluoroarene-substituted polystyrene synthesized by Vanderkooy et al. that controlled the self-assembly of nanostructures of polymer aggregates by halogen bonding.[8] According to recent reports, halogen bonding greatly contributes to molecular recognition in vivo and has thus been applied in designing drugs,[9] such as aldose reductase inhibitors[10] and HIV-1 inhibitors.[11] Therefore, fully understanding the characteristics of halogen bonding may drastically facilitate the advancement of materials chemistry.

Notably, halogen bonding between halogen groups and π electrons of aromatic rings or unsaturated bonds acting as electron donors, i.e., "halogen-π (X-π) interactions," plays important roles in biological systems.[12] Voth et al. reported the first X-π interactions in biological systems.[13] They found that the interactions between the aromatic rings of phenyl residues inhibited the protein kinases CDK2 and CK2. Data on X-π interactions in biological systems rapidly grew following Voth's report, and the X-π interaction now occupies about 30% of the current reports on halogen bonding in protein-ligand complexation.[14] The importance of X-π interactions is now recognized, and many properties (magnitude directionality and origin of the X-π interaction) have been clarified with high level computational methods based on theoretical chemistry.[15]

Despite the progress, additional experimental data on X-π interactions are necessary because the halogen bond is in physical competition with many other stronger noncovalent interactions, including the hydrophobic interaction, hydrogen bond, and electrostatic interaction.[16] High performance liquid chromatography (HPLC) is a powerful separation technique that utilizes the difference in partition coefficients between the solutes of the mobile and stationary phases, a factor that sensitively reflects the strength of the noncovalent interaction.[17] In our previous studies, we developed novel separation media immobilized with carbon materials.[18] These media exhibited strong π interactions because of their many π electrons. Characteristics of weak interactions from aromatic rings were clarified by evaluating their retention behaviors with HPLC measurements. This included the π-π interaction based on the spherical recognition of C_{60}- or C_{70}-fullerenes (C60/C70), the difference in intensity of the CH or CD-π interaction, and the strong CH-π interaction between corannulene and planar polycyclic aromatic hydrocarbons.

We also uncovered the possibility for the separation of halogenated aromatic compounds resulting from the efficient halogen-π interactions in HPLC.[19] The aromatic halogens, such as polychlorinated biphenyls (PCBs)[20] and polybrominated diphenyl ethers (PBDEs),[21] are widely known to be highly toxic; therefore, we need monitor the concertation of these pollutions in our environment. Usually, these aromatic halogens are analyzed by gas-chromatography or reverse-phase liquid chromatography, which involve complicated preparation processes. Even with these existing methods, the separation of the full variety of isomers by the direct analysis of the sample in oil or after extraction with non-polar solvents is difficult because only factors driving the separation are the differences in vaporization or hydrophobicity between the compounds. In addition, the halogen-π interaction has never been utilized for the separation of these aromatic halogens. Thus, we hypothesized that the effective halogen-π interaction would enable the efficient separation of the isomers of aromatic halogens and that the one-pot separation system will contribute to the straightforward monitoring of environmental pollutions like PCBs and PBDEs.

In the present study, we experimentally evaluated the strength of the X-π interaction between carbon materials and a variety of halogenated benzenes using normal phase liquid chromatography (NPLC). The hydrophobic interaction was completely suppressed in this technique, and thus the π interactions could be simply examined. Furthermore, we accurately evaluated the π interactions between halogenated benzenes and C70 using ultraviolet-visible (UV-Vis) and ^{1}H NMR spectroscopy. Finally, we demonstrate the one-pot separation of the entirety of the brominated benzenes (11 analogues) by optimizing the mobile phase conditions to control the X-π interactions.

3-2 Experimental Section

3-2-1 Materials

Acetone, diethyl ether, magnesium sulfate, sodium hydroxide, dichloromethane, chlorobenzene, *toluene, ethyl acetate,* methanol, *tetrahydrofuran, n*-hexane, *n*-heptane, *n*-octane, *n*-nonane, *n*-decane and chloroform were purchased from Nacalai Tesque (Kyoto, Japan). Methyl pentafluorobenzoate, diethyl amine, urea, acetic acid, 3-aminopropyltrimethoxysilane (APTMS), 2.6-lutidine and halogenated benzenes were from Tokyo Chemical Industry (Tokyo, Japan). Sodium azide, *N*-hydroxysuccinimide (NHS), 1-ethyl-3-(3-dimethylaminopropyl)carbodiimide (EDAC) were acquired from Wako Pure Chemical Industries (Osaka, Japan). Polyethylene glycol (PEG) (*M*n = 10,000), C60-fullerene (C60), C70-fullerene (C70) were purchased from Sigma-Aldrich Japan (Tokyo, Japan). Deionized water was obtained from a Milli-Q Direct-Q 3UV system (Merck Millipore, Tokyo, Japan). A COSMOSIL PYE® and πNAP® were purchased from Nacalai Tesque, and a fused-silica capillary from Polymicro Technologies Inc. (Phoenix, AZ, USA).

3-2-2 Instruments

A capillary liquid chromatographic system consisted of a DiNa S (KYA Technologies Co., Tokyo, Japan) as a pump, CE-2070 (JASCO, Tokyo, Japan) as a UV detector, CHEMINERT (Valco Instruments Co., Huston, TX) as a sample injector, and Chemco capillary column conditioner Model 380-b (Chemco Co. Osaka, Japan) as a column oven. An HPLC system consisted of a Prominence series (Shimadzu Co., Kyoto, Japan). UV-Vis spectroscopy was carried out by a UV-2450 (Shimadzu). FT-IR, NMR, elemental analysis, and fast atom bombardment mass spectrometry (FABMS) were carried out by a

Nicolet iS5 ATR (Thermo Fisher Scientific K. K., Yokohama, Japan), JNM-ECA500 spectrometer (JEOL, Tokyo, Japan), Flash EA1112 (Thermo Fisher Scientific K. K.), and JMS-700 (JEOL), respectively.

3-2-3 Preparation of C70-coated columns and their evaluation

C60 fullerene-coated silica monolithic column (C60 column) and C70 column were prepared following the protocols in previous chapter (Chapter 2). The silica-monolithic capillary was treated with 1.0 M aqueous sodium hydroxide at 40 ºC for 3 h. After washing with water and methanol, 3-aminopropyltrimethoxysilane (APTMS) in methanol (10%, v/v) was passed through the silica-monolithic capillary for 24 h and washed with methanol. C60/C70-4-azido-2,3,5,6-tetrafluorophenyl succinate (PFPA-NHS) in toluene (3.0 mg mL^{-1}) was charged into the NH_2-monolith for 24 h at room temperature and washed with toluene and methanol (Scheme 1). A column that was modified with only the linkers or PFPA column (Scheme 2) was also prepared and used as a control. NH_2 groups on the silica-monolith surface and C70-PFPA-NHS were reacted under the conditions in Table 1. (column 1 is defined as Type-1 and column 4 is defined as Type-2).

Table 1. Reaction condition of NH_2 group on silica-monolith surface and C70-PFPA-NHS.

	Column 1	Column 2	Column 3	Column 4
Reaction time with NH_2 group	1 day	2 day	1 day	2 day
Concentration of C70-PFPA-NHS	3 mg/mL	3 mg/mL	8 mg/mL	8 mg/mL

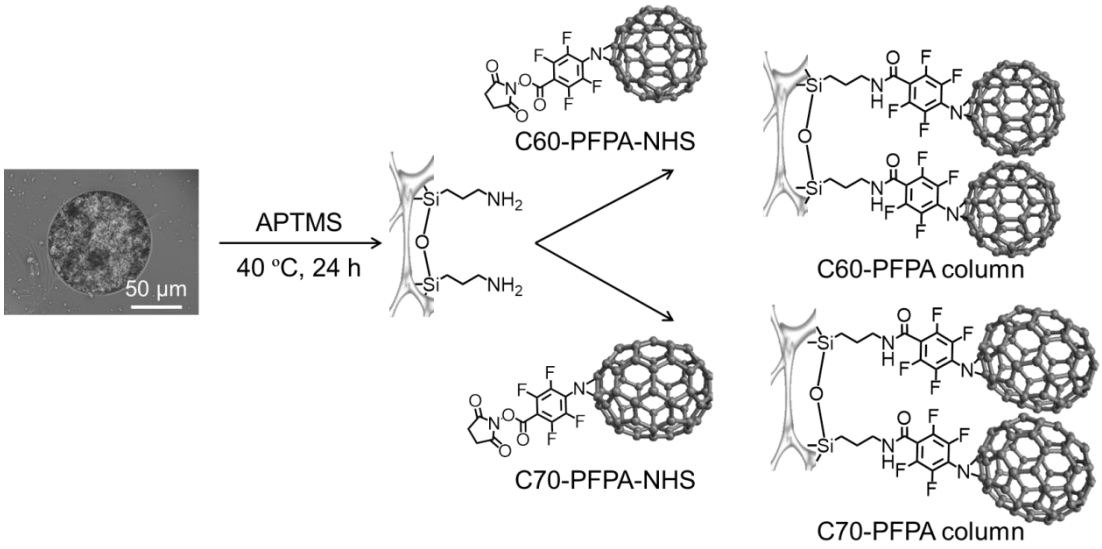

Scheme 1. Preparation of C60/C70-coated column.

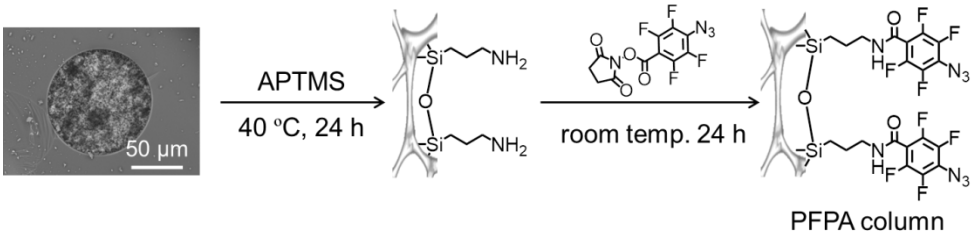

Scheme 2. Preparation of PFPA-coated column.

3-2-4 Computational methods

To obtain the initial 3D molecular coordinates of each molecule, Chem3D version 7.0 was used. *Ab initio* calculations using Gaussian 03 were performed on a Linux Cluster. All geometrical optimizations were carried out by using the RB3LYP/3-21G basis set. Calculations of charges based on Merz-Singh-Kollman were carried out by using the B3LYP/3-21G basis set, which can be applied to large molecules. This method required no significant calculation time. During *ab initio* calculations, all internal coordinates were optimized by means of the Berny algorithm, and convergence was tested against criteria for the maximum force component, root-mean-square force, maximum displacement component, and root-mean-square displacement.

.

3-3 Results and Discussion

3-3-1 Retention of halogenated benzenes on carbon-material coated columns in NPLC

We evaluated the retention of halogenated benzenes on four different carbon-material (πNAP, 5PYE, C60, and C70) coated columns (Figure 1). Figure 1a shows the retention factors k ($k = (t_R - t_0)/t_0$ where t_R is the retention time of a solute and t_0 is the elution time of non-retained solute) of brominated benzenes on each carbon-material coated column against the number of bromo substitutions in the solutes. All the carbon-material coated columns showed higher retentions as the number of bromo substitutions increased. The results indicated that the X-π interactions existed between the aromatic rings in the stationary phases and the bromo substitutions of the solutes. The C70-coated column showed significantly higher retentions for brominated benzenes. PFPA, the linker of the C70-coated column, did not provide such high retention, as shown in Table 2; therefore, we concluded that the C70 moiety was responsible for the high retentions of the brominated benzenes.

Furthermore, in order to evaluate the impact of the halogen species in the solutes on retention behaviors, the retention factors of benzenes with various halogens on the C70-coated column were measured and plotted in Figure 1b against the number of halogen substitutions in the solutes. The C70-coated column did not retain any fluorinated benzenes. This result suggested that fluorine substitutions were not capable of meaningful X-π interactions. Alternatively, the C70-coated column retained chlorinated and brominated benzenes and showed higher retentions as the number of halogen substitutions increased. However, the absolute retentions and the retention differences across the number of halogen substitutions of the chlorinated benzenes were much less than those of the brominated benzenes.

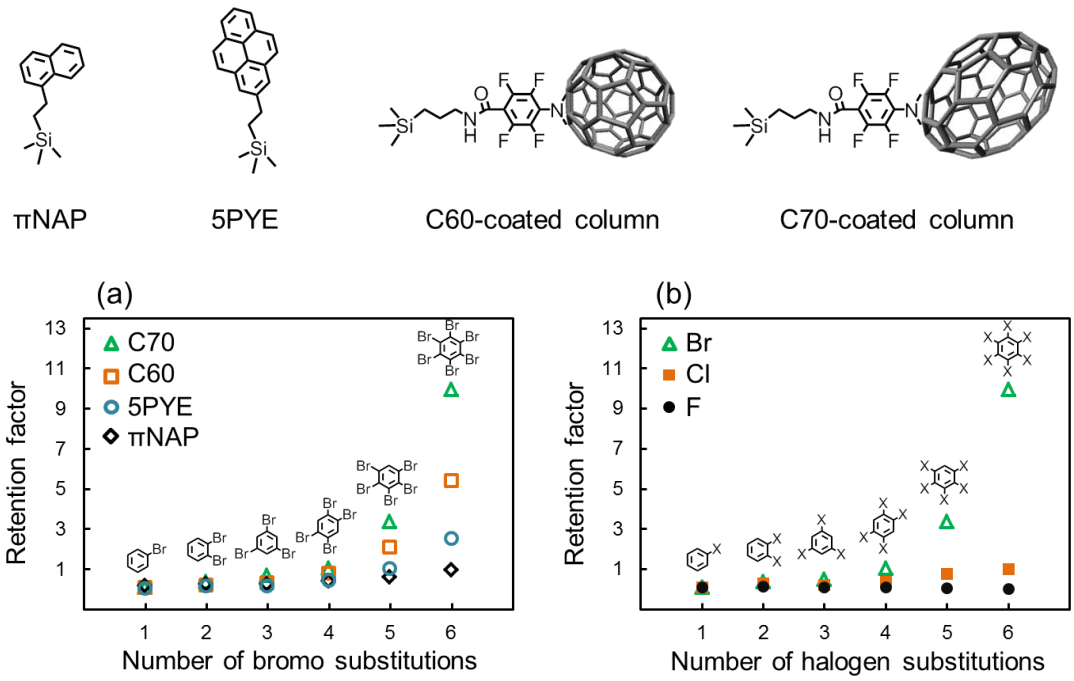

Figure 1. Structure of the stationary phases and retention behaviors of halogenated benzenes with carbon-material coated columns in NPLC. (a) retention factors of brominated benzenes with each column and the number of brominated substitutions. (b) retention factors of each halogenated benzene with the C70-coated column and the number of halogen substitutions.

Conditions: column, C60-coated (28.8 cm × 100 μm i.d.), C70-coated (Type-1, 25.5 cm × 100 μm i.d.), 5PYE (150 mm × 4.6 mm i.d.), πNAP (50 mm × 2.0 mm i.d.); flow rate; 2.0 μL min^{-1} (C70, C60-coated), 1.0 mL min^{-1} (5PYE), 0.5 mL min^{-1} (πNAP); mobile phase, *n*-hexane; temperature, 25 °C; detection, UV 228 nm.

Table 2. Retention factors of brominated benzenes on C70-coated column and PFPA column in *n*-hexane.

	C70 column	PFPA column
bromobenzene	0.11	0.02
o-dibromobenzene	0.39	0.02
m-dibromobenzene	0.25	0.01
p-dibromobenzene	0.21	0.01
1,2,3-tribromobenzene	0.68	0.04
1,2,4-tribromobenzene	0.54	0.02
1,3,5-ribromobenzene	0.50	0.04
1,2,4,5-tribromobenzene	1.03	0.04
pentabromobenzene	3.36	0.05
hexabromobenzene	9.93	0.11

Conditions: column, C60-coated (28.8 cm × 100 μm i.d.), C70-coated (Type-1, 25.5 cm × 100 μm i.d.), 5PYE (150 mm × 4.6 mm i.d.), πNAP (50 mm × 2.0 mm i.d.); flow rate; 2.0 μL min^{-1} (C70, C60-coated), 1.0 mL min^{-1} (5PYE), 0.5 mL min^{-1} (πNAP); mobile phase, *n*-hexane; temperature, 25 °C; detection, UV 228 nm.

The chromatograms of chlorinated benzenes (Figure 2a) and brominated benzenes (Figure 2b) also clearly showed poorer resolution for the chlorinated benzenes. These results indicated that the X-π interactions of chlorine substitutions were weaker than those of their bromine counterparts.

Here, we hypothesized that the X-π interaction becomes stronger as the size of the substituting halogen increases. A few reports in the literature support our hypothesis; briefly, the size of the σ hole increases with the size of the halogen.[49-51] In order to confirm our hypothesis, we evaluated the retention behaviors of the hexa-halogenated benzenes

(C_6F_6, C_6Cl_6, C_6Br_6, C_6I_6) in NPLC with the C70-coated column. Figure 2c shows the chromatograms of the mixed sample of hexa-halogenated benzenes. In consideration of the solubility of C_6I_6, tetrahydrofuran (THF) was added to the mobile phase in this separation. As shown in Fig. 2c, the elution order in the C70-coated column was C_6F_6 < C_6Cl_6 < C_6Br_6 < C_6I_6. As expected, larger halogen atoms enabled higher retentions; the differences in the X-π interactions should account for this trend.

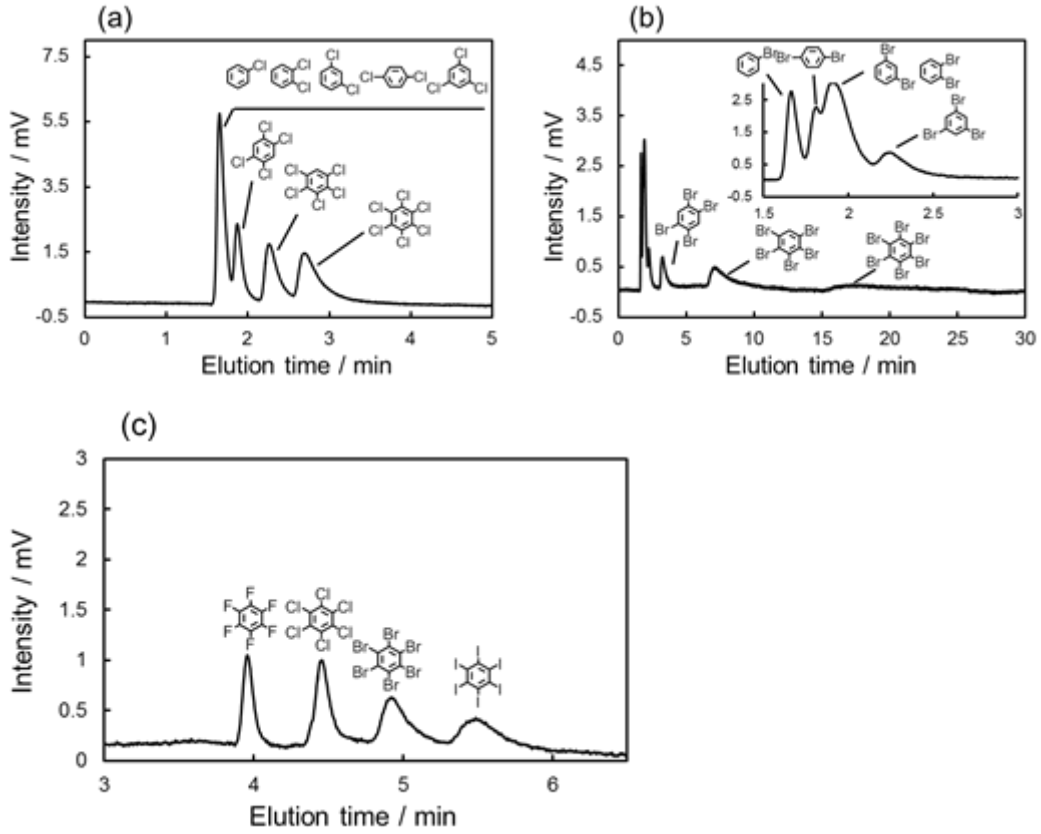

Figure 2. Chromatograms of the mixed sample of (a) chlorinated benzenes, (b) brominated benzenes, and (c) the mixture of hexa-halogenated benzenes with the C70-coated column.

Conditions: (a)(b) column, C70-coated (Type-1, 25.5 cm × 100 μm i.d.); flow rate; 2.0 μL min^{-1}; mobile phase, *n*-hexane; temperature, 25 °C; detection, UV 228 nm; (c) column, C70-coated (Type-1, 75.0 cm × 100 μm i.d.); flow rate; 2.0 μL min^{-1}; mobile phase, *n*-hexane/THF = 7/3; temperature, 25 °C; detection, UV 228 nm.

3-3-2 Retention selectivity for hemispherical structure

In the interaction between halogenated benzenes and aromatic carbon-materials, typical π-π interactions could also contribute in addition to the X-π interactions. In order to evaluate the contributions of π-π interactions to the retention of brominated benzenes, we focused on the differences in UV-Vis absorption spectra of halogenated benzenes with/without C70. Several previous studies reported that the π-π interaction attenuated a certain absorbance region in UV-Vis.[40, 52] The absorption spectra of *o*-dibromobenzene (10 μM) with/without C70 (10 μM) in *n*-hexane are shown in Figure 3a. Interestingly, the spectrum dramatically changed when C70 was added to the solution. Similar spectral alterations were observed for other brominated benzenes (Figure 4). These results suggested that the π-π interaction also contributes to the intermolecular interaction between brominated benzenes and C70. Alternatively, the absorption spectra with larger numbers of bromine substitutions ($n > 3$), especially hexabromobenzene, were almost unchanged. we assumed that the extent of contributions of the π-π interactions to the intermolecular interaction with C70 was different for these solutes. To evaluate the difference in detail, we calculated the difference in absorbance at the maximum wavelength (around 205 nm, typical specific absorption for the π-π* transition[53]) between columns with and without C70 (ΔA). Figure 3b summarizes ΔA for each solute against the number of bromine substitutions. Based on this Figure 4, we supposed that fewer bromine substitutions allowed stronger π-π interactions while higher bromine substitutions were mainly dominated by the X-π interaction. Briefly, the degree of the contribution by the π-π interaction between brominated benzenes and C70 followed a trend opposite to that of retention strength of brominated benzenes on the C70-coated column (Figure 1). In higher bromine substitutions, the relatively stronger X-π interaction

may dominantly contribute to the higher retentions on the C70-coated column. From these results, we conclude that both the X-π interaction and the π-π interaction are competitively involved in the intermolecular interaction between halogenated benzenes and C70.

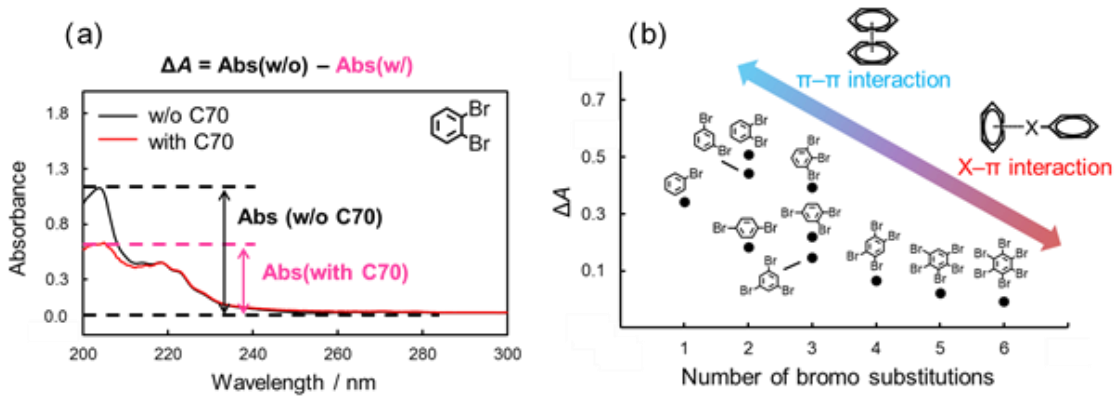

Figure 3. Absorption spectra of *o*-dibromobenzene in *n*-hexane with/without C70 (a) and difference of absorbance in maximum wavelength (205 nm) with/without C70.

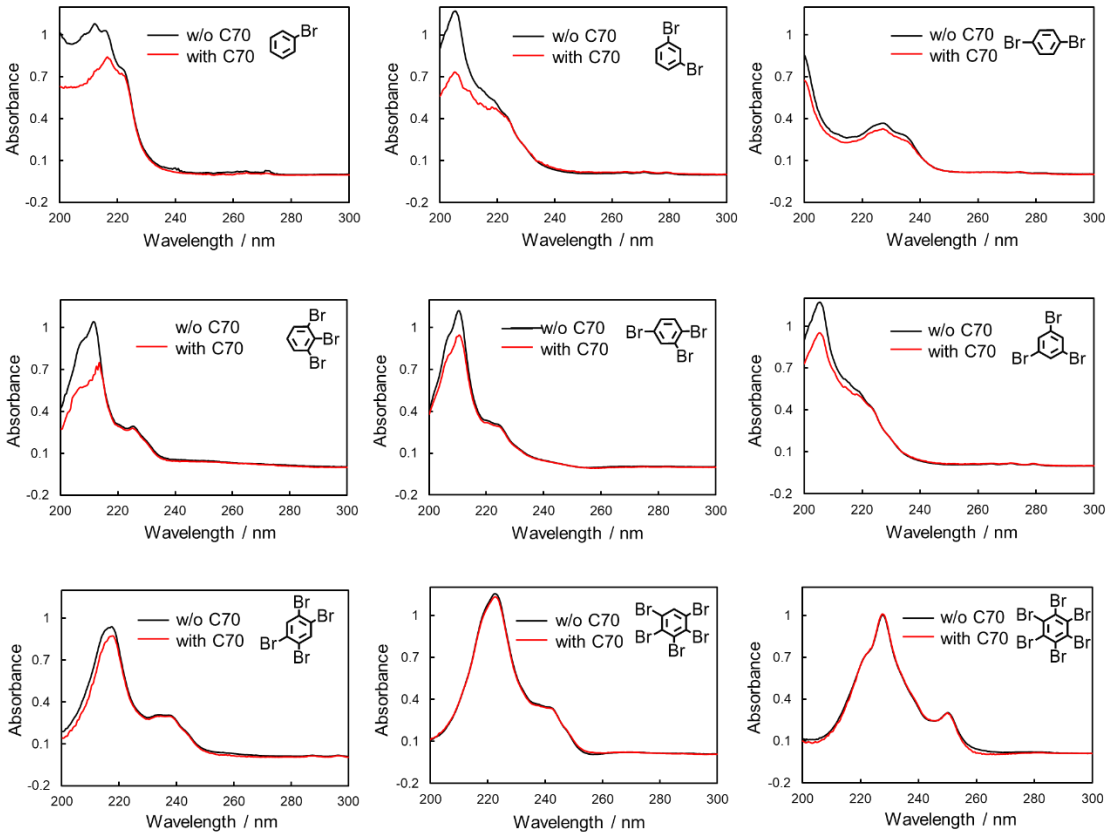

Figure 4. Absorption spectra of each brominated benzenes in n-hexane with/without C70.

3-3-3 Retention behaviors of PAHs with different π electron numbers

As described above, large differences of Δ*A* were also observed among the isomers of dibromo and tribromobenzenes. These absorbance changes were expected to indicate the strength of the π-π interaction between each structural isomer and C70. Thus, we anticipated that the C70-coated column could efficiently separate the isomers by optimizing the LC conditions to exploit the differences in the strength of the interactions. To achieve such separations, we improved the procedure of preparing a C70-coated column; in brief, we attempted to increase the concentration of C70-PFPA-NHS in the reaction solution to improve the immobilization amount of C70. Then, we obtained another C70-coated column (Type-2), in which a high density of C70 was immobilized. NH_2 groups on the silica-monolith surface and C70-PFPA-NHS were reacted under the conditions in Table 1. For comparing column performances, we evaluated retention factors and separation factors of phenanthrene and corannulene, which showed specific intermolecular interaction with C70 due to its spherical recognition. Figure 5 (a) shows the retention factors of phenanthrene and corannulene obtained and the separation factor for each column. The chromatograms of the phenathrene and corannulene mixture obtained with column 1 and column 4 are shown in Figure 5 (b). Column 4 showed the largest retention factor and separation factor. This result clearly suggested that the separation performance of the column was successfully improved by increasing the reaction time and concentration of C70-PFPA-NHS in the reaction solution.

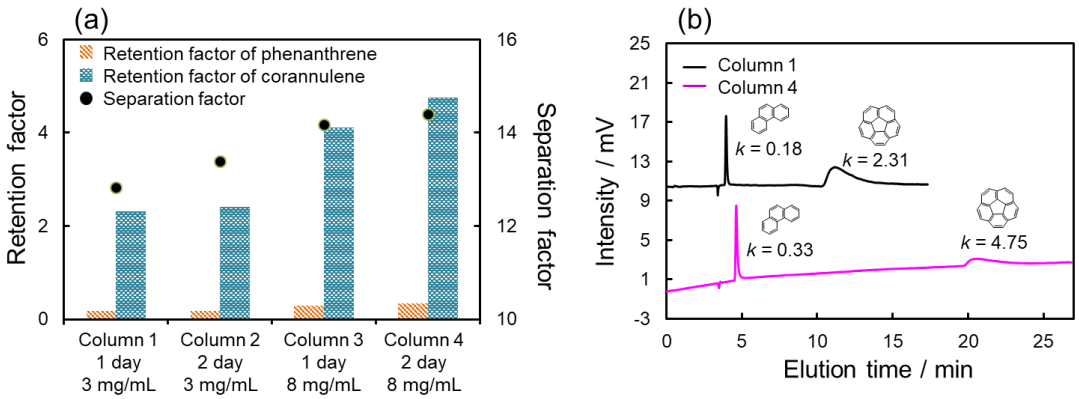

Figure 5. Improvement of column performance by increasing the reaction time and concentration of C70-PFPA-NHS in the reaction solution. (a) Retention factors of phenanthrene and corannulene and corresponding separation factor with each column. (b) Chromatograms of the mixed sample of phenanthrene and corannulene with the Column 1 or Column 4. Conditions: column, Column 1, 2, 3, and 4 (75.0 cm × 100 μm i.d.); flow rate; 2.0 μL min^{-1}; mobile phase, n-hexane/chloroform = 7/3; temperature, 25 ºC UV absorption (254 nm).

We then used column 4 to evaluate the separation performance of the structural isomers of halogenated benzenes. Figure 6 shows chromatograms for the mixture of isomers. As we expected, the separation of these structural isomers was successfully achieved. Furthermore, the elution orders on the column, *i.e.*, *o*-dibromobenzene > *m*-dibromobenzene > *p*-dibromobenzene, 1,2,3-tribromobenzene > 1,2,4-tribromobenzene > 1,3,5-tribromobenzene, followed the trend of π-π interaction contributions (Figure 3b). Consequently, we anticipated that the retention differences were a result of the differences in the strength of the π-π interaction.

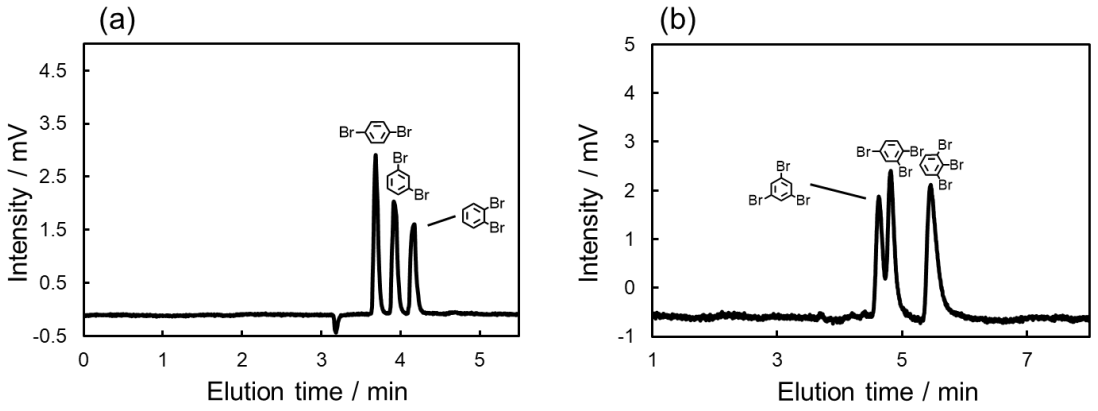

Figure 6. Chromatograms of the mixture of (a) di- or (b) tri-brominated benzenes with the C70-coated column (the C70-coated, Type-2). Conditions: column, C70-coated (Type-2, 75.0 cm × 100 μm i.d.); flow rate; 2.0 μL min^{-1}; mobile phase, *n*-hexane; temperature, 25 °C; detection, UV 228 nm.

To investigate the differences in strength of the π-π interactions, we considered the dipole moments of these structural isomers. The strength of the π interaction is considered to be determined by the induced dipole–dipole interaction or the induced dipole–induced dipole interaction.[33, 54-58] The potential energy of the induced dipole–dipole interaction is given as follows:

$$G_{\text{induced dipole–dipole}} = -\mu^2\alpha_1/(4\pi\varepsilon_0\varepsilon_r)^2 r^6 \qquad (1)$$

where, μ is the dipole moment of the polar molecule, α is the polarizability of the other interacting molecule, ε_0 is the permittivity of vacuum, ε_r is the relative permittivity of the solvent, and r is the distance between the molecules. In addition, the potential energy of the induced dipole–induced dipole interaction is given as follows:

$$G_{\text{induced dipole–induced dipole}} = -\mathrm{A}\alpha_1\alpha_2/(4\pi\varepsilon_0\varepsilon_r)^2 r^6 \qquad (2)$$

where, the polarizabilities of each interacting molecule are involved. Since halogen atoms have strong withdrawing properties and thus halogenated benzenes have large dipole moments across the aromatic ring, we could predict that the π-π interaction was a result of the induced dipole-dipole interaction and that higher dipole moments allowed stronger π-π interactions in our experiments. We then carried out computer simulations to calculate the dipole moments of the solutes (Table 3); Figure 7ab shows the retention factors and ΔA against μ^2. The logarithm of the retention factor was plotted in order to correspond to the potential energy based on the equation of distribution equilibrium.[59] Both di- and tri-brominated structural isomers showed stronger retentions and larger contributions of the π-π interaction as the dipole moment strength increased. The theoretical considerations also supported the notion that di- and tri-brominated benzenes express different strengths of π-π interactions based on the magnitude of their dipole moments.

Table 3. Dipole moment in each structural isomer.

	Dipole X	Dipole Y	Dipole Z	Total Dipole
o-dichlorobenzene	3.6242	0.0353	0.0000	3.6244
m-dichlorobenzene	-0.0079	-2.3155	0.0000	2.3155
p-dichlorobenzene	0.0003	0.0007	0.0015	0.0017
o-dibromobenzene	-1.8132	-1.4543	0.0000	2.3244
m-dibromobenzene	-0.0007	-1.4871	0.0000	1.4871
p-dibromobenzene	0.0114	-0.0007	0.0000	0.0114
1,2,3-tribromobenzene	-0.0004	2.0802	0.0000	2.0802
1,2,4-tribromobenzene	0.1986	1.0204	0.0000	1.0395
1,3,5-tribromobenzene	0.0000	0.0000	0.0000	0.0000
o-diiodobenzene	1.2614	1.6963	0.0000	2.1139
m-diiodobenzene	0.0007	1.4645	0.0000	1.4645
p-diiodobenzene	0.0000	0.0000	0.0000	0.0000

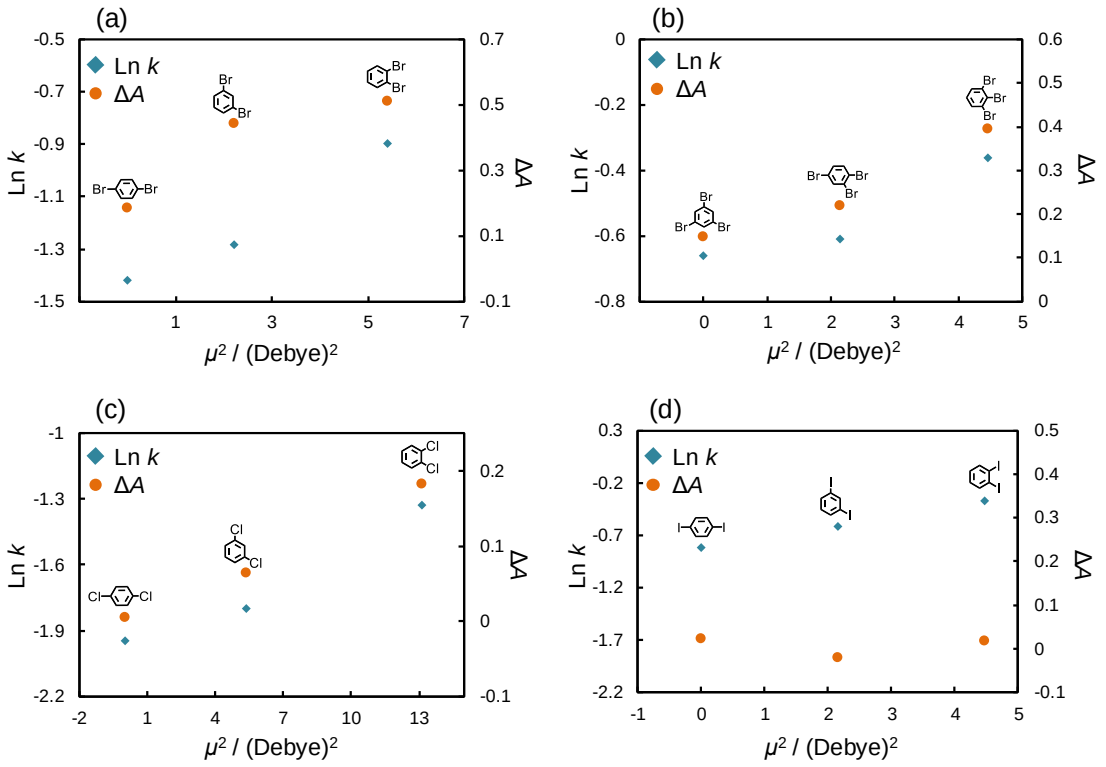

Figure 7. Logarithm of the retention factor or Δ*A* of (a) di- or (b) tri-brominated benzenes and (c) di-chlorinated or (d) di-iodinated benzenes with the C70-coated column against square of dipole moment in each solute. Conditions: column, C70-coated (Type-2, 75.0 cm × 100 μm i.d.); flow rate; 2.0 μL min^{-1}; mobile phase, *n*-hexane; temperature, 25 °C; detection, UV 228 nm.

In a fashion similar to the above experiments, we evaluated the effect of the π-π interaction for chlorine and iodine substitutions. Figure 8 shows the chromatograms of di-chlorinated and di-iodinated benzenes. The separation of these structural isomers was confirmed even though the separation efficiency was poorer than that of the bromine substitutions. Here, we again evaluated the retention factor and Δ*A* of each solute and calculated their dipole moments (Table 3). The absorption spectra of structural isomers of di-chloro and di-iodo benzenes (10 μM) with/without C70 (10 μM) in *n*-hexane are shown in Figure 9. Figure 7c and 7d show the retention factors and the Δ*A* of di-

chlorinated and iodinated benzenes against μ^2. Chlorinated benzenes showed larger retention factors and ΔA as their dipole moments increased in comparison to brominated benzenes (Figure 7c). The results indicated that structural isomers of chlorinated benzenes showed the differences in strength of π-π interactions with the magnitudes of their dipole moments as we expected. Surprisingly, di-iodinated benzenes showed little change in ΔA, and no correlation between ΔA and their dipole moment was observed. we considered that the differences in the retentions of di-iodo benzenes were not a result of the π-π interaction. As mentioned above, the σ hole of iodine groups is the largest and shows the strongest halogen-π interactions amongst the halogen groups. Additionally, Präsang et al. reported that halogenated compounds showed stronger X-π interactions as the electron withdrawing functional groups were coordinated to the closed position on the aromatic rings.[60] In this case, the X-π interaction strength could be shown in the order of *o*- > *m*- > *p*-di-iode benzenes. This is because iodine also has an electron withdrawing effect and the strength of the withdrawing effect follows the order of *o*- > *m*- > *p*-di-iode benzenes.

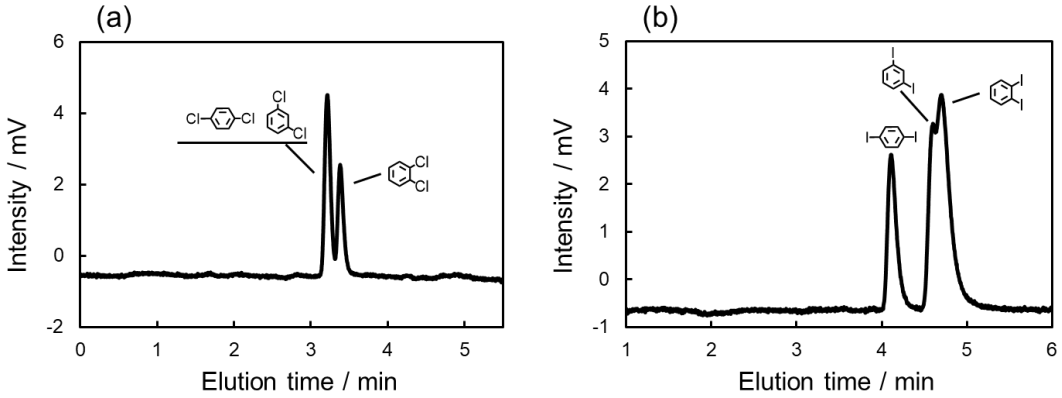

Figure 8. Chromatograms of the mixture of (a) di-chlorinated or (b) di-iodinated benzenes with the C70-coated column. Conditions: column, C70-coated (Type-2, 75.0 cm × 100 μm i.d.); flow rate; 2.0 μL min^{-1}; mobile phase, *n*-hexane; temperature, 25 ºC; detection, UV 228 nm.

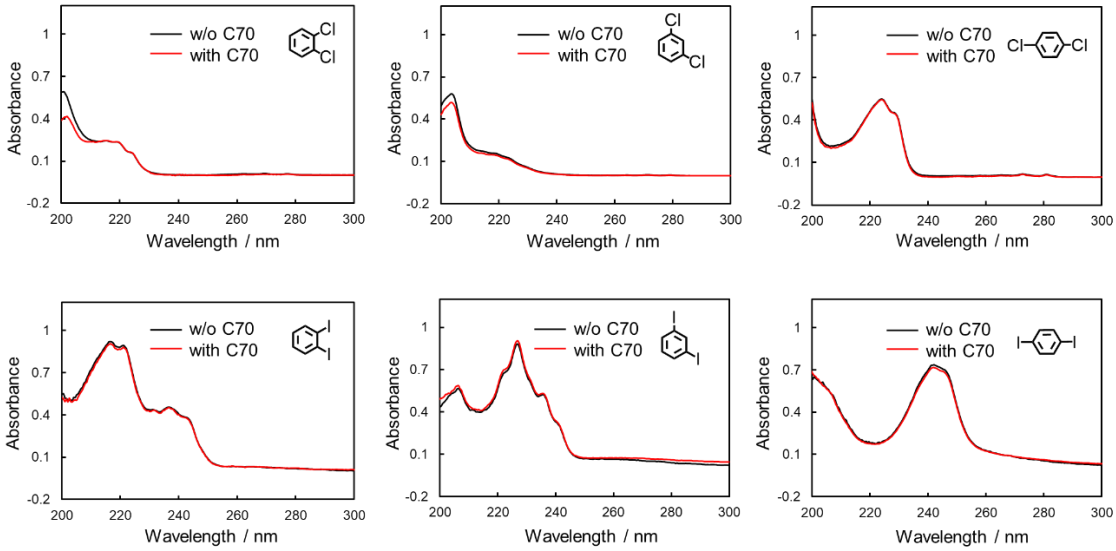

Figure 9. Absorption spectra of each chlorinated or iodinated benzenes solution in *n*-hexane with/without C70.

3-3-4 Effect of dielectric constants in mobile phases

As shown in equations (1) and (2), the induced-dipole interaction is strongly influenced by the dielectric constant (ε) of the solvents. Figure 10a shows the chromatograms of the mixtures of halogenated benzenes in *n*-hexane or *n*-octane mobile phases with the C70-coated column. As expected, the retentions for halogenated benzenes with the C70-coated column were drastically lower with *n*-octane than with *n*-hexane. To consider the effect of ε, we evaluated the retention behaviors of halogenated benzenes in several normal alkanes (NAs), which have different ε. Figure 10b shows a semilogarithmic plot of the retention factors for halogenated benzenes obtained with each NA against $1/\varepsilon^2$. The plot shows that ln k increased linearly with $1/\varepsilon^2$. This result was consistent with the expected trend given by equations (1) and (2) and clearly indicated that the retentions of halogenated benzenes were significantly impacted by the induced-dipole interaction.

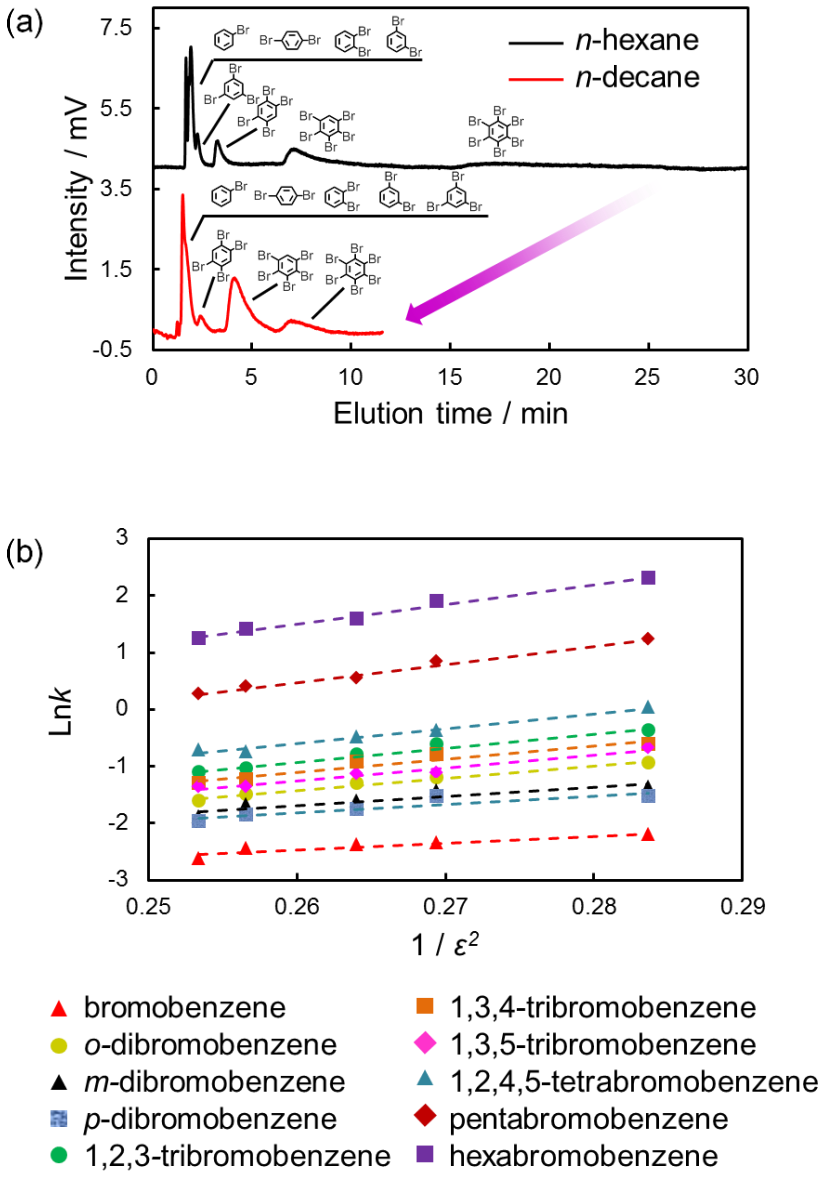

Figure 10. Chromatograms of the mixture of brominated benzenes with the C70-coated column (a) and ln *k* against $1/\varepsilon^2$ in each NA mobile phase (b). Conditions: column, C70-coated (Type-1, 25.5 cm × 100 μm i.d.); flow rate; 2.0 μL min^{-1}; mobile phase, *n*-hexane, *n*-heptane, *n*-octane, *n*-nonane, *n*-decane; temperature, 25 °C; detection, UV 228 nm.

3-3-5 Possibility of orbital interactions influencing X-π interactions

Because the σ hole behaves as an electron acceptor in halogen bonding, the contributions of the orbital interaction as well as electrostatic interaction have to be considered. Early in 1950, Mulliken showed experimental evidence of changes in the electronic structure occur upon formation of a halogen bonding.[61] Furthermore, many computational results have also supported the notion that orbital interactions affect halogen bonding.[62-65] However, several computational studies suggested an opposing view that the orbital interaction could not largely contribute to halogen bonding.[66-68] In order to promote such a complicated argument, We evaluated the contribution of orbital energy to the X-π interaction by ^{1}H NMR spectroscopy, which sensitively reflects the electronic state of protons. The No-D ^{1}H NMR spectra of *o*-dibromobenzene and pentabromobenzene in the presence of C70 in *n*-hexane were recorded and compared with each other. Peak shifts were not observed in *o*-dibromobenzene when *o*-dibromobenzene and C70 were mixed (Figure 11). However, when pentabromobenzene was mixed with C70, the peak in the pentabromobenzene spectrum shifted slightly upfield (Figure 11). These results suggested that a proton on the pentabromobenzene was placed into a more electron rich (more shielded) environment and that pentabromobenzene, as an electron acceptor of C70, might be subjected to the orbital interaction. Briefly, five bromine atoms on pentabromobenzene became electron rich from the molecular interaction with C70; this meant that the aromatic ring and its proton were also in electron rich conditions. In addition, we carried out computer simulations to determine the differences in orbital energy between the HOMO in C70-PFPA-NHS and the LUMO in each brominated benzene (Figure 11c). The differences in orbital energies of poly-brominated benzenes ($n > 2$) were much lower than that for dibromobenzenes and were more likely to cause orbital

interactions with C70-PFPA-NHS. Furthermore, the LUMOs of poly-brominated benzenes (n > 2) extended in the direction of the σ bond in the C—Br of the bromine atoms and matched the positions showing the X-π interactions (Figure 12). These results also suggested that orbital interactions might contribute to the X-π interaction.

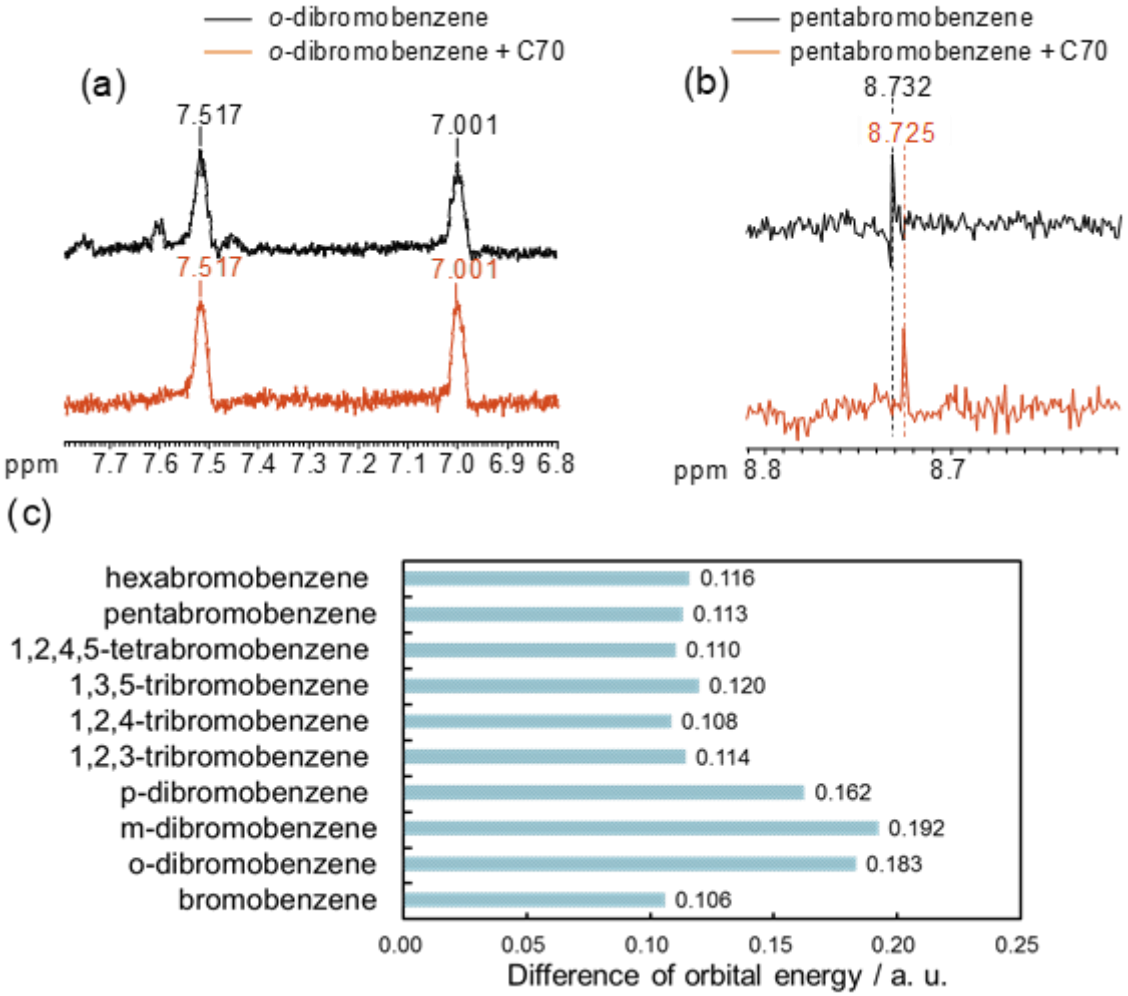

Figure 11. ^{1}H NMR spectra of *o*-dibromobenzene (a), pentabromobenzene (b) with/without C70 in *n*-hexane and the difference in orbital energy between HOMO in C70-PFPA-NHS and LUMO in each brominated benzene (c).

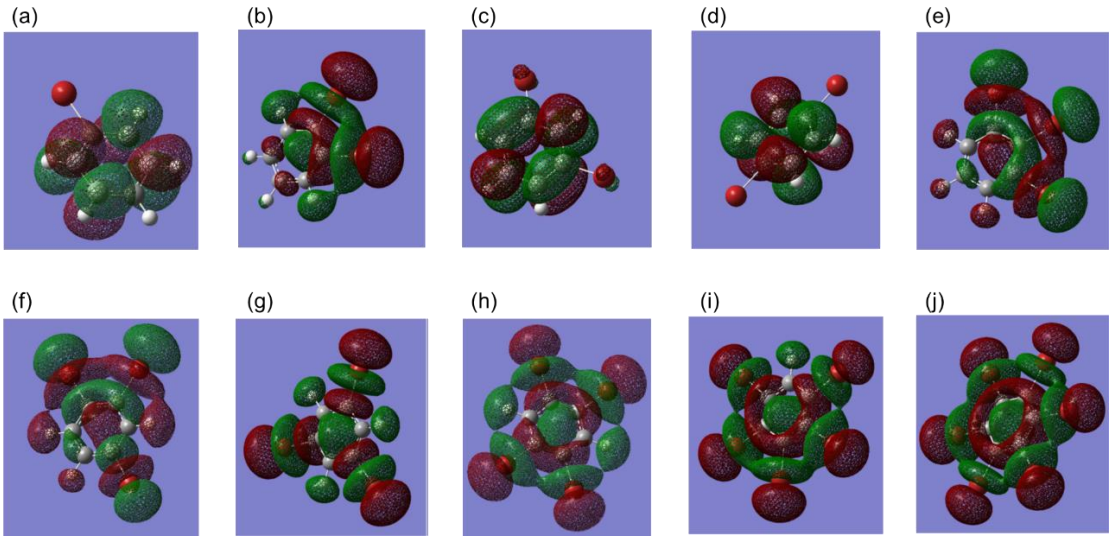

Figure 12. The LUMOs of each brominated benzene. (a) bromobenzene, (b) *o*-dibromobenznen, (c) *m*-dibromobenznene, (d) *p*-dibromobenznene, (e) 1,2,3-tribromobenzene, (f) 1,2,4-tribromobenznene, (g) 1,3,5-tribromobenzene, (h) 1,2,4,5-tetrabromobenzene, (i) pentabromobenzene, (j) hexabromobenznene.

3-3-6 One-pot separation of the entirety of brominated benzenes

In the above discussions, we clarified the presence of π-π and/or X-π interactions between halogenated benzenes and carbo-materials. In addition, we revealed the effect of the mobile phase as being against these π interactions. Finally, we were faced with the challenge of achieving the separation of halogenated benzenes in NPLC. This achievement will lead to efficient separations of aromatic halogens in oil. To realize this goal, we optimized the mobile phase conditions, in consideration of the dielectric effect, to achieve a one-pot separation of all isomers of brominated benzenes (11 analogues, Figure 13). The separation of halogenated benzenes in oil samples is a major issue in the field of environmental chemistry, since many halogenated benzenes are in waste oil and are highly toxic.[69-71] Therefore, the LC separation of halogenated benzenes has great importance in environmental chemistry and shows its potential for separating toxic aromatic halogens, such as polychlorinated biphenyls and polybrominated biphenyls.

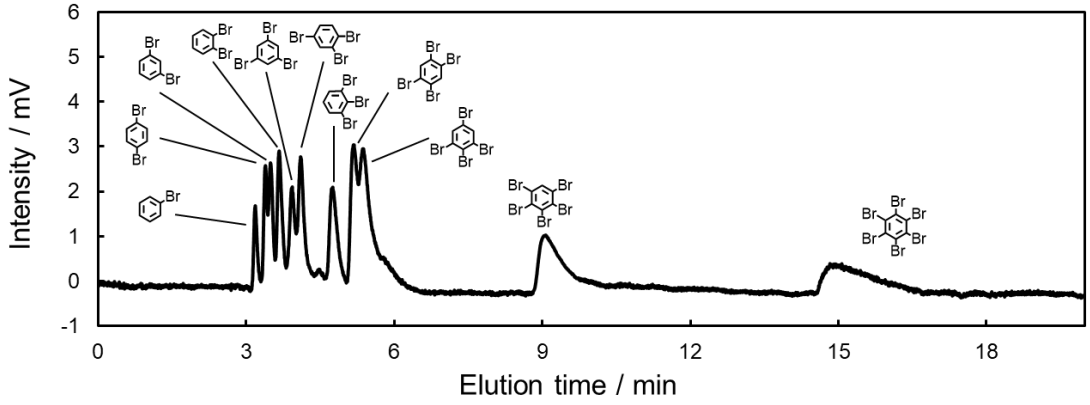

Figure 13. Chromatogram of all isomers of brominated benzenes with the C70-coated column in NPLC. Conditions: column, C70-coated (Type-2, 75.0 cm × 100 μm i.d.); flow rate; 2.0 μL min^{-1}; mobile phase, *n*-hexane/*n*-decane = 8/2; temperature, 25 °C; detection, UV 228 nm.

3-4 Conclusions

In this study, we experimentally evaluated the strength of the X-π interaction between carbon-materials and the variety of halogenated benzenes using NPLC, in which the hydrophobic interaction was completely suppressed. Higher retentions were observed as the number of Cl, Br, or we substitutions on the benzenes increased, especially for the C70-coated column, which showed higher retention efficiencies than other carbon materials. UV absorption spectra of mono- to tri- brominated benzenes were critically changed in the presence of C70, indicating that these compounds mainly interacted via the π-π interaction with C70. Furthermore, the number of bromine substitutions affected the strength of the X-π interaction with C70. The ^{1}H NMR spectra of *o*-dibromobenzene and pentabromobenzene in the presence of C70 also showed the possibility for orbital interactions based on the X-π interaction. Thus, we supposed the existence of bimodal interactions, the π-π and X-π interactions, between the halogenated benzenes and aromatic materials. Using this new knowledge, we successfully demonstrated the effective separation of di- or tri-bromo benzene isomers and 11 brominated benzene analogues with a C70-coated column in NPLC by optimizing the mobile phase conditions. We believe that this report greatly contributes to elucidation of the X-π interaction and efficient separations of halogenated environmental pollutants.

3-5 References

1. Kolar, M. H.; Hobza, P., Computer Modeling of Halogen Bonds and Other sigma-Hole Interactions. *Chem. Rev.* **2016,** *116*, 5155-5187.
2. Cavallo, G.; Metrangolo, P.; Milani, R.; Pilati, T.; Priimagi, A.; Resnati, G.; Terraneo, G., The Halogen Bond. *Chem. Rev.* **2016,** *116*, 2478-2601.
3. Wilcken, R.; Zimmermann, M. O.; Lange, A.; Joerger, A. C.; Boeckler, F. M., Principles and Applications of Halogen Bonding in Medicinal Chemistry and Chemical Biology. *J. Med. Chem.* **2013,** *56*, 1363-1388.
4. Kozuch, S.; Martin, J. M. L., Halogen Bonds: Benchmarks and Theoretical Analysis. *J. Chem. Theory Comput.* **2013,** *9*, 1918-1931.
5. Erdelyi, M., A big hello to halogen bonding. *Nat. Chem.* **2014,** *6*, 762.
6. Danelius, E.; Andersson, H.; Jarvoll, P.; Lood, K.; Gräfenstein, J.; Erdélyi, M., Halogen Bonding: A Powerful Tool for Modulation of Peptide Conformation. *Biochemistry* **2017,** *56*, 3265-3272.
7. Erdélyi, M., Application of the Halogen Bond in Protein Systems. *Biochemistry* **2017,** *56*, 2759-2761.
8. Mukherjee, A.; Tothadi, S.; Desiraju, G. R., Halogen Bonds in Crystal Engineering: Like Hydrogen Bonds yet Different. *Acc. Chem. Res.* **2014,** *47*, 2514-2524.
9. Arman, H. D.; Rafferty, E. R.; Bayse, C. A.; Pennington, W. T., Complementary Selenium···Iodine Halogen Bonding and Phenyl Embraces: Cocrystals of Triphenylphosphine Selenide with Organoiodides. *Cryst. Growth Des.* **2012,** *12*, 4315-4323.
10. Ouvrard, C.; Le Questel, J.-Y.; Berthelot, M.; Laurence, C., Halogen-bond geometry: a crystallographic database investigation of dihalogen complexes. *Acta Crystallogr.*

B **2003,** *59*, 512-526.

11. El-Sheshtawy, H. S.; Bassil, B. S.; Assaf, K. I.; Kortz, U.; Nau, W. M., Halogen Bonding inside a Molecular Container. *J. Am. Chem. Soc.* **2012,** *134*, 19935-19941.
12. Metrangolo, P.; Neukirch, H.; Pilati, T.; Resnati, G., Halogen Bonding Based Recognition Processes: A World Parallel to Hydrogen Bonding. *Acc. Chem. Res.* **2005,** *38*, 386-395.
13. Langton, M. J.; Robinson, S. W.; Marques, I.; Félix, V.; Beer, P. D., Halogen bonding in water results in enhanced anion recognition in acyclic and rotaxane hosts. *Nat. Chem.* **2014,** *6*, 1039.
14. Tresca, B. W.; Brueckner, A. C.; Haley, M. M.; Cheong, P. H. Y.; Johnson, D. W., Computational and Experimental Evidence of Emergent Equilibrium Isotope Effects in Anion Receptor Complexes. *Journal of the American Chemical Society* **2017,** *139*, 3962-3965.
15. Noh, J.; Jung, S.; Koo, D. G.; Kim, G.; Choi, K. S.; Park, J.; Shin, T. J.; Yang, C.; Park, J., Thienoisoindigo-Based Semiconductor Nanowires Assembled with 2-Bromobenzaldehyde via Both Halogen and Chalcogen Bonding. *Sci. Rep.* **2018,** *8*, 14448.
16. Priimagi, A.; Cavallo, G.; Metrangolo, P.; Resnati, G., The halogen bond in the design of functional supramolecular materials: recent advances. *Acc. Chem. Res.* **2013,** *46*, 2686-2695.
17. González-Rodríguez, D.; Schenning, A. P. H. J., Hydrogen-bonded Supramolecular π-Functional Materials. *Chem. Mater.* **2011,** *23*, 310-325.
18. Fernandez-Palacio, F.; Poutanen, M.; Saccone, M.; Siiskonen, A.; Terraneo, G.; Resnati, G.; Ikkala, O.; Metrangolo, P.; Priimagi, A., Efficient Light-Induced Phase

Transitions in Halogen-Bonded Liquid Crystals. *Chem. Mater.* **2016,** *28*, 8314-8321.

19. Nguyen, H. L.; Horton, P. N.; Hursthouse, M. B.; Legon, A. C.; Bruce, D. W., Halogen Bonding: A New Interaction for Liquid Crystal Formation. *J. Am. Chem. Soc.* **2004,** *126*, 16-17.
20. Barendt, T. A.; Docker, A.; Marques, I.; Félix, V.; Beer, P. D., Selective Nitrate Recognition by a Halogen-Bonding Four-Station [3]Rotaxane Molecular Shuttle. *Angew. Chem. Int. Ed.* **2016,** *55*, 11069-11076.
21. Vanderkooy, A.; Pfefferkorn, P.; Taylor, M. S., Self-Assembly of Polymer Nanostructures through Halogen Bonding Interactions of an Iodoperfluoroarene-Functionalized Polystyrene Derivative. *Macromolecules* **2017,** *50*, 3807-3817.
22. Auffinger, P.; Hays, F. A.; Westhof, E.; Ho, P. S., Halogen bonds in biological molecules. *Proc. Natl. Acad. Sci. U. S. A.* **2004,** *101*, 16789.
23. Lu, Y.; Shi, T.; Wang, Y.; Yang, H.; Yan, X.; Luo, X.; Jiang, H.; Zhu, W., Halogen Bonding—A Novel Interaction for Rational Drug Design? *J. Med. Chem.* **2009,** *52*, 2854-2862.
24. Hardegger, L. A.; Kuhn, B.; Spinnler, B.; Anselm, L.; Ecabert, R.; Stihle, M.; Gsell, B.; Thoma, R.; Diez, J.; Benz, J.; Plancher, J.-M.; Hartmann, G.; Banner, D. W.; Haap, W.; Diederich, F., Systematic Investigation of Halogen Bonding in Protein–Ligand Interactions. *Angew. Chem. Int. Ed.* **2011,** *50*, 314-318.
25. Yabe-Nishimura, C., Aldose Reductase in Glucose Toxicity: A Potential Target for the Prevention of Diabetic Complications. *Pharmacol. Rev.* **1998,** *50*, 21.
26. Himmel, D. M.; Das, K.; Clark, A. D.; Hughes, S. H.; Benjahad, A.; Oumouch, S.; Guillemont, J.; Coupa, S.; Poncelet, A.; Csoka, I.; Meyer, C.; Andries, K.; Nguyen, C. H.; Grierson, D. S.; Arnold, E., Crystal Structures for HIV-1 Reverse Transcriptase

in Complexes with Three Pyridinone Derivatives: A New Class of Non-Nucleoside Inhibitors Effective against a Broad Range of Drug-Resistant Strains. *J. Med. Chem.* **2005,** *48*, 7582-7591.

27. Cao, J.; Yan, X.; He, W.; Li, X.; Li, Z.; Mo, Y.; Liu, M.; Jiang, Y.-B., C–I···π Halogen Bonding Driven Supramolecular Helix of Bilateral N-Amidothioureas Bearing β-Turns. *J. Am. Chem. Soc.* **2017,** *139*, 6605-6610.
28. Heroven, C.; Georgi, V.; Ganotra, G. K.; Brennan, P.; Wolfreys, F.; Wade, R. C.; Fernández-Montalván, A. E.; Chaikuad, A.; Knapp, S., Halogen–Aromatic π Interactions Modulate Inhibitor Residence Times. *Angew. Chem. Int. Ed.* **2018,** *57*, 7220-7224.
29. Matter, H.; Nazaré, M.; Güssregen, S.; Will, D. W.; Schreuder, H.; Bauer, A.; Urmann, M.; Ritter, K.; Wagner, M.; Wehner, V., Evidence for C-Cl/C-Br· · ·π Interactions as an Important Contribution to Protein–Ligand Binding Affinity. *Angew. Chem. Int. Ed.* **2009,** *48*, 2911-2916.
30. Shah, M. B.; Liu, J.; Zhang, Q.; Stout, C. D.; Halpert, J. R., Halogen−π Interactions in the Cytochrome P450 Active Site: Structural Insights into Human CYP2B6 Substrate Selectivity. *ACS Chem. Biol.* **2017,** *12*, 1204-1210.
31. Voth Regier, A.; Ho Shing, P., The Role of Halogen Bonding in Inhibitor Recognition and Binding by Protein Kinases. *Curr. Top. Med. Chem.* **2007,** *7*, 1336-1348.
32. Lu, Y.; Wang, Y.; Zhu, W., Nonbonding interactions of organic halogens in biological systems: implications for drug discovery and biomolecular design. *Phys. Chem. Chem. Phys.* **2010,** *12*, 4543-4551.
33. Tsuzuki, S.; Uchimaru, T.; Wakisaka, A.; Ono, T., Magnitude and Directionality of Halogen Bond of Benzene with C6F5X, C6H5X, and CF3X (X = I, Br, Cl, and F). *J.*

Phys. Chem. A **2016,** *120*, 7020-7029.

34. Youn, I. S.; Kim, D. Y.; Cho, W. J.; Madridejos, J. M. L.; Lee, H. M.; Kołaski, M.; Lee, J.; Baig, C.; Shin, S. K.; Filatov, M.; Kim, K. S., Halogen−π Interactions between Benzene and X2/CX4 (X = Cl, Br): Assessment of Various Density Functionals with Respect to CCSD(T). *J. Phys. Chem. A* **2016,** *120*, 9305-9314.
35. Awwadi, F. F.; Taher, D.; Haddad, S. F.; Turnbull, M. M., Competition between Hydrogen and Halogen Bonding Interactions: Theoretical and Crystallographic Studies. *Cryst. Growth Des.* **2014,** *14*, 1961-1971.
36. Aakeröy, C. B.; Fasulo, M.; Schultheiss, N.; Desper, J.; Moore, C., Structural Competition between Hydrogen Bonds and Halogen Bonds. *J. Am. Chem. Soc.* **2007,** *129*, 13772-13773.
37. Zha, B.; Dong, M.; Miao, X.; Peng, S.; Wu, Y.; Miao, K.; Hu, Y.; Deng, W., Cooperation and competition between halogen bonding and van der Waals forces in supramolecular engineering at the aliphatic hydrocarbon/graphite interface: position and number of bromine group effects. *Nanoscale* **2017,** *9*, 237-250.
38. Kimata, K.; Hosoya, K.; Araki, T.; Tanaka, N., [2-(1-Pyrenyl)ethyl]silyl silica packing material for liquid chromatographic separation of fullerenes. *J. Org. Chem.* **1993,** *58*, 282-283.
39. Chen, S.; Meyerhoff, M., Shape-Selective Retention of Polycyclic Aromatic Hydrocarbons on Metalloprotoporphyrin−Silica Phases: Effect of Metal Ion Center and Porphyrin Coverage. *Analytical Chemistry* **1998,** *70*, 2523-2529.
40. Kubo, T.; Kanao, E.; Matsumoto, T.; Naito, T.; Sano, T.; Yan, M.; Otsuka, K., Specific Intermolecular Interactions by the Localized π-Electrons in C70-fullerene. *ChemistrySelect* **2016,** *1*, 5900-5904.

41. Kubo, T.; Murakami, Y.; Tsuzuki, M.; Kobayashi, H.; Naito, T.; Sano, T.; Yan, M.; Otsuka, K., Unique Separation Behavior of a C60 Fullerene-Bonded Silica Monolith Prepared by an Effective Thermal Coupling Agent. *Chem.: Eur. J.* **2015,** *21*, 18095-18098.
42. Kanao, E.; Kubo, T.; Naito, T.; Matsumoto, T.; Sano, T.; Yan, M.; Otsuka, K., Differentiating π interactions by constructing concave/convex surfaces using a bucky bowl molecule, corannulene in liquid chromatography. *Analytical chemistry* **2019,** *91*, 2439-2446.
43. Kanao, E.; Naito, T.; Kubo, T.; Otsuka, K., Development of a C70-Fullerene Bonded Silica-Monolithic Capillary and Its Retention Characteristics in Liquid Chromatography. *Chromatography* **2017,** *38*, 45-51.
44. Hadi, P.; Xu, M.; Lin, C. S. K.; Hui, C. W.; McKay, G., Waste printed circuit board recycling techniques and product utilization. *J. Hazard. Mater.* **2015,** *283*, 234-243.
45. Quinete, N.; Esser, A.; Kraus, T.; Schettgen, T., Determination of hydroxylated polychlorinated biphenyls (OH-PCBs) in human urine in a highly occupationally exposed German cohort: New prospects for urinary biomarkers of PCB exposure. *Environ. Int.* **2016,** *97*, 171-179.
46. Law, R. J.; Covaci, A.; Harrad, S.; Herzke, D.; Abdallah, M. A. E.; Femie, K.; Toms, L. M. L.; Takigami, H., Levels and trends of PBDEs and HBCDs in the global environment: Status at the end of 2012. *Environ. Int.* **2014,** *65*, 147-158.
47. Malliari, E.; Kalantzi, O. I., Children's exposure to brominated flame retardants in indoor environments - A review. *Environ. Int.* **2017,** *108*, 146-169.
48. McGrath, T. J.; Ball, A. S.; Clarke, B. O., Critical review of soil contamination by polybrominated diphenyl ethers (PBDEs) and novel brominated flame retardants

(NBFRs); concentrations, sources and congener profiles. *Environ. Pollut.* **2017,** *230*, 741-757.

49. Roper, L. C.; Präsang, C.; Whitwood, A. C.; Bruce, D. W., A halogen-bonded complex of DMAP with 4-bromoiodobenzene. *CrystEngComm* **2010,** *12*, 3382-3384.
50. Ibrahim, M. A. A., Molecular mechanical study of halogen bonding in drug discovery. *J. Comput. Chem.* **2011,** *32*, 2564-2574.
51. Vijay Solomon, R.; Angeline Vedha, S.; Venuvanalingam, P., A new turn in codon–anticodon selection through halogen bonds. *Phys. Chem. Chem. Phys.* **2014,** *16*, 7430-7440.
52. Karachevtsev, V. A.; Plokhotnichenko, A. M.; Karachevtsev, M. V.; Leontiev, V. S., Decrease of carbon nanotube UV light absorption induced by π–π-stacking interaction with nucleotide bases. *Carbon* **2010,** *48*, 3682-3691.
53. Wang, T.-H.; Hsu, C.-S.; Huang, W.-L.; Lo, Y.-H., Structures, molecular orbitals and UV–vis spectra investigations on Br2C6H4: A computational study. *Spectrochim. Acta A* **2013,** *115*, 866-875.
54. Trnka, J.; Sedlak, R.; Kolář, M.; Hobza, P., Differences in the Sublimation Energy of Benzene and Hexahalogenbenzenes Are Caused by Dispersion Energy. *J. Phys. Chem. A* **2013,** *117*, 4331-4337.
55. Forni, A.; Pieraccini, S.; Rendine, S.; Sironi, M., Halogen bonds with benzene: An assessment of DFT functionals. *J. Comput. Chem.* **2014,** *35*, 386-394.
56. Tsuzuki, S.; Honda, K.; Uchimaru, T.; Mikami, M.; Tanabe, K., Origin of Attraction and Directionality of the π/π Interaction: Model Chemistry Calculations of Benzene Dimer Interaction. *J. Am. Chem. Soc.* **2002,** *124*, 104-112.
57. Lima, C. F. R. A. C.; Rocha, M. A. A.; Gomes, L. R.; Low, J. N.; Silva, A. M. S.;

Santos, L. M. N. B. F., Experimental Support for the Role of Dispersion Forces in Aromatic Interactions. *Chem.: Eur. J.* **2012,** *18*, 8934-8943.

58. Wallnoefer, H. G.; Fox, T.; Liedl, K. R.; Tautermann, C. S., Dispersion dominated halogen–π interactions: energies and locations of minima. *Phys. Chem. Chem. Phys.* **2010,** *12*, 14941-14949.
59. Kanao, E.; Kubo, T.; Naito, T.; Matsumoto, T.; Sano, T.; Yan, M.; Otsuka, K., Isotope Effects on Hydrogen Bonding and CH/CD−π Interaction. *The Journal of Physical Chemistry C* **2018,** *122*, 15026-15032.
60. Präsang, C.; Whitwood, A. C.; Bruce, D. W., Halogen-Bonded Cocrystals of 4-(N,N-Dimethylamino)pyridine with Fluorinated Iodobenzenes. *Cryst. Growth Des.* **2009,** *9*, 5319-5326.
61. Mulliken, R. S., Structures of Complexes Formed by Halogen Molecules with Aromatic and with Oxygenated Solvents1. *J. Am. Chem. Soc.* **1950,** *72*, 600-608.
62. Palusiak, M., On the nature of halogen bond – The Kohn–Sham molecular orbital approach. *J. Mol. Struct.* **2010,** *945*, 89-92.
63. Wang, C.; Danovich, D.; Mo, Y.; Shaik, S., On The Nature of the Halogen Bond. *J. Chem. Theory Comput.* **2014,** *10*, 3726-3737.
64. Wolters, L. P.; Bickelhaupt, F. M., Halogen Bonding versus Hydrogen Bonding: A Molecular Orbital Perspective. *ChemistryOpen* **2012,** *1*, 96-105.
65. Desiraju Gautam, R.; Ho, P. S.; Kloo, L.; Legon Anthony, C.; Marquardt, R.; Metrangolo, P.; Politzer, P.; Resnati, G.; Rissanen, K., Definition of the halogen bond (IUPAC Recommendations 2013). *Pure Appl. Chem.* **2013**, *85*, 1711-1713.
66. Riley, K. E.; Hobza, P., Investigations into the Nature of Halogen Bonding Including Symmetry Adapted Perturbation Theory Analyses. *J. Chem. Theory Comput.* **2008,**

4, 232-242.

67. Tsuzuki, S.; Wakisaka, A.; Ono, T.; Sonoda, T., Magnitude and Origin of the Attraction and Directionality of the Halogen Bonds of the Complexes of C6F5X and C6H5X (X=I, Br, Cl and F) with Pyridine. *Chem.: Eur. J.* **2012,** *18*, 951-960.
68. Řezáč, J.; de la Lande, A., On the role of charge transfer in halogen bonding. *Phys. Chem. Chem. Phys.* **2017,** *19*, 791-803.
69. Jaward, F. M.; Farrar, N. J.; Harner, T.; Sweetman, A. J.; Jones, K. C., Passive Air Sampling of PCBs, PBDEs, and Organochlorine Pesticides Across Europe. *Environ. Sci. Technol.* **2004,** *38*, 34-41.
70. Jacobson, M. H.; Darrow, L. A.; Barr, D. B.; Howards, P. P.; Lyles, R. H.; Terrell, M. L.; Smith, A. K.; Conneely, K. N.; Marder, M. E.; Marcus, M., Serum Polybrominated Biphenyls (PBBs) and Polychlorinated Biphenyls (PCBs) and Thyroid Function among Michigan Adults Several Decades after the 1973-1974 PBB Contamination of Livestock Feed. *Environ. Health Perspect.* **2017,** *125*, 97020.
71. Safe, S.; Hutzinger, O., Polychlorinated Biphenyls (PCBs) and Polybrominated Biphenyls (PBBs): Biochemistry, Toxicology, and Mechanism of Action. *Crit. Rev. Toxicol.* **1984,** *13*, 319-395.

Chapter 4

Isotope Effects on Hydrogen Bonding and CH/CD-π Interaction

4-1 Introduction

As a simple approach for enhancing pharmacological effects, deuteration of drugs has attracted interests for more than 50 years.[1, 2] Deuteration of drugs can have significant effects for improving the circulation life time of drugs *in vivo* and for reducing toxic substances derived from the metabolism, because deuterated compounds are less susceptible to metabolism by enzymes such as Cytochrome P450s.[3] So far, a number of deuterated drugs have been developed,[4, 5] e.g. Venlafaxine for geriatric depression, Ivacaftor for cystic fibrosis, and Ruxolitinib for alopecia areata. Furthermore, the competition for the development of deuterated drugs among pharmaceutical companies might become more intense, as exemplified by the approval of deuterated Tetrabenazine,[6, 7] which is a drug for the symptomatic treatment of hyperkinetic movement disorders and was developed by Teva®, by the Food and Drug administration (FDA). In order to achieve such isotope effects, it is obviously important to isolate one isotope analogue from the others so that the deuterated drugs can be obtained in high concentrations. Therefore, purification techniques of deuterated compounds are expected to be in high demand.

However, as the chemical properties of isotopologues are exactly alike, it is therefore difficult to distinguish them. The isotopes have the same number of electrons and there

is no difference between the wave function and the potential curved surface in the Born-Oppenheimer approximation. On the other hand, there is a difference in vibration energy of C–H and C–D bonds due to the difference of the mass number.[8–10] Here, the Gibbs free energy can be expressed in the following equations.

$$\text{Vibration energy} \ : \ G_{\text{vibration}} = h\nu\,(n + 1)$$

$$\text{Stretching frequency} \ : \ \nu = (1 / 2\pi)\sqrt{}\,(ks / \mu)$$

where, h is the Planck constant, n is the principal number, k_S is the spring constant of chemical bond, and μ is the reduced mass of atoms involved in chemical bond. A chemical bond with a deuterium is more stable than that with a protium resulting from a lower vibration energy and deuterium has a larger mass number than protium. Vibration energy also contributes to intermolecular interactions.[11–13] In a computational study, Bell et al. reported isotope effects of the hydrogen bonding between formamidine and solvent molecules using *Ab* initio calculation.[14] In supramolecular chemistry, Tresca et al. demonstrated isotope effects between chloride ion and deuterated anion receptor complexes both by calculation and experimentally.[15] These studies imply the potential that the separation techniques of isotopologues might be established by utilizing isotope effect of intramolecular interactions.

High performance liquid chromatography (HPLC), which is the most used separation technique and is based on the difference in partition coefficients of the solute between the mobile and stationary phases, sensitively reflects the strength of intermolecular interactions. Tanaka et al. succeeded in the separation of compounds containing isotopes of ^{15}N and ^{18}O on a recycle HPLC system.[16] In another successful example, Tsurowski et al. reported the separation of isotopologues on reversed phase liquid chromatography (RPLC).[17] They found that the protiated compounds were more hydrophobic than

deuterated ones, and pointed out the CH-π interaction[18–20] was involved in the separation of the isotopologues by RPLC. However, the effect of the interactions with the mobile phases was not considered in this study, even though the affinity between the mobile phases and solutes contributed to the hydrophobic interaction. We hypothesize that the interaction with hydrophilic solvents cannot be ignored even with hydrophobic molecules. Our anticipation is also encouraged by a literature, which reported the presence of hydrogen bonding interaction between benzene and water.[21] In addition, the CH-π interaction deriving from their stationary phases was very weak, and the influence of the CH-π interaction for the separation of isotopologues has been ambiguous. In particular, Zhao et al. described that there is no difference in the intensity between the CH-π and CD-π interactions, and completely contradicted the report by Tsurowski.[22] Thus, it is necessary to reconsider the influence of the mobile phase–solute interaction or CH-π interaction in the separation of isotopologues.

We succeeded in the immobilization of fullerenes onto a silica-monolithic capillary[23, 24] in order to develop a new separation medium providing strong π interaction[25–27] derived from aromatic structures. We evaluated characteristics of the fullerene-coated silica monolithic capillaries by normal phase liquid chromatography (NPLC), in which hydrophobic interaction was completely reduced, and several polycyclic aromatic hydrocarbons (PAHs) were successfully separated by the effective π–π interaction.[28, 29] In particular, a C_{70} fullerene-coated silica monolithic capillary (C70 column) showed the retention of corannulene as a hemispherical molecule based on the π–π interaction and halogenated benzenes based on halogen-π interaction due to much stronger π interaction than any other commercially available columns.[30, 31]

In this article, we investigate the effect of solvents in the mobile phase and

isotopologues as the solutes in LC evaluations with a variety of columns. We discuss the contribution of intramolecular interactions to the separation of isotopologues by RPLC and evaluate the separation of isotopologues due to the hydrogen bonding. Furthermore, we examined the effect of the CH-π interaction with the C70 column to confirm the strength of the CH-π interaction and the effect of the CH-π interaction on the separation of isotopologues by NPLC.

4-2 Experimental Section

4-2-1 Materials

Acetone, benzene, diethyl ether, sodium hydroxide, dichloromethane, chlorobenzene, toluene, ethyl acetate, methanol, acetonitrile and n-hexane were purchased from Nacalai Tesque (Kyoto, Japan), methyl pentafluorobenzoate, diethyl amine, urea, acetic acid, and 3-aminopropyltrimethoxysilane (APTMS) from Tokyo Chemical Industry (Tokyo, Japan), sodium azide, *N*-hydroxysuccinimide (NHS), and 1-ethyl-3-(3-dimethylaminopropyl)carbodiimide (EDAC) from Wako Pure Chemical Industries (Osaka, Japan), polyethylene glycol (PEG) (Mn=10,000), benzene-d6, toluene-d8, naphthalene-d8, o-xylene, 1,2,4-trimethylbenzene, 1,2,4,5-tetramethylbenzene, pentamethylbenzene, C60-fullerene (C60), C70-fullerene (C70), phenanthrene, phenanthlene-d10, hexamethylbenzene (HMB), hexamethylbenzene-d18 (HMB-d18) from Sigma-Aldrich Japan (Tokyo, Japan), respectively. Deionized water was obtained from a Milli-Q Direct-Q 3UV system (Merck Millipore, Tokyo, Japan). A COSMOSIL PYE® and COSMOSIL PBB–R® (PBB) was purchased from Nacalai Tesque, Mightysil RP–18GPII® (ODS) was purchased from KANTO CHEMICAL (Tokyo, Japan), Silica-150 (silica-150) are purchased from TOSOH Corporation (Tokyo, Japan) and a fused-silica capillary from Polymicro Technologies Inc. (Phoenix, AZ).

4-2-2 Instruments

A capillary liquid chromatographic system consisted of a DiNa S (KYA Technologies Co., Tokyo, Japan) as a pump, CE-2070 (JASCO, Tokyo, Japan) as a UV detector, CHEMINERT (Valco Instruments Co., Huston, TX) as a sample injector, and Chemco

capillary column conditioner Model 380-b (Chemco Co. Osaka, Japan) as a column oven. An HPLC system consisted of a Prominence series (Shimadzu Co., Kyoto, Japan). FT-IR, NMR, elemental analysis, and fast atom bombardment mass spectrometry (FABMS) were carried out by a Nicolet iS5 ATR (Thermo Fisher Scientific K. K., Yokohama, Japan), JNM-ECA500 spectrometer (JEOL, Tokyo, Japan), Flash EA1112 (Thermo Fisher Scientific K. K.), and JMS-700 (JEOL), respectively.

4-2-3 HPLC and nano LC methods

C60 fullerene-coated silica monolithic column (C60 column) and C70 column were prepared following the protocols in previous chapter (Chapter 2). The commercially available columns containing 5PYE, PBB, ODS and silica-150 were evaluated by typical liquid chromatographic system, Prominence series. The capillary columns containing C60 or C70 columns were evaluated by a home-made nano flow system consisting of a DiNa S as the pump, CE-2070 as the UV detector, CHEMINERT as the sample injector, and Chemco capillary column conditioner Model 380-b as the column oven for isothermal operations. In both systems, we employed normal and reverse phase modes.

4-3 Results and Discussion

4-3-1 Effect of mobile phase on isotope effect in RPLC

In order to elucidate the mechanism of the separation of isotopologues in RPLC, we evaluated the separation behavior of isotopologues on various columns (Figure 1). The partition coefficient of an isotopologue in chromatography is expressed as the retention factor, *k*.

$$k_H = (t_H - t_0) / t_0,\ k_D = (t_D - t_0) / t_0$$

$$\alpha_{IE} = k_H / k_D$$

where, t_H and t_D are the retention times of protiated and deuterated compounds, respectively, and t_0 is the retention time of an unretained solute. α_{IE} shows the ratio of k_H to k_D. The obtained values of k_H, k_D and α_{IE} are summarized in Table 1-3. Comparing the retention factors, protiated compounds were retained more than deuterated ones. Additionally, it found that α_{IE} increased with the percent of water in the mobile phase for all columns (Figure 2). These results are consistent with the previous report by Tsurowski et al. stating that the hydrophobic interaction contributed to the separation of isotopologues since a protiated compound is more hydrophobic than a deuterated compound.

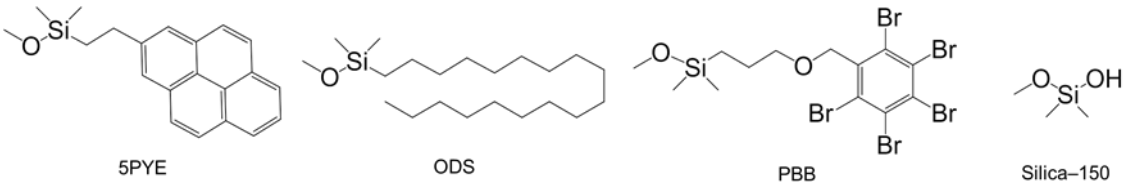

Figure 1. Structures of the stationary phases used.

Table 1. k_H, k_D, and α_{IE} in methanol / water mobile phase on ODS column.

	water / methanol (v / v)	k_H	k_D	α_{IE}
benzene	2 / 8	0.609	0.607	1.003
	3 / 7	1.162	1.150	1.011
	4 / 6	2.172	2.097	1.036
toluene	2 / 8	0.987	0.985	1.002
	3 / 7	2.038	1.996	1.021
	4 / 6	4.121	3.972	1.037
naphthalene	2 / 8	1.309	1.263	1.037
	3 / 7	2.965	2.822	1.051
	4 / 6	6.571	6.227	1.055
phenanthrene	2 / 8	2.847	2.670	1.066
	3 / 7	7.460	6.974	1.070
	4 / 6	19.247	17.878	1.077
HMB	2 / 8	6.896	6.405	1.077
	3 / 7	19.210	17.668	1.087
	4 / 6	59.327	53.618	1.106

Conditions: column, Conditions: column, ODS (Kanto kagaku, 150 mm × 4.6 mm i.d.); flow rate, 2.0 mL min^{-1}; mobile phase, water / methanol; detection, UV 254 nm (benzene, naphthalene, phenanthrene), 220 nm (toluene, HMB); temperature, 40.0 °C.

Table 2. k_H, k_D, and α_{IE} in methanol / water mobile phase on PBB column.

	water / methanol (v / v)	k_H	k_D	α_{IE}
benzene	2 / 8	0.231	0.230	1.005
	3 / 7	0.519	0.510	1.017
	4 / 6	1.084	1.046	1.037
toluene	2 / 8	0.398	0.398	1.000
	3 / 7	0.959	0.950	1.010
	4 / 6	2.106	2.028	1.039
naphthalene	2 / 8	1.283	1.280	1.003
	3 / 7	3.058	3.027	1.010
	4 / 6	7.225	6.846	1.055
phenanthrene	2 / 8	5.890	5.585	1.055
	3 / 7	15.853	14.895	1.064
	4 / 6	46.771	43.426	1.077
HMB	2 / 8	7.857	7.299	1.076
	3 / 7	22.747	20.776	1.095
	4 / 6	68.878	61.852	1.114

Conditions: column, Conditions: column, PBB (Nacalai Tesque, 150 mm × 2.0 mm i.d.); flow rate, 1.0 mL min^{-1}; mobile phase, water / methanol; detection, UV 254 nm (benzene, naphthalene, phenanthrene), 220 nm (toluene, HMB); temperature, 40.0 °C.

Table 3. k_H, k_D, and α_{IE} in methanol / water mobile phase on 5PYE column.

	water / methanol (v / v)	k_H	k_D	α_{IE}
benzene	2 / 8	0.371	0.370	1.002
	3 / 7	0.694	0.678	1.024
	4 / 6	1.347	1.292	1.043
toluene	2 / 8	0.544	0.540	1.006
	3 / 7	1.100	1.077	1.021
	4 / 6	2.315	2.200	1.052
naphthalene	2 / 8	1.058	1.046	1.011
	3 / 7	2.337	2.249	1.039
	4 / 6	5.388	5.105	1.055
phenanthrene	2 / 8	3.300	3.106	1.063
	3 / 7	8.741	8.177	1.069
	4 / 6	24.717	22.957	1.077
HMB	2 / 8	4.916	4.479	1.098
	3 / 7	13.753	12.400	1.109
	4 / 6	40.025	35.551	1.126

Conditions: column, Conditions: column, 5PYE (Nacalai Tesque, 150 mm × 4.6 mm i.d.); flow rate, 2.0 mL min^{-1}; mobile phase, water / methanol; detection, UV 254 nm (benzene, naphthalene, phenanthrene), 220 nm (toluene, HMB); temperature, 40.0 °C.

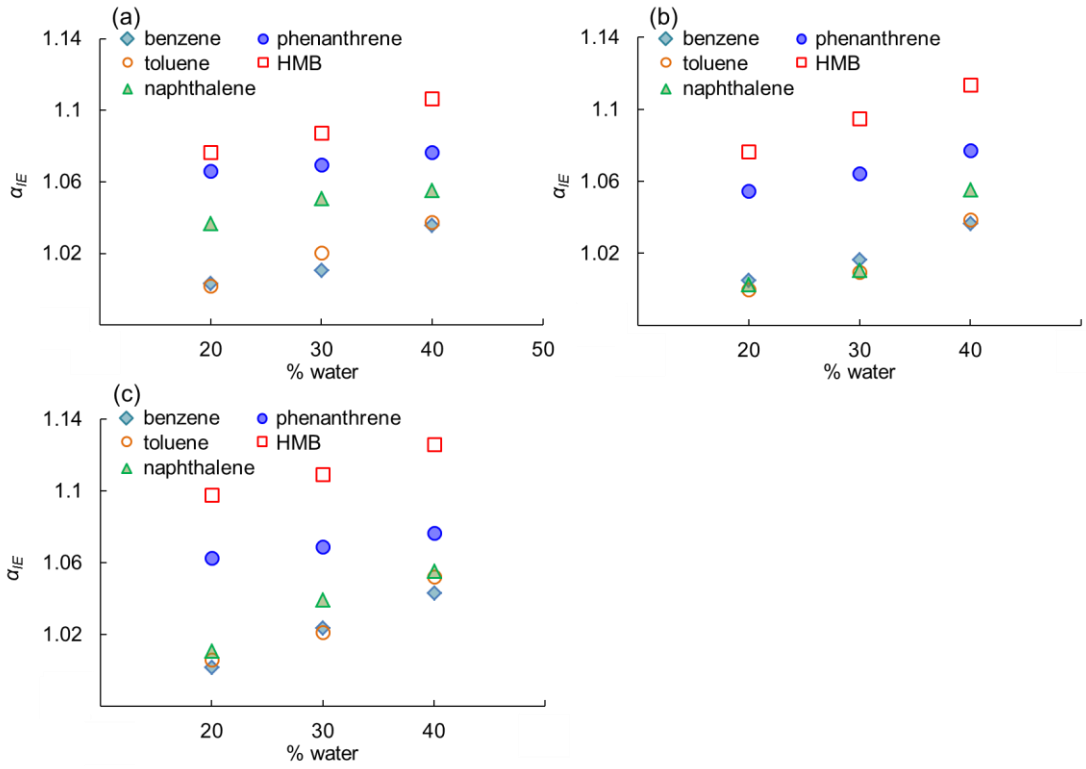

Figure 2. Plots of α_{IE} vs percent water in methanol as the mobile phase.

Conditions: column, (a) ODS (Kanto Chemicals, 150 mm × 4.6 mm i.d.), (b) PBB (Nacalai Tesque, 150 mm × 2.0 mm i.d.), (c) 5PYE (Nacalai Tesque, 150 mm × 4.6 mm i.d.); flow rate, (a), (c) 2.0 mL min^{-1}, (b) 1.0 mL min^{-1}; mobile phase, water / methanol; detection, UV 254 nm (for benzene, naphthalene, and phenanthrene), 220 nm (toluene and HMB); temperature, 40 °C.

We then employed acetonitrile instead of methanol as the mobile phase, and confirmed the effect of organic solvent in RPLC. The values of k_H, k_D, and α_{IE} in acetonitrile/water are summarized in Table 4-6. Even in acetonitrile/water, the similar separation pattern of isotopologues based on the hydrophobic interaction was obtained as in methanol/water. However, the relation between the retention factor and α_{IE} is slightly different in acetonitrile/water than in methanol/water (Figure 3). In general, the separation factor becomes higher with increasing retention factor.[32] Figure 3 showed that α_{IE} in acetonitrile was relatively lower than that in methanol, thus organic solvents might affect the retention difference. We hypothesize that the presence of hydroxy groups in the mobile phase or the separation medium might contribute to the hydrogen bonding with the hydrogen atoms in solutes, so that the differences of the hydrophobicity could be observed in protiated and deuterated compounds.

Table 4. k_H, k_D, and α_{IE} in acetonitrile / water mobile phase on ODS column.

	water / acetonitrile (v / v)	k_H	k_D	α_{IE}
benzene	4 / 6	1.210	1.210	1.000
	5 / 5	2.121	2.117	1.002
	6 / 4	3.994	3.983	1.003
toluene	4 / 6	1.905	1.904	1.000
	5 / 5	3.598	3.528	1.020
	6 / 4	7.545	7.354	1.026
naphthalene	4 / 6	2.168	2.169	1.000
	5 / 5	5.172	5.030	1.028
	6 / 4	12.558	11.767	1.067
phenanthrene	4 / 6	5.429	5.191	1.046
	5 / 5	12.328	11.734	1.051
	6 / 4	35.228	32.979	1.068
HMB	4 / 6	6.879	6.451	1.066
	5 / 5	12.349	11.560	1.068
	6 / 4	84.352	76.947	1.096

Conditions: column, Conditions: column, ODS (Kanto kagaku, 150 mm × 4.6 mm i.d.); flow rate, 2.0 mL min^{-1}; mobile phase, water / acetonitrile; detection, UV 254 nm (benzene, naphthalene, phenanthrene), 220 nm (toluene, HMB); temperature, 40.0 °C.

Table 5. k_H, k_D, and α_{IE} in acetonitrile / water mobile phase on PBB column.

	water / acetonitrile (v / v)	k_H	k_D	α_{IE}
benzene	4 / 6	0.231	0.230	1.005
	5 / 5	0.519	0.510	1.017
	6 / 4	1.084	1.046	1.037
toluene	4 / 6	0.398	0.398	1.000
	5 / 5	0.959	0.950	1.010
	6 / 4	2.106	2.028	1.039
naphthalene	4 / 6	1.283	1.280	1.003
	5 / 5	3.058	3.027	1.010
	6 / 4	7.225	6.846	1.055
phenanthrene	4 / 6	5.890	5.585	1.055
	5 / 5	15.853	14.895	1.064
	6 / 4	46.771	43.426	1.077
HMB	4 / 6	7.857	7.299	1.076
	5 / 5	22.747	20.776	1.095
	6 / 4	68.878	61.852	1.114

Conditions: column, Conditions: column, PBB (Nacalai Tesque, 150 mm × 2.0 mm i.d.); flow rate, 1.0 mL min^{-1}; mobile phase, water / acetonitrile; detection, UV 254 nm (benzene, naphthalene, phenanthrene), 220 nm (toluene, HMB); temperature, 40.0 °C.

Table 6. k_H, k_D, and α_{IE} in acetonitrile / water mobile phase on 5PYE column.

	water / acetonitrile (v / v)	k_H	k_D	α_{IE}
benzene	4 / 6	0.658	0.659	0.998
	5 / 5	1.155	1.154	1.001
	6 / 4	1.315	1.313	1.001
toluene	4 / 6	0.918	0.914	1.004
	5 / 5	1.731	1.711	1.012
	6 / 4	3.679	3.565	1.032
naphthalene	4 / 6	1.517	1.514	1.002
	5 / 5	3.053	2.950	1.035
	6 / 4	5.351	5.081	1.053
phenanthrene	4 / 6	3.617	3.439	1.052
	5 / 5	8.155	7.729	1.055
	6 / 4	22.980	21.488	1.069
HMB	4 / 6	6.397	5.910	1.082
	5 / 5	17.860	16.421	1.088
	6 / 4	30.666	27.933	1.098

Conditions: column, Conditions: column, 5PYE (Nacalai Tesque, 150 mm × 4.6 mm i.d.); flow rate, 2.0 mL min^{-1}; mobile phase, water / acetonitrile; detection, UV 254 nm (benzene, naphthalene, phenanthrene), 220 nm (toluene, HMB); temperature, 40.0 °C.

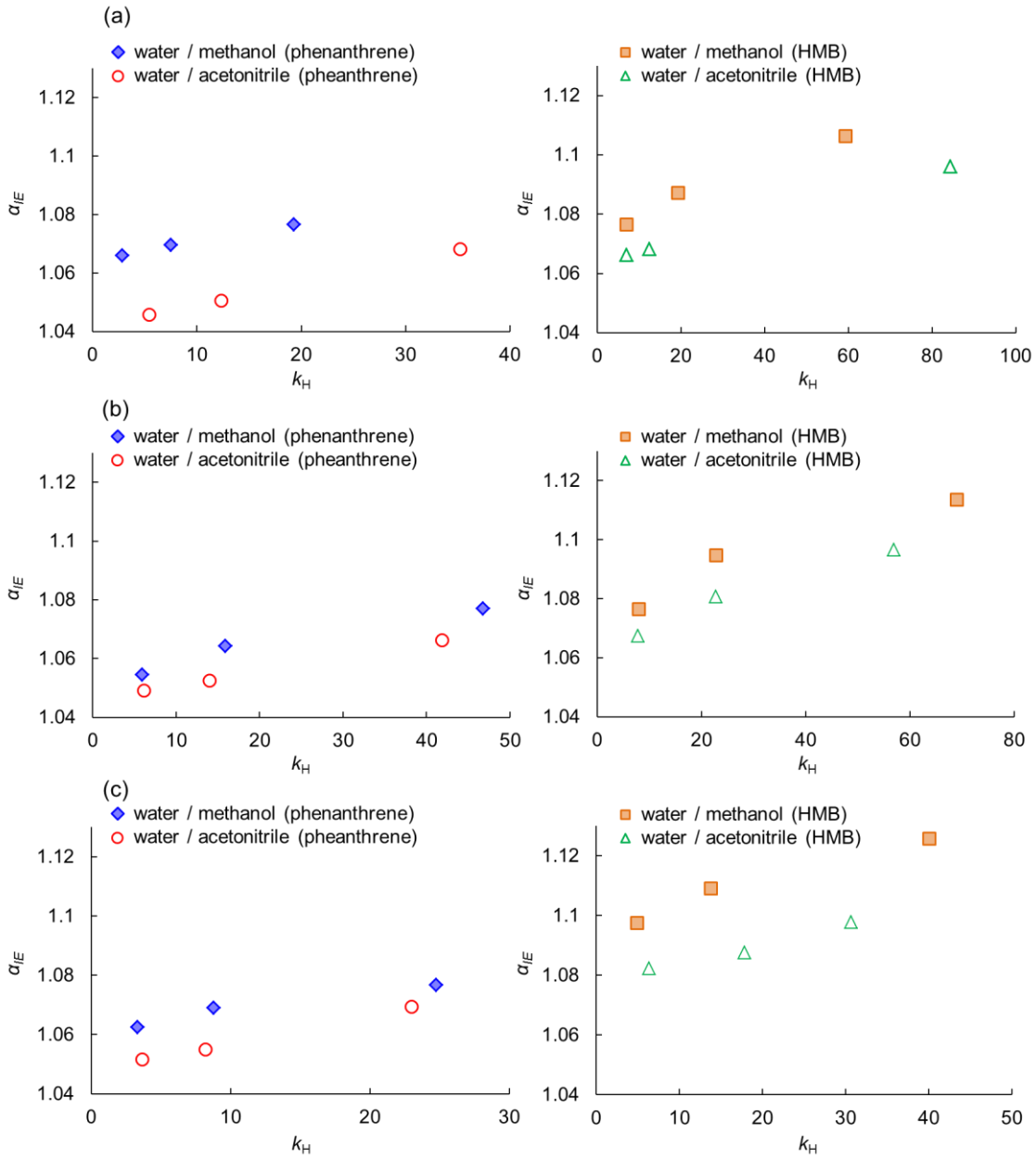

Figure 3. Plot of α_{IE} vs k_H for phenanthrene and HMB in methanol / water and acetonitrile / water as mobile phases. Mobile phase, water / methanol and water / acetonitrile. Other conditions are the same as in Figure 2.

4-3-2 Retention behavior of isotopologues on stationary phase having hydroxy groups

As mentioned above, the results in RPLC suggested the possibility that the difference in the hydrophobicity of protiated and deuterated compounds might be due to the hydrogen bonding between hydroxy groups and solutes. To test the hypothesis, we evaluated the retention behavior of isotopologues using a silica column (silica-150) since silanol groups on the surface of silica gel should contribute the separation of isotopologues due to hydrogen bonding. LC analyses were carried out under the normal phase condition to suppress the hydrophobic interaction.

The chromatograms of isotopologues on silica-150 are shown in Figure 4. Interestingly, all the deuterated compounds eluted later than protiated compounds. In fact, the elution order was reversed from RPLC. In particular, the difference of retention time of isotopologues was clearly observed, thus the peak top separations were achieved for the isotopologues of phenanthrene and HMB. The results strongly suggested that the deuterated compounds allowed stronger hydrogen bonding than the protiated compounds. Consequently, it is believed that the separation of isotopologues in RPLC was caused by the hydrogen bonding between the mobile phase and solutes. In RPLC, deuterated compounds decreased the affinity toward the hydrophobic stationary phase because of their stronger hydrogen bonding to hydroxy groups in the mobile phase than that of protiated compounds.

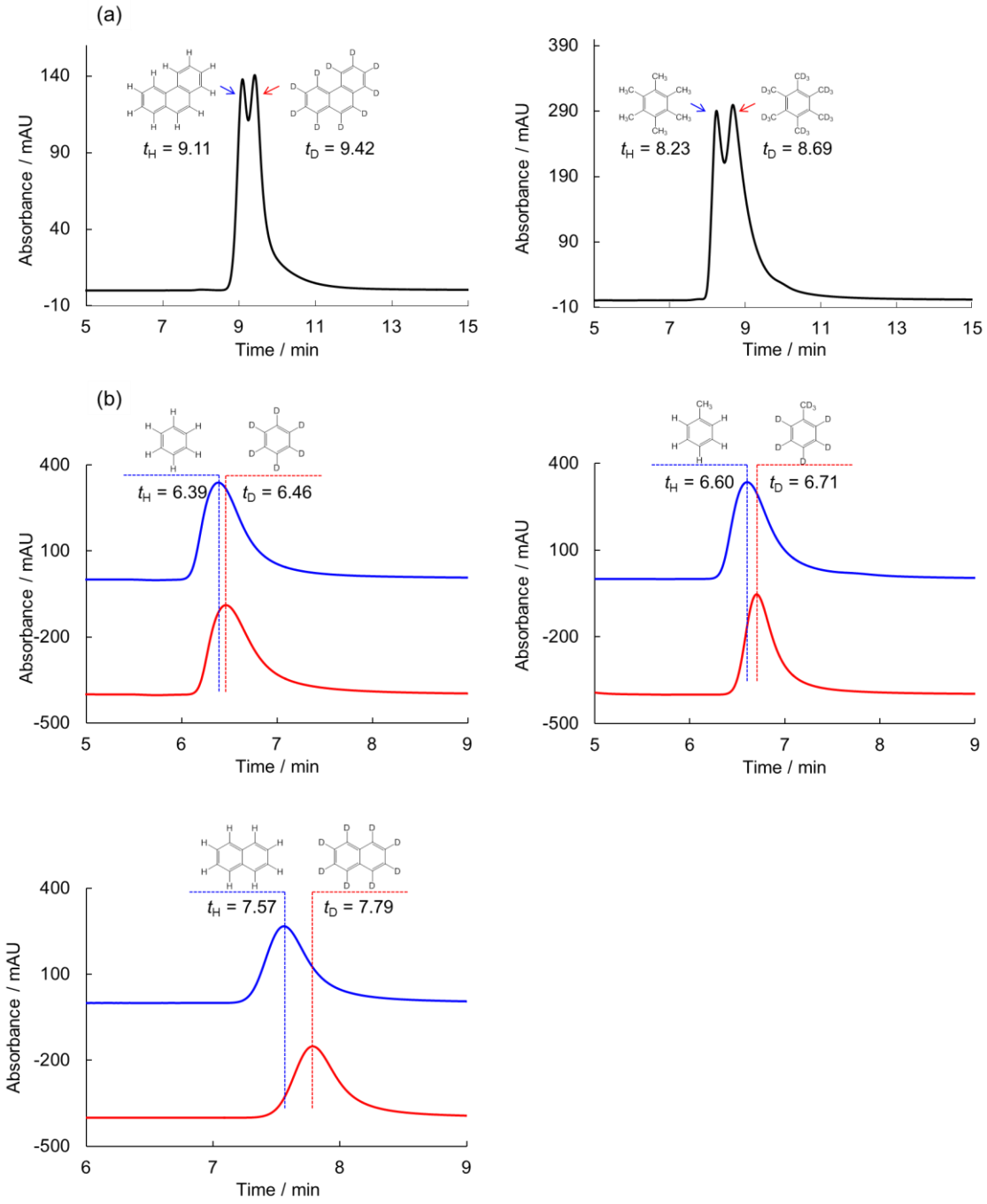

Figure 4. Representative chromatograms of isotopologues on silica-150. (a) Mixed sample of isotopologue pairs of phenanthrene and HMB, (b) single samples of isotopologues of benzene, toluene, and naphthalene.

Conditions: column, silica-150 (TOSOH, 250 × 2.0 mm i.d.); flow rate, 0.8 mL min^{-1}; mobile phase, *n*-hexane; detection, UV 254 nm (for benzene, naphthalene, and phenanthrene), 220 nm (toluene and HMB); temperature, 40 °C.

4-3-3 Difference in isotope effect due to atmosphere of hydrogen atoms by evaluation of free energy changes

The retention factor (k) relates to free energy changes (ΔG) in the chromatographic partition equilibrium as

$$\Delta G = -\mathrm{R}\ T \ln (C\mathrm{s} / C_\mathrm{M}) = -\mathrm{R}\ T \ln (V_\mathrm{M}\ k / V_\mathrm{S})$$

where, R is gas constant, T is temperature, Cs and C_M are the concentrations of the solute in the stationary and mobile phases, respectively, V_M and V_S are the volumes of the mobile and stationary phases, respectively. The difference in ΔG between protiated and deuterated compounds ($\Delta\Delta G_\mathrm{TIE}$) can be obtained with α_IE in RPLC as follows.

$$\Delta G_\mathrm{H} - \Delta G_\mathrm{D} = \Delta\Delta G_\mathrm{TIE} = -\mathrm{R}\ T \ln (k_\mathrm{H} / k_\mathrm{D}) = -\mathrm{R}\ T \ln (\alpha_\mathrm{IE})$$

We then calculated the single isotope effect ($\Delta\Delta G_\mathrm{IE}$), which reflects the average influence of a single H/D substitution, given by

$$\Delta\Delta G_\mathrm{IE} = \Delta\Delta G_\mathrm{TIE} / n_\mathrm{HD}$$

where, n_HD is the number of D atoms substituted for H. Figure 5 shows $\Delta\Delta G_\mathrm{IE}$ for each solute obtained by the RPLC evaluation. We found that $\Delta\Delta G_\mathrm{IE}$ of aromatic compounds without any functional groups (benzene, naphthalene, and phenanthrene) was larger than that of methyl substituted benzene (toluene and HMB) in every column. In general, the acidity of hydrogen atoms on sp^2 carbon (aromatic) is higher than the hydrogen atoms on sp^3 carbon (methyl).[33, 34] Thus, aromatic compounds without any functional groups showed larger isotope effect than methyl substituted benzene by stronger hydrogen bonding with the mobile phase.

Furthermore, $\Delta\Delta G_\mathrm{IE}$ of benzene, toluene, and HMB decreased for columns in the order of ODS > PBB > 5PYE, suggesting that the CH/CD-π interactions between aromatic rings of the stationary phase and hydrogen bonding of solutes contribute to the

isotopologue separation. On the other hand, naphthalene and phenanthrene, which have multiple aromatic rings, showed almost no difference in $\Delta\Delta G_{IE}$, regardless of the column stationary phase. The result might be caused by the π–π interaction to be dominant over the CH/CD-π interactions in the stationary phase.

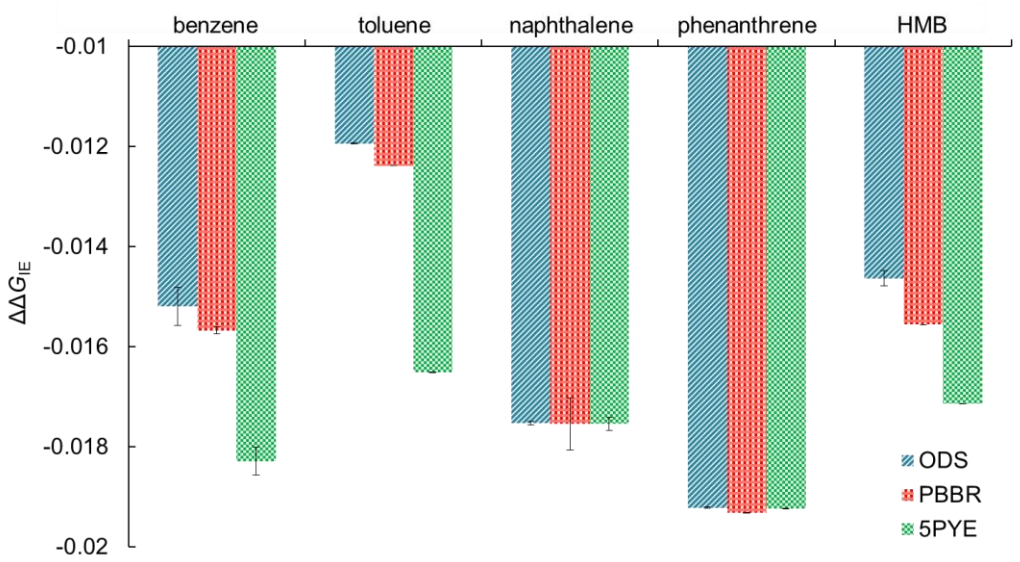

Figure 5. $\Delta\Delta G_{IE}$ of aromatic solutes by RPLC using hydrophobic columns. Mobile phase, water / methanol = 4 / 6. Other conditions are the same as in Figure 2.

To test this hypothesis, it is nessesary to know the strength of CH-π and CD-π interactions. To solve this question, we considered a schematic diagram of free energy among the mobile phases and the stationary phases (Figure 6). This diagram is based on the assumption that isotopologues are more stable in hydrophobic stationary phases than in hydrophilic mobile phases since all solutes are hydrophobic, and the free energy of the hydrogen bonding between the mobile phase and solute for the protiated compound is lower than for the deuterated one because of stronger hydrogen bonding with protiated compounds.

In the case that the CD-π interaction is stronger than the CH–π interaction, $\Delta\Delta G_{IE}$ increases by CH/CD-π interactions with the stationary phase, and then $\Delta\Delta G_{IE}$ increases in the order of ODS < PBB < 5PYE. But this model contradicts our experimental results that $\Delta\Delta G_{IE}$ decreased in the order of ODS > PBB > 5PYE. On the other hand, in the case that the CH-π interaction is stronger than the CD-π interaction (Figure 6), $\Delta\Delta G_{IE}$ decreases by CH/CD-π interactions with the stationary phase and $\Delta\Delta G_{IE}$ decreases in the order of ODS > PBB > 5PYE, which is consistent with the experimental results. Therefore, we conclude that the CH-π interaction is slightly stronger than the CD-π interaction.[35, 36]

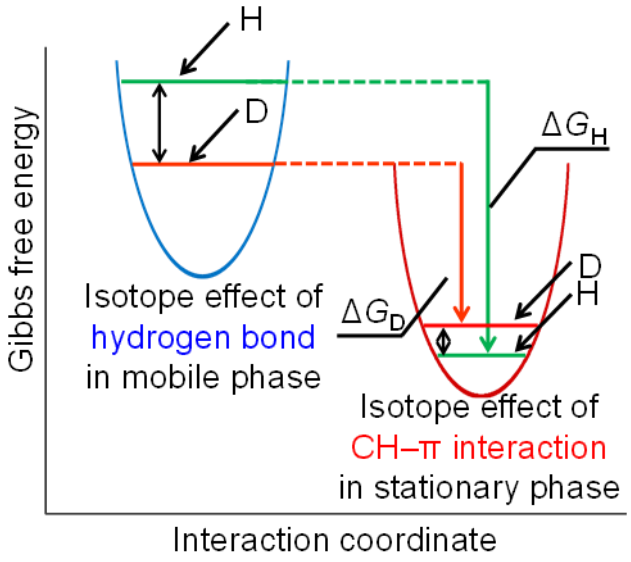

Figure 6. Schematic diagram of free energy caused by hydrogen bonding and CH-π interaction due to isotope effect in the case that CH-π is stronger than CD-π.

4-3-4 Evaluation of CH–π interaction on fullerene-coated stationary phases

Based on the results in NPLC, we suggest that the CH-π interaction was stronger than the CD-π interaction. Additionally, as described in our report regarding specific retention ability of the C70 column, we expect that the separation of isotopologues based on CH/CD-π interactions can be achieved with the C70 column. We therefore evaluated various columns modified with aromatic moieties as well as fullerene-coated columns. As results of evaluations in NPLC, we confirmed that the C70 column showed stronger CH-π interaction toward methyl substituted benzenes than any other columns. Figure 7 (a) shows the relation between the retention factors on each column and the number of methyl substitution in each solute, and the chromatogram of the mixed sample of methylbenzenes on the C70 column is shown in Figure 7 (b). These results clearly indicate that the number of methyl substitutions increased retention factors especially on the fullerene-modified columns due to effective CH-π interaction.

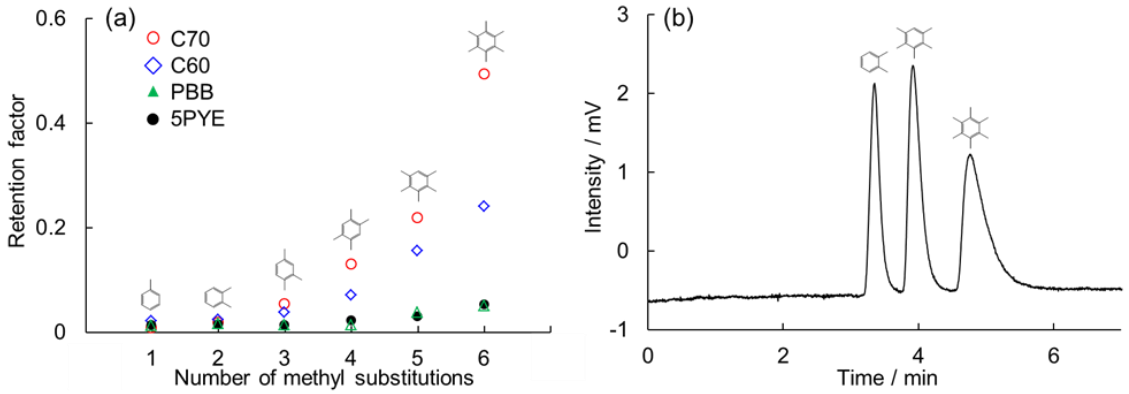

Figure 7. Retention of methyl-substituted benzenes by CH-π interaction on stationary phases immobilized with aromatic compounds. (a) the plots of retention factors on each column vs number of methyl substitutions in each solute, (b) the chromatogram of the mixed sample of methyl-substituted benzenes on C70 column.

Conditions: column, PBB (Nacalai Tesque, 150 mm × 2.0 mm i.d.), 5PYE (Nacalai Tesque, 150 mm × 4.6 mm i.d.), C60 (32.0 cm × 100 mm i.d.), C70 (32.0 cm × 100 mm i.d.); flow rate, 2.0mL min^{-1} (PBB, 5PYE), 2.0 µL min^{-1} (C70, C60); mobile phase, n-hexane; detection, UV 220 nm; temperature, 40 ºC.

Furthermore, we carried out NPLC on mixed isotopologue pairs of HMB and phenanthrene on the C70 column. We successfully confirmed the peak top separation of isotopologue pairs of HMB as shown in Figure 8 (a), where protiated HMB was eluted earlier than deuterated one. These results also supported that the CH-π interaction is stronger than the CD-π interaction. On the other hand, despite the stronger retention of phenanthrene than HMB, isotopologue separation was not observed as shown in Figure 8 (b). In this case, the π-π interaction was preferentially acted instead of the CH-π interaction due to the multiple aromatic rings in phenanthrene.

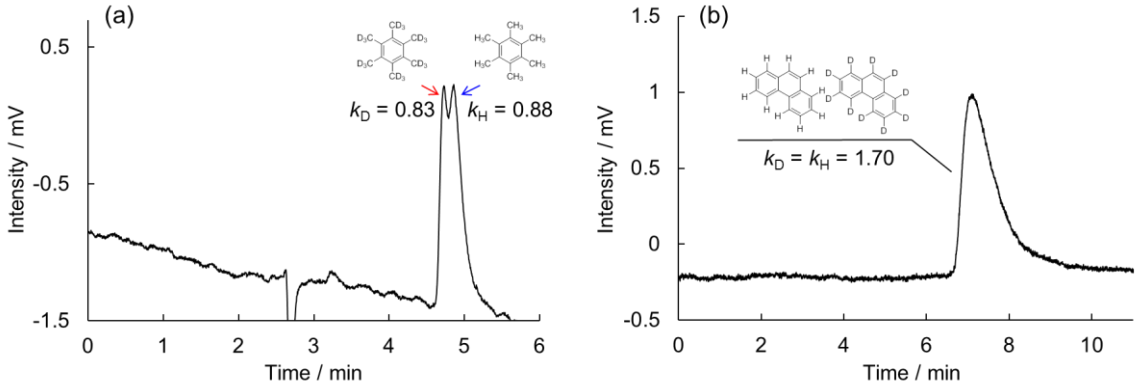

Figure 8. Chromatograms for H/D isotopologue pairs of (a) HMB and (b) phenanthrene in NPLC using C70 column.
Conditions: column, C70 column (32.0 cm × 100 mm i.d.); flow rate, 2.0 μL min^{-1}; mobile phase, n-hexane; detection, UV (a) 220 nm, (b) 254 nm, temperature, 40 ºC.

4-4 Conclusions

In this report, we studied the contribution of intermolecular interactions to chromatographic isotope effect on various LC conditions. In particular on RPLC, we found that the hydrogen bonding between hydrogen atom of isotopologues and hydroxy groups of the mobile phase was responsible for the separation of isotopologues. In fact, we succeeded in the peak top separation of isotopologues by the hydrogen bonding with hydroxy group of the silica stationary phase on NPLC, and found that deuterated compounds showed stronger hydrogen bonding than protiated compounds. Furthermore, the stationary phase immobilized with aromatic compounds showed good separation of the pairs of isotopologues of methyl substituted benzenes, a result which can be attributed to the fact that the CH-π interaction was stronger than the CD-π interaction by considering free energies in chromatographic partition equilibrium. Finally, we demonstrated the peak top separation of isotopologues of HMB with the C70 column, which showed extremely strong π interactions, by the isotope effect of CH/CD-π interactions on NPLC.

Our reports demonstrated the importance of H/D isotope effect in the hydrogen bonding and CH/CD-π interactions by simple LC evaluations. The separation of isotopologues on LC and their strength from the view point of free energy in chromatographic partition equilibrium were discussed. In particular, this is the first report to discuss about the separation of isotopologues on NPLC by the isotope effect of the hydrogen bonding or CH/CD-π interactions. we believe that this report greatly advanced our understanding of isotope effects based on weak interactions, and contribute to the development of new separation techniques for deuterated drugs.

4-5 References

1. Belleau, B.; Burba, J.; Pindell M.; Reiffenstein, J. Effect of Deuterium Substitution in Sympathomimetic Amines on Adrenergic Responses. *Science* **1961,** *133*, 102–104.
2. Sharma, R.; Strelevitz, T. J.; Gao, H.; Clark, A. J.; Schildknegt, K.; Obach, R. S.; Ripp, S. L.; Spracklin, D. K.; Tremaine, L. M.; Vaz, A. D. Deuterium Isotope Effects on Drug Pharmacokinetics. I. System-dependent Effects of Specific Deuteration with Aldehyde Oxidase Cleared Drugs. *Drug Metab. Dispos.* **2012,** *40*, 625–634.
3. Foster, A. B. Deuterium Isotope Effects in Studies of Drug Metabolism. *Trends Pharmacol. Sci*. **1984,** *5*, 524–527.
4. Mullard, A. Deuterated Drugs Draw Heavier Backing. *Nat. Rev. Drug Discov.* **2016,** *15*, 219–221.
5. Sanderson, K. Big Interest in Heavy Drugs. *Nature* **2009,** *458*, 269.
6. Schmidt, C. First Deuterated Drug Approved. *Nat. Biotechnol.* **2017,** *35*, 493–494.
7. Mullard, A. FDA Approves First Deuterated Drug. *Nat. Rev. Drug Discov.* **2017,** *16*, 305.
8. Bubin, S.; Pavanello, M.; Tung, W. C.; Sharkey, K. L.; Adamowicz, L. Born-Oppenheimer and Non-Born–Oppenheimer, Atomic and Molecular Calculations with Explicitly Correlated Gaussians. *Chem. Rev.* **2013,** *113*, 36–79.
9. Sullivan, J. H. Deuterium Kinetic Isotope Effect in the Hydrogen–Iodine Reaction. *J. Chem. Phys.* **1963,** *39*, 3001–3009.
10. Wiberg, K. B. The Deuterium Isotope Effect. *Chem. Rev.* **1955,** *55*, 713–743.
11. Wade, D. Deuterium Isotope Effects on Noncovalent Interactions between

Molecules. *Chem. Biol. Interact.* **1999,** *117*, 191–217.

12. Moncada, F.; Uribe, L. S.; Romero, J.; Reyes, A. Hydrogen Isotope Effects on Covalent and Noncovalent Interactions: The Case of Protonated Rare Gas Clusters. *Int. J. Quantum Chem.* **2013,** *113*, 1556–1561.
13. Shi, C.; Zhang, X.; Yu, C. H.; Yao, Y. F.; Zhang, W. Geometric Isotope Effect of Deuteration in a Hydrogen-bonded Host-Guest Crystal. *Nat. Commun.* **2018,** *9*, 481–489.
14. Bell, R. L.; Truong, T. N. *J. Phys. Chem. A* Primary and Solvent Kinetic Isotope Effects in the Water-Assisted Tautomerization of Formamidine: An *ab* Initio Direct Dynamics Study. **1997,** *101*, 7802–7808.
15. Tresca, B. W.; Brueckner, A. C.; Haley, M. M.; Cheong, P. H.; Johnson, D. W. Computational and Experimental Evidence of Emergent Equilibrium Isotope Effects in Anion Receptor Complexes. *J. Am. Chem. Soc.* **2017,** *139*, 3962–3965.
16. Tanaka, N.; Hosoya K.; Nomura, K.; Yoshimura, T.; Ohki, T.; Yamamoto, R.; Kimata K.; Araki, M. Separation of Nitrogen and Oxygen Isotopes by Liquid Chromatography. Nature **1989,** *341*, 727–728.
17. Turowski, M.; Yamakawa, N.; Meller, J.; Kimata, K.; Ikegami, T.; Hosoya, K.; Tanaka, N.; Thornton, E. R. Deuterium Isotope Effects on Hydrophobic Interactions: The Importance of Dispersion Interactions in the Hydrophobic Phase. *J. Am. Chem. Soc.* **2003,** *125*, 13836–13849.
18. Kobayashi, K.; Asakawa, Y.; Kato, Y.; Aoyama, Y. Complexation of Hydrophobic Sugars and Nucleosides in Water with Tetrasulfonate Derivatives of Resorcinol Cyclic Tetramer Having a Polyhydroxy Aromatic Cavity: Importance of Guest-Host CH-π interaction. *J. Am. Chem. Soc.* **1992,** *114*, 10307–10313.

19. Plevin, M. J.; Bryce, D. L.; Boisbouvier, J. Direct Detection of CH/π Interactions in Proteins. *Nat. Chem.* **2010,** *2*, 466–471.
20. Asensio, J. L.; Ardá, A.; Cañada, F. J.; Jiménez-Barbero, J. Carbohydrate-Aromatic Interactions. *Acc. Chem. Res.* **2013,** *46*, 946–954.
21. Suzuki, S.; Green, P. G.; Bumgarner, R. E.; Dasgupta, S.; Goddard, W. A.; Blake, G. A., Benzene Forms Hydrogen Bonds with Water. *Science* **1992,** *257*, 942–945.
22. Zhao, C.; Parrish, R. M.; Smith, M. D.; Pellechia, P. J.; Sherrill, C. D.; Shimizu, K. D. Do Deuteriums Form Stronger CH-π Interactions? *J. Am. Chem. Soc.* **2012,** *134*, 14306–14309.
23. Hara, T.; Kobayashi, H.; Ikegami, T.; Nakanishi, K.; Tanaka, N. Performance of Monolithic Silica Capillary Columns with Increased Phase Ratios and Small-Sized Domains. *Anal. Chem.* **2006,** *78*, 7632–7642.
24. Tanaka, N.; McCalley, D. V. Core–Shell, Ultrasmall Particles, Monoliths, and Other Support Materials in High-Performance Liquid Chromatography. *Anal. Chem.* **2016,** *88*, 279–298.
25. Hunter, C. A.; Sanders, J. K. M. The nature of π-π Interactions. *J. Am. Chem. Soc.* **1990,** *112*, 5525–5534.
26. Yarkony, D. R. Diabolical Conical Intersections. *Rev. Mod. Phys.* **1996,** *68*, 985–1013.
27. Tsuzuki, S.; Honda, K.; Uchimaru, T.; Mikami, M.; Tanabe, K. The Magnitude of the CH / π Interaction between Benzene and Some Model Hydrocarbons. *J. Am. Chem. Soc.* **2000,** *122*, 3746–3753.
28. Kubo, T.; Murakami, Y.; Tominaga, Y.; Naito, T.; Sueyoshi, K.; Yan, M.; Otsuka, K. Development of a C60-fullerene bonded open-tubular capillary using a photo /

thermal active agent for liquid chromatographic separations by π-π interactions. *J. Chromatogr. A* **2014,** *1323*, 174–178.

29. Kubo, T.; Murakami, Y.; Tsuzuki, M.; Kobayashi, H.; Naito, T.; Sano, T.; Yan, M.; Otsuka, K. Unique Separation Behavior of a C60 Fullerene-Bonded Silica Monolith Prepared by an Effective Thermal Coupling Agent. *Chem. Eur. J.* **2015,** *21*, 18095–18098.
30. Kubo, T.; Kanao, E.; Matsumoto, T.; Naito, T.; Sano, T.; Yan, M.; Otsuka, K. Specific Intermolecular Interactions by the Localized π-Electrons in C70-fullerene. *ChemistrySelect* **2016,** *1*, 5900–5904.
31. Kanao, E.; Naito, T.; Kubo, T.; Otsuka, K. Development of a C70-Fullerene Bonded Silica-Monolithic Capillary and Its Retention Characteristics in Liquid Chromatography. *Chromatography* **2017,** *38*, 45–51.
32. Leslie, E. S. Relative Retention Expressions in Chromatography. *J. Chromatogr. A* **1980,** *17*, 229–234.
33. Hartmann, M.; Wetmore, S. D.; Radom, L. C-H···X Hydrogen Bonds of Acetylene, Ethylene, and Ethane with First- and Second-Row Hydrides. *J. Phys. Chem. A* **2001,** *105*, 4470–4479.
34. Miao, K.; Hu, Y.; Zha, B.; Xu, L.; Dong, M.; Miao, X.; Deng, W. Polymorphic Self-Assemblies of 2,7-Bis(decyloxy)-9-fluorenone at the Solid/Gas Interface: Role of C–H···O=C Hydrogen Bond. *J. Phys. Chem. C* **2017,** *121*, 3947–3957.
35. Zhao, Y.; Houk, K. N.; Rechavi, D.; Scarso, A.; Rebek, J. Jr. Equilibrium Isotope Effects as a Probe of Nonbonding Attractions. *J. Am. Chem. Soc.* **2004,** *126*, 11428–11429.
36. Rechavi, D. Scarso, A. Rebek, J. Jr. Isotopomer Encapsulation in a Cylindrical

Molecular Capsule: A Probe for Understanding Noncovalent Isotope Effects on a Molecular Level. *J. Am. Chem. Soc.* **2004,** *126*, 7738–7739.

Chapter 5

Tunable Liquid Chromatographic Separation of H/D Isotopologues Enabled by Aromatic π Interactions

5-1 Introduction

Deuterium (D) is a natural isotope of hydrogen (H) that has an additional neutron and therefore two times more mass. The chemical and physical properties of deuterated molecules are nearly identical to those of hydrogenated molecules. However, the differences between hydrogen and deuterium are easily identified by mass spectrometry and nuclear magnetic resonance (NMR) techniques, such that deuterium can be used to label molecules.[1-4] This differentiation is known as the deuterium isotope effect. In previous literature, deuteration of molecules has been necessary for exploring routes in organic synthesis, biosynthesis, and metabolism.[5-11] Thus, deuterated molecules are now widely applied in various fields because of the deuterium isotope effect. In particular, this effect aids the design of organic molecules and the development of novel pharmaceuticals.[12-15] In these applications, a deeper understanding of the effects of the deuterium isotope effect is greatly needed.

In general, the Gibbs free energies of isotopologues differ because the vibration energy of each bond in the molecules depends on the mass difference of the bonding atoms. This is shown in the relations for the Gibbs free energy, G, and stretching frequency, v,

$$G = hv\,(n + 1) \qquad (1)$$

$$v = (1 / 2\pi)\,(k_S / \mu)^{1/2} \qquad (2)$$

where h, n, k_S, and μ are the Planck constant, principal number, spring constant, and reduced mass of each atom, respectively. The reduced mass of deuterium is slightly larger than that of hydrogen, and therefore, bonds with deuterium are more stable.[16-18] This property is widely known as the kinetic isotope effect and has been widely studied by theoretical and experimental evaluations.[19-24] In contrast, An increased understanding of the isotope effects related to intermolecular interactions contributes to new theoretical findings and developments of functional smart materials.[25-30]

Liquid chromatography (LC) is a separation method based on the partition of stationary and mobile phases. Since the retention strength of an analyte in LC is highly sensitive to intermolecular interactions, the method is suitable for evaluating weak interactions.[31-36] We previously reported the development of novel stationary phases modified with carbon nanomaterials.[37] For example, C_{60}-fullerene and C_{70}-fullerene (C60, C70) molecules provided effective interactions, such as π-π stacking, spherical recognition, and dipole-induced dipole interactions.[38-40] Furthermore, we revealed the contributions of hydrogen bonding and CH-π interactions for the H/D isotopologues in reverse phase LC (RPLC) and normal phase LC (NPLC).[41,42] However, detailed examinations regarding these isotope effects were not conducted in these cases.

In this paper, we evaluated the mechanism of the isotope effect by LC based on the interactions of isotopologues of aromatic molecules with polar functional groups and with π-conjugated moieties. Various analytes with a number of stationary phases and mobile phases were employed in NPLC, where the hydrophobic interaction was almost completely suppressed. We utilized a few hydrophilic stationary phases modified with polar functional groups and a C70-bonded silica monolithic capillary. Based on the isothermal evaluations from NPLC, the dependence of enthalpy and entropy on the H/D

isotope effects was estimated by the van't Hoff equations. Furthermore, the influence of the dielectric constant of mobile phases on the H/D isotope effects was examined. Following these experiments, we demonstrated H/D separations by harnessing the complementary behaviors of CH-π interactions with a stationary phase and OH-π interactions with a mobile phase.

5-2 Experimental Section

5-2-1 Materials

Acetone, benzene, diethyl ether, sodium hydroxide, dichloromethane, chlorobenzene, toluene, ethyl acetate, methanol, acetonitrile and *n*-hexane were purchased from Nacalai Tesque (Kyoto, Japan), methyl pentafluorobenzoate, diethyl amine, urea, acetic acid, and 3-aminopropyltrimethoxysilane (APTMS) from Tokyo Chemical Industry (Tokyo, Japan), sodium azide, *N*-hydroxysuccinimide (NHS), and 1-ethyl-3-(3-dimethylaminopropyl)carbodiimide (EDAC) from Wako Pure Chemical Industries (Osaka, Japan), polyethylene glycol (PEG) (*M*n=10,000), benzene-d6, toluene-d8, naphthalene-d8, *o*-xylene, 1,2,4-trimethylbenzene, 1,2,4,5-tetramethylbenzene, pentamethylbenzene, C70, phenanthrene, phenanthlene-d10, hexamethylbenzene (HMB), hexamethylbenzene-d18 (HMB-d18) from Sigma-Aldrich Japan (Tokyo, Japan), respectively. Deionized water was obtained by a Milli-Q Direct-Q 3UV system (Merck Millipore, Tokyo, Japan). A COSMOSIL PYE® was purchased from Nacalai Tesque, Mightysil RP–18GPII® (ODS) was purchased from KANTO CHEMICAL (Tokyo, Japan) and CHEMCOSORB 3-120-Si® (Silica) and 3-NH_2® (Amino) were purchased from CHEMCO PLUS (Osaka, Japan) and fused-silica capillaries from Polymicro Technologies (Phoenix, AZ).

5-2-2 Instruments

A capillary liquid chromatographic system consisted of a DiNa S (KYA Technologies, Tokyo, Japan) as a pump, a CE-2070 (JASCO, Tokyo, Japan) as a UV detector, a CHEMINERT (Valco Instruments, Houston, TX) as a sample injector, and a Chemco capillary column conditioner Model 380-b (Chemco, Osaka, Japan) as a column oven. As

an HPLC system, a Prominence series (Shimadzu, Kyoto, Japan) was used. FT-IR, NMR, elemental analysis, and fast atom bombardment mass spectrometry (FABMS) were carried out by a Nicolet iS5 ATR (Thermo Fisher Scientific, Yokohama, Japan), a JNM-ECA500 spectrometer (JEOL, Tokyo, Japan), a Flash EA1112 (Thermo Fisher Scientific), and a JMS-700 (JEOL), respectively.

5-2-3 Preparation of Amide column

3-NH_2 (3.0 g) was dispersed in acetone (10 mL) and triethylamine (1.0 mL) was added to the dispersion liquid. Acetyl chloride (1.0 mL) was instilled into the dispersion liquid at 0 °C and stirred at room temperature for 24 h (Scheme 1). After the reaction, the particles were collected by centrifugal sedimentation and washed with acetone. After drying, the particles were packed into an HPLC column by utilization of packing service in CHEMCO (Amide column).

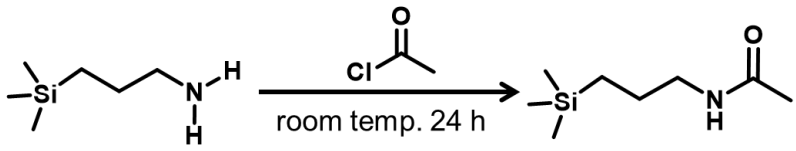

Scheme 1. Preparation of an amide column.

5-2-4 Preparation of C70-coated columns and their evaluation

C70 column were prepared following the protocols in the previous chapter (Chapter 3). The commercially available columns containing 5PYE, ODS, Silica, Amino and Amide column were evaluated by typical liquid chromatographic system, Prominence series. The capillary columns containing C70 column was evaluated by a home-made nano flow system consisting of a DiNa S as the pump, CE-2070 as the UV detector, CHEMINERT

as the sample injector, and Chemco capillary column conditioner Model 380-b as the column oven for isothermal operations. In both systems, we employed normal and reverse phase modes.

5-3 Results and Discussion

5-3-1 Effect of polar functional groups on the isotope effect in NPLC

In order to evaluate the isotope effect under the interactions of the aromatic molecules with polar functional groups, we studied the separation behaviour of the isotopologues in NPLC on various hydrophilic columns containing either silica (Si-OH, Silica column), amino (NH_2, Amino column), or amide (NHCO, Amide column) functional groups. The density of the functional groups in these columns was estimated by elemental analysis (Table 1). The immobilisation of amino groups in the Amino column and carbonyl groups in the Amide column was confirmed by alterations of the nitrogen content. These columns were then evaluated by NPLC. The partition coefficient of an isotopologue in chromatography is expressed by the retention factor, k.[41-42]. The retention factors of the protiated and deuterated isotopologues are given by,

$$k_H = (t_H - t_0) / t_0,\ k_D = (t_D - t_0) / t_0 \qquad (3)$$

$$\alpha_{IE} = k_D / k_H \qquad (4)$$

where t_H and t_D are the retention times of the protiated and deuterated analytes, respectively, and t_0 is the retention time of a non-retained analyte. The quantity α_{IE} is the ratio of k_D to k_H.

Comparing the separation factor of phenanthrene and hexamethylbenzene (HMB) for each column, the deuterated analytes were eluted later than the protiated ones in all the columns (Figure 1 (a)). The results clearly suggest that the deuterated analytes provided stronger interactions with the polar functional groups, which is consistent with our previous report.[42] In addition, the absolute strength of the α_{IE} values followed the order of Silica > Amino > Amide for all the analytes. In fact, the effective separation of isotopologue pairs of phenanthrene was confirmed only in the Silica column; the other

columns hardly showed separations (Figure 1 (b-d)). In our previous study,[42] we considered that the chromatographic isotope effect resulted from hydrogen bonding, in which the heteroatoms in the polar functional group acted as hydrogen donors. In general, the oxygen atom of a carbonyl group shows stronger hydrogen bonding than that of a hydroxyl group.[43-44] In spite of this fact, the Amide column exhibited a worse separation than the Silica column; therefore, we have reconsidered the interactions that cause the isotope effect of polar functional groups.

Table 1. Results of elemental analysis of the packed particles.

	Silica			Amino			Amide		
	C wt %	H wt %	N wt %	C wt %	H wt %	N wt %	C wt %	H wt %	N wt %
	0.04	0.00	0.00	2.59	0.66	0.93	0.54	0.99	0.96
Amino group	–			0.67 mmol/g			–		
Carbonyl group	–			–			1.10 mmol/g		

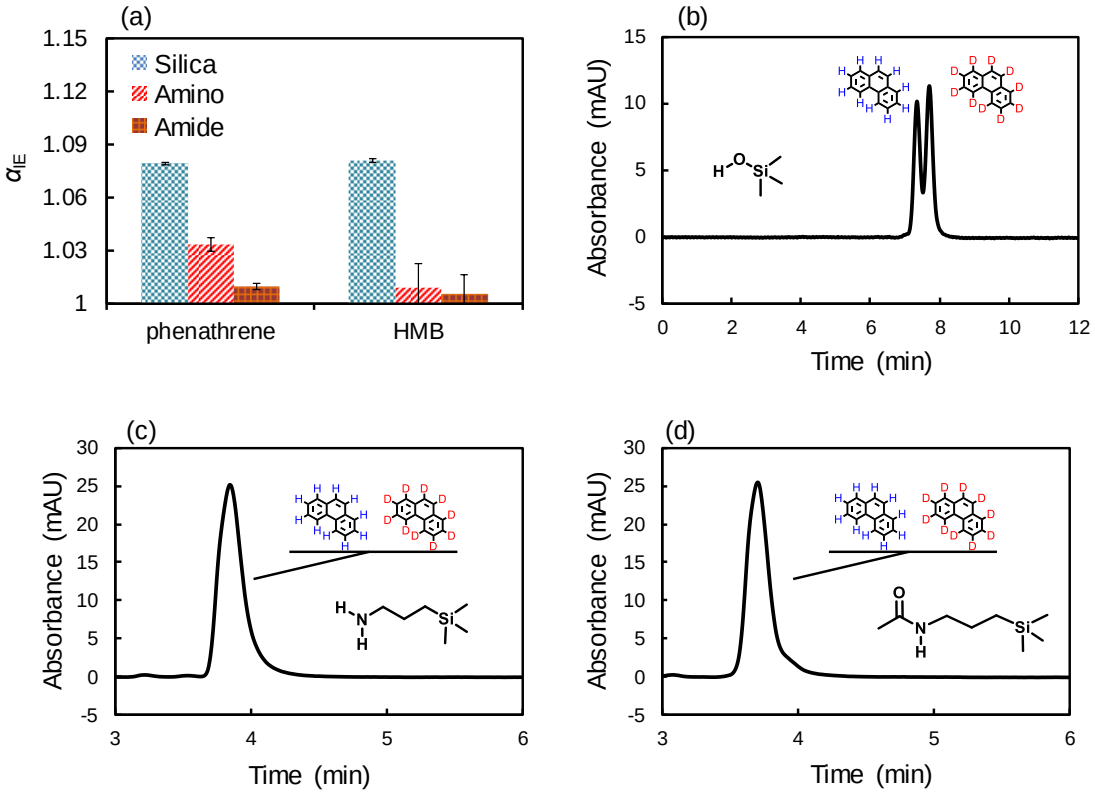

Figure 1. Separation behavior of the H/D isotopologue pairs on hydrophilic columns. (a) α_{IE} values of phenanthrene and HMB in NPLC with hydrophilic columns. Chromatograms of the H/D isotopologue pairs of phenanthrene with (b) Silica, (c) Amino, and (d) Amide in NPLC.

Conditions: column, Silica (CHEMCO, 150 mm × 2.1 mm i.d.), Amino (CHEMCO, 150 mm × 2.1 mm i.d.), Amide (CHEMCO, 150 mm × 2.1 mm i.d.); flow rate, 2.0 mL min^{-1}; mobile phase, *n*-hexane; detection, UV 254 nm (phenanthrene), 220 nm (HMB); temperature, 25.0 °C.

Here, to explain the retention differences, we consider that the isotope effect might be caused by OH- or NH-π interactions, in which the aromatic rings of the analytes act as donors for hydrogen atoms on the polar functional groups in each stationary phase.[45-48] The C-D bond will have more electron density around the carbon atom than the C-H bond because a shorter bond results in a smaller volume for electrons to reside in, leading to a higher electron density. To test our hypothesis, we measured ^{13}C NMR spectra of phenanthrene and HMB H/D isotopologue pairs (Figure 2). According to these spectra, the carbon atoms bonding with deuterium gave triplet peaks because the spin-spin coupling between the ^{13}C and deuterium atoms was not eliminated during proton decoupling. Interestingly, the peaks of deuterated compounds appeared at lower magnetic fields than those of protiated ones. This result suggested that aromatic carbon atoms in the deuterated analytes have higher electron densities than in the protiated ones. Therefore, we assumed that the deuterated analytes showed stronger electrostatic interactions between their aromatic rings and the protons on the OH or NH groups in the columns due to the higher electron densities around the aromatic carbon atoms. In addition, OH-π interactions were stronger than NH-π interactions because OH-π interactions with hydrogen atoms were weaker than NH-π interactions with hydrogen atoms.[47] Consequently, the Silica column exhibited a better separation than the Amino column.

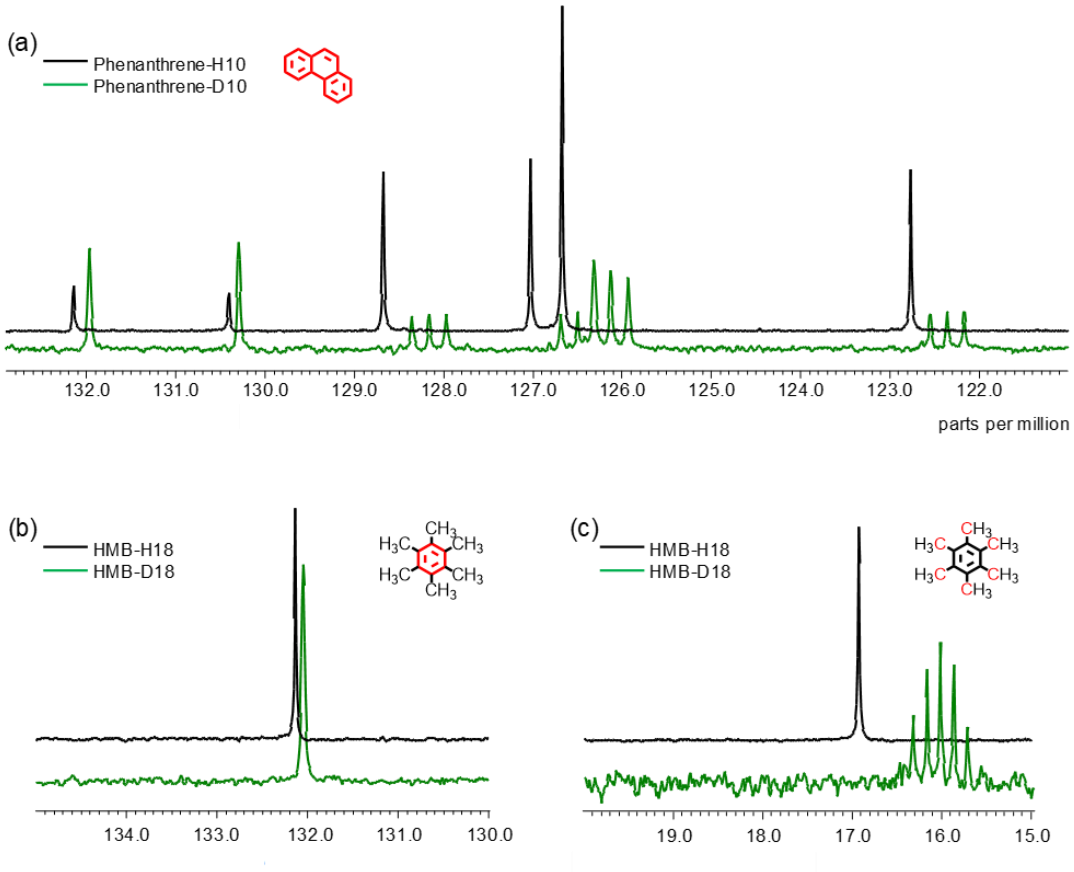

Figure 2. ^{13}C NMR spectra of phenanthrene and HMB H/D isotopologue pairs in chloroform-d. (a) phenanthrene, (b) aromatic ring in HMB, (c) methyl group in HMB.

Our previous studies [41-42] reported that hydrogen atoms on sp^2 carbon (aromatic) atoms showed greater isotope effects than those on sp^3 carbon (methyl) atoms in RPLC. Here, we hypothesize that the difference in the isotope effect between hydrogen atoms on sp^2 and sp^3 carbon atoms can also be observed in NPLC. To verify this hypothesis, we evaluated the isotope effect for a single hydrogen atom in each analyte using the same method of our previous reports. The retention factor, k, is related to the free energy change, ΔG, in the chromatographic partition equilibrium by,

$$\Delta G = -R\,T \ln (C_S / C_M) = -R\,T \ln (V_M\,k / V_S) \qquad (5)$$

where R, T, C_S, C_M, V_M, and V_S are the gas constant, temperature, concentration of the analyte in the stationary or mobile phase, and volume of the mobile or stationary phase, respectively. The difference in ΔG between protiated and deuterated analytes, $\Delta\Delta G_{TIE}$, obtained with an α_{IE} is given by the following equation.

$$\Delta G_H - \Delta G_D = \Delta\Delta G_{TIE} = -\mathrm{R}\,T\,|\ln (k_D / k_H)| = -\mathrm{R}\,T\,|\ln \alpha_{IE}| \quad (6)$$

The isotope effect for a single hydrogen atom ($\Delta\Delta G_{IE}$) was then calculated by taking the average of a single H/D substitution, given by,

$$\Delta\Delta G_{IE} = \Delta\Delta G_{TIE} / n_{HD} \qquad (7)$$

where n_{HD} is the number of D atoms substituted for H atoms. Figure 3 shows the $\Delta\Delta G_{IE}$ for each analyte obtained in NPLC evaluations with the Silica column. We found that the $\Delta\Delta G_{IE}$ for aromatic compounds without any functional groups (benzene, naphthalene, and phenanthrene) were smaller than that of methyl-substituted benzene (toluene and HMB), and the analytes with a higher number of aromatic rings showed smaller $\Delta\Delta G_{IE}$ values (phenanthrene showed the smallest $\Delta\Delta G_{IE}$). The results suggested that the analytes with hydrogen atoms on sp^2 carbon atoms showed a greater isotope effect than those on sp^3 carbon atoms. Hydrogen atoms bonded to sp^2 carbon atoms may induct electrons

directly to the aromatic carbon atoms, while hydrogen atoms bonded to sp^3 carbon atoms donate electrons indirectly to aromatic carbon atoms through sp^3 carbon atoms. Therefore, hydrogen atoms on sp^2 carbon atoms could show stronger inductive effects toward aromatic rings than those on sp^3 carbon atoms, and thus the aromatic compounds without methyl groups showed stronger OH-π interactions.

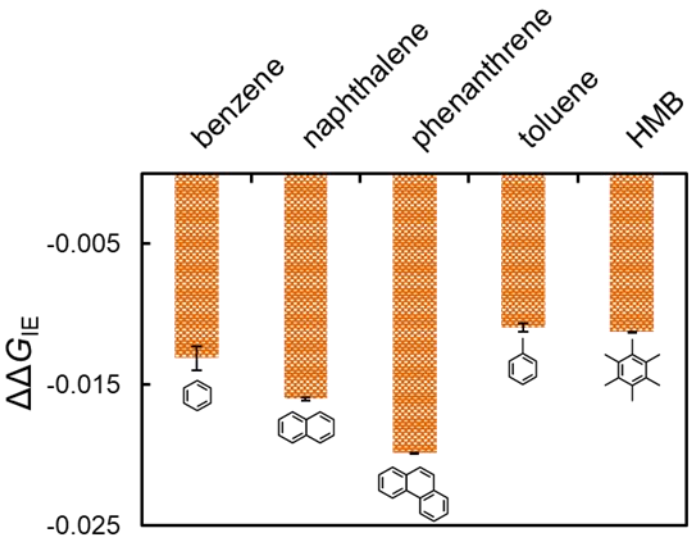

Figure 3. $\Delta\Delta G_{IE}$ of aromatic solutes on Silica column in NPLC. Conditions were the same as Figure 1.

5-3-2 Thermodynamic parameters of isotope effects on the OH-π interaction

The OH-π interaction is a kind of π interaction and is caused by dipole-induced dipole interactions or induced dipole-induced dipole interactions.[49] The potential energy of the dipole-induced dipole interaction ($E_{\text{dipole-induced dipole}}$) is given by the following equation.[40]

$$E_{\text{dipole-induced dipole}} = -\mu^2\alpha/16\pi\,\varepsilon_0{}^2\varepsilon_r{}^2\,r^6 \qquad (8)$$

The potential energy of the induced dipole-induced dipole interaction ($E_{\text{induced-dipole-induced dipole}}$) is given by,

$$E_{\text{induced-dipole-induced dipole}} = -A\alpha_1\alpha_2/16\pi\,\varepsilon_0{}^2\varepsilon_r{}^2\,r^6 \qquad (9)$$

where A, μ, and α are constants that depend on the ionisation energy, the dipole moment of polar molecules, and the polarisabilities of the molecules, respectively. Both interactions are based on the electrostatic force. We can derive the temperature dependence from the application of van't Hoff's equation for chromatography,[50-51]

$$\ln k = \ln V_S / V_M - \Delta G/\mathrm{R}\,T = \ln V_S / V_M - \Delta H / \mathrm{R}\,T + \Delta S / \mathrm{R} \qquad (10)$$

where ΔH and ΔS are alterations of the enthalpy and entropy, respectively, in the chromatographic partition equilibrium. Thus, the differences in ΔH_{TIE} and ΔS_{TIE} between protiated and deuterated compounds ($\Delta\Delta H_{\text{TIE}}$, $\Delta\Delta S_{\text{TIE}}$) could be obtained. We then calculated $\Delta\Delta H_{\text{IE}}$ and $\Delta\Delta S_{\text{IE}}$, which reflected the average influence of a single H/D substitution, with the following equations.

$$\Delta\Delta H_{\text{IE}} = \Delta\Delta H_{\text{TIE}} / n_{\text{HD}} \qquad (11)$$

$$\Delta\Delta S_{\text{IE}} = \Delta\Delta S_{\text{TIE}} / n_{\text{HD}} \qquad (12)$$

The chromatograms and the plots of the separation factors of phenanthrene and HMB H/D isotopologue pairs at different temperatures are shown in Figure 4 (a-c). As expected from Equation 10, the separation factors for the Silica column tended to decrease as the temperature increased. We prepared the van't Hoff plots for phenanthrene and HMB

(Figure 4 (d, e)) and summarised the $\Delta\Delta H_{IE}$ and $T\Delta\Delta S_{IE}$ values (T = 25 °C) in Table 2. For both analytes, $\Delta\Delta H_{IE}$ and $T\Delta\Delta S_{IE}$ were negative values. Furthermore, the $\Delta\Delta H_{IE}$ of phenanthrene was slightly smaller than that of HMB. These results are consistent with our hypothesis that the hydrogen atoms on sp^2 carbon atoms show stronger electrostatic attractions and greater isotope effects than those on sp^3 carbon atoms. Consequently, we supposed that the isotope effects on OH-π interactions were due to electrostatic attraction.

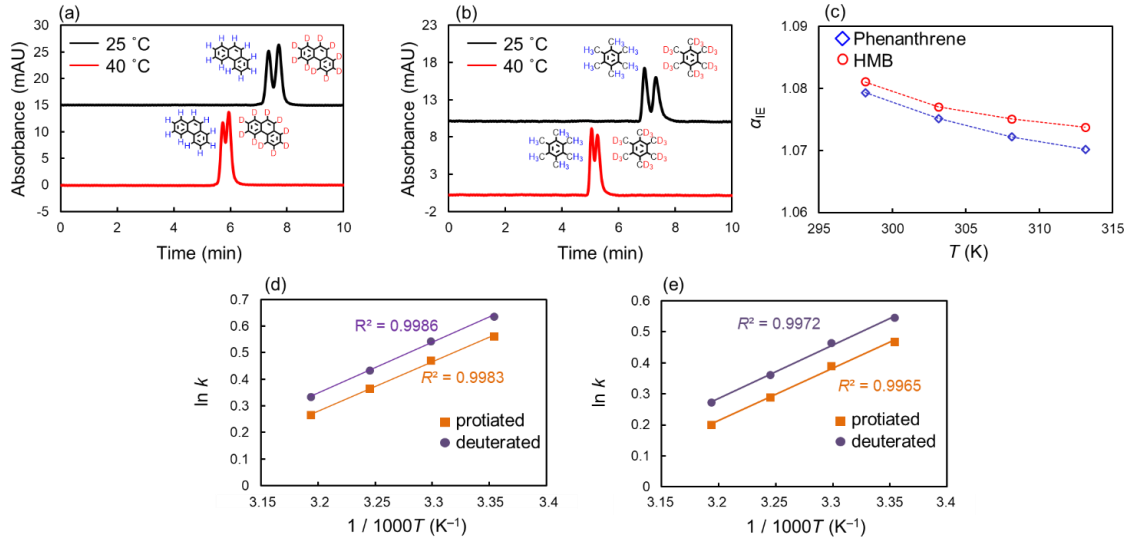

Figure 4. Separation behaviors of H/D isotopologue pairs with the Silica column at different temperatures. Chromatograms of (a) phenanthrene and (b) HMB; (c) plots of the separation factors on the Silica column as a function of measured temperature. Van't Hoff plots of (d) phenanthrene and (e) HMB with the Silica column. Conditions were the same as in Figure 1.

Table 2. Thermodynamic parameters (T = 25 °C) obtained from van't Hoff plots with Silica column.

	$\Delta\Delta H_{IE}$	$T\Delta\Delta S_{IE}$
Phenanthrene	-43.92 J / mol	-0.08 J / mol
HMB	-19.24 J / mol	-0.03 J / mol

5-3-3 Solvent effects on the OH-π interaction

As mentioned above, the OH-π interaction is an electrostatic attraction and can be described with Equations 8 and 9. From these equations, we developed a hypothesis that the strength of the OH-π interaction and the isotope effect are strongly affected by the dielectric constant of the solvents involved. To confirm this hypothesis, we evaluated the separation behaviour of the H/D isotopologue pairs of phenanthrene and HMB on the Silica column with normal alkanes (NAs) having dielectric constants different from those of the mobile phases. The chromatograms of the isotopologues in *n*-pentane, *n*-hexane, and *n*-octane on the Silica column are shown in Figure 5 (a, b), and the plots of α_{IE} for each analyte against the dielectric constants are shown in Figure 5 (c). As we expected, both analytes showed decreases in the retention factors with increases to the dielectric constant of the mobile phase. The results supported the notion that the electrostatic attraction with the Silica column caused the retention of these analytes.

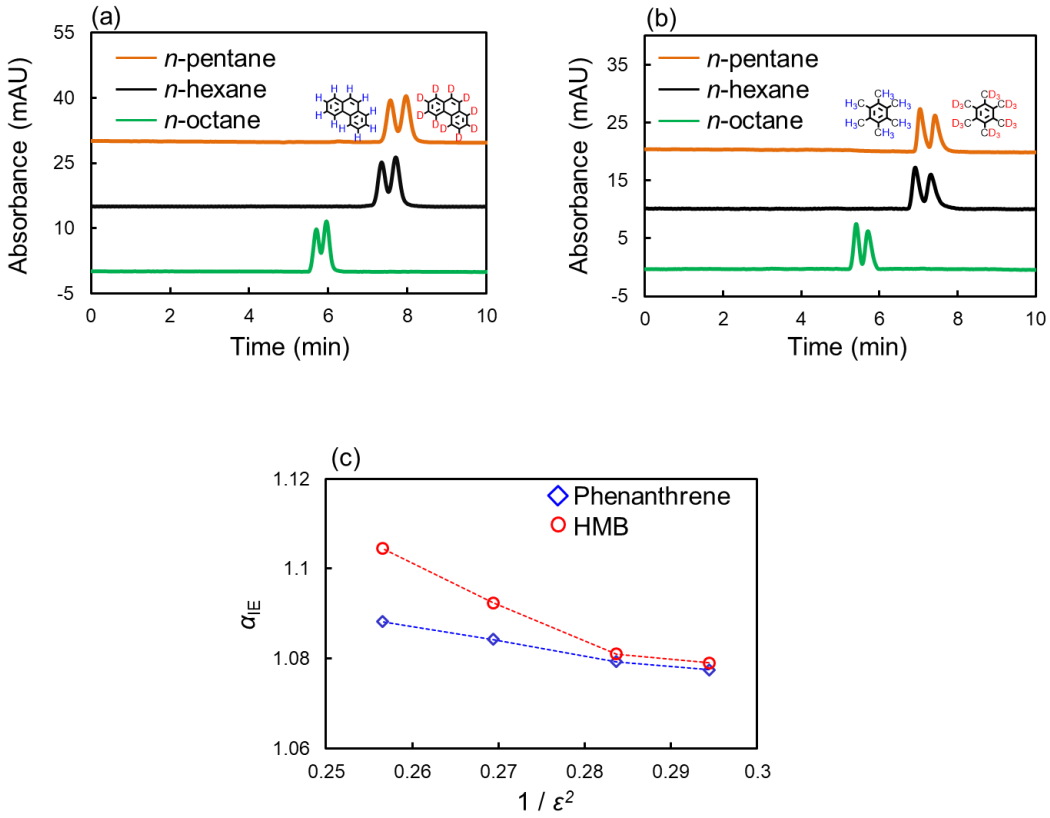

Figure 5. Separation behaviors of H/D isotopologue pairs with the Silica column in various NAs. Chromatograms of (a) phenanthrene and (b) HMB; (c) the plots of α_{IE} on the Silica column as a function of $1/\varepsilon^2$. Conditions were the same as in Figure 1.

In contrast, the α_{IE} values of both analytes increased slightly with the increase in the dielectric constant of the mobile phase. We considered that the increase in the strength of the isotope effect in these analytes might have been due to the dipole-induced dipole interactions or the induced dipole-induced dipole interactions between the mobile phase and analytes. As many reports have shown,[52-55] the dipole-induced dipole interaction and the induced dipole-induced dipole interaction are caused by the dispersion force. For non-polar molecules, such as NAs, the induced dipole interaction is similarly affected. These interactions are enhanced by longer chains in NAs,[56-58] which explains why induced dipole interactions occurred partially between the NAs and analytes in our evaluation. Briefly, when the isotope effect due to the induced dipole interaction between the analytes and NAs as mobile phases became greater, the separation factor of the H/D isotopologue pairs also became greater. In this case, NAs with longer chains provide stronger interactions with protiated analytes. As shown in a schematic energy diagram (Figure 6), the alteration of the free energy of the analytes between the mobile phases and the Silica column was higher in NAs with longer chains. Therefore, although the absolute retention of the analytes decreased, the α_{IE} values increased slightly in NAs with longer chains.

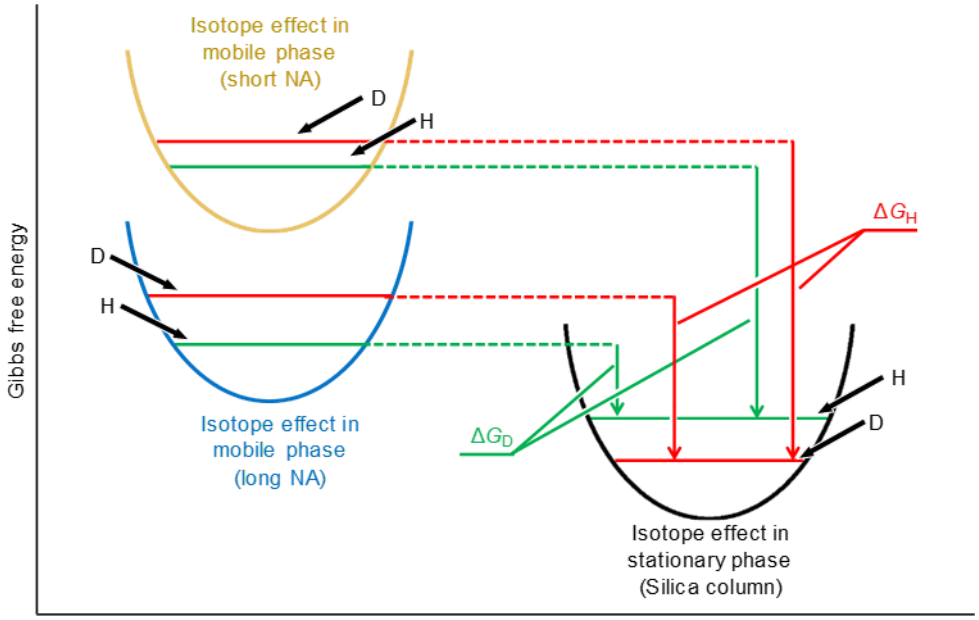

Figure 6. Schematic diagram of free energies caused by the intermolecular interaction with the Silica column under NAs as mobile phases.

5-3-4 Evaluation of the isotope effect on CH–π interactions

In this section, we suggested that weak interactions, such as the dipole-induced dipole interaction and the induced dipole-induced dipole interaction, contributed to the isotope effect on the hydrophilic columns. Furthermore, we previously succeeded in confirming the isotope effect of the CH-π interaction in the C70 column.[42] Here, we evaluated the dependence of the isotope effect of the CH-π interaction on the temperature and dielectric constant in the same way as the previous sections. Figure 7 shows the chromatograms for the H/D isotopologue pairs on the C70 column. Although the divided peaks were not observed for benzene, toluene, and naphthalene, separations at the tops of the peaks were confirmed for phenanthrene and HMB. In agreement with our previous study, the protiated analytes were strongly retained on the C70 column but not the hydrophilic columns. The results showed that the CH-π interaction effected the opposite force compared to the intermolecular interaction with polar functional groups. Here, we consider the geometric isotope effect (GIE) contributing towards the CH-π interactions.[59-60] H/D isotope effects in intermolecular interactions are often caused by the GIE, based on intermolecular distance. Briefly, the longer bonding distance of C-H bonds could provide a preferable interaction compared to C-D bonds; thus the CH-π interaction is slightly stronger than the CD-π interaction. Meanwhile, the covalent bond between a deuterium and a carbon atom was stronger and had a shorter bonding length than that between a proton and a carbon atom; therefore, the shorter intermolecular distance allows the CH-π interaction to be stronger than the CD-π interaction (Figure 8 (a)). Furthermore, we evaluated $\Delta\Delta G_{IE}$ to quantify the isotope effect for phenathrene and HMB (Figure 8 (b)). According to Figure 8, the isotope effect of HMB was slightly greater than that of phenanthrene. In this case, the π-π interactions with HMB were not competitive because

of the steric hindrance from the methyl groups[61-63]; the effect from the CH-π interaction could then be observed.

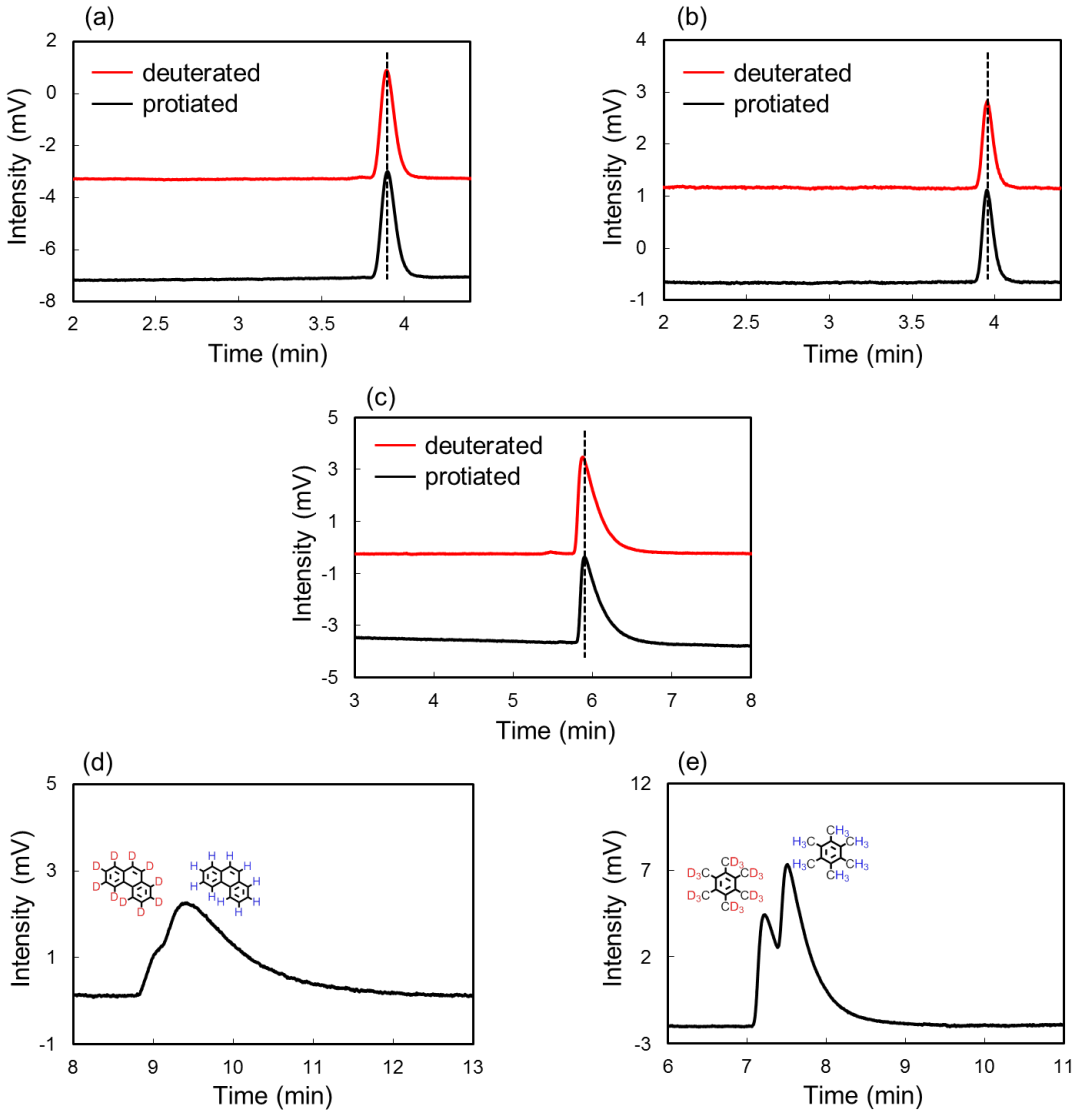

Figure 7. Separations of hte H/D isotopologue pairs of (a) benzene, (b) toluene, (c) naphthalene (d) phenanthrene, and (e) HMB on C70 column.
Conditions: column, C70 column (75.0 cm × 100 μm i.d.); flow rate, 2.0 μL min^{-1}; mobile phase, *n*-hexane; detection, UV (a), (c), (d) 254 nm, (b), (e) 220 nm; temperature, 25 °C.

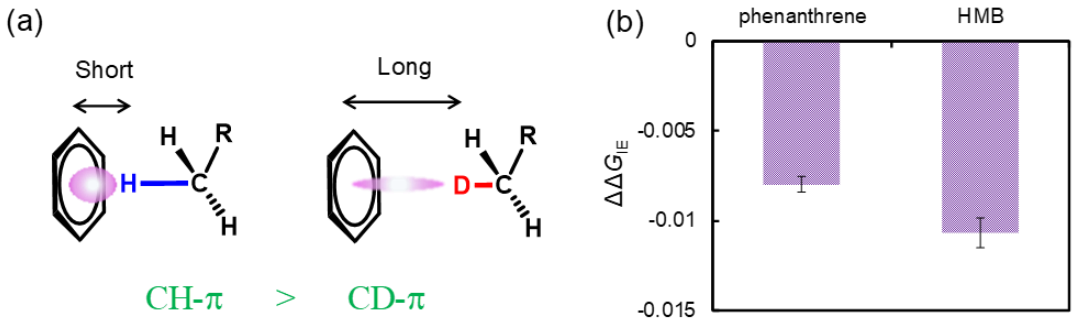

Figure 8. Schematic image of the interaction distance between CH-π and CH-π interactions (a) and $\Delta\Delta G_{IE}$ of the aromatic analytes on the C70 column in NPLC. Conditions: column, C70 column (75.0 cm × 100 μm i.d.); flow rate, 2.0 μL min^{-1}; mobile phase, *n*-hexane; detection, UV 254 nm (phenanthrene), 220 nm (HMB); temperature, 25 °C.

5-3-5 Thermodynamic parameters of isotope effects on CH-π interactions

The temperature dependence of the CH-π interaction was evaluated. The chromatograms and plots of the separation factors are shown in Figure 9 (a, b) and (c), respectively. In Figure 9 (c), we employed the quantity $1/\alpha_{IE}$ because of the higher retention of protiated analytes. Similar to the case of the OH-π interaction, a temperature increase caused a decrease in the separation factors. Considering Equations 8 and 9, the temperature alteration did not affect the CH-π interaction, so that the typical van't Hoff equation could be applied. Figure 9 (d, e) and Table 3 summarise the van't Hoff plots and each parameter, respectively. According to these results, negative values were observed for both $T\Delta\Delta S_{IE}$ and $\Delta\Delta H_{IE}$. Therefore, the isotope effects on the CH-π interaction were also caused by the electrostatic attraction.

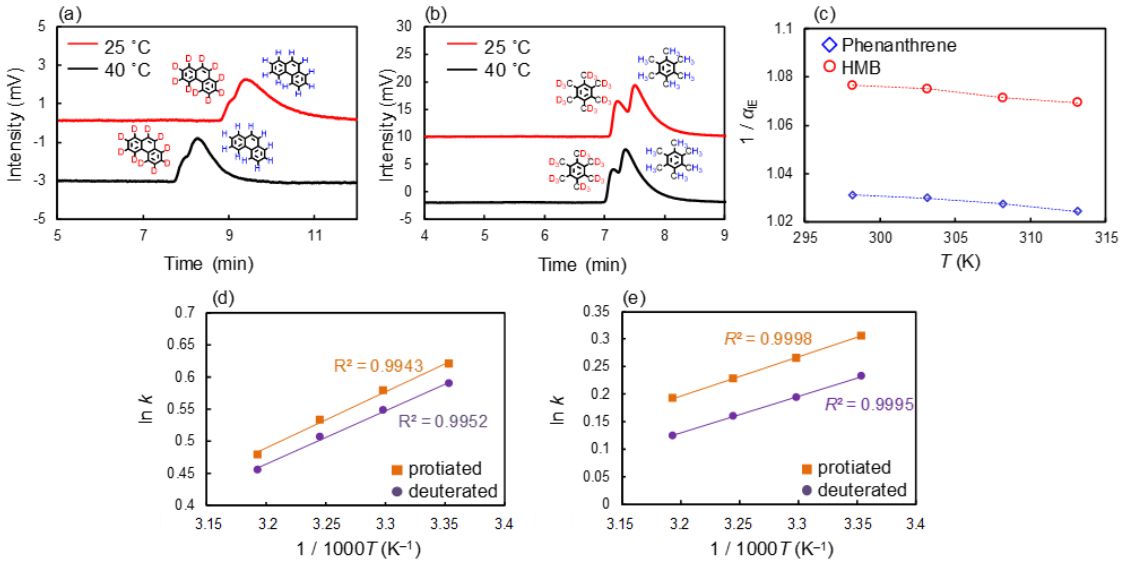

Figure 9. Separation of H/D isotopologue pairs with the C70 column at different temperature. Chromatograms of (a) phenanthrene and (b) HMB; (c) the plots of separation factors in the C70 column as a function of measured temperature. van't Hoff plots of (d) phenanthrene and (e) HMB in C70 column. Conditions: column, C70 column (75.0 cm × 100 µm i.d.); flow rate, 2.0 µL min^{-1}; mobile phase, *n*-hexane; detection, UV 254 nm (phenanthrene), 220 nm (HMB); temperature, 25, 30, 35, and 40 °C.

Table 3. Thermodynamic parameters (T = 25 ºC) obtained from van't Hoff plots with Silica column.

	$\Delta\Delta H_{IE}$	$T\Delta\Delta S_{IE}$
Phenanthrene	-34.47 J / mol	-0.09 J / mol
HMB	-20.07 J / mol	-0.03 J / mol

5-3-6 Solvent effects on CH-π interactions

As mentioned above, we proposed that the isotope effect on the CH-π interaction was caused by the GIE. Following from Equations 8 and 9, this interaction is inversely proportional to the dielectric constant of the mobile phase. Thus, the retention behaviors of the H/D isotopologue pairs of phenanthrene and HMB were evaluated with the C70 column using various NAs. As shown in Figures 10 and 11 (a), the separations of the H/D isotopologue pairs worsened and their separation factors decreased as the dielectric constant increased. In addition, the rate of the decreases in the separation factor as the dielectric constant increased for the CH-π interaction was steep in comparison to the interaction with polar functional groups. This result was caused not only by suppression of the CH-π interactions but also by competition from the isotope effect due to the dipole-induced dipole or induced dipole-induced dipole interactions from the longer chains of the NAs. Briefly, stronger isotope effects from these interactions in the mobile phases allowed stronger affinities toward the protiated analytes; then, the difference in the stabilizing energy between the mobile phase (NAs) and stationary phase (C70) became smaller (Figure 11 (b)).

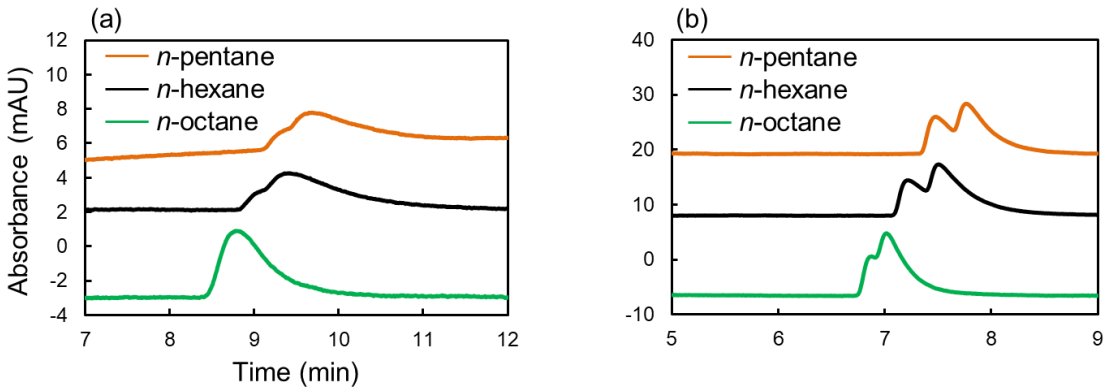

Figure 10. Chromatograms of (a) phenanthrene and (b) HMB.
Conditions: column, C70 column (75.0 cm × 100 μm i.d.); flow rate, 2.0 μL min^{-1}; mobile phase, *n*-pentane, *n*-hexane, *n*-heptane, *n*-octane; detection, UV 254 nm (phenanthrene), 220 nm (HMB); temperature, 25 °C.

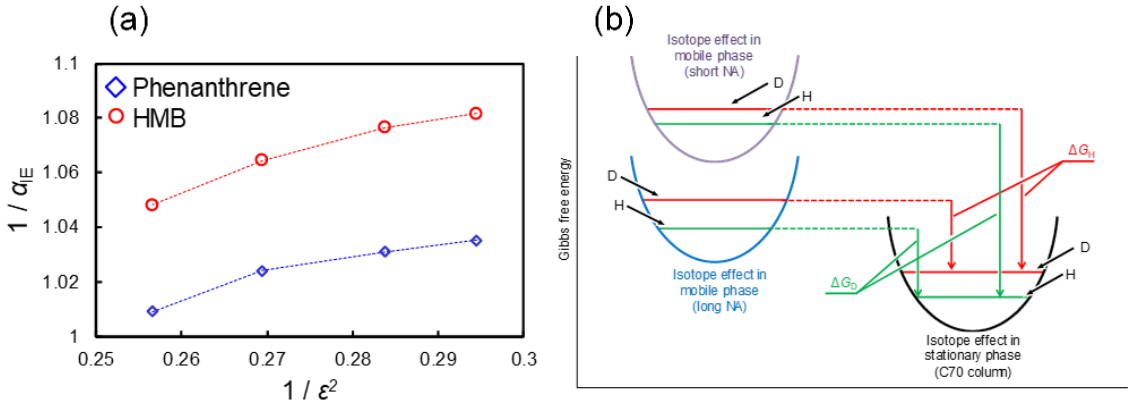

Figure 11. Separation behaviors of H/D isotopologue pairs on the C70 column in various NAs.
(a) the plots of separation factors on the C70 column as a function of 1 / ε^2. (b) schematic diagram of free energies caused by the CH-π interaction with the C70 column under NAs as mobile phases. Conditions: column, C70 column (75.0 cm × 100 μm i.d.); flow rate, 2.0 μL min^{-1}; mobile phase, *n*-pentane, *n*-hexane, *n*-heptane, *n*-octane; detection, UV 254 nm (phenanthrene), 220 nm (HMB); temperature, 25 °C.

5-3-7 Separation of isotopologues on the C70 column by complementary intermolecular interactions

As discussed above, the strength of the isotope effects can be controlled by optimising the intermolecular interactions with polar functional groups and CH-π interactions. We were then finally able to demonstrate an effective isotope separation by employing both interactions. We utilised the intermolecular interaction with the polar mobile phase and the CH-π interaction with the stationary phase. In brief, methanol was used as a mobile phase to cause stronger interactions with the deuterated analytes by OH-π interactions, and the C70 column was used as a stationary phase to cause stronger interactions with deuterated analytes by CH-π interactions. To find suitable separation conditions, the flow rate of the mobile phase was optimised according to the van Deemter plots for the C70 column (Figure 12).[64] For comparison, an octadecylsilyl column (ODS column) for confirming the influence of the effective hydrophobic interactions and a commercially available LC column for confirming the influence of the effective π-π interactions, PYE®, in which the spherical silica particles modified with pyrene moieties were packed, were also employed under the same conditions. The chromatograms with the ODS, PYE, and C70 columns are summarised in Figure 13. For the ODS column, isotope separation was not observed, whereas PYE provided a slight H/D separation. The C70 column showed clear H/D separations of phenanthrene that were almost baseline ($1.18 > 1 / \alpha_{IE}$) (Figure 13 (c)). These results suggested that the H/D separations in the C70 column with methanol were not due to the hydrophobic interaction, and preferable H/D separation might be achieved by the complementary actions of the OH-π interactions in the mobile phase and CH-π interactions with C70.

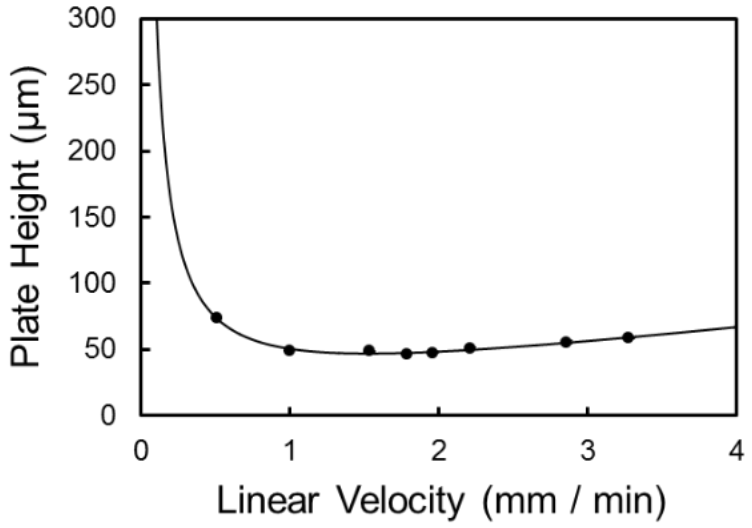

Figure 12. van Deemter plot for C70 column.
Conditions: column, C70 column (75.0 cm × 100 μm i.d.); mobile phase, methanol; detection, UV 254 nm; temperature, 25 °C.

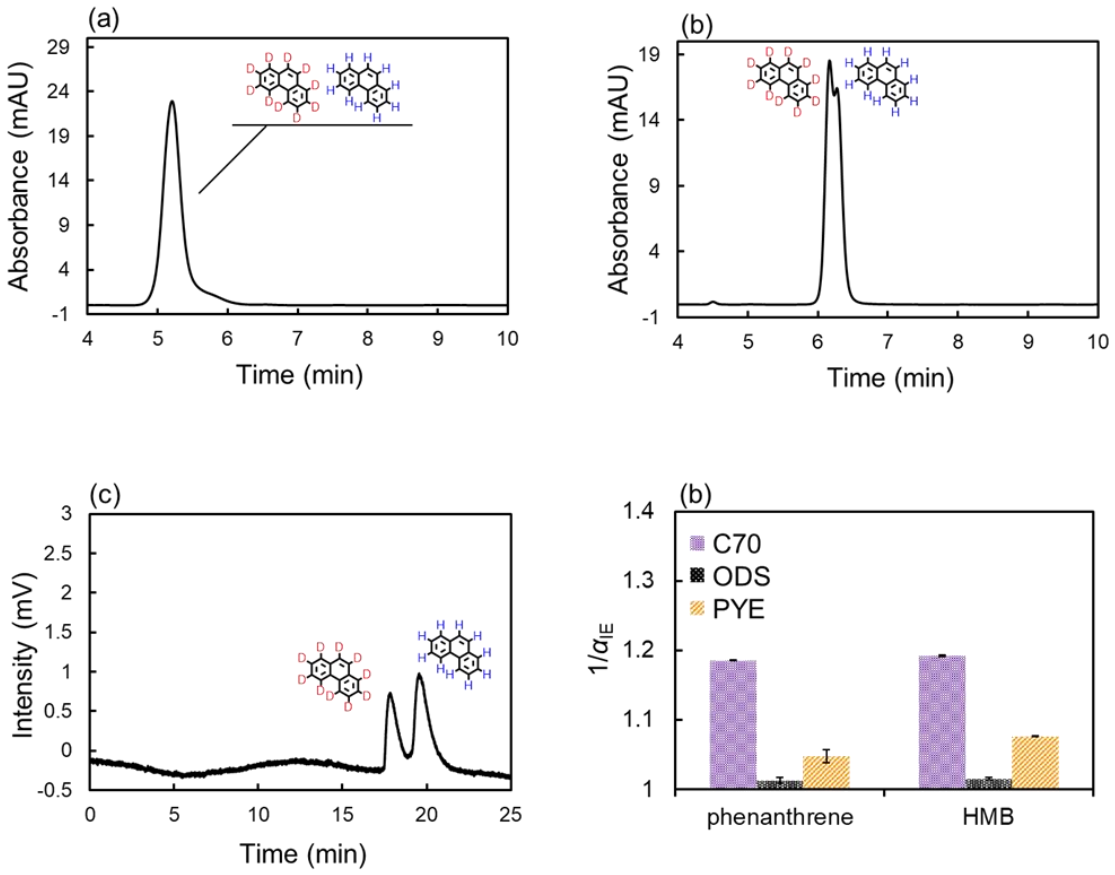

Figure 13. Separation behaviors of H/D isotopologue pairs in ODS, PYE, and C70 column with methanol as a mobile phase. (a), (b), (c) Chromatograms of phenanthrene H/D isotopologue pairs in (a) ODS, (b) PYE®, and (c) the C70 columns, (d) separation factors of phenanthrene and HMB in each column. Conditions: column, (a) Mightysil-C18 column (Kanto Chemicals, 150 mm × 4.6 mm i.d.), (b) PYE (Nacalai Tesque, 150 mm × 4.6 mm i.d.) and (c) C70 column (75.0 cm × 100 μm i.d.); flow rate, (a), (b) 0.5 mL min^{-1}, (c) 0.8 μL min^{-1}; mobile phase, methanol; detection, UV 254 nm (phenanthrene), 220 nm (HMB); temperature, 25 °C.

5-4 Conclusions

In order to understand the H/D isotope effect based on the intermolecular interactions with polar functional groups and aromatic rings, liquid chromatography experiments were conducted under various conditions. The intermolecular interaction with polar functional groups affected the deuterated isotopologues significantly more than the protiated isotopologues. Furthermore, the ^{13}C NMR spectra of the H/D isotopologues and the van't Hoff evaluations suggested that the isotope effect of the intermolecular interaction with polar functional groups was based on the electrostatic OH or NH-π interaction, in which the aromatic rings of the H/D isotopologues acted as donors to the protons of the polar functional groups in the hydrophilic stationary phases. Furthermore, NPLC evaluation of the C70 column suggested that the CH-π interaction showed an isotope effect opposite to that based on the GIE. Finally, we successfully demonstrated the effective H/D separation of phenanthrene by introducing the complementary isotope effect to the OH-π interaction and CH-π interaction. we believe that the isotope effect based on these weak intermolecular interactions can be useful for the effective and rapid separation of H/D isotopologues.

5-5 References

1 Atzrodt, J.; Derdau, V.; Kerr, W. J.; Reid, M., Deuterium- and Tritium-Labelled Compounds: Applications in the Life Sciences. *Angew. Chem. Int. Ed.* **2018,** *57*, 1758-1784.

2 Zhang, Z.; Zhang, A.; Xiao, G., Improved Protein Hydrogen/Deuterium Exchange Mass Spectrometry Platform with Fully Automated Data Processing. *Anal. Chem.* **2012,** *84*, 4942-4949.

3 Merlet, D.; Ancian, B.; Courtieu, J.; Lesot, P., Two-Dimensional Deuterium NMR Spectroscopy of Chiral Molecules Oriented in a Polypeptide Liquid Crystal: Applications for the Enantiomeric Analysis through Natural Abundance Deuterium NMR. *J. Am. Chem. Soc.* **1999,** *121*, 5249-5258.

4 Thibblin, A.; Ahlberg, P., Reaction branching and extreme kinetic isotope effects in the study of reaction mechanisms. *Chem. Soc. Rev.* **1989,** *18*, 209-224.

5 Liu, C.; Chen, Z.; Su, C.; Zhao, X.; Gao, Q.; Ning, G.-H.; Zhu, H.; Tang, W.; Leng, K.; Fu, W.; Tian, B.; Peng, X.; Li, J.; Xu, Q.-H.; Zhou, W.; Loh, K. P., Controllable deuteration of halogenated compounds by photocatalytic D2O splitting. *Nat. Commun.* **2018,** *9*, 80.

6 Miyashita, M.; Sasaki, M.; Hattori, I.; Sakai, M.; Tanino, K., Total Synthesis of Norzoanthamine. *Science* **2004,** *305*, 495.

7 Sorensen, J. L.; Sleeman, M. C.; Schofield, C. J., Synthesis of deuterium labelled l- and d-glutamate semialdehydes and their evaluation as substrates for carboxymethylproline synthase (CarB)—implications for carbapenem biosynthesis. *Chem. Commun.* **2005,** 1155-1157.

8 Zhang, Z.; Chen, L.; Liu, L.; Su, X.; Rabinowitz, J. D., Chemical Basis for Deuterium

Labeling of Fat and NADPH. *J. Am. Chem. Soc.* **2017,** *139*, 14368-14371.

9 Billault, I.; Mantle, P. G.; Robins, R. J., Deuterium NMR Used To Indicate a Common Mechanism for the Biosynthesis of Ricinoleic Acid by Ricinus communis and Claviceps purpurea. *J. Am. Chem. Soc.* **2004,** *126*, 3250-3256.

10 Markai, S.; Marchand, P. A.; Mabon, F.; Baguet, E.; Billault, I.; Robins, R. J., Natural Deuterium Distribution in Branched-Chain Medium-Length Fatty Acids is Nonstatistical: A Site-Specific Study by Quantitative 2H NMR Spectroscopy of the Fatty Acids of Capsaicinoids. *ChemBioChem* **2002,** *3*, 212-218.

11 Englander, J. J.; Del Mar, C.; Li, W.; Englander, S. W.; Kim, J. S.; Stranz, D. D.; Hamuro, Y.; Woods, V. L., Protein structure change studied by hydrogen-deuterium exchange, functional labeling, and mass spectrometry. *Proc. Natl. Acad. Sci. USA* **2003,** *100*, 7057.

12 Jiang, Y.; Geng, H.; Shi, W.; Peng, Q.; Zheng, X.; Shuai, Z., Theoretical Prediction of Isotope Effects on Charge Transport in Organic Semiconductors. *J. Phys. Chem. Lett.* **2014,** *5*, 2267-2273.

13 Gant, T. G., Using Deuterium in Drug Discovery: Leaving the Label in the Drug. *J. Med. Chem.* **2014,** *57*, 3595-3611.

14 Atzrodt, J.; Derdau, V.; Kerr, W. J.; Reid, M., C−H Functionalisation for Hydrogen Isotope Exchange. *Angew. Chem. Int. Ed.* **2018,** *57*, 3022-3047.

15 Mullard, A., FDA approves first deuterated drug. *Nat. Rev. Drug Discov.* **2017,** *16*, 305.

16 Simon, H.; Palm, D., Isotope Effects in Organic Chemistry and Biochemistry. *Angew. Chem. Int. Ed.* **1966,** *5*, 920-933.

17 Wiberg, K. B., The Deuterium Isotope Effect. *Chem. Rev.* **1955,** *55*, 713-743.

18 Wolfsberg, M., Theoretical evaluation of experimentally observed isotope effects. *Acc. Chem. Res.* **1972,** *5*, 225-233.

19 Westheimer, F. H., The Magnitude of the Primary Kinetic Isotope Effect for Compounds of Hydrogen and Deuterium. *Chem. Rev.* **1961,** *61*, 265-273.

20 Clive, D. L. J.; Tao, Y.; Khodabocus, A.; Wu, Y.-J.; Angoh, A. G.; Bennett, S. M.; Boddy, C. N.; Bordeleau, L.; Kellner, D., Total Synthesis of Crystalline (.+-.)-Fredericamycin A. Use of Radical Spirocyclization. *J. Am. Chem. Soc.* **1994,** *116*, 11275-11286.

21 Vedejs, E.; Little, J., Aziridinomitosenes by Anionic Cyclization: Deuterium as a Removable Blocking Group. *J. Am. Chem. Soc.* **2002,** *124*, 748-749.

22 Huang, J.; Buchowiecki, M.; Nagy, T.; Vaníček, J.; Meuwly, M., Kinetic isotope effect in malonaldehyde determined from path integral Monte Carlo simulations. *Phys. Chem. Chem. Phys.* **2014,** *16*, 204-211.

23 González-Lafont, À.; Lluch, J. M., Kinetic isotope effects in chemical and biochemical reactions: physical basis and theoretical methods of calculation. *Wiley Interdiscip. Rev. Comput. Mol. Sci.* **2016,** *6*, 584-603.

24 Bartell, L. S.; Roskos, R. R., Isotope Effects on Molar Volume and Surface Tension: Simple Theoretical Model and Experimental Data for Hydrocarbons. *J. Chem. Phys.* **1966,** *44*, 457-463.

25 Haino, T.; Fukuta, K.; Iwamoto, H.; Iwata, S., Noncovalent Isotope Effect for Guest Encapsulation in Self-Assembled Molecular Capsules. *Chem.: Eur. J.* **2009,** *15*, 13286-13290.

26 Tresca, B. W.; Brueckner, A. C.; Haley, M. M.; Cheong, P. H. Y.; Johnson, D. W., Computational and Experimental Evidence of Emergent Equilibrium Isotope Effects

in Anion Receptor Complexes. *J. Am. Chem. Soc.* **2017,** *139*, 3962-3965.

27 Paris, A.; Verbitskiy, N.; Nefedov, A.; Wang, Y.; Fedorov, A.; Haberer, D.; Oehzelt, M.; Petaccia, L.; Usachov, D.; Vyalikh, D.; Sachdev, H.; Wöll, C.; Knupfer, M.; Büchner, B.; Calliari, L.; Yashina, L.; Irle, S.; Grüneis, A., Kinetic Isotope Effect in the Hydrogenation and Deuteration of Graphene. *Adv. Funct. Mater.* **2013,** *23*, 1628-1635.

28 Bai, Y.; Chen, B. W. J.; Peng, G.; Mavrikakis, M., Density functional theory study of thermodynamic and kinetic isotope effects of H2/D2 dissociative adsorption on transition metals. *Catal. Sci. Technol.* **2018,** *8*, 3321-3335.

29 Zhao, C.; Parrish, R. M.; Smith, M. D.; Pellechia, P. J.; Sherrill, C. D.; Shimizu, K. D., Do Deuteriums Form Stronger CH−π Interactions? *J. Am. Chem. Soc.* **2012,** *134*, 14306-14309.

30 Tsuji, H.; Mitsui, C.; Nakamura, E., The hydrogen/deuterium isotope effect of the host material on the lifetime of organic light-emitting diodes. *Chem. Commun.* **2014,** *50*, 14870-14872.

31 Claessens, H. A., Trends and progress in the characterization of stationary phases for reversed-phase liquid chromatography. *Trends Anal. Chem.* **2001,** *20*, 563-583.

32 Tanaka, N.; Tanigawa, T.; Kimata, K.; Hosoya, K.; Arai, T., Selectivity of carbon packing materials in comparison with octadecylsilyl- and pyrenylethylsilylsilica gels in reversed- phase liquid chromatography. *J. Chromatogr. A* **1991,** *549*, 29-41.

33 Kimata, K.; Hosoya, K.; Tanaka, N.; Araki, T.; Tsuboi, R.; Haginaka, J., Effect of stationary phase structure on retention and selectivity of restricted-access reversed-phase packing materials. *J. Chromatogr. A* **1991,** *558*, 19-30.

34 Kawachi, Y.; Ikegami, T.; Takubo, H.; Ikegami, Y.; Miyamoto, M.; Tanaka, N.,

Chromatographic characterization of hydrophilic interaction liquid chromatography stationary phases: Hydrophilicity, charge effects, structural selectivity, and separation efficiency. *J. Chromatogr. A* **2011,** *1218*, 5903-5919.

35 Kimata, K.; Hosoya, K.; Araki, T.; Tanaka, N., [2-(1-Pyrenyl)ethyl]silyl silica packing material for liquid chromatographic separation of fullerenes. *J. Org. Chem.* **1993,** *58*, 282-283.

36 Chen, S.; Meyerhoff, M., Shape-Selective Retention of Polycyclic Aromatic Hydrocarbons on Metalloprotoporphyrin−Silica Phases: Effect of Metal Ion Center and Porphyrin Coverage. *Anal. Chem.* **1998,** *70*, 2523-2529.

37 Kubo, T.; Murakami, Y.; Tominaga, Y.; Naito, T.; Sueyoshi, K.; Yan, M.; Otsuka, K., Development of a C60-fullerene bonded open-tubular capillary using a photo/thermal active agent for liquid chromatographic separations by π–π interactions. *J. Chromatogr. A* **2014,** *1323*, 174-178.

38 Kubo, T.; Murakami, Y.; Tsuzuki, M.; Kobayashi, H.; Naito, T.; Sano, T.; Yan, M.; Otsuka, K., Unique Separation Behavior of a C60 Fullerene-Bonded Silica Monolith Prepared by an Effective Thermal Coupling Agent. *Chem.: Eur. J.* **2015,** *21*, 18095-18098.

39 Kubo, T.; Kanao, E.; Matsumoto, T.; Naito, T.; Sano, T.; Yan, M.; Otsuka, K., Specific Intermolecular Interactions by the Localized π-Electrons in C70-fullerene. *ChemistrySelect* **2016,** *1*, 5900-5904.

40 Kanao, E.; Kubo, T.; Naito, T.; Matsumoto, T.; Sano, T.; Yan, M.; Otsuka, K., Differentiating π interactions by constructing concave/convex surfaces using a bucky bowl molecule, corannulene in liquid chromatography. *Anal. Chem.* **2019,** *91*, 2439-2446.

41 Turowski, M.; Yamakawa, N.; Meller, J.; Kimata, K.; Ikegami, T.; Hosoya, K.; Tanaka, N.; Thornton, E. R., Deuterium Isotope Effects on Hydrophobic Interactions: The Importance of Dispersion Interactions in the Hydrophobic Phase. *J. Am. Chem. Soc.* **2003,** *125*, 13836-13849.

42 Kanao, E.; Kubo, T.; Naito, T.; Matsumoto, T.; Sano, T.; Yan, M.; Otsuka, K., Isotope Effects on Hydrogen Bonding and CH/CD−π Interaction. *J. Phys. Chem. C* **2018,** *122*, 15026-15032.

43 Gilli, P.; Pretto, L.; Bertolasi, V.; Gilli, G., Predicting Hydrogen-Bond Strengths from Acid−Base Molecular Properties. The pKa Slide Rule: Toward the Solution of a Long-Lasting Problem. *Acc. Chem. Res.* **2009,** *42*, 33-44.

44 Steiner, T., Donor and acceptor strengths in C–H···O hydrogen bonds quantified from crystallographic data of small solvent molecules. *New J. Chem.* **1998,** *22*, 1099-1103.

45 Tsuzuki, S.; Honda, K.; Uchimaru, T.; Mikami, M.; Tanabe, K., Origin of the Attraction and Directionality of the NH/π Interaction: Comparison with OH/π and CH/π Interactions. *J. Am. Chem. Soc.* **2000,** *122*, 11450-11458.

46 Maier, J. M.; Li, P.; Vik, E. C.; Yehl, C. J.; Strickland, S. M. S.; Shimizu, K. D., Measurement of Solvent OH−π Interactions Using a Molecular Balance. *J. Am. Chem. Soc.* **2017,** *139*, 6550-6553.

47 Mohan, N.; Vijayalakshmi, K. P.; Koga, N.; Suresh, C. H., Comparison of aromatic NH···π, OH···π, and CH···π interactions of alanine using MP2, CCSD, and DFT methods. *J. Comput. Chem.* **2010,** *31*, 2874-2882.

48 Takahashi, H.; Suzuoka, D.; Morita, A., Why is Benzene Soluble in Water? Role of OH/π Interaction in Solvation. *J. Chem. Theory Comput.* **2015,** *11*, 1181-1194.

49 Albertí, M.; Aguilar, A.; Huarte-Larrañaga, F.; Lucas, J. M.; Pirani, F., Benzene–Hydrogen Bond (C6H6–HX) Interactions: The Influence of the X Nature on their Strength and Anisotropy. *J. Phys. Chem. A* **2014,** *118*, 1651-1662.

50 Chester, T. L.; Coym, J. W., Effect of phase ratio on van't Hoff analysis in reversed-phase liquid chromatography, and phase-ratio-independent estimation of transfer enthalpy. *J. Chromatogr. A* **2003,** *1003*, 101-111.

51 Kim, Y.; Ahn, S.; Chang, T., Isotopic effect in the separation of polystyrene by normal phase and reversed phase liquid chromatography. *Anal. Chem.* **2010,** *82*, 1509-1514.

52 Nishio, M., The CH/π hydrogen bond in chemistry. Conformation, supramolecules, optical resolution and interactions involving carbohydrates. *Phys. Chem. Chem. Phys.* **2011,** *13*, 13873-13900.

53 Sherrill, C. D., Energy Component Analysis of π Interactions. *Acc. Chem. Res.* **2013,** *46*, 1020-1028.

54 Kobayashi, K.; Asakawa, Y.; Kikuchi, Y.; Toi, H.; Aoyama, Y., CH-π interaction as an important driving force of host-guest complexation in apolar organic media. Binding of monools and acetylated compounds to resorcinol cyclic tetramer as studied by proton NMR and circular dichroism spectroscopy. *J. Am. Chem. Soc.* **1993,** *115*, 2648-2654.

55 Kim, E.-i.; Paliwal, S.; Wilcox, C. S., Measurements of Molecular Electrostatic Field Effects in Edge-to-Face Aromatic Interactions and CH-π Interactions with Implications for Protein Folding and Molecular Recognition. *J. Am. Chem. Soc.* **1998,** *120*, 11192-11193.

56 Yang, L.; Adam, C.; Nichol, G. S.; Cockroft, S. L., How much do van der Waals dispersion forces contribute to molecular recognition in solution? *Nat. Chem.* **2013,**

5, 1006.

57 Inoue, S.; Minemawari, H.; Tsutsumi, J. y.; Chikamatsu, M.; Yamada, T.; Horiuchi, S.; Tanaka, M.; Kumai, R.; Yoneya, M.; Hasegawa, T., Effects of Substituted Alkyl Chain Length on Solution-Processable Layered Organic Semiconductor Crystals. *Chem. Mater.* **2015,** *27*, 3809-3812.

58 Takamuku, T.; Sakurai, H.; Ogawa, A.; Tashiro, A.; Kawano, M.; Kawazu, Y.; Sadakane, K.; Iwase, H.; Ozutsumi, K., Effects of the long octyl chain on complex formation of nickel(ii) with dimethyl sulfoxide, methanol, and acetonitrile in ionic liquid of [C8mim][TFSA]. *Phys. Chem. Chem. Phys.* **2019,** *21*, 3154-3163.

59 Shi, C.; Zhang, X.; Yu, C.-H.; Yao, Y.-F.; Zhang, W., Geometric isotope effect of deuteration in a hydrogen-bonded host–guest crystal. *Nat. Commun.* **2018,** *9*, 481.

60 Shibl, M. F.; Tachikawa, M.; Kühn, O., The geometric (H/D) isotope effect in porphycene: grid-based Born–Oppenheimer vibrational wavefunctions vs. multi-component molecular orbital theory. *Phys. Chem. Chem. Phys.* **2005,** *7*, 1368-1373.

61 Nishio, M., CH/π hydrogen bonds in crystals. *CrystEngComm* **2004,** *6*, 130-158.

62 Saraswatula, V. G.; Sharada, D.; Saha, B. K., Stronger π···π Interaction Leads to a Smaller Thermal Expansion in Some Charge Transfer Complexes. *Cryst. Growth Des.* **2018,** *18*, 52-56.

63 Kawase, T.; Seirai, Y.; Darabi, H. R.; Oda, M.; Sarakai, Y.; Tashiro, K., All-Hydrocarbon Inclusion Complexes of Carbon Nanorings: Cyclic [6]- and [8]Paraphenyleneacetylenes. *Angew. Chem. Int. Ed.* **2003,** *42*, 1621-1624.

64 Tanaka, N.; McCalley, D. V., Core–Shell, Ultrasmall Particles, Monoliths, and Other Support Materials in High-Performance Liquid Chromatography. *Anal. Chem.* **2016,** *88*, 279-298.

Chapter 6

Differentiating π Interactions by Constructing Concave/Convex Surfaces Using a Bucky Bowl Molecule, Corannulene in Liquid Chromatography

6-1 Introduction

The π interaction is a type of non-covalent interaction with aromatic compounds, and plays an important role in the molecular recognition processes in biological systems and organic functional materials.[1–5] For example, Nakagawa et al. revealed an oncogenic promoter recognition mechanism caused by the CH-π interaction between kinase C and indole-V derivatives.[6] Recently, many studies suggest that the π interaction is profoundly involved in photo and electronic behaviors of organic functional materials. Okamoto et al. developed organic transistors based on a laminating π-π interaction, which exhibited ten times higher electron mobility than conventional transistors.[7] Wu et al. developed an organic thin film capable of regulating visible singlet and near infrared triplet emissive properties by CH-π interaction-assisted self-assembly.[8] As can be observed by these and many other reports, a deep understanding and the ability to control π interactions will greatly facilitate the development of new functional materials.

The bowl-shaped π-conjugated molecule, known as the “bucky bowl” and first synthesized by Barth and Lawton in 1966,[9] has attracted much interest because of its many unique properties including hemispherical structure,[10] large dipole moment,[11]

high electron acceptability,[12,13] and bowl to bowl inversion.[14,15] The bucky bowls have been widely used in the synthesis of new functional materials.[16,17] For example, Sygula et al. designed a clip as a fullerene host, in which two bucky bowl units were connected through a rigid benzo cyclooctatetraene linker.[18] Mack et al. synthesized extended bucky bowl π-systems having potential applications as blue emitters in OLEDs.[19] Despite the outstanding properties of bucky bowls and increased research interest, very little is known regarding the precise mechanism of the π interactions. A comprehensive understanding of π interactions from π-conjugated structures is vital to the development of bucky bowl-based high performance functional materials.

It is challenging to study π interactions especially in the presence of other molecular interactions because π interactions are much weaker than most molecular interactions, such as hydrophobic interaction, hydrogen bonding, and electrostatic bonding. Computational approaches to study molecular interactions using quantum mechanical models have seen much progress in recent years due to the significant improvement in both algorithms and computing power.[20–23] These calculations, however, only generate theoretical hypotheses that still need experimental verification. Nuclear magnetic resonance (NMR) spectroscopy, which has been successfully applied to study strong molecular interactions such as H bonding, often lacks sufficient sensitivity to detect the weak π interaction.[24–27] There is still no straightforward experimental methods that can directly determine π interaction.

High performance liquid chromatography (HPLC) is a powerful separation technique that is able to distinguish the partition coefficients of solutes between the mobile and stationary phases and can sensitively reflect the strength of molecular interactions. Using HPLC, Kimata et al. determined the difference of strength in π interactions

between allotropes by studying the retention behavior of fullerene allotropes in pyrenylethyl-modified columns [28] In another study, Chen et al. evaluated the influence of metal species on the strength of π-π interactions using metallo protoporphyrins covalently-linked silica surface.[29] In previous studies, Kubo, T. et al. successfully immobilized C_{60}-fullerene (C60) and C_{70}-fullerene (C70) onto a silica-monolithic capillary and evaluated the characteristics of π interactions of fullerenes.[30–34] In these studies, we succeeded in separating several polycyclic aromatic hydrocarbons (PAHs) by the effective π–π interactions. We also showed that fullerenes exhibited specific π–π interaction with corannulene resulting from the hemispherical recognition and induced dipole of fullerenes.

In this study, we developed new Crn-coated silica monoliths for the precise understanding of π interactions on the curved π-conjugated surface using LC. Crn is known to have convex and concave surfaces,[35,36] which is expected to lead to different molecular recognition at each surface. Towards this end, we developed two kinds of Crn-functionalized silica monoliths, namely, Crn-ester column and Crn-PFPA (perfluorophenyl azide) column. The Crn-ester column was prepared from a Crn derivative that was edge functionalized with a -CH_2OH group, which was then conjugated to a carboxy-functionalized silica monolith. It was anticipated that both surfaces of the Crn structure could interact with solutes [37] in the Crn-ester column. The Crn-PFPA column was prepared from a Crn derivative that was functionalized with PFPA to form an azridine on a spoke of Crn.[38] In this case, the aziridine structure suppresses the inversion of convex–concave surface by asserting large steric hindrance on the concave surface, thus only the concave surface of Crn structure could interact with solutes. Using these two new columns, we evaluated the strength of π interactions

between Crn and several PAHs by normal phase liquid chromatography (NPLC), in which hydrophobic interaction was completely reduced and thus π interaction could be examined [33]. To further understand the π-π interactions between Crn structure on the stationary phase and Crn as a solute, computational simulations were carried out. In addition, ^{1}H-NMR spectroscopy was employed to examine the interaction between Crn and coronene in details. This represents the first report that evaluates the shape-based specific interactions on π-conjugated hemispherical surface and multiple CH-π interactions in bucky bowls.

6-2 Experimental Section

6-2-1 Materials

Acetone, diethyl ether, magnesium sulfate, sodium hydroxide, dichloromethane, chlorobenzene, *toluene, ethyl acetate,* methanol, *tetrahydrofuran, n*-hexane, and chloroform were purchased from Nacalai Tesque (Kyoto, Japan). Methyl pentafluorobenzoate, diethyl amine, urea, acetic acid, 3-aminopropyltrimethoxysilane (APTMS), [3-(trimethoxysilyl)propyl]succinic anhydride (TMSPSA), 2.6-lutidine, *N*,*N*'-dicyclohexylcarbodiimide (DCC), 4-dimethylaminopyridine (DMAP) and polycyclic aromatic hydrocarbons (PAHs) were from Tokyo Chemical Industry (Tokyo, Japan). Sodium azide, *N*-hydroxysuccinimide (NHS), 1-ethyl-3-(3-dimethylaminopropyl)carbodiimide (EDAC), titanium (IV) chloride ($TiCl_4$), dichloromethyl methyl ether and sodium borohydride were acquired from Wako Pure Chemical Industries (Osaka, Japan). Polyethylene glycol (PEG) (*M*n = 10,000), Crn, C60 and C70 were purchased from Sigma-Aldrich Japan (Tokyo, Japan). Deionized water was obtained from a Milli-Q Direct-Q 3UV system (Merck Millipore, Tokyo, Japan). A COSMOSIL PYE® and πNAP® was purchased from Nacalai Tesque, and a fused-silica capillary from Polymicro Technologies Inc. (Phoenix, AZ).

6-2-2 Instruments

The capillary liquid chromatographic system consists of a DiNa S (KYA Technologies Co., Tokyo, Japan) as the pump, CE-2070 (JASCO, Tokyo, Japan) as the UV detector, CHEMINERT (Valco Instruments Co., Huston, TX) as the sample injector, and Chemco capillary column conditioner Model 380-b (Chemco Co. Osaka, Japan) as the column oven. The HPLC system is a Prominence series (Shimadzu Co., Kyoto, Japan).

FT-IR, NMR, elemental analysis, and direct analysis in real time mass spectroscopy (DARTMS) were carried out on a Nicolet iS5 ATR (Thermo Fisher Scientific Inc., Waltham, MA, USA), JNM-ECA500 spectrometer (JEOL, Tokyo, Japan), Flash EA1112 (Thermo Fisher Scientific), and DART (JEOL), respectively.

6-2-3 Synthesis of hydroxymethyl-substituted Crn (Crn-CH_2OH)

Derivatization of corannulene with the hydroxymethyl group was carried out according to the reported procedures (Scheme 1-(a)). Briefly, Crn (100.0 mg, 0.40 mmol) and dichloromethyl methyl ether (0.20 mL, 2.25 mmol) were dissolved dichloromethane (50 mL). The mixture was added dropwise under N_2 atmosphere to a solution of $TiCl_4$ (0.25 mL, 2.28 mmol) in dichloromethane (5 mL) at 0 °C, stirred at 0 °C for 1 h and then at room temperature for 20 h. After completion of the reaction, the mixture was poured into water and extracted with dichloromethane. The organic phase was dried over sodium sulfate, and the filtrate was concentrated under vacuum. The product, Crn-CHO (50 mg, 0.18 mmol), was dissolved in THF/methanol 1/3 v/v (100 mL) together with $NaBH_4$ (18.0 mg, 0.47 mmol), and the mixture was stirred at room temperature for 2 h under N_2 atmosphere. The mixture was poured into water, extracted with dichloromethane, dried over sodium sulfate, and concentrated under vacuum. The crude was finally purified by silica-gel column chromatography using toluene/ethyl acetate 4/1 (v/v) as the eluent to give Crn-CH_2OH (25.6 mg, 50.6% yield). Crn-CH_2OH was characterized by FT-IR, DARTMS and ^1H NMR. ^1H NMR (400 MHz, $CDCl_3$).

6-2-4 Synthesis of Crn-PFPA-NHS

4-azido-2,3,5,6-tetrafluorophenyl succinate (PFPA-NHS)

Methyl pentafluorobenzoate (MPFB, 18.3 mmol) and sodium azide (20 mmol) was dissolved in water/acetone = 5/12 (v/v), and the mixture was stirred at 120 °C for 20 h under N_2 atmosphere. After extraction with diethyl ether and dried over sodium sulfate, the solvent was evaporated to give PFPA-CO_2CH_3. Then, the residue was dissolved in methanol/10% NaOH aq. = 4/1 (v/v), and the mixture was stirred at room temperature for 30 min. After neutralization with 6 M HCl to pH ~1, the solution was extracted with chloroform, the organic layer was dried over sodium sulfate, and the solvent was removed. The product (PFPA-CO_2H, 17.4 mmol) was dissolved in dichloromethane with EDAC (17.2 mmol) and NHS (17.2 mmol), and the mixture was stirred at room temperature for 16 h under N_2 atmosphere. The mixture was washed with water to remove unreacted EDAC and NHS. The chloroform layer was dried over sodium sulfate and the solvent was removed. Finally, 4-azido-2,3,5,6-tetrafluorophenyl succinate (PFPA-NHS) was obtained after purification by silica-gel column chromatography with dichloromethane as the eluent.

Synthesis of Crn-PFPA-NHS

Crn was first derivatized with PFPA-NHS, which was then conjugated to silica monolith by amide coupling. 4-Azido-2,3,5,6-tetrafluorophenyl succinate (PFPA-NHS) was synthesized as described in Chapter 2. PFPA-derivatized Crn was synthesized following Scheme 1-b. In brief, Crn 40.0 mg (0.16 mmol) and PFPA-NHS 79.7 mg (0.24 mmol) were dissolved in chlorobenzene (20 mL). After bubbling with N_2 for 3 min, the mixture was stirred at 108 °C for 120 h. After silica-gel chromatography using

hexane/toluene/ethyl acetate =20/20/1 (v/v/v) as the eluent, the title product (Crn-PFPA-NHS) was isolated (3.20 mg, 5.77 μmol, 3.61% yield against Crn). For structural determination, we prepared Crn derivatized with PFPA-CO_2CH_3, which can be more conveniently synthesized than Crn-PFPA-NHS, according Scheme 1-(b). Crn (20.0 mg, 0.16 mmol) and PFPA-CO_2CH_3 (59.8 mg, 0.24 mmol) were dissolved in chlorobenzene (20 mL). After bubbling in N_2 for 3 min, the mixture was stirred at 108 °C for 120 h. After column chromatography using hexane/toluene/ethyl acetate =20/20/1 (v/v/v) as the eluent, the product (Crn-PFPA-CO_2CH_3) was isolated (5.48 mg 11.6 μmol, 7.27% yield against Crn).

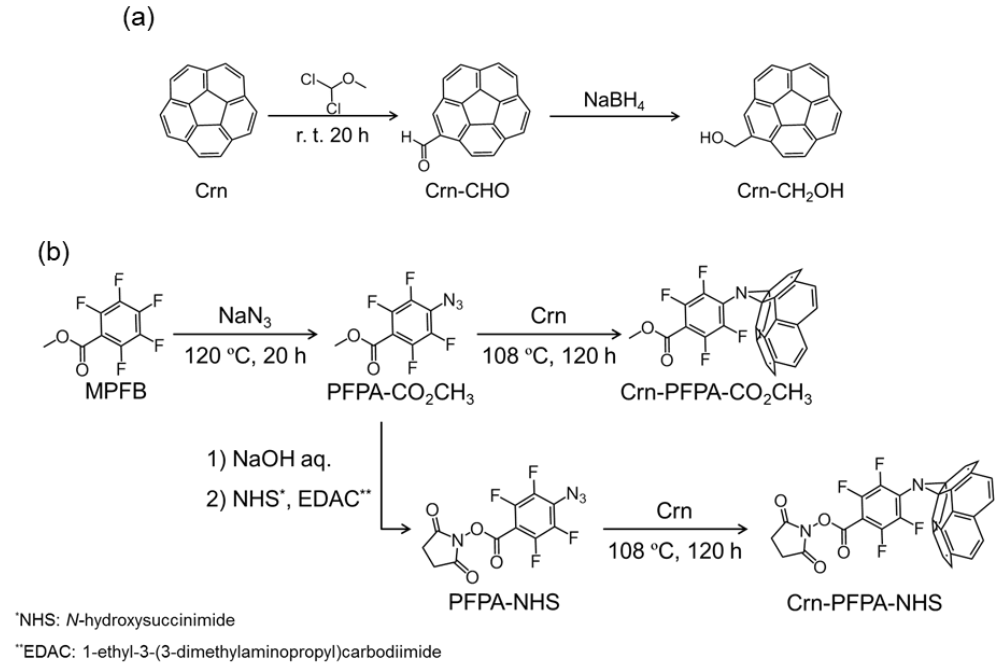

Scheme 1. Synthesis of (a) Crn-CH_2OH, (b) Crn-PFPA-CO_2CH_3 and Crn-PFPA-NHS.

6-2-5 Preparation of carbon material-coated column

Preparation of silica-monolithic capillary

A fused-silica capillary (2-3 m in length) was treated with a 1.0 M aqueous sodium hydroxide solution at 40 °C for 3 h. Then, the capillary was washed with water and acetone, and dried. TMOS (56 mL) was added to a solution of PEG (11.9 g) and urea (9.0 g) in 0.01 M acetic acid (100 mL), and the mixture stirred at 0 °C for 30 min. The resulting homogeneous solution was charged into the fused-silica capillary and remained at 30 °C overnight. The resulting monolithic silica column was treated for 3 h at 120 °C to form mesopores with ammonia generated by the hydrolysis of urea, followed by water and methanol washes. After drying, a heat treatment was carried out at 330 °C for 25 h, resulting in the decomposition of the organic moieties in the capillary.

Surface modification of silica monolith with Crn-CH_2OH

The silica-monolithic capillary, which was prepared by the same method as the previous study, was treated with 1.0 M aqueous HCl at 40 °C for 3 h. After washing with water, methanol, THF and toluene, [3-(trimethoxysilyl)propyl]succinic anhydride (TMSPSA) / 2,6-lutidine / toluene = 20/1/100 (v/v/v) was passed through the silica-monolithic capillary at 40 °C for 24 h, and washed with toluene and THF. Then THF / water = 1/1 (v/v) was passed through the silica-monolithic capillary for 24 h at 100 °C, and washed with THF and toluene to give carboxy-functionalized silica-monolith. Afterwards, a mixture of Crn-CH_2OH (1.0 mg, 3.58 μmol), DCC (2.0 mg, 9.69 μmol) and DMAP (1.2 mg, 9.82 μmol) in toluene (1 mL) was charged into the CO_2H-modified silica column for 24 h at room temperature, and washed with toluene to give the Crn-ester column (see Scheme 2-(a)). A control was also prepared by treating CO_2H-modified silica monolith in a similar manner except without Crn-CH_2OH to give the Ester column.

Surface modification of the silica monolith with Crn-PFPA-NHS

The silica-monolithic capillary was treated with 1.0 M aqueous HCl at 40 °C for 3 h, and washed with water and methanol. It was then filled with APTMS in methanol (10%, v/v), remained at room temperature for 24 h and then washed with methanol to give NH_2-modified silica monolith. A solution of Crn-PFPA-NHS in toluene (1.0 mg mL^{-1}) was charged into the NH_2-modified column. After remaining at room temperature for 24 h, the column was washed with toluene and methanol to give the Crn-PFPA column (see Scheme 2-(b)). A control was prepared by charging the NH_2-modified silica monolith with PFPA-NHS in toluene (1.0 mg mL^{-1}) at room temperature for 24 h, and

washing with toluene and methanol to give the PFPA column. Additionally, C60 column and C70 column were prepared following the protocols in Chapter 2. The detailed preparation procedures are described in Scheme 3.

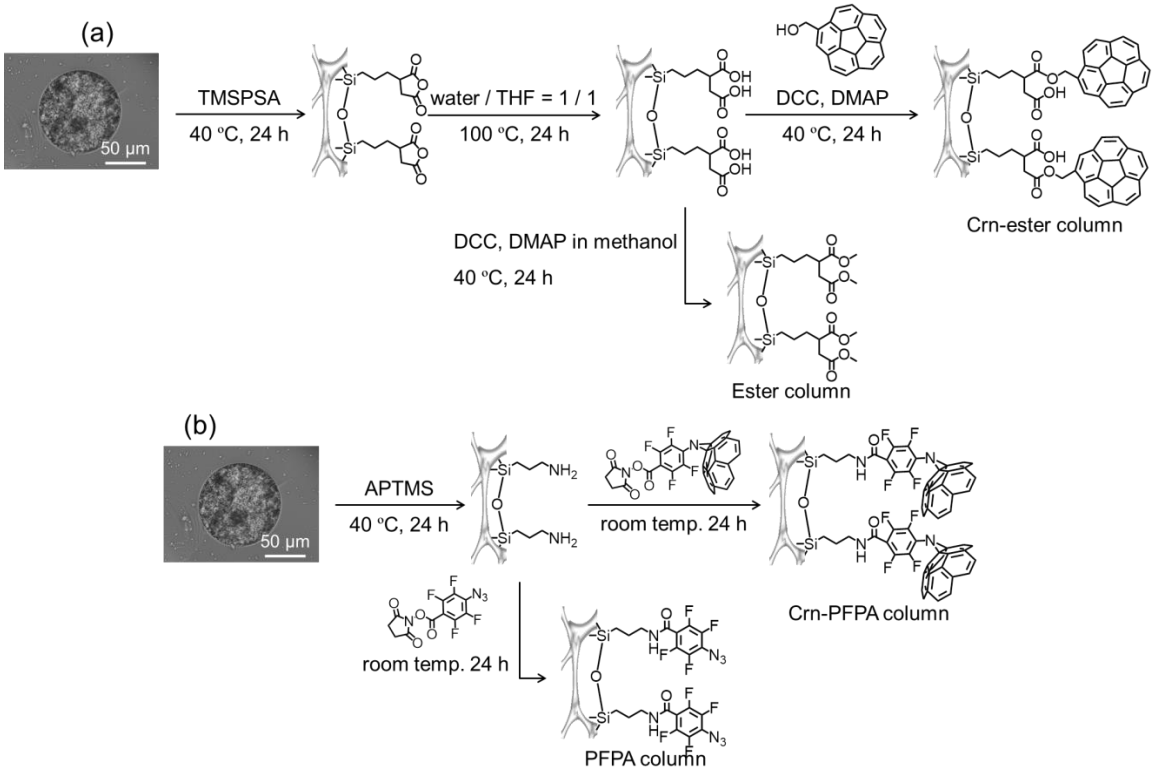

Scheme 2. Preparation of (a) Crn-ester and Ester columns, and (b) Crn-PFPA and PFPA columns.

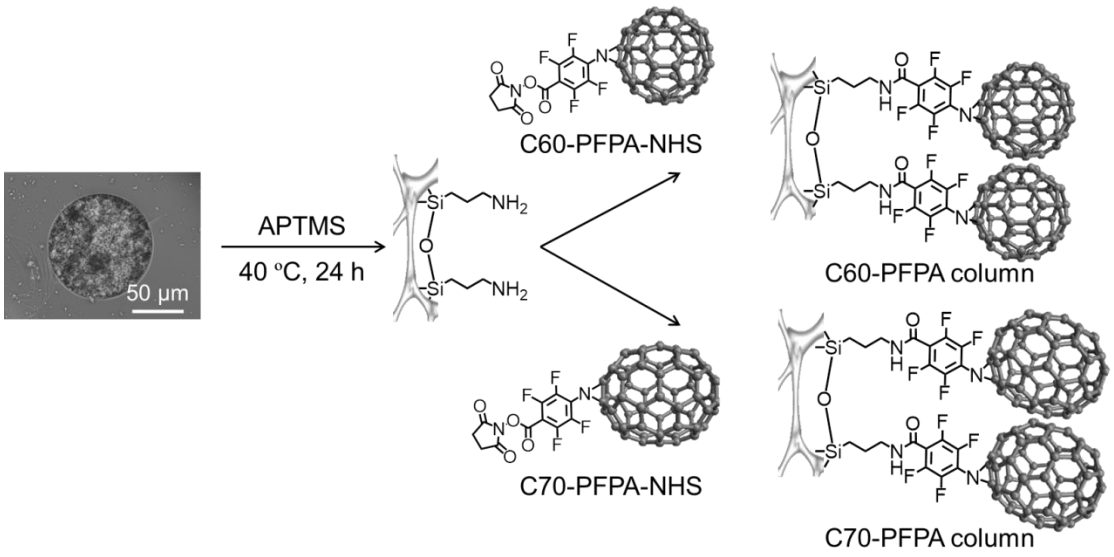

Scheme 3. Preparation of C60/C70 column.

6-2-6 Computational methods

To obtain the initial 3D molecular coordinates of each molecule, Chem3D version 7.0 was used. *Ab initio* calculations using Gaussian 03 were performed on a Linux Cluster. All geometrical optimizations were carried out by using the RB3LYP/3-21G basis set. Calculations of charges based on Merz-Singh-Kollman were carried out by using the B3LYP/3-21G basis set, which can be applied to large molecules. This method required no significant calculation time. During *ab initio* calculations, all internal coordinates were optimized by means of the Berny algorithm, and convergence was tested against criteria for the maximum force component, root-mean-square force, maximum displacement component, and root-mean-square displacement.

6-3 Results and Discussion

6-3-1 Preparation of Crn-modified silica monoliths

Two types of Crn derivatives were used to construct the columns: one was edge functionalized with hydroxymethyl (Crn-CH_2OH) and the other was functionalized PFPA-NHS (Crn-PFPA-NHS) (Scheme 1). Crn-CH_2OH was synthesized by first reacting Crn with an excess amount of dichloromethyl methyl ether in the presence of $TiCl_4$ at room temperature for 24 hours to give the aldehyde derivative Crn-CHO, which was then reduced with $NaBH_4$ to give Crn-CH_2OH in an overall 51% yield [37]. Crn-CH_2OH was characterized by FT-IR, DARTMS and ^1H NMR. ^1H NMR (400 MHz, $CDCl_3$): δ = 8.1 (*d*, 1 H, OH), 8.20 (m, 9 H, aromatic), 5.3 (s, 2 H, CH_2) ppm. DARTMS: calcd. for $C_{21}H_{12}O$ $[M]^+$ 280.10, found 280.03 (Figures 1-3).

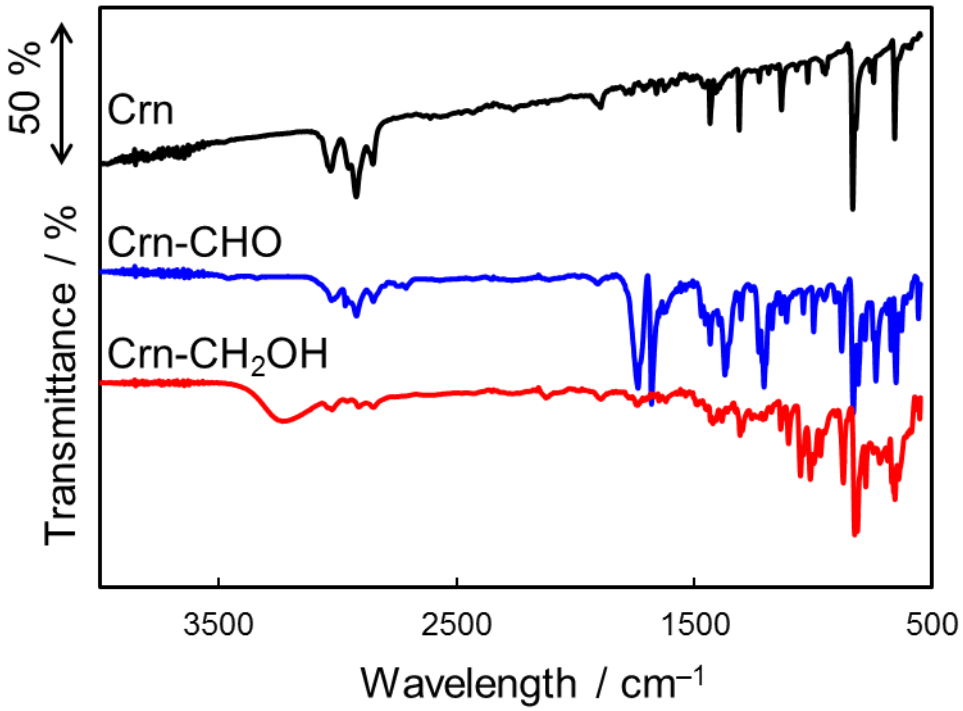

Figure 1. FT-IR spectra of Crn-CH_2OH and its precursors. All spectra were obtained using an ATR attachment. See Scheme 1 for compound structures.

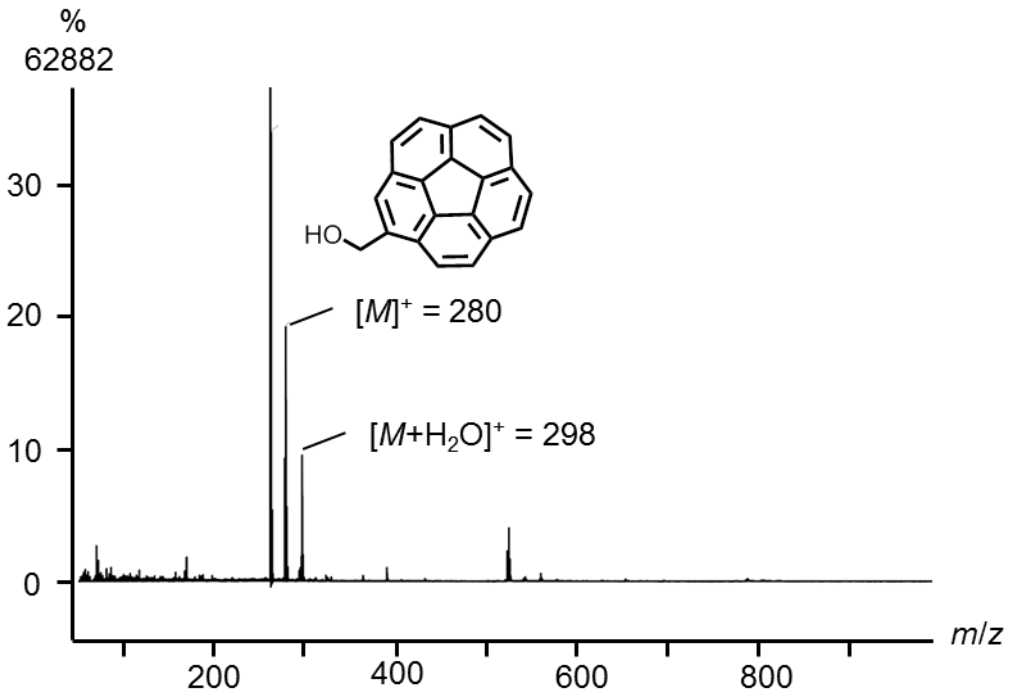

Figure 2. DARTMS spectrum of Crn-CH_2OH.

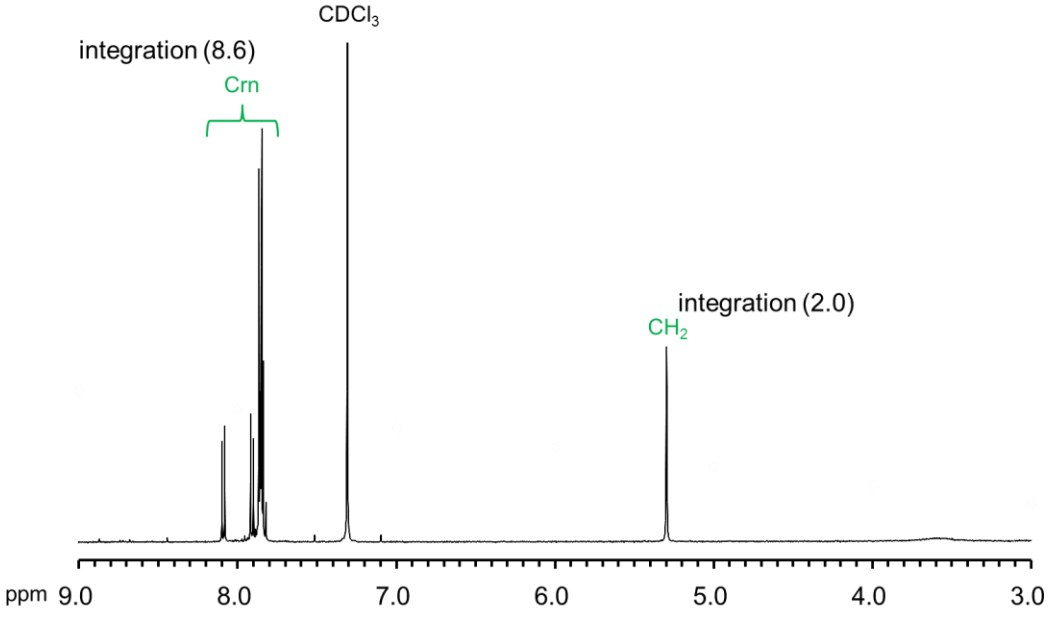

Figure 3. ^{1}H-NMR spectrum of Crn-CH_2OH. The spectrum was obtained in $CDCl_3$ as the solvent.

PFPA-derivatized Crn, Crn-PFPA-NHS, was synthesized by heating Crn with PFPA-NHS in chlorobenzene at 108 °C for 5 days. PFPA undergoes cycloaddition with double bonds to form aziridine structures. Perfluorination of phenyl azide lowers the LUMO of the azide, facilitating its reaction with dipolarophiles and electrophiles[39]. PFPAs have also demonstrated good reactivity towards carbon materials such as fullerenes[30,40], carbon nanotubes [41] and graphene [42–44] which are otherwise quite inert chemically. There are four types of double bonds in Crn, and therefore four different products are possible from the reaction with PFPA (Figure 4). To facilitate structure determination of the product, a PFPA methyl ester, PFPA-CO_2CH_3, was used as a model compound for its simpler structure than PFPA-NHS. The aliphatic region of the ^{1}H NMR spectrum of the product only showed the methyl peak from PFPA-CO_2CH_3, thus ruling out the arizidine products from the addition to the flank and rim of Crn (B and D, Figure 4).

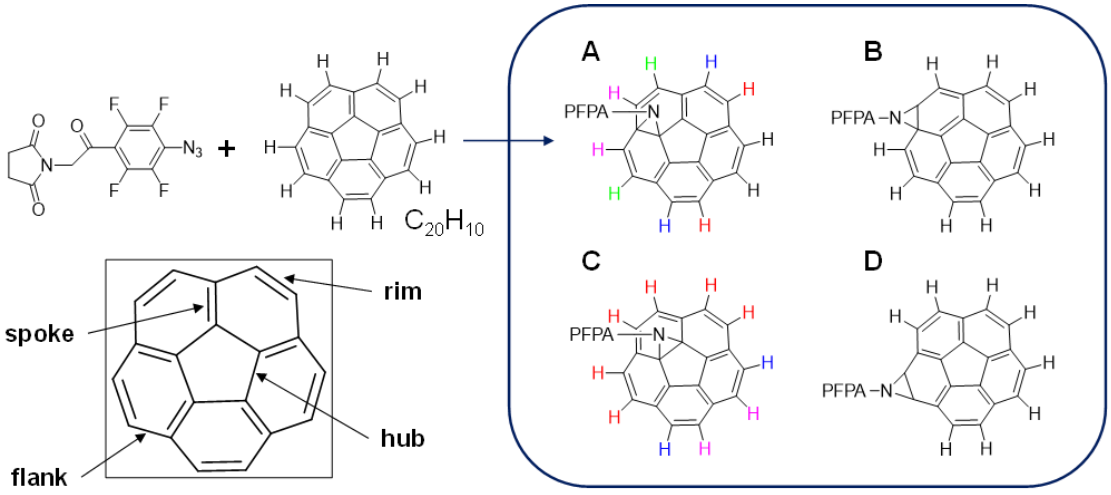

Figure 4. Possible products in the reaction between PFPA-NHS and Crn.

Crn-PFPA-CO_2CH_3 was characterized by FT-IR, DARTMS, ^{1}H NMR and ^{13}C NMR. ^{1}H NMR (400 MHz, $CDCl_3$): δ = 7.9–7.7 (complex, 10 H, aromatic), 4.0 (s, 3 H, CH_3) ppm. ^{13}C NMR (101 MHz, $CDCl_3$): δ = 130–115 (CH, aromatic), 52 (CH_3, methyl) ppm. DARTMS: calcd. for $C_{28}H_{13}NO_2F_4$ $[M+H]^+$ 472.40, found 472.03 (Figures 5-8). The ^{1}H NMR spectrum of the product showed the peak patterns in the aromatic region (Figure 7) that support the structure of spoke addition (A, Figure 4, i.e., Crn-PFPA-CO_2CH_3) rather than hub addition (C, Figure 4). The product was furthermore characterized by DEPT ^{13}C NMR (Figure 8). The structure assignment is additionally confirmed by simulations. Computation of the orbital energies of PFPA and Crn supports the reaction between the LUMO of the azide in PFPA and the HOMO (Figure 9, 10). Results of the stabilization energy computed from the Hartree–Fock (HF) method indicated that the most stable structure is structure A, which is consistent with our experimental data (Table 1).

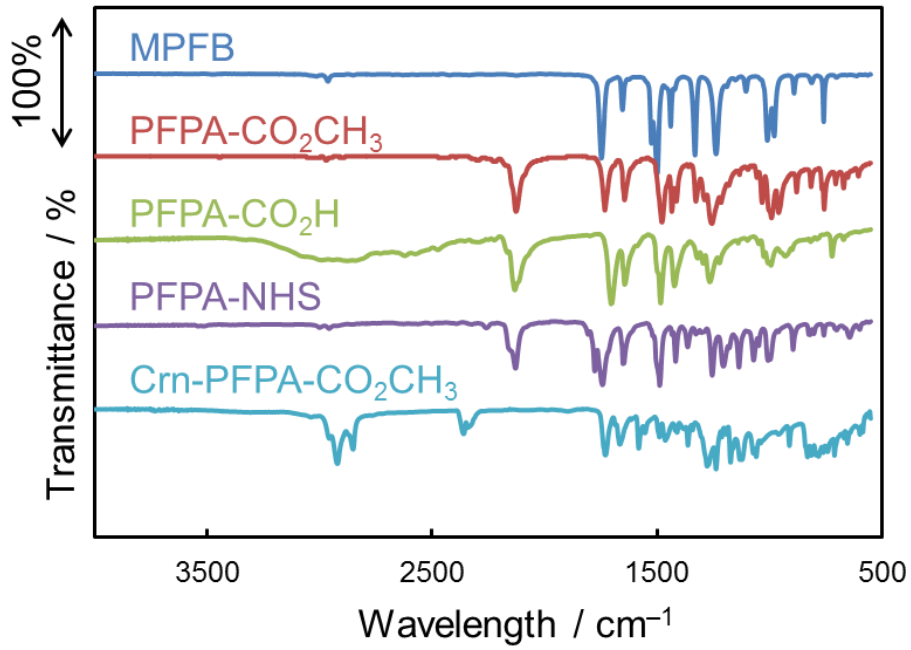

Figure 5. FT-IR spectra of Crn-PFPA-CO_2CH_3 and its derivatives. All spectra were obtained using an ATR attachment. See Scheme 1 for compound structures.

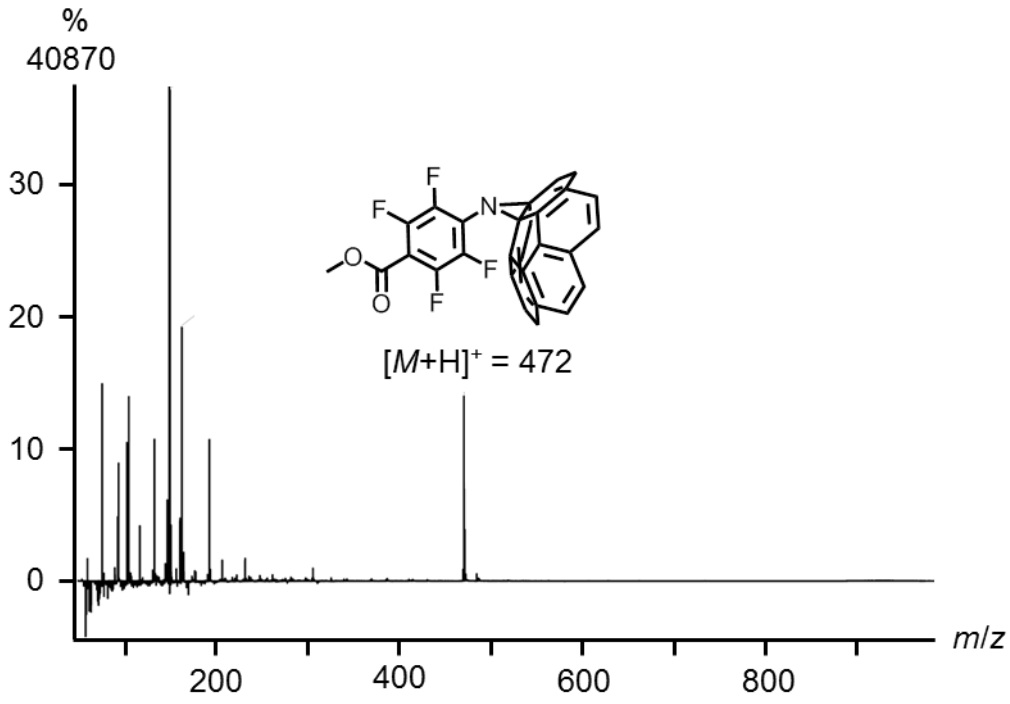

Figure 6. DARTMS spectrum of Crn-PFPA-CO_2CH_3.

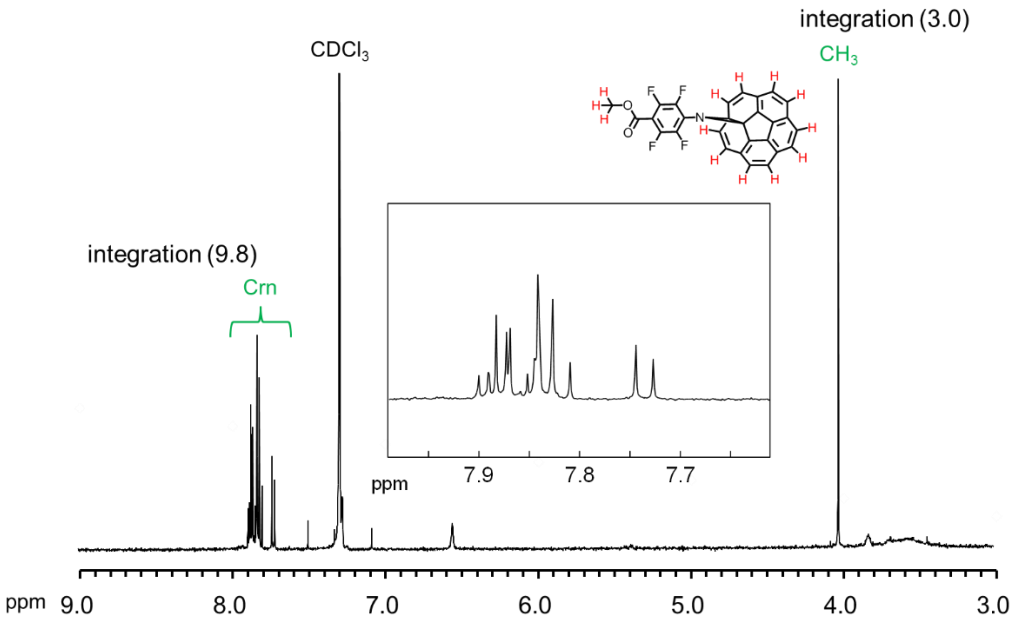

Figure 7. ^{1}H-NMR spectrum of Crn-PFPA-CO_2CH_3. The spectrum was obtained in $CDCl_3$ as the solvent.

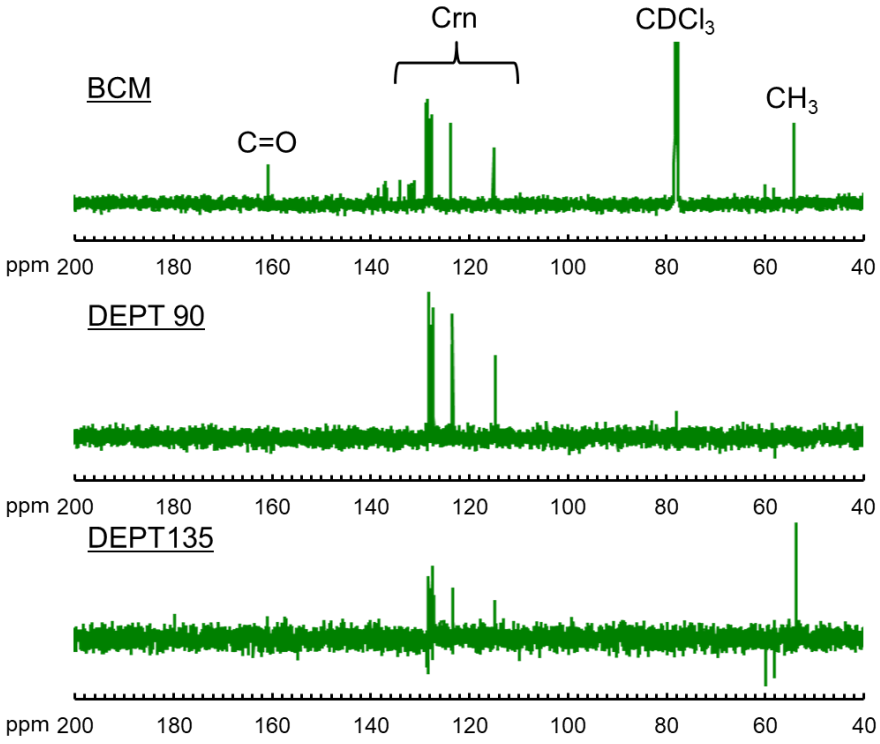

Figure 8. ^{13}C-NMR spectrum of Crn-PFPA-CO_2CH_3. The spectrum was obtained in the DEPT mode using $CDCl_3$ as the solvent.

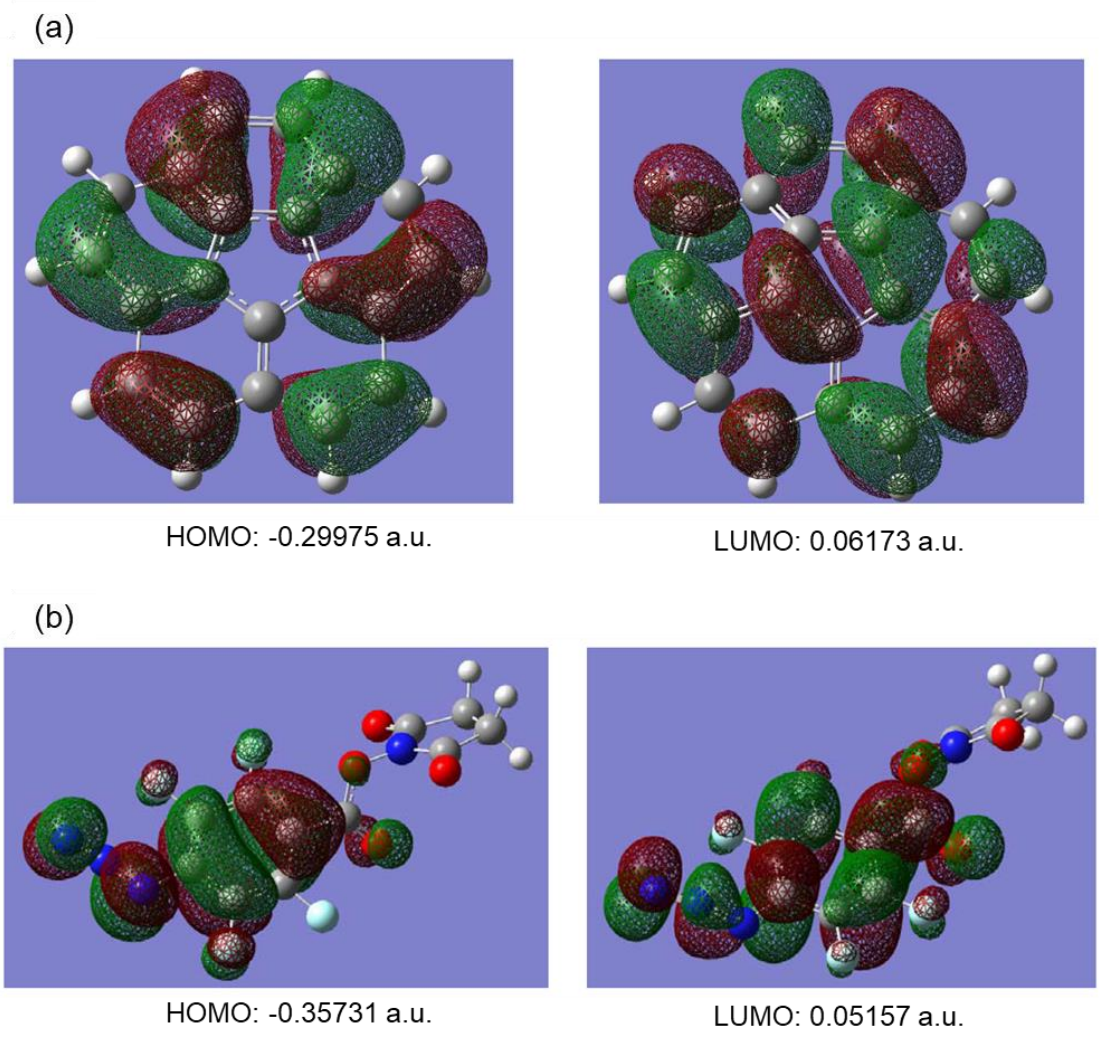

Figure 9. HOMO, LUMO and their orbital energies of (a) Crn, (b) PFPA-NHS.

Table 1. Stabilization energy of the possible products from the reaction of Crn and PFPA. See Figure 4 for structures. SCF, the self-consistent field method, is the same as the Hartree–Fock (HF) method.

Candidates	SFC energy / a. u.	ΔE / kcal mol^{-1}
A	**-1988.4822**	**21.42**
B	**-1988.4573**	**37.04**
C	**-1988.4573**	**37.04**

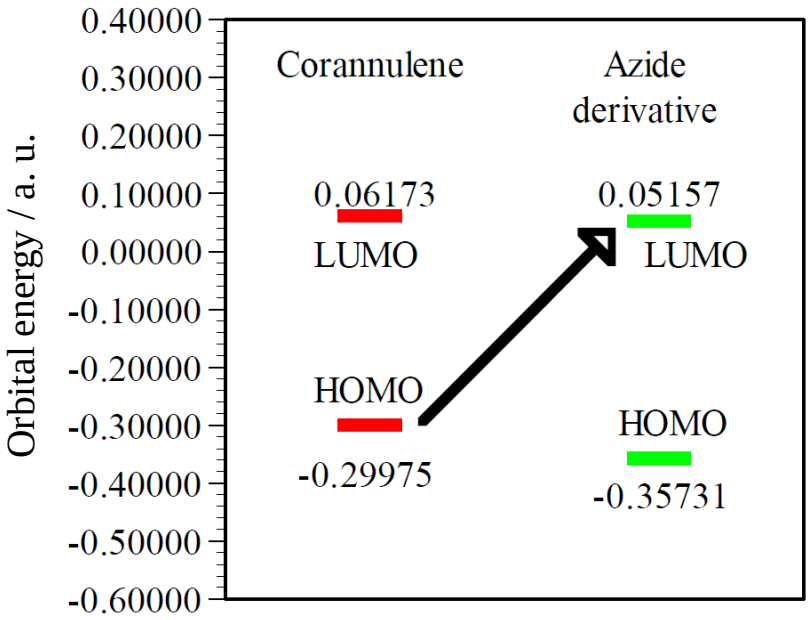

Figure 10. Orbital energies of Crn and PFPA.

These Crn derivatives were then conjugated to CO_2H- or NH_2-functionalized silica monolith by esterification or amidation to give the Crn-ester column and Crn-PFPA column, respectively (Scheme 2). Columns that were modified with only the linkers, Ester column and PFPA column (Scheme 2), were also prepared and used as controls. Figure 11 (a) shows the surface structure of the stationary phase in Crn-ester column, Crn-PFPA column, ester column and PFPA column.

Corannulene is highly hydrophobic, and when immobilized on silica monoliths, is expected to show strong affinity to hydrophobic compounds in hydrophilic solvents. In order to confirm that the π interaction is present in Crn-immobilized columns and can change their retention properties, the retention behaviors of alkylbenzenes (ABs) and PAHs were evaluated with typical reverse phase LC.

Figure 11 (b) plots the retention factor k ($k = (t_R – t_0 / t_0$; t_R, retention time of a solute; t_0, elution time of non-retained solute (acetone)) of different AB and PAH in these columns vs. the water/octanol partition coefficient (Log $P_{O/W}$), which indicates the hydrophobicity of the molecule. When the columns were modified with Crn (i.e., Crn-ester and Crn-PFPA columns), they showed stronger retention of ABs than other columns. Log k increased linearly with Log $P_{O/W}$. Additionally, Crn-ester column and Crn-PFPA column showed stronger retention for hydrophobic PAHs, while this was not observed on the control columns (Ester and PFPA columns) that were not modified with Crn. The results confirmed the existence of the hydrophobic interaction and π interaction derived from the Crn structure. Furthermore, these results clearly demonstrated the successful immobilization of Crn on Crn-ester and Crn-PFPA columns.

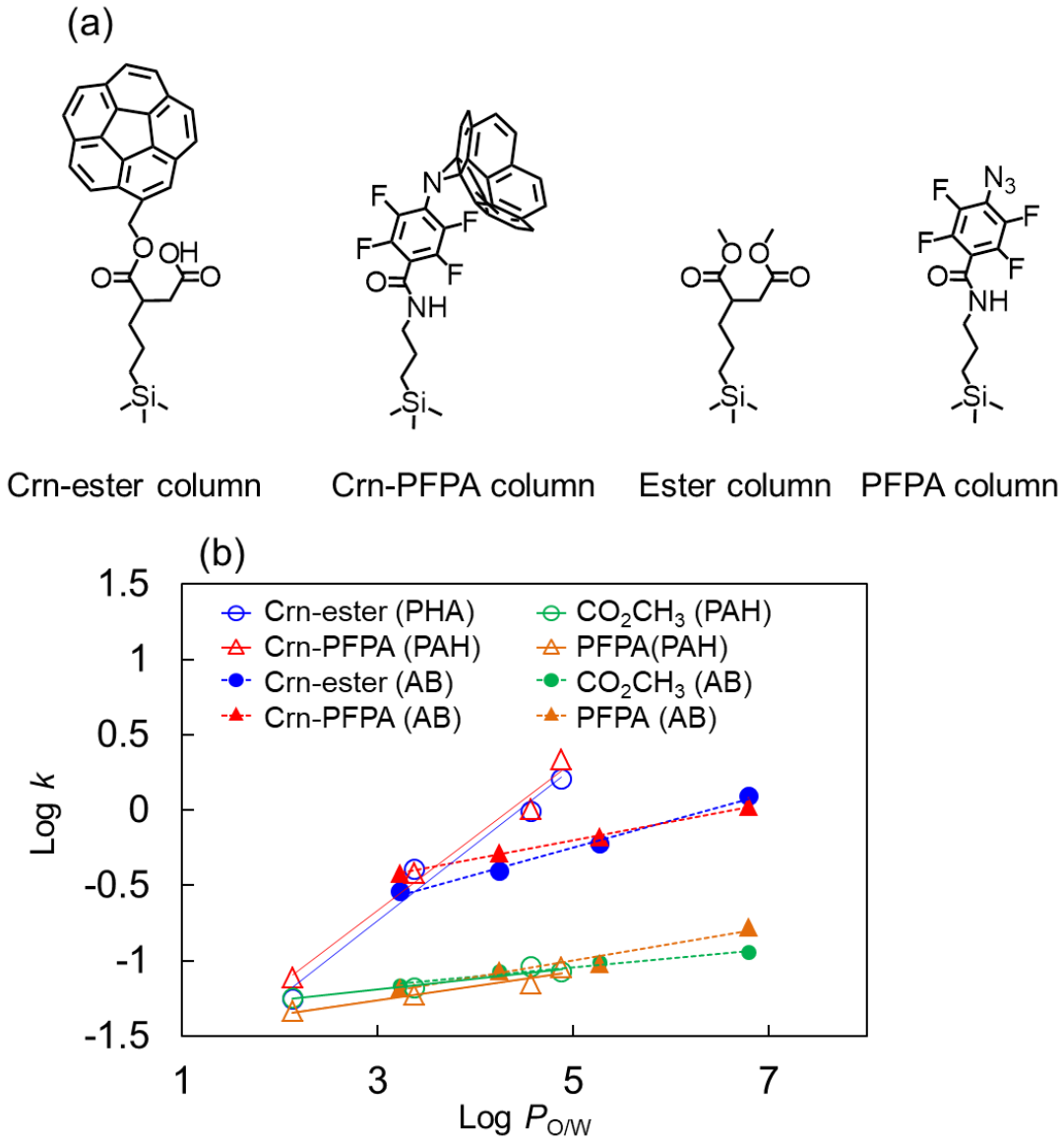

Figure 11. (a) Surface structure of the stationary phase in Crn-ester column, Crn-PFPA column and the controls, Ester column and PFPA column. (b) Log *k* vs. log *P*o/w in each column. Condition: Crn-ester column (32.0 cm × 100 mm i.d.), Crn-PFPA column (32.0 cm × 100 mm i.d.), Ester column (32.0 cm × 100 mm i.d.), PFPA column (32.0 cm × 100 mm i.d.); flow rate, 2.0 μL min^{-1}; mobile phase, water / methanol = 1 / 9; detection, UV 254 nm; temperature 40 ºC.

6-3-2 Retention selectivity for hemispherical structure

In Chapter 2, C60 and C70 showed higher recognition for Crn than typical planar PAH structures owing to the specific π-π interaction between the spherical π-conjugated surfaces [31,32]. We expect that Crn-modified silica monoliths should show similarly spherical recognition owing to the hemispherical structure of Crn. To test the hypothesis, we included benzo[a]pyrene, which has the same number of π electrons as Crn but has a planar structure rather than the hemispherical structure in Crn, and evaluated the elution behavior of Crn and benzo[a]pyrene using Crn modified silica monoliths. For a comparison, C60 and C70 columns, and commercially available LC columns that are known for their effective π interaction (PYE and πNAP (Nacalai Tesque, Kyoto, Japan)) were tested under the same conditions.

Chromatograms of the mixed sample of Crn and benzo[a]pyrene on each column are shown in Figure 12. On the commercially LC columns PYE and πNAP, there were no differences in the strength of π interactions between Crn and benzo[a]pyrene, likely due to the small-planar π-conjugated structure that are used to modify the columns (Figure 12 (a)). On the other hand, fullerene-modified silica monoliths showed stronger retention for Crn than that of benzo[a]pyrene, which can be attributed to spherical recognition (Figure 12 (b)). Surprisingly, Crn-modified silica monoliths showed lower retentions for Crn than benzo[a]pyrene (Figure 12 (c)). This result implies a significantly lower interaction between Crn structures themselves than their interaction with fullerene. A previous study showed repulsion of Crn with hemispherical structures despite its hemispherical structure, which was attributed to the presence of intramolecular dipole as one of the major differences between fullerene and Crn.[11] In Chapter 2, we confirmed that the effective retention of Crn on C70 column was caused

by the dipole of Crn inducing dipoles in C70 [32]. Hence, we hypothesize that the repulsion between the hemispherical structure of Crn is caused by the dipole moment.

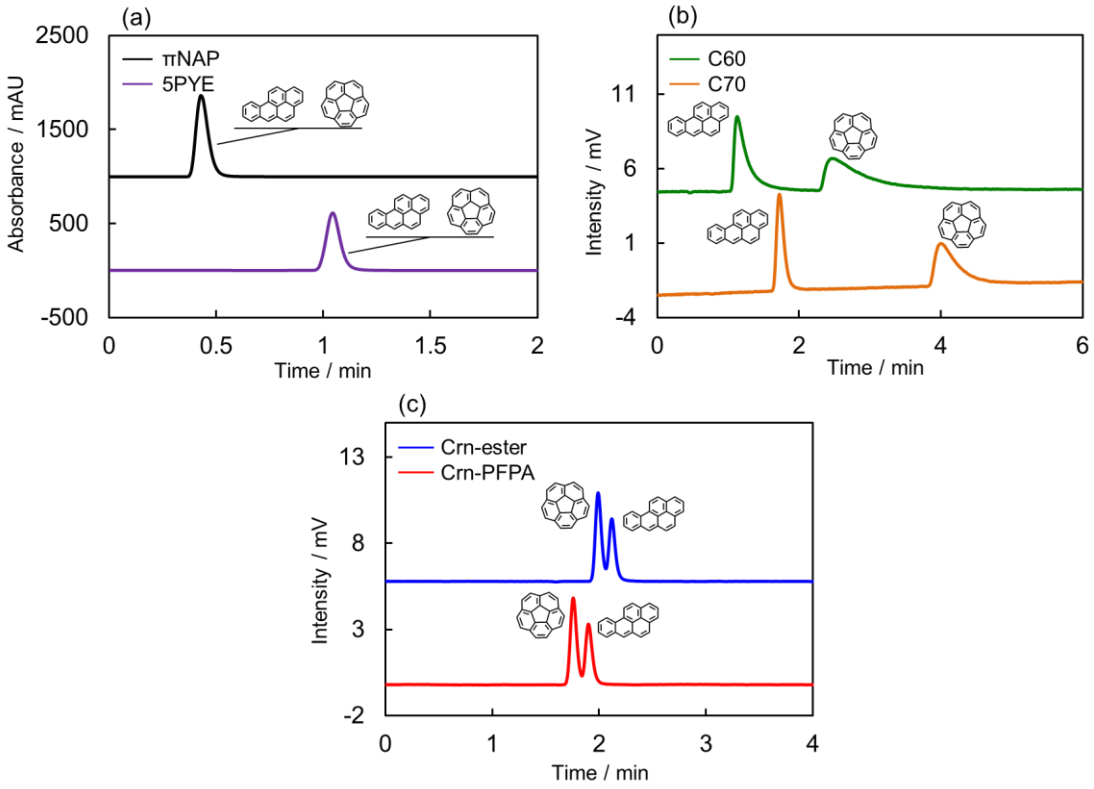

Figure 12. Chromatograms of the mixed sample of Crn and benzo[a]pyrene on (a) πNAP (Nacalai Tesque, 50 mm × 2.0 mm i.d.), 5PYE (Nacalai Tesque, 150 mm × 4.6 mm i.d.), (b) C60 column (32.0 cm × 100 mm i.d.), C70 column (32.0 cm × 100 mm i.d.), (c) Crn-ester column (32.0 cm × 100 mm i.d.), Crn-PFPA column (32.0 cm × 100 mm i.d.). Condition: flow rate, (a) 2.0 mL min^{-1}, (b), (c) 2.0 μLmin^{-1}; mobile phase, chloroform / *n*-hexane = 3 / 7; detection, UV 254 nm; temperature 40 ºC.

A computational simulation was carried out in order to understand the charge state of each carbon atom on Crn and Crn derivatives. Figure 13 shows the charge on each carbon atom and the charge distribution in Crn and Crn derivatives. The carbon atoms in Crn exhibited alternating negative and positive charges (Figure 13 (b) and (c)). Crn derivatives exhibited similar trend, with the exception of those carbon atoms that were functionalized (C3, and to a lesser extent C2 and C4 in Crn-CH_2OH; C1 and C2, and to

a lesser extent C3 and C4 in Crn-PFPA, Fig. 13 (b)). As such, if Crn in the mobile phase overlaps with the Crn structure on the stationary phase, electrostatic repulsions would occur between their dipole moments. In this case, Crn-modified silica monoliths would not be able to interact with Crn in the mobile phase due to the electrostatic repulsion resulting from the same arrangements of atomic charges in the Crn structures. Similar result was reported by Wang et al. that neighboring Crn structures were not completely stacked in the crystal structure, which is consistent with our observation [45].

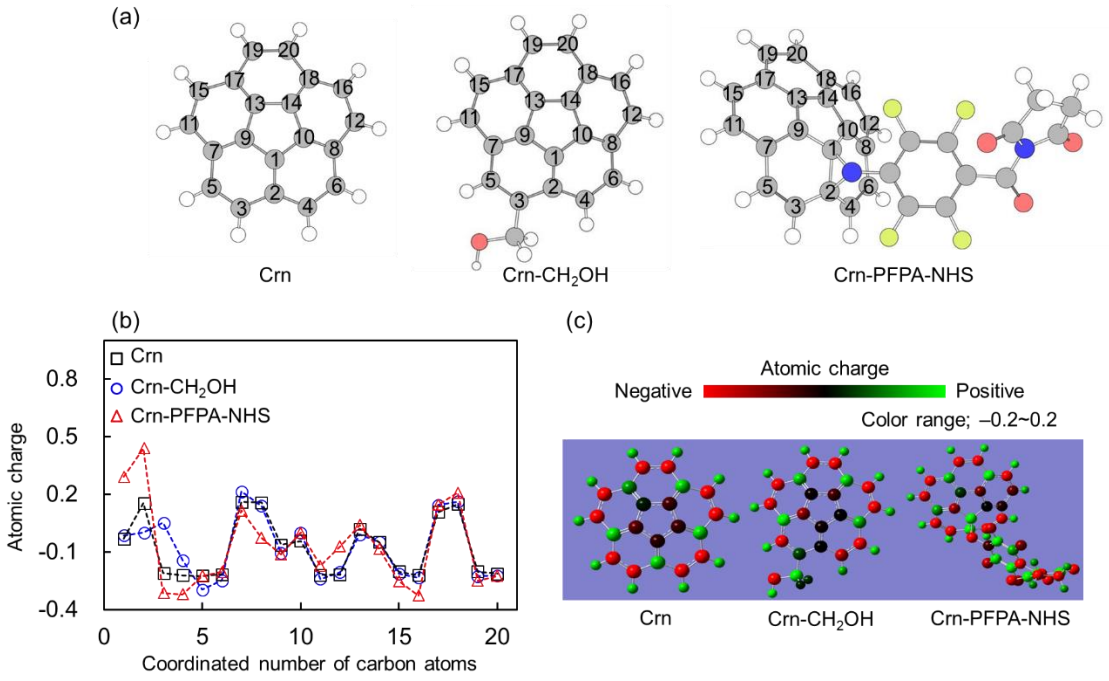

Figure 13. Computer simulations of Crn and Crn derivatives. (a) The numbering of carbon atoms, (b) atomic charges of carbon atoms, (c) charge distribution. The C atoms are numbered such that they remain the same in all Crn structures.

Based on the above results, we hypothesize that intramolecular dipoles in aromatic compounds could decrease the strength of π-π interactions with other polar aromatic compounds resulting from charge repulsion. To test this, we evaluated separation behaviors between the non-polar naphthalene and the polar azulene [46], both of which are of planar structures and have the identical number of π electrons.

The chromatograms of the mixed sample of naphthalene and azulene, together with the separation factor and retention factor on each column are shown in Figure 14 (a-d) and Figure 14 (e), respectively. From the chromatograms, it can be seen that the elution trend was slightly different. The fullerene- modified columns showed higher retention to azulene, whereas Crn-modified columns showed relatively stronger retention to naphthalene although the retention order was same in both columns. These data suggested fullerene interacts stronger with azulene than naphthalene, and Crn interacts stronger with naphthalene than azulene, a result that implied additional dipole-induced interactions in addition to π-π interaction. We found that Crn-modified silica monoliths showed weaker retention and lower selectivity to azulene than the fullerene-modified columns. On the other hand, Crn-modified silica monoliths exhibited stronger retentions than fullerene-modified columns for naphthalene due to intramolecular dipoles in Crn structures and induced dipole in naphthalene. Thus, we suggest that polar aromatic compounds showed lower affinity to other polar aromatic compounds than nonpolar compounds regardless of plane or curved structures.

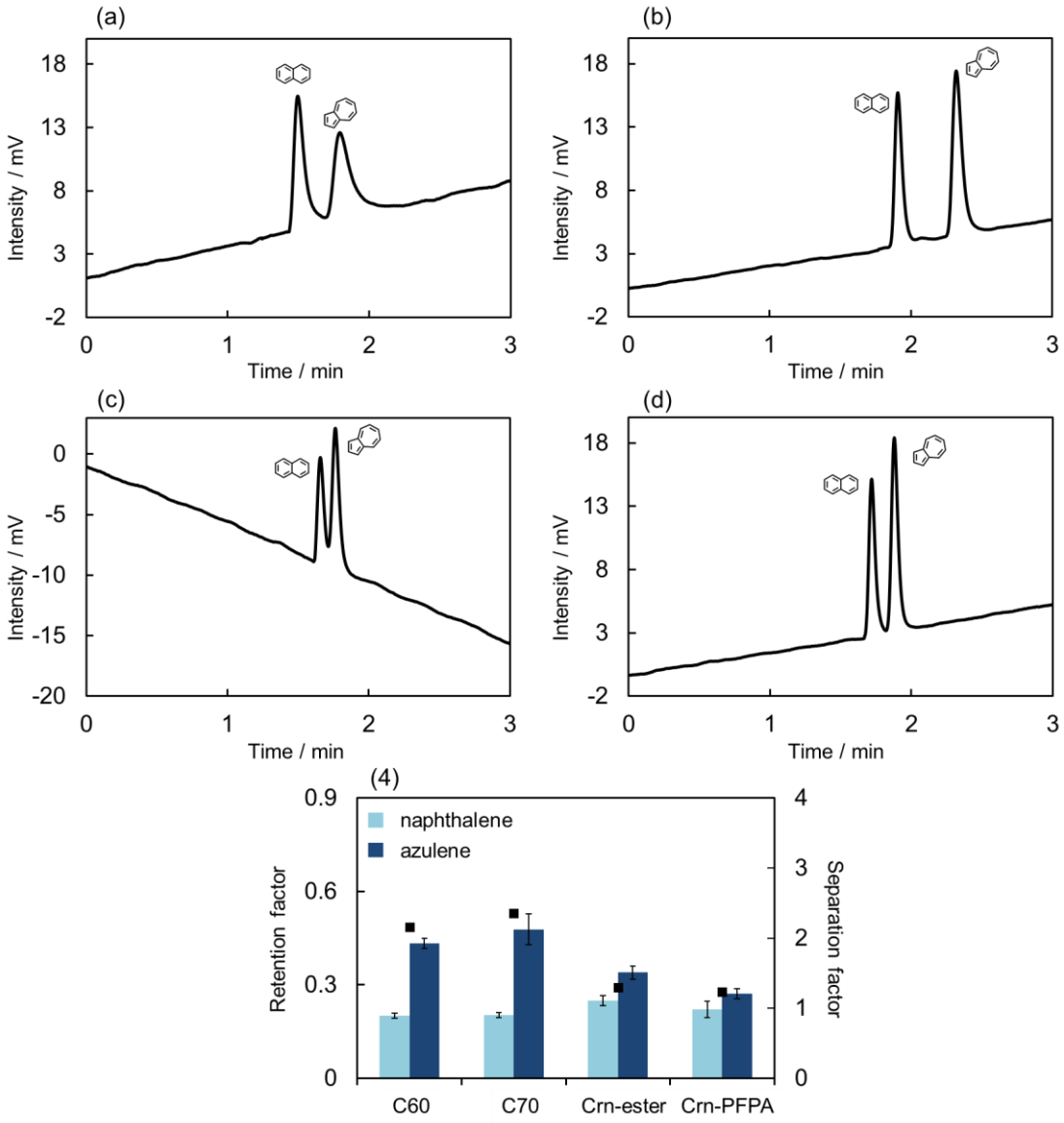

Figure 14. Chromatograms of the mixed sample of naphthalene and azulene on (a) C60 column (32.0 cm × 100 mm i.d.), (b) C70 column (32.0 cm × 100 mm i.d.), (c) Crn-ester column (32.0 cm × 100 mm i.d.), (d) Crn-PFPA column (32.0 cm × 100 mm i.d.), (e) retention factors and separation factors between azulene and naphtahlene on each column. Condition: flow rate, 2.0 μLmin^{-1}; mobile phase, *n*-hexane; detection, UV 254 nm; temperature 40 ºC. Separation factor on each column was calculated as follows; Separation factor = $k_{azulene}/k_{napthalene}$.

6-3-3 Retention behaviors of PAHs with different π electron numbers

In the last section, we clarified the interaction of Crn with polar aromatic compounds and elucidated the retention behavior based on the nature of charge interactions. In this section, we evaluate the retention selectivity of non-polar and planar PAHs in Crn-modified silica monoliths. The typical chromatograms obtained by normal phase mode of PAHs, including phenanthrene, pyrene, chrysene, benzo[a]pyrene, and coronene are shown in Figure 15 (a) and (b). Both Crn-ester and Crn-PFPA columns strongly retained PAHs. The retention increased with the number of π electrons, and showed high separation resolution owing to the strong π-π interaction. To demonstrate the retention selectivity in the Crn-modified silica monoliths, the retention factor for each PAH is plotted against the number of π electrons. As shown in Figure 15 (c), PAHs were retained in Crn columns slightly better than other columns, which can be attributed to the dipole of Crn. Interestingly, in both Crn-ester and Crn-PFPA columns, coronene was significantly retained compared to other planar PAHs, whereas a linear relation was observed for all the PAHs in the C60, C70, PYE and πNAP columns. Especially, the retention of coronene was much higher in Crn-PFPA column than in Crn-ester column. In Crn-PFPA, since PFPA derivatization occurs on the spoke of Crn (Scheme 2b), only the concave surface of Crn structure in Crn-PFPA column could interact with coronene because of the large steric hindrance of nitrogen atom on the concave surface. In Crn-ester column, however, because the derivatization occurs at the edge of the structure, both concave and convex surfaces of the Crn structure could interact with coronene.

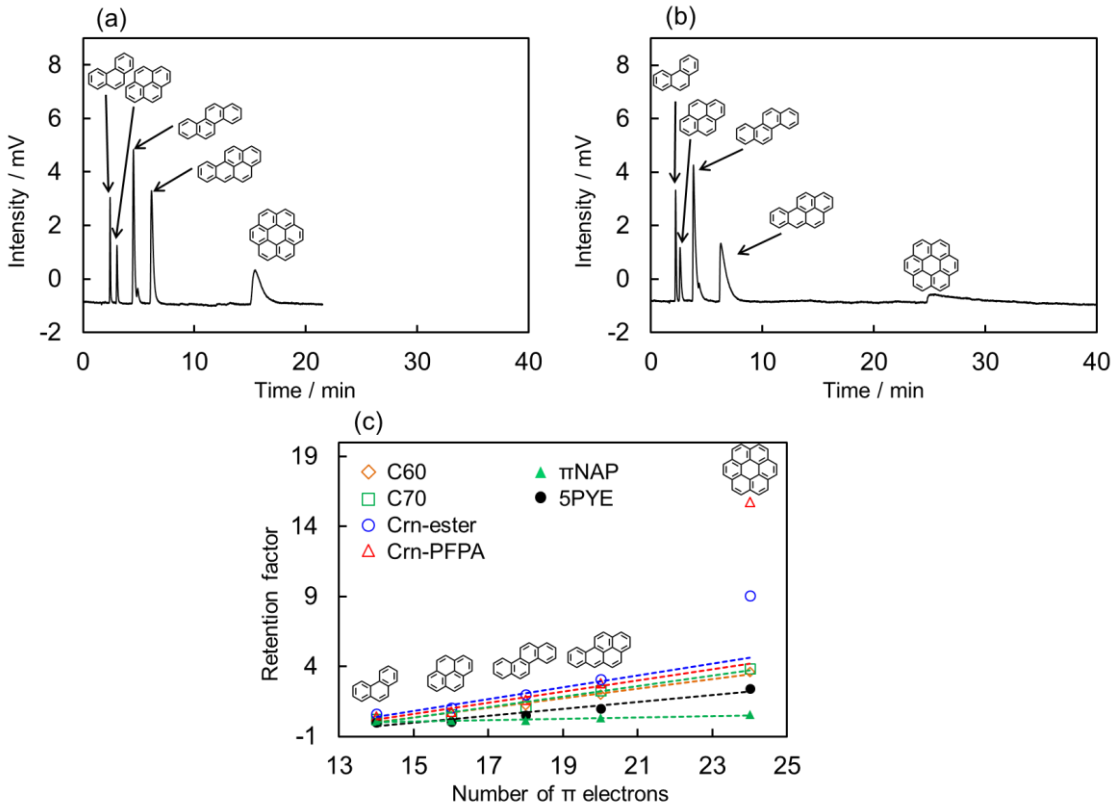

Figure 15. Retention behaviors of nonpolar and planar PAHs in Crn-modified silica monoliths. Chromatograms of the mixed sample of PAHs on (a) Crn-ester column, (b) Crn-PFPA column. (c) Plots of retention factor on each column vs. the number of π electrons in PAH. Condition: column, C60 column (32.0 cm × 100 mm i.d.), C70 column (32.0 cm × 100 mm i.d.), Crn-ester column (32.0 cm × 100 mm i.d.), Crn-PFPA column (32.0 cm × 100 mm i.d.), πNAP (Nacalai Tesque, 50 mm × 2.0 mm i.d.), 5PYE (Nacalai Tesque, 150 mm × 4.6 mm i.d.); mobile phase, *n*-hexane; detection, UV 300 nm; temperature 40 ºC.

To elucidate the additional intramolecular interactions between coronene and Crn structures, the ^{1}H NMR spectra of Crn-CH_2OH or Crn-PFPA-CH_2OCH_3 in the presence of coronene were recorded and compared to those of coronene or the Crn derivatives. No significant peak shifts were observed in either coronene or Crn-CH_2OH when the two molecules were mixed (Figure 16 (a)). However, when coronene was mixed with Crn-PFPA-CH_2OCH_3, the aromatic peaks in Crn-PFPA-CH_2OCH_3 shifted upfield and the width of several peaks were also broadened, while no shift was observed for the methyl protons.

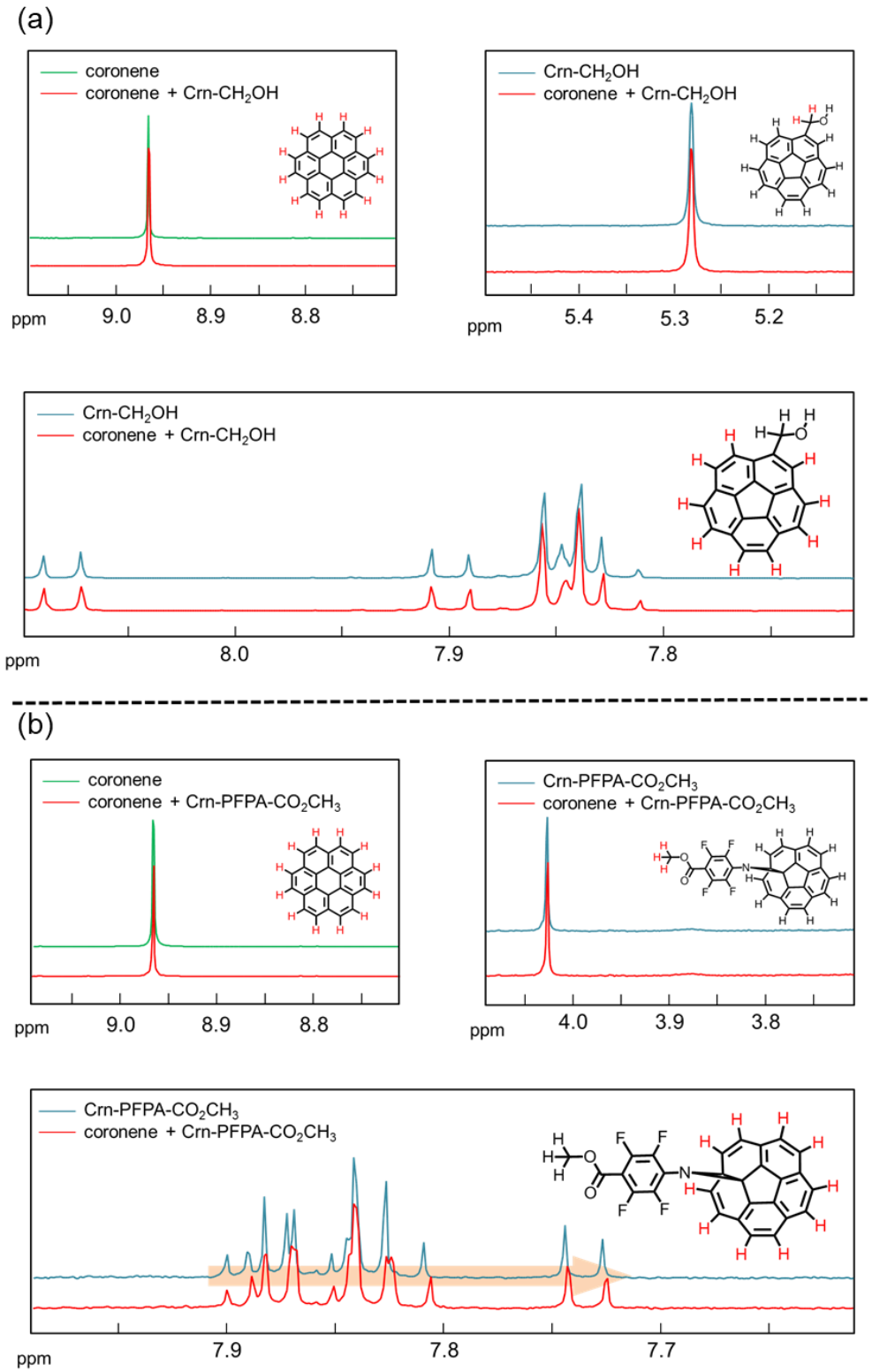

Figure 16. ^{1}H NMR spectra of coronene, Crn derivatives, or their mixture in $CDCl_3$. (a) Crn-CH_2OH with/without coronene, (b) Crn-PFPA-CH_2OCH_3 with/without coronene.

In general, π interactions can be interfered by polar molecules such as halogenated compounds, thus the interaction between Crn and coronene may not be fairly evaluated in chloroform. In fact, the retentions due to π interactions were dramatically decreased by adding chloroform to the mobile phase in LC [34]. Therefore, to better evaluate the chemical shifts in NMR, we added *n*-hexane-*d*14 to chloroform-*d* because π interactions appear more strongly in *n*-hexane, due to its lower dielectric constant, than in chloroform. As expected, significant shifts of the aromatic protons in both coronene and Crn-PFPA-CH_2OCH_3 were observed in *n*-hexane-*d*14/chloroform-*d*. As shown in Figure 17, the aromatic peak in coronene shifted downfield after mixing with Crn-PFPA-CH_2OCH_3, whereas all Crn aromatic protons in Crn-PFPA-OCH_3 shifted upfield. In addition, these peaks were bifurcated and broadened. These drastic changes suggest the presence of extremely strong intermolecular interactions. Thus, the protons on the Crn structure were placed in a more electron rich environment (i.e., more shielded), whereas the protons on coronene were placed in a more electron poor environment (i.e., less shielded). In other words, as the Crn structure approached the π conjugated surface of coronene, it attracted the π electrons in coronene making its aromatic protons more shielded[47].

This is likely mediated by the strong electron-withdrawing PFPA on Crn-PFPA-CH_2OCH_3, which pulls the electron density away from Crn, and subsequently coronene. Briefly, strong CH-π interaction at multiple points working between the hydrogen atom of Crn and the aromatic ring of coronene was confirmed. Matsuno et al. recently reported multipoint and strong π interaction between (P)-(12,8)-[4]cyclo-2,8-chrysenylene, which is a cylindrical molecules made of linked chrysen structure in a hoop-like structure, and Crn. These results are also strongly

supported from this report.[48]

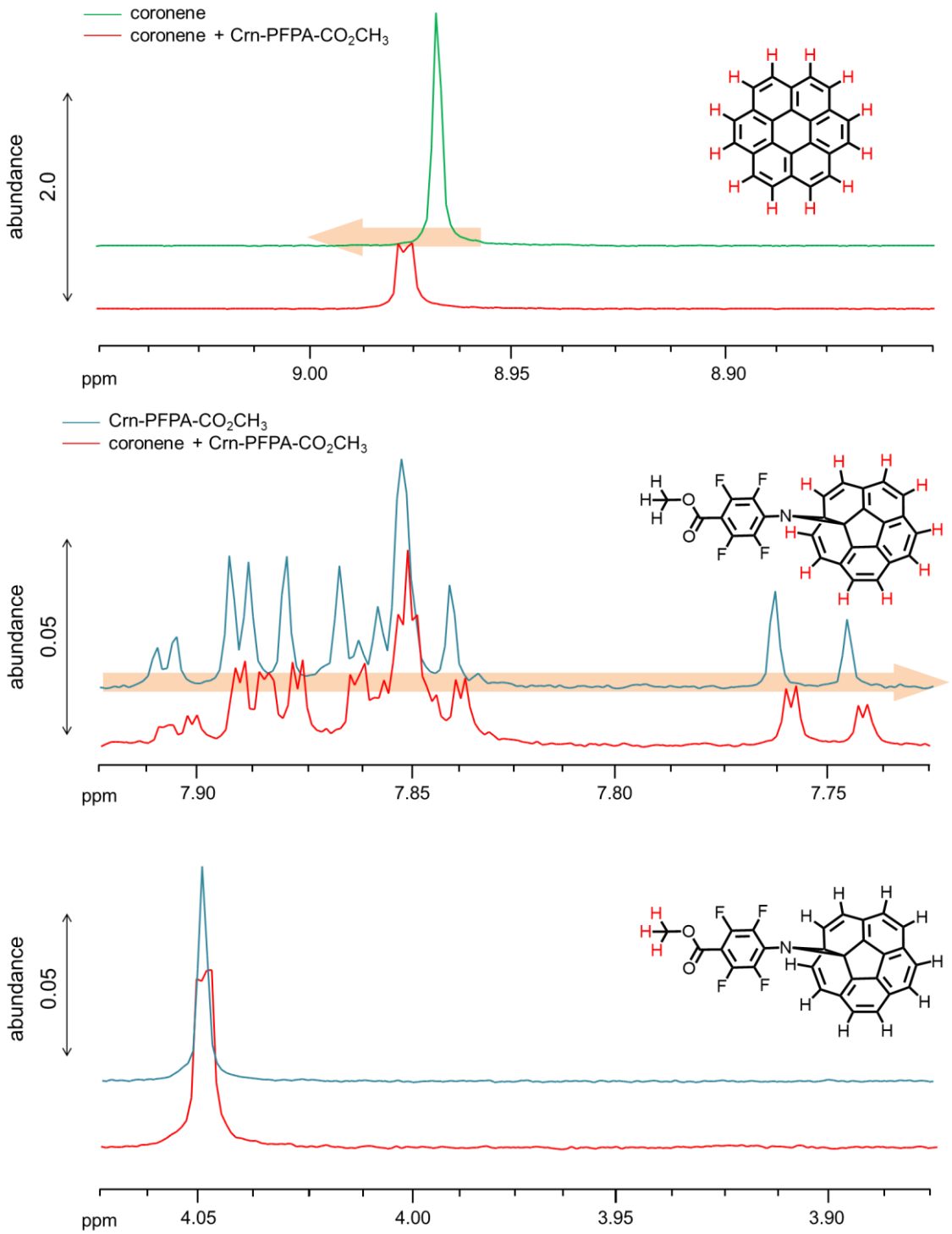

Figure 17. ^{1}H NMR spectral comparisons of coronene, Crn-PFPA-CH_2OCH_3 or their mixture in hexane-*d*14/chloroform-*d* = 1/1.

Figure 18 shows a schematic diagram illustrating the π interaction of coronene with Crn in Crn-ester or Crn-PFAP column. On the Crn-ester column, Crn was edge-functionalized and the linker is away from the Cr surface. As such, both concave and the convex surfaces of Crn can interact with coronene. On the Crn-PFPA column, because the modification by PFPA occurs on the spoke of Crn, the strong steric hindrance puts the PFPA group on the convex surface of the Crn structure. This leaves mainly the concave surface of Crn to interact with coronene. The fact that the Crn-PFPA column had significantly higher retention for coronene than the Crn-ester column demonstrate that the CH-π interaction on this concave surface is much stronger than the interaction from both surfaces in Crn-ester.

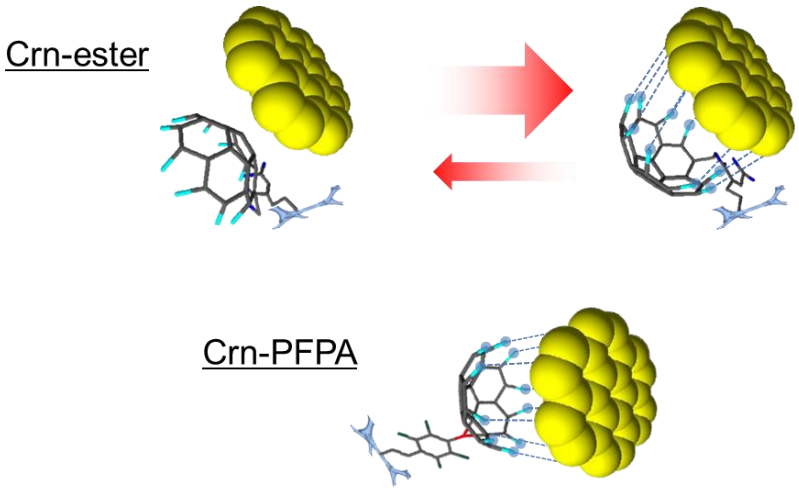

Figure 18. Schematic diagram of π interaction between coronene and Crn in Crn-ester or Crn-PFPA column.

6-3-4 Shape recognition

We show in last section that both convex and concave surfaces of the Crn structure contributed to the molecular recognition in the Crn-ester column, while only the concave surface of the Crn structure contributed in the Crn-PFPA column. To investigate whether the shape recognition plays a role, we evaluated the retention selectivity of naphthacene and triphenylene, which are planar aromatic compounds that have the same number of π electrons and the only difference is the molecular shape. The chromatograms obtained by normal phase mode of naphthacene and triphenylene are shown in Figure 19. Interestingly, the elution order was reversed; triphenylene eluted faster than naphthacene on the Crn-ester column, while the opposed result was obtained on the Crn-PFPA column.

To investigate the difference in shape recognition, we consider the difference in the polarizability of these PAHs. In the case of nonpolar molecules in π interaction, the strength of π interaction is considered to be due to induced dipole–dipole interaction or induced dipole–dipole interaction [49,50]. The potential energy of induced dipole–induced dipole interaction is given as follows:

$$G_{\text{induced dipole}-\text{dipole}} = -\mu^2\alpha_1/(4\pi\varepsilon_0\varepsilon_r)^2 r^6$$

The potential energy of induced dipole–dipole interaction is given as follows:

$$G_{\text{induced dipole-induced dipole}} = -\mathrm{A}\alpha_1\alpha_2/(4\pi\varepsilon_0\varepsilon_r)^2 r^6$$

where, μ is the dipole moment of polar molecules, α are polarizabilities of the molecules, ε_0 is the permittivity of vacuum, ε_r is the permittivity of the solvent, and r is the distance between the molecules, respectively [51,52]. In this case, the strength of π interaction increases as the polarizability of the solute increases.

Then, we consider that the difference in shape recognition was caused by the

polarizability of these PAHs. The polarizability of PAHs was summarized in Table 2, and the polarizability is plotted against the number of π electrons (Figure 20). As shown in Figure 20, the polarizability of each solute increases roughly with the number of π electrons. This trend is consistent with increasing in retention and the stronger π interaction as the number of π electrons increases (Figure 15). For those PAHs with identical number of π electrons, small differences in the polarizability were observed; *e.g.* naphthacene, benzo[a]anthracene, chrysene, and triphenylene.

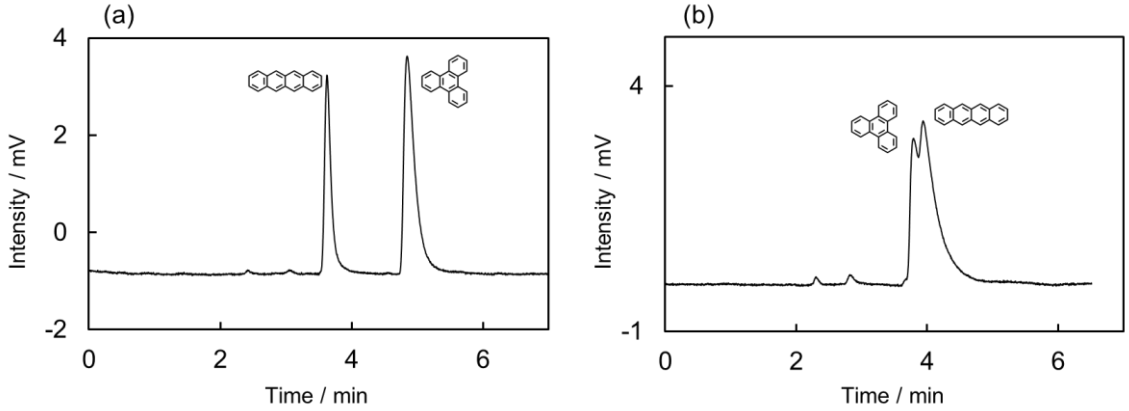

Figure 19. Chromatograms of the mixed sample of naphthacene and triphenylene on (a) Crn-ester column, (b) Crn-PFPA column. Condition: column, Crn-ester column (32.0 cm × 100 mm i.d.), Crn-PFPA column (32.0 cm × 100 mm i.d.); mobile phase, *n*-hexane; detection, UV 280 nm; temperature 40 ºC.

Table 2. Polarizability of PAHs.

Compounds	Porarizability (C m^2 V^{-1})
Anthracene	273.359
Phenanthrene	253.655
Pyrene	324.861
Tetracene	410.029
Benzo[a]anthracene	376.997
Chrycene	360.369
Triphenylene	342.915
Benzo[a]pyrene	431.079
Coronene	522.719

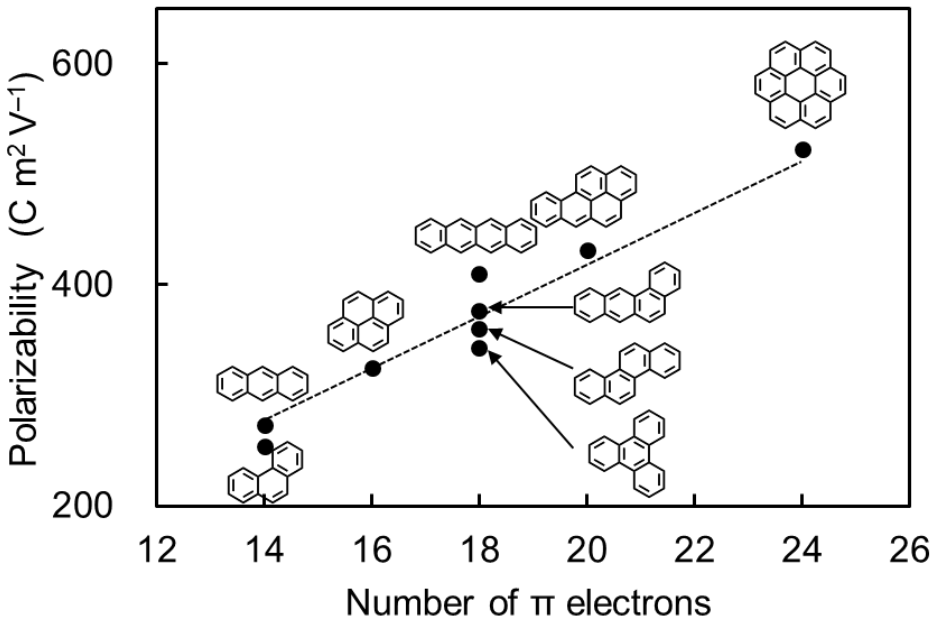

Figure 20. Plot of polarizability vs. the number of π electrons in PAH.

We subsequently calculated the retention factors of naphthacene, benzo[a]anthracene, chrysene, and triphenylene on different columns from the results of LC, and plotted them against the polarizability of each PAH (Figure 21 (a)). In commercially available LC columns, πNAP and 5PYE, separation of these solutes could not be realized because the π conjugated structure of these stationary phases have small numbers of π electrons. As mentioned earlier, the retention factor increased with the polarizability in the Crn-PFPA column. However, the trend in the Crn-ester column was completely reversed that the retention factor decreased with the polarizability. The same is true for C60/C70 columns. As illustrated in Figure 21 (b), C60 and C70 have the convex face of Crn as their partial structure. Therefore, this result supports that the convex surface of Crn contributes to retention in the Crn-ester column in contrast to the Crn-PFPA column that the concave surface contributed to the retention. In summary, the convex surface of Crn in Crn-PFPA column dominated the interactions with the solutes.

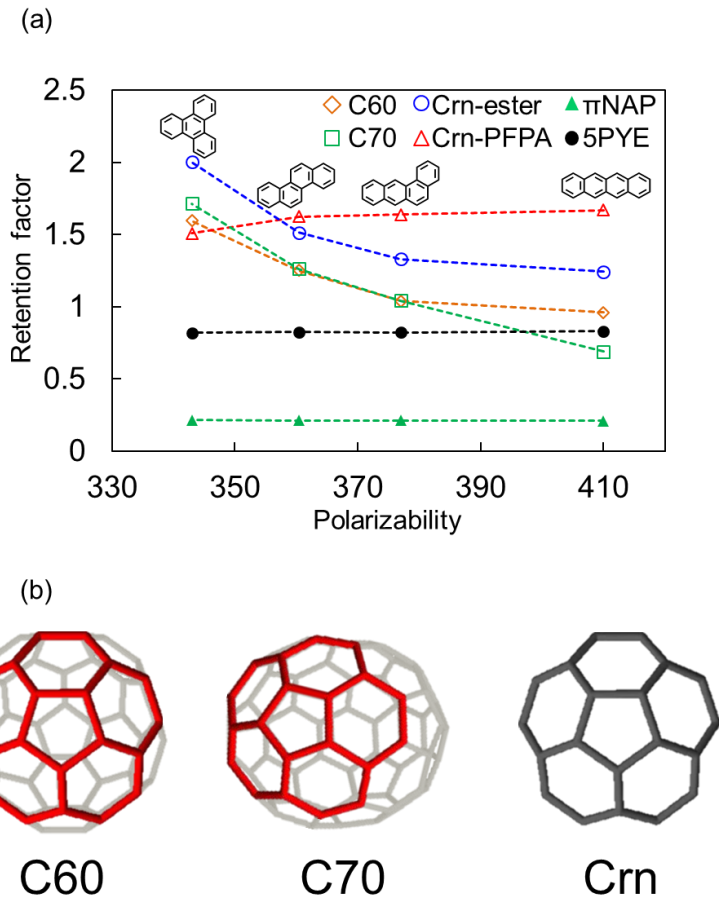

Figure 21. (a) Plot of retention factors of naphthacene, benzo[a]anthracene, chrysene, and triphenylene on different columns. (b) The convex surface of Crn shown as a partial structure in C60 and C70.

6-4 Conclusions

In this report, we revealed the molecular recognition of Crn by evaluating the retention of Crn as well as a number of aromatic compounds on Crn-modified silica monoliths in LC. We synthesized two kinds of Crn derivatives, Crn-ester by introducing the functional group on the edge of Crn, and Crn-PFPA by modifying the spoke structure of corannulene, and successfully prepared the Crn-modified columns Crn-ester and Crn-PFPA. Both columns showed low retention for Crn, despite its hemispherical structure. Computer simulation of Crn and Crn derivatives suggested electrostatic repulsion resulting from the same arrangements of charge and charge distributions in the Crn structures. On the other hand, both columns exhibited strong interactions with the planar molecule, coronene, especially Crn-PFPA which showed significantly strong interactions. The evaluation of ^{1}H-NMR shifts suggested that the specific retention caused by CH-π interaction at multiple points between the hydrogen atoms of the concave surface of Crn structure and the planar π conjugated surface of coronene. Furthermore, we demonstrated that the molecular recognition in Crn-ester was due to π–π interaction on the convex surface of Crn. We believe that this report greatly advanced understanding on the π interactions, which should aid the development of novel functional materials.

6-5 References

1 Cornil, B. J.; Beljonne, D.; Calbert, J.; Brødas, J. *Adv. Mater.* Interchain Interactions in Organic π-Conjugated Materials: Impact on Electronic Structure, Optical Response, and Charge Transport. **2001**, *13*, 1053–1067.

2 Mignon, P.; Loverix, S.; Steyaert, J.; Geerlings, P. Influence of the π–π interaction on the hydrogen bonding capacity of stacked DNA/RNA bases. *Nucleic Acids Res.* **2005**, *33*, 1779–1789.

3 Wilson, K. A.; Kellie, J. L.; Wetmore, S. D. DNA–protein π-interactions in nature: abundance, structure, composition and strength of contacts between aromatic amino acids and DNA nucleobases or deoxyribose sugar. *Nucleic Acids Res.* **2014**, *42*, 6726–6741.

4 Salonen, L. M.; Ellermann, M.; Diederich, F. Aromatic Rings in Chemical and Biological Recognition: Energetics and Structures. *Angew. Chemie - Int. Ed.* **2011**, *50*, 4808–4842.

5 Neel, A. J.; Hilton, M. J.; Sigman, M. S.; Toste, F. D. Exploiting non-covalent π interactions for catalyst design. *Nature* **2017**, *543*, 637–646.

6 Nakagawa, Y.; Irie, K.; Yanagita, R. C.; Ohigashi, H.; Tsuda, K. I. Indolactam-V Is Involved in the CH/π Interaction with Pro-11 of the PKCδ C1B Domain: Application for the Structural Optimization of the PKCδ Ligand. *J. Am. Chem. Soc.* **2005**, *127*, 5746–5747.

7 Okamoto, T.; Nakahara, K.; Saeki, A.; Seki, S.; Oh, J. H.; Akkerman, H. B.; Bao, Z.; Matsuo, Y. Aryl−Perfluoroaryl Substituted Tetracene: Induction of Face-to-Face π−π Stacking and Enhancement of Charge Carrier Properties. *Chem. Mater.* **2011**, *23*, 1646–1649.

8 Wu, H.; Zhao, P.; Li, X.; Chen, W.; Ågren, H.; Zhang, Q.; Zhu, L. Tuning for Visible Fluorescence and Near-Infrared Phosphorescence on a Unimolecular Mechanically Sensitive Platform via Adjustable CH−π Interaction. *ACS Appl. Mater. Interfaces* **2017**, *9*, 3865–3872.

9 Barth, W. E.; Lawton, R. G. Dibenzo[ghi,mno]fluoranthene. *J. Am. Chem. Soc.* **1966**, *88*, 380–381.

10 Olson, A. J.; Hu, Y. H. E.; Keinan, E. Chemical mimicry of viral capsid self-assembly. *Proc. Natl. Acad. Sci.* **2007**, *104*, 20731–20736.

11 Lovas, F. J.; McMahon, R. J.; Grabow, J. U.; Schnell, M.; Mack, J.; Scott, L. T.; Kuczkowski, R. L. Interstellar Chemistry: A Strategy for Detecting Polycyclic Aromatic Hydrocarbons in Space. *J. Am. Chem. Soc.* **2005**, *127*, 4345–4349.

12 Wang, L.; Wang, W. Y.; Qiu, Y. Q.; Lu, H. Z. Second-Order Nonlinear Optical Response of Electron Donor–Acceptor Hybrids Formed between Corannulene and Metallofullerenes. *J. Phys. Chem. C* **2015**, *119*, 24965–24975.

13 Lu, R. Q.; Xuan, W.; Zheng, Y. Q.; Zhou, Y. N.; Yan, X. Y.; Dou, J. H.; Chen, R.; Pei, J.; Weng, W.; Cao, X. Y. A corannulene-based donor–acceptor polymer for organic field-effect transistors. A *RSC Adv.* **2014**, *4*, 56749–56755.

14 Hashemi, M. M.; Bratcher, M. S.; Scott, L. T. Corannulene bowl-to-bowl inversion is rapid at room temperature. *J. Am. Chem. Soc.* **1992**, *114*, 1920–1921.

15 Juríček, M.; Strutt, N. L.; Barnes, J. C.; Butterfield, A. M.; Dale, E. J.; Baldridge, K. K.; Stoddart, J. F.; Siegel, J. S. Induced-fit catalysis of corannulene bowl-to-bowl inversion. *Nat. Chem.* **2014**, *6*, 222–228.

16 Kawasumi, K.; Zhang, Q.; Segawa, Y.; Scott, L. T.; Itami, K. A grossly warped nanographene and the consequences of multiple odd-membered-ring defects. *Nat.*

Chem. **2013**, *5*, 739–744.

17 Mishra, A.; Ulaganathan, M.; Edison, E.; Borah, P.; Mishra, A.; Sreejith, S.; Madhavi, S.; Stuparu, M. C. Polymeric Nanomaterials Based on the Buckybowl Motif: Synthesis through Ring-Opening Metathesis Polymerization and Energy Storage Applications. *ACS Macro Lett.* **2017**, *6*, 1212–1216.

18 Sygula, A.; Fronczek, F. R.; Sygula, R.; Rabideau, P. W.; Olmstead, M. M. A double concave hydrocarbon buckycatcher. *J. Am. Chem. Soc.* **2007**, *129*, 3842–3843.

19 Mack, J.; Vogel, P.; Jones, D.; Kaval, N.; Sutton, A. The development of corannulene-based blue emitters. *Org. Biomol. Chem.* **2007**, *5*, 2448–2452.

20 Wells, R. A.; Kellie, J. L.; Wetmore, S. D. Significant strength of charged DNA–protein π–π interactions: a preliminary study of cytosine. *J. Phys. Chem. B* **2013**, *117*, 10462–10474.

21 Tsuzuki, S.; Honda, K.; Uchimaru, T.; Mikami, M.; Tanabe, K. Origin of the Attraction and Directionality of the NH/π Interaction: Comparison with OH/π and CH/π Interactions. *J. Am. Chem. Soc.* **2000**, *122*, 11450–11458.

22 Huber, R. G.; Margreiter, M. A.; Fuchs, J. E.; Von Grafenstein, S.; Tautermann, C. S.; Liedl, K. R.; Fox, T. Heteroaromatic π-stacking energy landscapes. *J. Chem. Inf. Model.* **2014**, *54*, 1371–1379.

23 Kawahara, S. I.; Tsuzuki, S.; Uchimaru, T. Ab initio calculation of interaction nature of borazine ($B_3N_3H_6$) dimer. *J. Chem. Phys.* **2003**, *119*, 10081–10087.

24 Kohn, S. C.; Dupree, R.; Smith, M. E. Proton environments and hydrogen-bonding in hydrous silicate glasses from proton NMR. *Nature* **1989**, *337*, 539–541.

25 Ramı, K.; Alonso-rı, R. Enthalpic Nature of the CH/π Interaction Involved in the

Recognition of Carbohydrates by Aromatic Compounds, Confirmed by a Novel Interplay of NMR, Calorimetry, and Theoretical Calculations. *J. Am. Chem. Soc.* **2009**, *131*, 18129–18138.

26 Li, P.; Zhao, C.; Smith, M. D.; Shimizu, K. D. Comprehensive Experimental Study of N-Heterocyclic π-Stacking Interactions of Neutral and Cationic Pyridines. *J. Org. Chem.* **2013**, *78*, 5303–5313.

27 Del Bene, J. E.; Perera, S. A.; Bartlett, R. J. Hydrogen Bond Types, Binding Energies, and 1H NMR Chemical Shifts. *J. Phys. Chem. A* **1999**, *103*, 8121–8124.

28 Kimata, K.; Hosoya, K.; Araki, T.; Tanaka, N. The effects of cold preservation on steatotic graft viability in rat liver transplantation.. *J. Org. Chem.* **1993**, *58*, 282–283.

29 Chen, S.; Meyerhoff, M. Shape-Selective Retention of Polycyclic Aromatic Hydrocarbons on Metalloprotoporphyrin−Silica Phases: Effect of Metal Ion Center and Porphyrin Coverage. *Anal. Chem.* **1998**, *70*, 2523–2529.

30 Kubo, T.; Murakami, Y.; Tominaga, Y.; Naito, T.; Sueyoshi, K.; Yan, M.; Otsuka, K. Development of a C_{60}-fullerene bonded open-tubular capillary using a photo/thermal active agent for liquid chromatographic separations by π–π interactions. *J. Chromatogr. A* **2014**, *1323*, 174–178.

31 Kubo, T.; Murakami, Y.; Tsuzuki, M.; Kobayashi, H.; Naito, T.; Sano, T.; Yan, M.; Otsuka, K. Unique Separation Behavior of a C_{60}- Fullerene-Bonded Silica Monolith Prepared by an Effective Thermal Coupling Agent. *Chem. - A Eur. J.* **2015**, *21*, 18095–18098.

32 Kubo, T.; Kanao, E.; Matsumoto, T.; Naito, T.; Sano, T.; Yan, M.; Otsuka, K. Specific Intermolecular Interactions by the Localized π-Electrons in C_{70}-fullerene.

ChemistrySelect **2016**, *1*, 5900–5904.

33 Kanao, E.; Kubo, T.; Naito, T.; Matsumoto, T.; Sano, T.; Yan, M.; Otsuka, K. Isotope effects on hydrogen bonding and CH/CD-π interaction. *J. Phys. Chem. C* **2018**, *122*, 15026–15032.

34 Kanao, E.; Naito, T.; Kubo, T.; Otsuka, K. Development of a C_{70}-Fullerene Bonded Silica-Monolithic Capillary and Its Retention Characteristics in Liquid Chromatography. *Chromatography* **2017**, *38*, 45–51.

35 Mizyed, S.; Georghiou, P. E.; Bancu, M.; Cuadra, B.; Rai, A. K.; Cheng, P.; Scott, L. T. Embracing C_{60} with Multiarmed Geodesic Partners. *J. Am. Chem. Soc.* **2001**, *123*, 12770–12774.

36 Li, J.; Liu, Y.; Qian, Y.; Li, L.; Xie, L.; Shang, J.; Yu, T.; Yi, M.; Huang, W. Describing curved–planar π–π interactions: modeled by corannulene, pyrene and coronene. *Phys. Chem. Chem. Phys.* **2013**, *15*, 12694–12701.

37 Rajeshkumar, V.; Lee, Y. T.; Stuparu, M. C. Corannulenecarbaldehyde: High-Yielding Synthesis by Rieche Form-ylation and Facile Access to a Variety of Corannulene Derivatives. *European J. Org. Chem.* **2016**, *2016*, 36–40.

38 Liu, L.-H.; Yan, M. Perfluorophenyl azides: new applications in surface functionalization and nanomaterial synthesis. *Acc. Chem. Res.* **2010**, *43*, 1434–1443.

39 Xie, S.; Lopez, S. A.; Ramström, O.; Yan, M.; Houk, K. N. 1, 3-Dipolar cycloaddition reactivities of perfluorinated aryl azides with enamines and strained dipolarophiles. *J. Am. Chem. Soc.* **2015**, *137*, 2958–2966.

40 Yan, M.; Cai, S. X.; Keana, J. F. W. Photochemical and thermal reactions of C_{60} with *N*-succinimidyl 4-azido-2, 3, 5, 6-tetrafluorobenzoate: a new method for

functionalization of C_{60}. *J. Org. Chem.* **1994**, *59*, 5951–5954.

41 Kong, N.; Shimpi, M. R.; Ramström, O.; Yan, M. Carbohydrate conjugation through microwave-assisted functionalization of single-walled carbon nanotubes using perfluorophenyl azides. *Carbohydr. Res.* **2015**, *405*, 33–38.

42 Park, J.; Yan, M. Covalent Functionalization of Graphene with Reactive Intermediates. *Acc. Chem. Res.* **2013**, *46*, 181–189.

43 Park, J.; Jayawardena, H. S.; Chen, X.; Jayawardana, K. W.; Sundhoro, M.; Ada, E.; Yan, M. A general method for the fabrication of graphene–nanoparticle hybrid material. *Chem. Commun.* **2015**, *51*, 2882–2885.

44 Park, J.; Jin, T.; Liu, C.; Li, G.; Yan, M. Three-Dimensional Graphene-TiO2 Nanocomposite Photocatalyst Synthesized by Covalent Attachment. *ACS Omega* **2016**, *1*, 351–356.

45 Wang, B. T.; Petrukhina, M. A.; Margine, E. R. Electronic transport properties of selected carbon π-bowls with different size, curvature and solid state packing. *Carbon* **2015**, *94*, 174–180.

46 Grimme, S. Ab initio study of the structure and dipole moment of azulene. *Chem. Phys. Lett.* **1993**, *20*, 67–74.

47 Jennings, W. B.; McCarthy, N. J. P.; Kelly, P.; Malone, J. F. Topically resolved intramolecular CH-π interactions in phenylalanine derivatives. *Org. Biomol. Chem.* **2009**, *7*, 5156–5162.

48 Matsuno, T.; Fujita, M.; Fukunaga, K.; Sato, S.; Isobe, H. Concyclic CH-π arrays for single-axis rotations of a bowl in a tube. *Nat. Commun.* **2018**, *9*, 3779–3786.

49 Lima, C. F. R. A. C.; Rocha, M. A. A.; Gomes, L. R.; Low, J. N.; Silva, A. M. S.; Santos, L. M. N. B. F. Experimental support for the role of dispersion forces in

aromatic interactions *Chem. - A Eur. J.* **2012**, *18*, 8934–8943.

50 Wagner, J. P.; Schreiner, P. R. London dispersion in molecular chemistry-reconsidering steric effects. *Angew. Chemie - Int. Ed.* **2015**, *54* , 12274–12296.

51 Liang, Y. Q.; Hunt, K. L. C. Intramolecular screening of intermolecular forces. *J. Chem. Phys.* **1993**, *98*, 4626–4635.

52 Bowen, W. R.; Jenner, F. The calculation of dispersion forces for engineering applications. *Adv. Colloid Interface Sci.* **1995**, *56*, 201–243.

General Conclusions

In this thesis, the author investigated the strength and natures of the π interactions by evaluating the properties of the newly developed carbon materials-coated columns in liquid chromatography (LC) and applied various π interactions to specific separation analyses.

In the Chapter 2, the author developed a new silica-monolithic capillary column, which was modified with C70-fullerene (C70) via a particular thermal reactive molecule, perfluorophenyl azide. As a result of LC, the C70-coated column showed specific retention toward a hemispherical molecule, corannulene (Crn), and the most of PAHs were more retained in the C70-coated column than in the C60-fullerene (C60)-coated column. Results of the computer simulation of the molecules suggested that the specific interaction might be caused by the deflection of the π-electrons-density in C70. Furthermore, the absorption spectrometry also indicated that the absorption spectra of C70 with/without Crn were dramatically changed by the specific interaction, whereas no spectrum differences were observed with C60. This results strongly supported that the significant changing of the polarity based on the electron density on C70 was occurred by the interaction with Crn.

The Chapter 3 described the experimental evaluations of the X-π interaction using LC with various carbon-material coated columns providing strong π interactions in normal phase LC (NPLC), where the hydrophobic interaction was completely suppressed. The C70-coated column showed higher retentions for halogenated aromatic compounds as the

number of halogen substitutions increased by the X-π interactions. In addition, the strength of the X-π interaction increased in the order of F < Cl < Br < I. Changes to the UV absorption of C70 toward the brominated benzenes suggested that the intermolecular interactions were changed from the π-π interaction to X-π interaction as increasing the number of bromine substitutions. Computer simulations also showed that the difference in dipole moments among structural isomers affected the strength of the π-π interaction. Furthermore, the author concluded that the orbital interaction might contribute to the X-π interactions from small peak shifts in ^{1}H NMR and computer simulations. Finally, the author succeeded in the one-pot separation of all isomers of brominated benzenes using the C70-coated column by optimizing the mobile phase conditions.

In the Chapter 4, the author evaluated the isotope effect by LC with variety of separation media under reversed phase LC (RPLC) and NPLC using the H/D isotopologue pairs as the solutes. Results of RPLC suggested that the protiated compounds were more hydrophobic than that of deuterated compounds due to the isotope effect based on the hydrogen bonding between hydrogen atoms of isotopologues and hydroxy groups in the mobile phase. The importance of the hydrogen bonding was also supported by the separation of isotopologues with a silica stationary phase in NPLC, where the deuterated compounds showed stronger hydrogen bonding to hydroxy groups on silanol. Furthermore, comparison of free energies of the isotopologues in RPLC suggested that the CH-π interaction was slightly stronger than the CD-π interaction. Finally, the separation of a few isotopologues by NPLC using the C70-coated column was demonstrated according to the effective CH/CD-π interactions.

In Chapter 5, the author had deeper discussion about the H/D isotope effects in LC. Various LC experimental with different aromatic analytes, separation media, and non-polar mobile phases were conducted under NPLC. The separation media that had polar functional groups, such as a silanol group, allowed higher separation efficiencies for the pairs of aromatic H/D isotopologues. In comparison of ^{13}C NMR spectra of the protiated and deuterated aromatic analytes, the electron density on the carbon atoms in the deuterated analyte was found to be slightly higher than that of the protiated analytes. According to the results, it seemed that the aromatic rings of the analyte acted as donors through the OH-π interaction to hydrogen atoms in the silanol groups. Thus, the deuterated analytes were able to be strongly retained by the stronger OH-π interactions. Furthermore, the C70-coated column allowed the opposite isotope effect. Briefly, an electrostatic attraction based on the dipole-(induced) dipole interaction dominated in the CH-π interactions, according to the van't Hoff analysis. Hence, the bonding lengths of the C-H or D bonds in the analytes were sensitively affected, such that we were able to conclude the CH-π interaction depended on the geometric effect. Applying these opposing H/D isotope effects, the author was able to finally demonstrate the effective H/D isotopologue separations by utilizing the complimentary action of the OH-π and CH-π interactions.

In Chapter 6, the author revealed the molecular recognition of Crn by evaluating the retention of Crn as well as a number of aromatic compounds on the Crn-modified silica monolith in LC. He synthesized two kinds of Crn derivatives, Crn-ester by introducing the functional group on the edge of Crn, and Crn-PFPA by modifying the spoke structure of corannulene, and successfully prepared the Crn-modified columns with Crn-ester and

Crn-PFPA. Both columns showed low retention for Crn, despite its hemispherical structure. Computer simulation of Crn and the Crn derivatives suggested the electrostatic repulsion from the same arrangements of charge and charge distributions in the Crn structures. On the other hand, both columns exhibited strong interactions with the planar molecule, coronene, especially in Crn-PFPA. The evaluation of ^{1}H-NMR shifts suggested that the specific retention caused by the CH-π interaction at multiple points between the hydrogen atoms of the concave surface of Crn structure and the planar π conjugated surface of coronene. Furthermore, the author demonstrated that the molecular recognition in the Crn-ester was due to the π–π interaction on the convex surface of Crn.

In conclusion, the obtained findings throughout these studies will be greatly advance for understanding on the π interactions, which should aid the development of novel functional materials and the apprehension for bio-systems in our body. Furthermore, the new separation media developed in these studies allowed the selective and effective separations based on the various strong π interactions. The author believes that the studies will be contributing for practical separation science, such as removal of environmental pollutant and quantitative determination of medicinal compounds in the future.

List of Publications

Chapter 2.

"Specific Intermolecular Interactions by the Localized π-Electrons in C_{70}-fullerene",

Kubo, T.; **Kanao, E.**; Matsumoto, T.; Naito, T.; Sano, T.; Yan, M.; Otsuka, K.:

ChemistrySelect **2016**, *1*, 5900-5904.

"Development of a C_{70}-Fullerene Bonded Silica-Monolithic Capillary and its Retention Characteristics in Liquid Chromatography",

Kanao, E.; Naito, T.; Kubo, T.; Otsuka, K.:

Chromatography **2017**, *38*, 45-51.

Chapter 3.

"Separation of Halogenated Benzenes Enabled by Investigation of Halogen-π Interactions with Carbon Materials",

Kanao, E.; Morinaga, T.; Kubo, T.; Naito, T.; Matsumoto, T.; Sano, T.; Maki, H.; Yan, M.; Otsuka, K.:

Chem. Sci. **2020**, *11*, 409-418.

Chapter 4.

"Isotope Effects on Hydrogen Bonding and CH/CD-π Interaction",

Kanao, E.; Kubo, T.; Naito, T.; Matsumoto, T.; Sano, T.; Yan, M.; Otsuka, K.:

J. Phys. Chem. C **2018**, *122*, 15026-15032.

Chapter 5.

"Tunable Liquid Chromatographic Separation of H/D Isotopologues Enabled by Aromatic π Interactions",

Kanao, E.; Kubo, T.; Naito, T.; Sano, T.; Yan, M.; Tanaka, N.; Otsuka, K.:

Anal. Chem. **2020**, *92*, 4065-4072.

Chapter 6.

"Differentiating π Interactions by Constructing Concave/Convex Surfaces Using a Bucky Bowl Molecule, Corannulene in Liquid Chromatography",

Kanao, E.; Kubo, T.; Naito, T.; Matsumoto, T.; Sano, T.; Yan, M.; Otsuka, K.:

Anal. Chem. **2019**, *91*, 2439-2446.

Other publications not included in this thesis

"Recycle Reversed-Phase Liquid Chromatography to Achieve Separations Based on One H/D Substitution on Aromatic Hydrocarbons",

Kimata, K.; Hirose, T.; **Kanao, E.**; Kubo, T.; Otsuka, K.; Hosoya, K.; Yoshikawa, K.; Fukusaki, E.; Tanaka, N.:

LC GC Europe **2019**, *32*, 14-19.

"Carbon-based Nanomaterials for Separation Media",

Kanao, E.; Kubo, T.; Otsuka, K.

Bull. Chem. Soc. Jpn. **2020**, *93*, 482-489.

Acknowledgments

The present studies have been carried out under the direction of Professor Koji Otsuka, Department of Material Chemistry, Graduate School of Engineering, Kyoto University.

The author would like to express his great appreciation to Professor Koji Otsuka for his support and encouragement throughout the research and his intellectual capability, knowledge, valuable suggestions and adept discussions. He inspired the author to take up "Chemistry" as his career, and his guidance and creative criticism enriched the quality of the present studies.

The author is very grateful to Professor Seijiro Matsubara and Professor Kazunari Akiyoshi (Graduate School of Engineering, Kyoto University) for their splendid comments and discussions.

The author wishes to acknowledge Professor Nobuo Tanaka (Osaka University), Dr. Tomoharu Sano (National Institute for Environmental Studies), and Professor Mingdi Yan (University of Massachusetts Lowell), for their valuable suggestions and experimental instructions.

The author is highly indebted to his beloved Associate Professor Takuya Kubo (Graduate School of Engineering, Kyoto University) for his constant guidance, support, and kind cooperation for the author's career, and his guidance and unstilted support helped in completion of the present studies. His vision and adept discussion improved the author to learn and understand the challenges and/or potentiality of the present studies.

The author would like to give a special gratitude to Assistant Professor Toyohiro Naito (Graduate School of Engineering, Kyoto University). The completion of the thesis would not be possible without his cooperation, friendly and continuous support and thoughtful guidance throughout the present studies.

The author also thanks Dr. Takatoshi Matsumoto (Tohoku University) and Mr. Hiroshi Kobayashi (Shinwa Chemical Industries, Ltd.) for providing their expertise.

The author would like to express his sincere thanks to all the members of Professor Koji Otsuka's laboratory for their constant encouragements during the course of his research works. They have helped him grow professionally and personally in all efforts of his life.

The present work has been supported in part by the Japan Society for the Promotion of Science (JSPS) through its ''Research Fellowship for Young Scientists''.

Finally, the author wishes to express his indebtedness to his family for their endless love, understanding, support, encouragement, and sacrifice throughout his studies.

Eisuke Kanao

March, 2020